THE TROPOSPHERIC ABUNDANCES, EMISSIONS, AND TRANSPORT OF HALOGENATED SUBSTANCES ON REGIONAL AND GLOBAL SCALES

NORFAZRIN MOHD HANIF

DOCTOR OF PHILOSOPHY
2019

The tropospheric abundances, emissions, and transport of halogenated substances on regional and global scales

By

Norfazrin Mohd Hanif

A thesis presented for the
degree of Doctor of Philosophy
to the University of East Anglia

School of Environmental Sciences

University of East Anglia

June 2019

Declaration

I hereby declare that the thesis is my original work except for quotations and citations which have been duly acknowledged. I also declare that it has not previously and is not concurrently submitted for any other degree at the University of East Anglia or at any other institution. This thesis contains 54983 words including appendices.

Abstract

The primary aim of this thesis was to use models to study the (a) regional emissions of very short-lived (i.e. chlorinated VSLS) and short-lived (i.e. methyl halides) halogenated gases, as well as (b) global emissions of long-lived halogenated gases (i.e. CFC-114 & CFC-114a). The 3-D dispersion model was employed to determine the impact of different source types and regions on the variability of halogenated gases measured during the campaigns in Taiwan and Bachok, Malaysia. On the other hand, the 2-D global model was used for estimating the emissions of CFC-114 and -114a in archived remote Southern Hemispheric tropospheric air and firn air data.

Overall, this thesis has demonstrated that the measured chlorinated VSLS and methyl halides were observed at significantly high abundances. In addition, the quantitative analyses of the NAME backwards trajectories (i.e. using ArcGIS-generated shapefile and emissions data of carbon monoxide (CO) taken from Representative Concentration Pathway 8.5) and the usage of the cold surge index have further shed some light on the potential sources of emission & regions and transport of halogenated gases; these in turn could inform as well as guide future campaigns. Importantly, the studies highlighted the important roles of the (a) Northeast Monsoon's cold surges and (b) East Asian and South East Asian emissions in the enhancements of halogenated substances levels in that regions.

In addition, this thesis presented the first long-term trends and emissions of CFC-114 and-114a. The mixing ratios of both isomers were no longer increasing significantly but significant global atmospheric emissions have persisted until at least 2014, suggesting a need for continual efforts to ensure that these substances eventually disappear from the atmosphere. Evidently, complementary ground-based observations of the Taiwanese air samples in Taiwan suggested the presence of persistent emissions of CFC-114a in East Asia.

Table of Contents

List of Figures

List of Tables

Dedication

In the name of God, the most Beneficent, the most Merciful

This thesis is dedicated to my beloved family, my lovely husband (Ibrahim) and my children (Ilman and upcoming little bundle of joy).

You have made me stronger, better and more fulfilled
than I could have ever imagined.

I love you all so much.

Acknowledgments

This journey is made possible through the endless support and encouragement of many lovely people. To them goes my greatest thanks. From the bottom of my heart, I would like to express my deepest thanks to my main supervisor, Prof. Dr. Claire Reeves for her faith in me, for her tremendous support and guidance in every possible way throughout this journey. I could not have hoped for a better supervisor. Her insights, words of wisdom, encouragement and willingness to share her knowledge, expertise and time made the completion of this PhD journey possible. I would also like to express my sincere appreciation to my co-supervisor, Dr. David Oram, for always making the time to listen when I have doubts and offering insightful advice, constructive suggestions and lots of encouragement along the way. Also, thank you to my examiners i.e. Prof. Dr. Alex Baker and Prof. Dr. Mathew Heal for the hard work to evaluate my thesis with positive, fruitful notes and comments. Special thanks also to Prof. Dr. Mohd Talib Latif, my lifelong mentor who has been with me throughout my study journey. I extend my appreciation and gratitude to the Ministry of Higher Education of Malaysia and Universiti Kebangsaan Malaysia for the opportunity, guidance and financial assistance throughout this PhD endeavour.

I have been very fortunate to form some great friendships and very fortunate to work with such great people in University of East Anglia. To all lovely friends in 01.37K, the UEA Atmospheric Chemistry group and 'Warga Norwich' family, thank you very much for the friendship, support and help. On a more personal note, I would like to thank Alia, Chata, Huslinda, Johana and Rhosanna for the long coffee breaks and all of the laughter and pep talks. I have been very lucky to have all of you that always helped to cheer me up and encouraged me whenever I was doubting myself.

Most importantly, my sincere appreciation goes to my beloved husband, Ibrahim Mohamed. I owe my deepest gratitude towards my better half for his endless love, understanding, patience, sacrifice, support and encouragement throughout this journey. I'm not sure I would have got this far without you, Abang. Thank you for

believing in me. Your unconditional love and support has meant the world to me. You were always around and you helped me to keep things in perspective. To my dearest son, Ahmad Ilman Faheem, thank you for all the joy and happiness. Words would never say how grateful I am to have you. Your love is what has gotten me through at times I thought that it is impossible to continue. I would also like to dedicate my years of hard work to my parents, Mohd Hanif and Rosnah, all family members and in-laws for their unconditional love, encouragement, understanding and prayers in my entire life. Above all, I thank the Almighty for giving me the strength and patience to work through all these years. Indeed, this journey is not merely a professional journey for me but it is truly a spiritual one and I would not trade all the life lessons I learnt with anything else. Alhamdulilah, I am so blessed that along the way, I crossed paths with people who directly or indirectly set me on the right path. I pray that each and every one of you is in Allah's blessings, always.

Finally, I am grateful to have had the privilege of attending the University of East Anglia. This experience has afforded me the opportunity to work with some of the best and brightest, and the resources for me to achieve great success. Thank you for this opportunity.

Chapter 1

Introduction

Halogenated substances are employed in multiple aspects of life, particularly in industrial processes, consumer products, and building materials (Midgley et al., 1999). Despite their beneficial domestic and industrial applications, there is scientific evidence that the production and release of halogenated compounds into the atmosphere had considerable ramifications on the atmosphere and the environment. This was especially true for the natural balance of the stratospheric ozone as well as global warming (Molina et al., 1974). The environmental impact of halogenated gases became prominent following the discovery of the Antarctic ozone hole in 1985 (Farman et al., 1985). Since then, such compounds have garnered the interest of scientists and policymakers, apart from triggering an unprecedented level international cooperation which resulted in the enactment of the Montreal Protocol in 1987. This protocol was created with the aim of regulating the release of halogenated gases, or ozone-depleting substances (ODSs), by reducing and phasing out the global production as well as consumption of ODSs. Evidently, the stabilisation of the global atmospheric mixing ratios of certain ODSs was proof of the success of the Montreal Protocol (Derwent et al., 1998). However, recent observations have revealed the existence of unexpected and persistent atmospheric emissions of Montreal Protocol ODSs and non-Montreal Protocol ODSs, both of which were a potential threat to the recovery of the aforementioned ozone hole (Laube et al. (2014), Hossaini et al. (2015). This phenomenon has highlighted the need for further investigations and continued efforts to ensure the elimination of the said ODSs from the atmosphere, which forms the motivation of this thesis.

The aim of this chapter is to briefly introduce the relevant aspects of atmospheric chemistry, especially halogenated substances and their effects on the ozone layer. It starts off with descriptions of the ozone layer, followed by an overview of the halogenated substances in the atmosphere and their roles in the depletion of stratospheric ozone (Sections 1.1 and 1.2). Meanwhile, Section 1.3

introduces the global legislation on the control of the production of halogenated substances. Also included are several recent and significant evidences of new and increasing threats from halogenated substances on the stratospheric ozone (Section 1.4). Next, this chapter states the research problems statements of the current thesis (Section 1.5). In the final section (Section 1.6), the aims and contents of the subsequent chapters are outlined.

1.1 The ozone layer

Natural ozone can be found in two main regions of the atmosphere. Almost 90% of ozone occurs in the stratosphere – the region which begins at about 10 - 16 kilometres above the surface of the Earth and extends up to ~50 kilometres– while the rest (~10%) occurs in the troposphere i.e. the lowest region of the atmosphere, between the surface of the Earth and the stratosphere (Hegglin et al., 2014). While high tropospheric ozone can cause harm to humans, plants and other living system (Hegglin et al., 2014), the high concentration of ozone in the stratosphere (otherwise referred to as the "ozone layer") acts as a protective layer that reduces the intensity of ultraviolet-B (UV-B) radiation from the sun which reaches the surface of the Earth (Wallace et al., 2006). Human exposure to UV-B increases the risks of skin cancer, immunosuppression, and cataract. In addition, UV-B also disrupts terrestrial plant life and aquatic ecosystems (Hegglin et al., 2014) Owing to the great importance of stratospheric ozone layer, the maintenance of its concentration is therefore crucial.

The concentration of ozone in the stratosphere is maintained via a chemical scheme (Equations 1.1 – 1.4) proposed by Chapman (1930):

$$O_2 + h\nu \longrightarrow O + O \qquad \text{(Equation 1.1)}$$

$$O + O_2 + M \longrightarrow O_3 + M \qquad \text{(Equation 1.2)}$$

$$O_3 + h\nu \longrightarrow O_2 + O \qquad \text{(Equation 1.3)}$$

$$O + O_3 \longrightarrow 2O_2 \qquad \text{(Equation 1.4)}$$

The reaction involves the dissociation of O_2 by solar UV radiation ($\lambda < 242$ nm) (Equation 1.1). The combination of atomic oxygen and molecular oxygen in Equation 1.2 forms ozone (O_3) and M (which represents N_2 and O_2). The reaction continues with the photodissociation of O_3 which occurs in the presence of UV radiation ($\lambda <$ 366 nm) (Equation 1.3). Finally, atomic oxygen and O_3 recombine to form O_2 (Equation 1.4).

1.2 Halogenated substances in the atmopshere

The concentration of stratospheric ozone as described in Section 1.1 can decrease in view of imbalances between the sources and sinks of O_3. A good example is the presence of halogens (i.e. chlorine and bromine radicals) in the stratosphere (Molina et al., 1974). These halogens are released into the atmosphere from a variety of anthropogenic and biogenic sources. Table 1.1 summarises the halogen source gases as well as their characteristics, uses/ sources, and atmospheric lifetimes.

Table 1.1 *Halogen source gases and their characteristics, uses/sources, atmospheric lifetimes*

Halogen source gases	Characteristics [a,c]	Uses or sources [a]	Atmospheric lifetimes [a]
Chlorofluorocarbons (CFCs)	• Are long lived gases, non- toxic, - corrosive, and - flammable • Are ozone-depleting substances; controlled under Montreal Protocol • Introduced in the 1930s, but has been replaced by hydrofluorocarbons (HFCs). HFCs are greenhouse gases that do not deplete stratospheric ozone	Refrigerants, cleaning solvents, blowing agents for plastic foam, maufacturing of aerosol sprays	~ 50 to 600 years

Carbon tetrachloride (CCl_4)	• Is an ozone-depleting substance; controlled under Montreal Protocol	Industrial cleaning solvents, feedstock fumigants, fire extinguishers	26 years
Methyl chloroform (CH_3CCl_3)	• Is an ozone-depleting substance; controlled under Montreal Protocol • Toxic	Industrial cleaning solvents, inks, correction fluids	5 years
Hydrochlorofluorocarbons (HCFCs)	• Have similar structure with CFCs, but contain at least one hydrogen atom • Transtitional CFC replacement • Low toxicity and flammability; reasonable cost[c] • Gives smaller impact than CFCs on stratopsheric chlorine[d]. However, HCFCs are greenhouse gases	Refrigerants, solvents, blowing agents for plastic foam, fire extinguishers	1.2 to 11.9 years
Halons	• Are bromine-containing halogenated hydrocarbons • Introduced in the 1960s • Volatile, electrically non-conductive, lack damaging residue or toxicity • Inexpensive to produce (IPCC/TEAP 2005) • Are ozone-depleting	Mobile fire extinguishers, fire-suppression systems (in places such as computer rooms and airplanes), explosion-protective agents	2.5 – 16 years

	substances; controlled under Montreal Protocol		
Methyl bromide (CH_3Br)	• Is an ozone-depleting substance; controlled under Montreal Protocol	Quarantine and pre-shipment (QPS) uses of CH3Br are exempted uses according to the Montreal Protocol. Comes from natural source similar to methyl chloride	0.8 years
Methy chloride (CH_3Cl)	• Not a controlled substance under Montreal Protocol	Primarily of natural origin (i.e. oceanic and terrestial ecosystems). Minimal anthropogenic sources.	0.9 years
Very short-lived substances (VSLSs) containing chlorine and bromine	• Not a controlled substance under Montreal Protocol	Brominated species (e.g. bromoform, $CHBr_3$) are predominantly of oceanic origin, while chlorinated species (e.g. dichloromethane, CH_2Cl_2) come mostly from industrial sources	Less than 6 months

Sources: [a] Carpenter et al. (2014), [b]Hegglin et al. (2014), [c]Kim et al. (2010), [d]Tsai (2002)

Halogenated gases that arise from human activities and mixed sources (human and natural emissions) are controlled by the Montreal Protocol (more details on Montreal Protocol in Section 1.4) and are classified as ozone-depleting substances (ODSs). On the other hand, halogenic substances of mainly natural origin are not referred to as ODSs (Table1.1).

Figure 1.1 shows the contributions of ODSs and natural halogen source gases to the stratospheric chlorine and bromine in 2012. The prime source of tropospheric chlorine is predominantly anthropogenic. Chlorofluorocarbons (CFCs), which consisted primarily of CFC-11, -12, and -113, accounted for the largest portion of man-made sources of tropospheric chlorine in 2012. This was followed by carbon tetrachloride (CCl_4), hydrochlorofluorocarbons (HCFCs), and methyl chloroform (CH_3CCl_3). Meanwhile, natural halogen source gases were mainly accounted for by methyl chloride (CH_3Cl) (about 16%) and very short-lived compounds (VSLSs) (approximately 3%).

Evidently, the contributions of natural and man-made sources towards tropospheric bromine are comparable. Halons and methyl bromide are the largest sources of stratospheric bromine; other sources include very short-lived brominated gases [e.g. bromoform ($CHBr_3$)], which are responsible for 24% of stratospheric bromine.

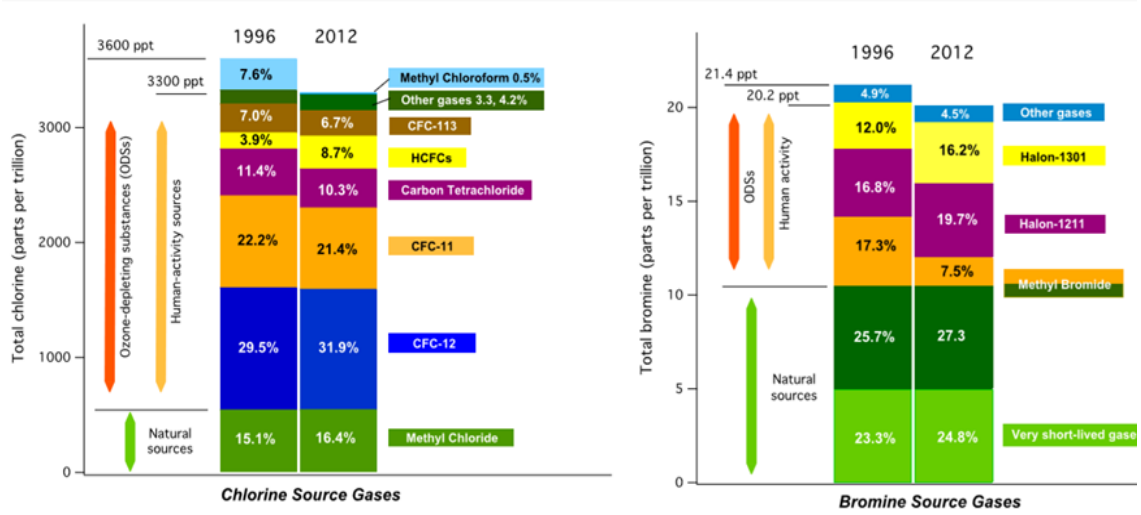

Figure 1.1: *Relative contributions of individual and groups of compounds to total tropospheric chlorine and total tropospheric bromine in 1996 and 2012 (Carpenter et al., 2014).*

Overall, the amount of chlorine which enters the stratosphere is 150 times that of bromine. Nevertheless, the atmospheric concentrations of bromine source gas, i.e. CH_3Br are still of great interest because their ozone depletion potential is 25 times

that of CH_3Cl. This phenomenon is attributable to the fact that on the atomic basis, bromine destroys ozone 60 times more effectively than chlorine (WMO, 2007).

1.3 Effects of halogenated substances on ozone layer

The following subsection describes the three main stages of stratopsheric ozone depletion by halogenated gases.

Stage 1 : Emission, accumulation, and transport of halogenated substances from troposphere to stratopshere

The said process starts with the release of the gases from a variety of sources on the Earth's surface. Small quantities of the aforementioned gases are liberated from natural sources, while substantial quantities of the same originate from anthropogenic emissions, as described in Section 1.2.

Once emitted, the halogen source gases accumulate in the troposhere prior to being transported to the stratosphere. It is important to note that this occurrence is also dependent on the lifetimes of the gases. The atmospheric lifetime of a molecule can be simply thought of as the time for which it remains in the atmosphere. Specifically, the atmospheric lifetime (τ) of trace gas is the time required for the removal or chemical transformation of approximately 63% of its global atmospheric burden (B). Calculations of the amopsheric lifetimes rely on a basic equation that relates the said burden, B, of an atmospheric constituent to its sources (emissions or *in situ* production) to its total global rate of removal, L (Equation 1.5) (Carpenter et al., 2014).

$$\tau = \frac{B\ (molecules)}{L\ (molecules\ s^{-1})} \qquad \text{(Equation 1.5)}$$

Halocarbon removal from the atmosphere can be achieved via numerous processes, including oxidation by hydroxyl radicals, photolysis, as well as uptake by the oceans, and terrestrial ecosystems. For instance, long-lived compounds (e.g. CFCs) which

are mainly removed through photolysis in the upper troposphere have lifetimes of around 100 years (Table 1.1). However, other gases (e.g. VSLSs) that are predominantly lost through multiple processes in the troposphere have lifetimes of under a year. The difference in lifetimes means that CFCs can remain in the atmosphere much longer and get accumulated to a much greater extent as compared to VSLSs.

Stage 2: Transport of halogenated substances from troposphere to stratopshere

The accumulated halogenated substances are then transported via natural air motions from the troposphere to the stratosphere. In general, the transportation of trace gases and aerosols from the troposphere to the stratosphere occurs primarily at the tropics where convective activities and vertical uplifts are most intense (Oram et al., 2017). In order to get to the stratosphere, an air parcel has to pass through the tropical tropopause layer (TTL) – the transitional layer which shares the characteristics of the upper troposphere (UT) and lower stratosphere (LS). Apart from being the gateway for troposphere-to-stratosphere transportations (TST), TTL also plays a key role in the global composition and circulation of the stratosphere (Fueglistaler et al., 2009).

Interestingly, the details of troposphere-to-stratosphere transport are of minor importance for long-lived and thus, well-mixed halogenated source gases. However, for VSLSs – whose lifetimes may be comparable to the tropospheric transport timescales (i.e. weeks to months), transportation processes may strongly impact their stratospheric source gas and product gas injections (Carpenter et al., 2014). Recent evidences by Oram et al. (2017) have suggested that it was possible for VSLSs to be transported from the boundary layer into the stratosphere, where they contributed to the stratospheric halogen-loading. In the TTL, higher VSLSs concentrations are predicted to occur during winter as compared to the rest of the year ((Aschmann et al., 2009, Gettelman et al., 2009). This is because of a combination of higher convective cloud tops reach the TTL and have higher vertical velocities within the TTL (Gettelman et al., 2009). During winters, deep convection currents over the Western Tropical Pacific are the dominant pathway through which

surface air is transported to the TTL (altitude: 13 - 17 km) and stratosphere. As such, the tropospheric composition and chemistry play a disproportionately large role in the determination of the stratospheric composition (Baker et al., 2016). Overall, the findings have supported that the Western Tropical Pacific was a region where VSLSs emissions could be efficiently transported to the TTL (Aschmann et al., 2009). Therefore, these highlight the importance of transport mechanisms in the making of VSLSs; previously, the said mechanism has not considered to play a significant role in stratospheric ozone depletion.

Stage 3 : Conversion , reaction, and removal of halogenated substances

In the stratosphere, halogenated compounds do not directly react with ozone. Instead, they dissociate via photolysis (in the presence of short-wave radiation from the sun) and release substantial amounts of halogen which are stable as well as not easily degradable (McGivern et al., 2000; Salawitch et al., 2005). Later, these halogens will take part in chemical chain reactions and destroy thousands of ozone molecules before being removed from the stratosphere (Montzka & Reimann, 2011) (Equations 1.6 - 1.8). Consequently, the natural balance between the production and loss of ozone is shifted the latter.

$$CF_2Cl_2 + h\nu \longrightarrow CF_2Cl + Cl \ (\lambda < 346 \text{ nm}) \quad \text{(Equation 1.6)}$$

$$Cl + O_3 \longrightarrow ClO + O_2 \quad \text{(Equation 1.7)}$$

$$ClO + O \longrightarrow Cl + O_2 \quad \text{(Equation 1.8)}$$

It is important to note that the chemical conversion rates of halogenated substances depend on their atmospheric lifetimes. Compounds with longer atmopsheric lifetimes (in the order of years) circulate multiple times between the troposphere and stratosphere before conversion occurs. After a few years, the reactive halogen gases, along with the stratospheric air, return to the troposphere and are removed via rain/ precepitation or deposition on the surfaces of the ground and oceans (Hegglin et al., 2014).

1.4 The global legislation to controls the production of halogenated substances (ODS)

Concerns over the roles of halogenated compounds in ozone depletion have been put forward in the 1970s by two scientists – Molina and Rowland. In 1974, they had theorised that CFCs, which originated from aerosol propellants and refrigerants, were chemically inert, and that their degradation via photodissociation in the stratosphere generated significant amounts of chlorine atoms which eventually led to the destruction of the atmospheric ozone. The prominent impact of CFCs has acknowledged since the early years of the discovery of the Antarctic ozone hole (Farman et al., 1985). Immense efforts have then been channelled towards the regulation of CFCs as well as other halogenated compounds. This subsequently galvanised the interest of scientists and policymakers, hence prompting unprecedented international action.

The 1987 Montreal Protocol on Substances that Deplete the Ozone Layer was enacted with the mission of regulating the release of halogenated gases by developed and developing countries, apart from providing a mechanism to reduce and phase-out the global production and consumption of ODSs (Derwent et al., 1998, Velders et al., 2007) (Figure 1.2). The Montreal Protocol took effect on 1st January 1989, following which the production of CFCs and other related halogenated compounds were to be phased out according to different schedules. For example, developed countries had to phase out CFCs by 1 January 1996, while developing countries could still produce (and purchase) CFCs until 2010 (AFEAS, 2006).

Since its inception, a total of eight amendments – which mainly concerned the inclusion of additional compounds – have been made to the Protocol (Hegglin et al., 2014). Currently signed by 197 countries, it has become the first treaty in the history of the United Nations to achieve universal ratification (UNEP, 2018).

ODSs are categorised into Class I or Class II controlled substances. Class I substances comprise those which have higher ozone depletion potentials (ODPs) and have been completely phased out by now, with a few exceptions. Therefore no production and

importing of class I substances are allowed, except for (1) those which are used in metered-dose inhalers for the treatment of asthma and chronic obstructive pulmonary disease; (2) small quantities of ODSs for laboratory tests and other procedures; as well as (3) methyl bromide that is essential for certain agricultural processes (e.g. quarantine and pre-shipment applications to prevent the spread of plant pests that may have huge economic and/ or environmental consequences). On the other hand, Class II substances are ODSs that have less ozone depletion potentials of less than 0.2. These include all HCFCs, which are the transitional substitutes for their Class I counterparts.

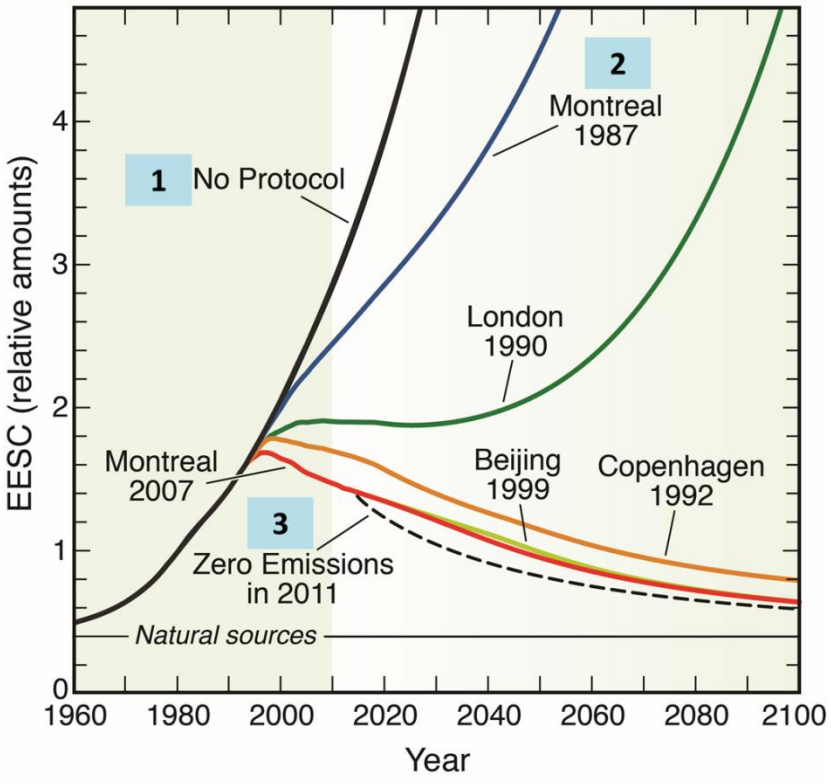

Figure 1.2: *Effects of Montreal Protocol and its amendments on long-term changes in terms of equivalent effective stratospheric chlorine (EESC). EESC refers to the sum of chlorine and bromine which is derived from ODS tropospheric abundances. It acts as a relative measure of the stratospheric ozone depletion potential. Projections of the future abundances of mid-latitude stratospheric ODSs have been made for the following cases: (1) no Protocol provisions, (2) provisions of the original 1987 Montreal Protocol, and (3) zero emissions of ODSs starting from 2014. The city names and years indicate the sites and times at which changes in the original Protocol's provisions were agreed upon (Hegglin et al., 2014).*

Enforcements of the 1989 Montreal Protocol and its subsequent amendments have resulted in the successful phasing-out of the production and consumption of CFCs (apart from relatively minor critical-use exemptions) by industrialised and developing nations in 2010. As a result, the atmospheric abundances of most documented CFCs started to decline (Montzka et al., 1996, Rigby et al., 2013, Carpenter et al., 2014, Laube et al., 2014, UNEP, 2014). Additionally, the Montreal Protocol and national regulations have given rise to significant reductions in the productions, usage, emissions, and observed atmospheric concentrations of CFC-11, CFC113, methyl chloroform, as well as several other ODSs. There is also evidence of the recovery of the stratospheric ozone as well (Velders et al., 2007) .

1.5 Emerging challenges in stratospheric ozone recovery

The balance between the emissions and removal of a substance determines the changes in its global atmospheric abundance. Following the implementation of the 1987 Montreal Protocol, the emissions of the majority of ODSs became significantly lower than their removal. This explained the decline in their atmospheric abundances. As a result, the reduction of stratospheric ozone was halted in the late 1990s, and the ozone levels in most parts of the stratosphere have remained roughly constant since 2000 or so (Carpenter et al., 2014). At present, the long-term recovery of the ozone layer from the effects of ODSs is still on track. However, significant uncertainties in the predictions of ozone and climate patterns still exist. These can be explained by the following three main categories of scientific evidences:

1.5.1 Newly-detected emissions of Montreal Protocol ODSs

The first challenge is the discovery of new emissions of Montreal Protocol ODSs; the major cause for concern is the unexpected increase in the atmospheric levels of certain CFCs. Hitherto this, enforcements and subsequent amendments of the Montreal Protocol have resulted in the successful phasing-out of CFC productions and consumptions in industrialised as well as developing nations by 2010. Therefore, the recent increase in the atmospheric abundance of CFCs has not been anticipated (Montzka et al., 2018). Recent study has found a persistent increase in the global emissions of ozone-depleting CFC-11 – one of the most abundant CFCs other than CFC-12 and -113 (Montzka et al., 1996). Back-trajectory analyses have revealed higher mole fractions of the chemical owing to their production at eastern Asia. It has been suggested that a possible pathway of inadvertent CFC-11 production was the fluorination of chlorinated methane to produce HCFC-22, although the amount of emission was small. Importantly, this work has highlighted that the increase in CFC-11 emission originated from new productions that were (1) inconsistent with the agreed phasing-out of CFC production as per the Montreal Protocol, as well as (2) have not been reported to the UNEP's Ozone Secretariat. Evidently, CFCs other than CFC-11 have also been detected in the atmosphere, an example of which was the discovery of four previously-undetected ODSs – CFC-112 ($CFCl_2CFCl_2$), CFC-112a (CF_2ClCCl_3), CFC-113a (CF_3CCl_3), and HCFC-133a (CF_3CH_2Cl) – in the atmosphere (Laube et al., 2014). Even though these compounds are regulated under the Montreal Protocol, two of them (i.e CFC-113a and HCFC-133a) suprisingly continued to accumulate in the atmosphere. While the abundances of these gases were low (i.e. mole fractions of less than 1 part per trillion (ppt) in 2010), the facts that these four gases were still present in the atmosphere, and that two of them were increasing in level, indicated the likely presence of limitations in the protocol, which subsequently raised questions over the sources of these gases. Following the work of Laube et al. (2004), atmospheric measurements of CFC-113a from ground-based stations in Australia, Taiwan, Malaysia, and the United Kingdom have been conducted in an attempt to investigate the sources of the said chemicals (Adcock et al., 2018). As per the evidences, the emission of CFC-113a was most likely attributable to its utilisation as a chemical in the production of hydrofluorocarbons.

While the sources of CFC-113a remained unclear, it has been found that significant emissions of the same were taking place in East Asia.

1.5.2 Unexpected emissions of Non-Montreal Protocol ODSs

The second possible factor of the uncertainty of the ozone layer's long-term recovery is the unexpected emissions of Non-Montreal Protocol ODSs. Although it is well-established that halogens from Montreal Protocol ODSs are the main contributors to the stratospheric halogen loading, recent observations have shown that increasing emissions of VSLSs are also an important source of stratospheric halogens. Historically, VSLSs were not considered as ozone-damaging because they had relatively short atmospheric lifetimes and were not expected to reach the stratosphere in sufficient quantities to damage the ozone layer. Hence, they were excluded from the Montreal Protocol. However, the atmospheric abundance of one of these VSLSs – dichloromethane (CH_2Cl_2) – is growing rapidly, and its continuous increase in concentration poses a potential threat to the ozone layer. CH_2Cl_2 is mainly anthropogenic in origin; its uses range from paint-stripping to agricultural fumigation and pharmaceutical production. The atmospheric concentration of this substance decreased in the 1990s and early 2000s, but over the past decade, dichloromethane has become approximately 60% more abundant (Carpenter et al., 2014, Hossaini et al., 2015, Leedham et al., 2015). The relative contributions of these emissions could become important as the levels of Montreal Protocol-controlled ODSs decline (Carpenter et al., 2014). According to Hossaini et al. (2017), the factor that drives the growth of dichloromethane is still uncertain. However, it could be due to the fact that CH_2Cl_2 is used in the manufacturing of some HFCs – the "ozone-friendly" gases which have been developed to replace CFCs. This ironically means that the production of ozone-friendly chemicals actually releases some ozone-destroying gases into the atmosphere.

On another note, the amounts of VSLSs's halogens that reach the stratosphere primarily depend on the location of their emissions (Chipperfield, 2006). This highlights the importance of the site of emission because the closer the source of emission to the regions where convective activities and vertical uplifts are most intense (i.e. the tropics), the higher the chances of the VSLSs to be transported to the

stratosphere (Navarro et al. (2015). Studies have provided evidences that East Asia – a region that is undergoing rapid industrialisation, has a substantial influence on the growth of anthropogenic VSLSs emissions. Evidently, 80% of all East Asian halocarbon emissions were identified to originate from China (Li et al., 2011). Emissions of pollutants, including ozone-depleting chemicals, in places like China are especially damaging because the cold-air surges in this region can rapidly carry significant quantities of industrial pollutants to the tropics (Ashfold et al., 2015, Oram et al., 2017). Recent measurements of Cl-VSLSs in Taiwan and Malaysia, as well as aircrafts flying above South East Asia, have revealed that (1) there were substantial regional emissions of these compounds; (2) these emissions could be rapidly transported over long distances into the deep tropics; as well as (3) an equally rapid vertical transport of the said substance to the upper tropical troposphere was a regular occurrence (Oram et al., 2017). The findings further emphasised that the increasing emissions of chlorinated VSLSs from East Asia, in conjuction with the transportation of chlorinated VSLSs to tropical regions of the western Pacific, could potentially slow down the recovery of stratospheric ozone. However, in view of the fact that most of the reported measurements have not been made in these two key regions (where the strongest troposphere-to-stratosphere transport occurred), there have been limitations in the abovementioned assessments.

1.5.3 Relative influence of naturally-emitted halocarbons

Most of the ODSs that contribute to the stratospheric halogens are produced by industries. Following the implementations of the Montreal Protocol and its amendments, the absence of production will cause the emissions of anthropogenic ODSs and hence, atmospheric concentrations of the same to dwindle (Montzka et al., 2018). As a result, there is less ozone damage. However, this causes the relative importance of naturally-produced halocarbons to increase, making them an increasingly important factor of future ozone and climactic chemistries. As stated in Section 1.2, methyl chloride (CH_3Cl) and methyl bromide (CH_3Br) are the main natural sources of stratospheric chlorine and bromine respectively. The atmospheric abundance of CH_3Cl currently accounts for around 17% of

tropospheric chlorine. On the other hand, atmospheric CH_3Br has recently accounted for up to 50% of tropospheric bromine (Carpenter et al., 2014). It is estimated that the contributions of natural CH_3Cl and CH_3Br to the equivalent effective stratospheric chlorine will exceed 50% by 2050 (WMO, 2007), thus highlighting the significant role of naturally-produced halogenated substances in the future stratospheric halogen loading. Previous researches (e.g. Yokouchi et al. (2000), Yokouchi et al. (2002), Lee-Taylor et al. (2005), Blei et al. (2010) have identified tropical terrestrial sources of CH_3Cl and CH_3Br (apart from the oceans and biomass-burning). However, the sparseness of these methyl halide measurements have resulted in huge uncertainties over the nature and strength of the tropical sources (Gebhardt et al., 2008). With regards to the global CH_3Br budget, the sinks seem to outweigh the sources, hence pointing to an underestimated or still-unknown source of the same (Gebhardt et al., 2008). The said imbalance also may be due to an underestimation of the atmospheric lifetime of CH_3Br as well (Reeves, 2003).

1.6 Problem statement

Uncertainties over the long-term recovery of the ozone layer still exist because some halogenated substances are still being emitted from exempted-use items, existing equipment, natural processes, unreported activities, or new technologies. Recent and significant evidences of the increasing emissions of both Montreal and Non-Montreal Protocol ODSs (Section 1.5) have highlighted the presence of an emerging threat by halogenated substances to the stratospheric ozone.

For Montreal Protocol ODSs like CFCs, the fact that their emissions are yet to hit zero until now stresses the importance of monitoring their atmospheric abundances and understanding the exact origins of these emissions. Doing so will ensure compliance with the Montreal Protocol for the environmental protection against ozone loss. Similarly, the recent increase in VSLSs emissions (e.g. dichloromethane) suggests a need to investigate the origins of these compounds. Evidently, the lack of global VSLS control measures leads to their significant impact on the atmosphere. This will consequently offset some of the gains achieved by the Montreal Protocol and further

delay the recovery of Earth's ozone layer. Natural emissions of methyl halides, particularly those in tropical regions, are also an emerging problem with regards to stratospheric ozone. The relative contributions of these emissions may become important as the levels of Montreal Protocol-controlled ODSs decline. Further evidences have also suggested that there are high levels of emissions in East Asia, and that these can be rapidly transported to Southeast Asia. However, assessments of the same are currently limited owing to lack of observational data. This has limited the ability to figure out the sites at which there is an increase in VSLSs emission, and whether they can have substantial effects on the ozone layer.

Overall, a delay in the recovery of the ozone layer is anticipated, depending on the volumes of emissions and atmospheric concentrations of ODSs in the future. Hence, there is a need for further regional and global studies on the origins of the halogenated gases. These data will provide more descriptions of the halogenated compounds, including an analysis of its factors and causes (e.g. sources of emission, meteorological processes), apart from providing some guidance for the implementation of control measures.

1.7 Aims and structure of thesis

This thesis concerns the tropospheric abundances, emissions, and transportation of halogenated substances on regional and global scales, with focus on very short-lived gases (chlorinated VSLS), short-lived gases (methyl halides), and long-lived gases (CFC-114 and -114a). Overall, the main reason of studying these compounds was their importance in stratospheric chemistry and lack of information on their exact origins.

This thesis was aimed to conduct a modelling study by using various observational datasets to constrain two different numerical models i.e. the 3-D dispersion model and 2-D global model. It is important to note that all observational datasets used were not generated by myself but kindly provided by others; I was involved in neither sample collection nor chemical analysis.

The overall structure of this thesis is as follows:

Chapter 2: Methodology

This section describes the methods that were used to conduct the study. It includes descriptions of different types of modelling systems and various sources of observational data that were used to constrain the model.

Chapter 3: Chlorinated VSLSs in East Asia and Southeast Asia

This chapter described the assessments of the abundances of four chlorinated VSLSs in East Asia and Southeast Asia. The findings from the sampling stations in Taiwan and Bachok, Malaysia are presented. The specific aims of this chapter are as follows:

1. To assess the variability of chlorinated VSLSs at both sampling locations and identify the presence of above-background levels of the chlorinated VSLSs.

2. To investigate the potential source regions and emission sectors that could contribute to the variation of chlorinated VSLSs.

3. To examine the influence of meteorological features in the long-range transportation of chlorinated VSLSs to Bachok.

Chapter 4: Methyl halides in East Asia and Southeast Asia

This chapter is similar to the part of the study in Chapter 3, except that the focus is on the methyl halides which were measured in Taiwan and Bachok. The specific aims of this chapter are as described below:

1. To assess the variability of methyl halides at both sampling locations and identify the presence of above-background levels of the methyl halides.

2. To investigate the potential source regions and emission sectors that could contribute to the variation of methyl halides.

Chapter 5: Long-term trends and emissions of CFC-114 and CFC-114a

This chapter presents the first long-term measurement of CFC-114 and CFC-114a separately. Also presented are their emission estimates that were derived from an air measurement dataset from campaigns in Cape Grim and the Antarctic to constrain the 2D atmospheric chemistry transport model. The specific aims of this chapter are as follows:

1. To derive the "top-down" emissions and compare the same against the industries' "bottom-up" estimates in order to verify the reports of CFC-114 and CFC-114a usage by the industries.

2. To identify potential sources of CFC-114 and CFC-114a emissions based on the data from Taiwan.

Chapter 6: Conclusions

This section summarises the key research findings and outlines future research directions.

1.8 References

Adcock, K. E., Reeves, C. E., Gooch, L. J., Leedham Elvidge, E. C., Ashfold, M. J., Brenninkmeijer, C. A., Chou, C., Fraser, P. J., Langenfelds, R. L. and Mohd Hanif, N.: Continued increase of CFC-113a mixing ratios in the global atmosphere: emissions, occurrence and potential sources, Atmospheric Chemistry and Physics, 18, 7, 4737-4751, 2018.

Aschmann, J., Sinnhuber, B. M., Atlas, E. L. and Schauffler, S. M.: Modeling the transport of very short-lived substances into the tropical upper troposphere and lower stratosphere, Atmospheric Chemistry and Physics, 9, 23, 9237-9247, 10.5194/acp-9-9237-2009, 2009.

Ashfold, M. J., Pyle, J. A., Robinson, A. D., Meneguz, E., Nadzir, M. S. M., Phang, S. M., Samah, A. A., Ong, S., Ung, H. E., Peng, L. K., Yong, S. E. and Harris, N. R. P.: Rapid transport of East Asian pollution to the deep tropics, Atmospheric Chemistry and Physics, 15, 6, 3565-3573, 10.5194/acp-15-3565-2015, 2015.

Baker, A. K., Sauvage, C., Thorenz, U. R., Van Velthoven, P., Oram, D. E., Zahn, A., Brenninkmeijer, C. A. M. and Williams, J.: Evidence for strong, widespread chlorine radical chemistry associated with pollution outflow from continental Asia, Scientific Reports, 6, 10.1038/srep36821, 2016.

Blei, E., Hardacre, C. J., Mills, G. P., Heal, K. V. and Heal, M. R.: Identification and quantification of methyl halide sources in a lowland tropical rainforest, Atmospheric Environment, 44, 8, 1005-1010, http://www.sciencedirect.com/science/article/pii/S1352310090105772010.

Carpenter, L. J., Reimann, S., Burkholder, J. B., Clerbaux, C., Hall, B. D., Hossaini, R., Laube, J. C. and Yvon-Lewis, S. A. Ozone-Depleting Substances (ODSs) and Other Gases of Interest to the Montreal Protocol, Chapter 1 in Scientific Assessment of Ozone Depletion: 2014, Global Ozone Research and Monitoring Project – Report No. 55. Geneva, Switzerland, World Meteorological Organization.2014

Chapman, S.: A theory of upper-atmospheric ozone, Memoirs of the Royal Meteorological Society, 3, 26, 103–125, 1930.

Chipperfield, M. P., et al. . Global ozone: Past and present, in Scientific Assessment of Ozone Depletion: 2006 Global Ozone Res. and Monit. Proj., Rep.**:** 3.1 – 3.57.2006

Derwent, R., Simmonds, P., O'doherty, S. and Ryall, D.: The impact of the Montreal Protocol on halocarbon concentrations in Northern Hemisphere baseline and European air masses at Mace Head, Ireland over a ten year period from 1987–1996, Atmospheric Environment, 32, 21, 3689-3702, 1998.

Farman, J. C., Gardiner, B. G. and Shanklin, J. D.: Large losses of total ozone in Antarctica reveal seasonal ClOx/NOx interaction, Nature, 315, 6016, 207-210, 10.1038/315207a0, 1985.

Fueglistaler, S., Dessler, A. E., Dunkerton, T. J., Folkins, I., Fu, Q. and Mote, P. W.: Tropical tropopause layer, Reviews of Geophysics, 47, 1, 10.1029/2008RG000267, 2009.

Gebhardt, S., Colomb, A., Hofmann, R., Williams, J. and Lelieveld, J.: Halogenated organic species over the tropical South American rainforest, Atmospheric Chemistry and Physics, 8, 12, 3185-3197, 2008.

Gettelman, A., Lauritzen, P. H., Park, M. and Kay, J. E.: Processes regulating short-lived species in the tropical tropopause layer, Journal of Geophysical Research: Atmospheres, 114, D13, doi:10.1029/2009JD011785, 2009.

Hegglin, M. I., Fahey, D. W., McFarland, M., Montzka, S. A. and Nash, E. R. Twenty Questions and Answers About the Ozone Layer: 2014 Update, Scientific Assessment of Ozone Depletion, World Meteorological Organization, Geneva, Switzerland, 2015**:** 84 pp.2014

Hossaini, R., Chipperfield, M. P., Montzka, S. A., Leeson, A. A., Dhomse, S. S. and Pyle, J. A.: The increasing threat to stratospheric ozone from dichloromethane, Nature Communications, 8, 15962, 10.1038/ncomms15962, 2017.

Hossaini, R., Chipperfield, M. P., Montzka, S. A., Rap, A., Dhomse, S. and Feng, W.: Efficiency of short-lived halogens at influencing climate through depletion of stratospheric ozone, Nature Geoscience, 8, 3, 186-190, 10.1038/ngeo2363, 2015.

Kim, J., Li, S., Kim, K. R., Stohl, A., Mühle, J., Kim, S. K., Park, M. K., Kang, D. J., Lee, G. and Harth, C. M.: Regional atmospheric emissions determined from measurements at Jeju Island, Korea: Halogenated compounds from China, Geophysical Research Letters, 37, 12, 2010.

Laube, J. C., Newland, M. J., Hogan, C., Brenninkmeijer, C. A. M., Fraser, P. J., Martinerie, P., Oram, D. E., Reeves, C. E., Röckmann, T., Schwander, J., Witrant, E. and Sturges, W. T.: Newly detected ozone-depleting substances in the atmosphere, Nature Geoscience, 7, 4, 266-269, 10.1038/ngeo2109, 2014.

Lee-Taylor, J. and Redeker, K.: Reevaluation of global emissions from rice paddies of methyl iodide and other species, Geophysical Research Letters, 32, 15, 2005.

Leedham, E. C., Oram, D. E., Laube, J. C., Baker, A. K., Montzka, S. A., Humphrey, S., O'Sullivan, D. A. and Brenninkmeijer, C. A. M.: Increasing concentrations of dichloromethane, inferred from CARIBIC air samples collected 1998-2012, Atmospheric Chemistry and Physics, 15, 4, 1939-1958, 10.5194/acp-15-1939-2015, 2015.

Li, S., Kim, J., Kim, K.-R., Mühle, J., Kim, S.-K., Park, M.-K., Stohl, A., Kang, D.-J., Arnold, T. and Harth, C. M.: Emissions of halogenated compounds in East Asia determined from measurements at Jeju Island, Korea, Environmental Science & Technology, 45, 13, 5668-5675, 2011.

Midgley, P. M. and McCulloch, A. Properties and applications of industrial halocarbons. Reactive Halogen Compounds in the Atmosphere, Springer**:** 129-153. 1999

Molina, M. J. and Rowland, F. S.: Stratospheric sink for chlorofluoromethanes: chlorine atom-catalysed destruction of ozone, Nature, 249, 5460, 810, 1974.

Montzka, S. A., Butler, J. H., Myers, R. C., Thompson, T. M., Swanson, T. H., Clarke, A. D., Lock, L. T. and Elkins, J. W.: Decline in the tropospheric abundance of halogen from halocarbons: Implications for stratospheric ozone depletion, Science, 272, 5266, 1318-1322, 1996.

Montzka, S. A., Dutton, G. S., Yu, P., Ray, E., Portmann, R. W., Daniel, J. S., Kuijpers, L., Hall, B. D., Mondeel, D., Siso, C., Nance, J. D., Rigby, M., Manning, A. J., Hu, L., Moore, F., Miller, B. R. and Elkins, J. W.: An unexpected and persistent increase in global emissions of ozone-depleting CFC-11, Nature, 557, 7705, 413-417, 10.1038/s41586-018-0106-2, 2018.

Navarro, M. A., Atlas, E. L., Saiz-Lopez, A., Rodriguez-Lloveras, X., Kinnison, D. E., Lamarque, J. F., Tilmes, S., Filus, M., Harris, N. R. P., Meneguz, E., Ashfold, M. J., Manning, A. J., Cuevas, C. A., Schauffler, S. M. and Donets, V.: Airborne measurements of organic bromine compounds in the Pacific tropical tropopause layer, Proceedings of the National Academy of Sciences of the United States of America, 112, 45, 13789-13793, 10.1073/pnas.1511463112/-/DCSupplemental, 2015.

Oram, D. E., Ashfold, M. J., Laube, J. C., Gooch, L. J., Humphrey, S., Sturges, W. T., Leedham-Elvidge, E., Forster, G. L., Harris, N. R. P., Mead, M. I., Abu Samah, A., Phang, S. M., Chang-Feng, O. Y., Lin, N. H., Wang, J. L., Baker, A. K., Brenninkmeijer, C. A. M. and Sherry, D.: A growing threat to the ozone layer from short-lived anthropogenic chlorocarbons, Atmospheric Chemistry and Physics, 7, 19, 11929-11941, 2017.

Reeves, C. E.: Atmospheric budget implications of the temporal and spatial trends in methyl bromide concentration, Journal of Geophysical Research: Atmospheres, 108, D11, 2003.

Rigby, M., Prinn, R. G., O'Doherty, S., Montzka, S. A., McCulloch, A., Harth, C. M., Mühle, J., Salameh, P. K., Weiss, R. F., Young, D., Simmonds, P. G., Hall, B. D., Dutton, G. S., Nance, D., Mondeel, D. J., Elkins, J. W., Krummel, P. B., Steele, L. P. and Fraser, P. J.: Re-evaluation of the lifetimes of the major CFCs and CH_3CCl_3 using atmospheric trends, Atmospheric Chemistry and Physics, 13, 5, 2691-2702, 10.5194/acp-13-2691-2013, 2013.

Tsai, W.-T.: A review of environmental hazards and adsorption recovery of cleaning solvent hydrochlorofluorocarbons (HCFCs), Journal of loss prevention in the process industries, 15, 2, 147-157, 2002.

UNEP (2014, last access: 27 May 2016). "Status of Ratification, List of Parties Categorised as Operating under Article 5 Paragraph 1 of the Montreal Protocol."

UNEP (2018). "https://www.epa.gov/ozone-layer-protection/international-actions-montreal-protocol-substances-deplete-ozone-layer." Retrieved last accessed on 9 September 2018.

Velders, G. J., Andersen, S. O., Daniel, J. S., Fahey, D. W. and McFarland, M.: The importance of the Montreal Protocol in protecting climate, Proceedings of the National Academy of Sciences, 104, 12, 4814-4819, 2007.

Wallace, J. M. and Hobbs, P. V. Atmospheric science: an introductory survey, Elsevier. 2006

WMO. Scientific Assessment of Ozone Depletion: 2006, Chapter 8: Halocarbon Scenarios, ODPs ans GWPs, Global Ozone Research and Monitoring Project - Report No. 50. Geneva, Switzerland, World Meteorological Organization**:** 8.1–8.39.2007

Yokouchi, Y., Ikeda, M., Inuzuka, Y. and Yukawa, T.: Strong emission of methyl chloride from tropical plants, Nature, 416, 6877, 163, 2002.

Yokouchi, Y., Noijiri, Y., Barrie, L. A., Toom-Sauntry, D., Machida, T., Inuzuka, Y., Akimoto, H., Li, H. J., Fujinuma, Y. and Aoki, S.: A strong source of methyl chloride to the atmosphere from tropical coastal land, Nature, 403, 295, 10.1038/35002049, 2000.

Chapter 2

Methodology

2.1 Introduction

The primary aim of this thesis was to use two different numerical models to study (a) the regional emissions of short and very short-lived halogenated gases and (b) the global emissions of long-lived halogenated gases. Depending on the specific questions which both studies attempt to answer, two different types of modelling systems and various sources of observational data to constrain the model have been utilised. The overview of the methodology used to study both groups of gases is depicted in Figure 2.1.

For study of short and very short-lived gases, the study required the usage of two observational datasets generated from the ground-based campaigns in East Asia and South East Asia, regions where emissions of greenhouse and ozone-depleting substances are rapidly increasing. The study then used the 3-D dispersion model to determine the impact of different source types and regions. In contrast, the study of long lived-gases used four sources of measurement data. The air samples collected from Cape Grim, Tasmania and extracted from deep firn snow in the Antarctic are used to serve as the long-term atmospheric measurement dataset. The combined dataset is then used to constrain the 2-D global model for deriving the emission estimates of CFC-114 and CFC-114a. Additionally, to put the study of long-lived gases into a wider context and to obtain further insight on the derived emission estimates, this study also used upper tropospheric samples collected using a commercial aircraft from the CARIBIC project and also air samples collected during ground-based campaigns in East Asia.

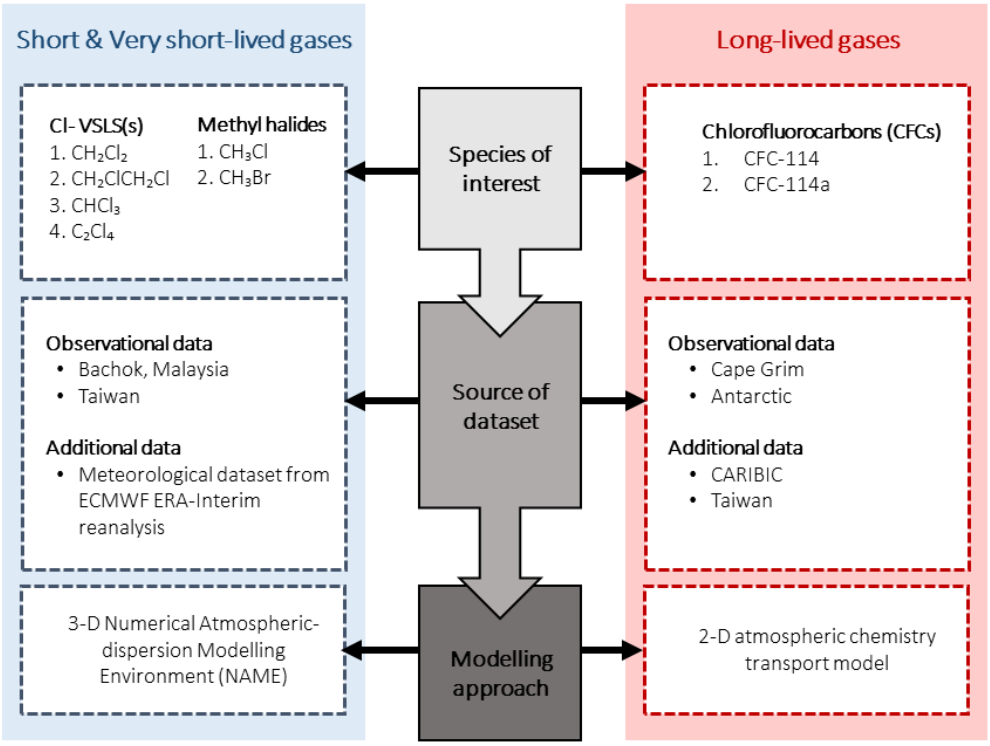

Figure 2.1*: Overview of the methodology to study the atmospheric budget of short and very short-lived gases (in blue) and long-lived gases (in red). The fundamental components that shape the methodology of this study have been identified and were split into three categories (in shades of grey). For the source of dataset, the observational dataset generated from air sampling campaigns were essential to evaluate and constrain the model simulations, whilst the additional datasets were used to support and facilitate the interpretation of the model output. Not shown in this diagram is the input data to run the models. The input data will be introduced in the section on atmospheric modelling.*

It is important to note that all observational datasets used were not generated by myself but kindly provided by others. My contribution is predominantly conducting the modelling study by using the observational datasets to constrain the 3-D dispersion model and 2-D global model. As such, the detection, quantification and measurement techniques, will not be discussed in detail in this chapter. More information can be found in Oram et al. (2017) and Laube et al. (2016). Also, this work used a model that was readily available and widely-used. As the focus is mainly on the use of the models rather than model development, it is not the intention here

to describe in detail the development of the models. Instead, important features of the model, the model setup and the methods used to specifically study the compounds of interest are described in this chapter.

Therefore, in this chapter, I have focussed on what I consider to be the most important aspects to conduct the study. In the first section of this chapter, the descriptions of all the source of data used in this thesis were outlined. This includes a brief description of the campaigns (Section 2.2), air samples collection and analysis methods (Section 2.3). The chapter then continues with the detailed description of the modelling approaches (Section 2.4). Finally, a summary of this chapter is presented in Section 2.5.

2.2 Sampling locations

The sampling locations and the general description of the sources of observational datasets used in this study are presented in Figure 2.2 and Table 2.1, respectively. The details on each dataset are describe in Sections 2.2.1 to 2.2.5.

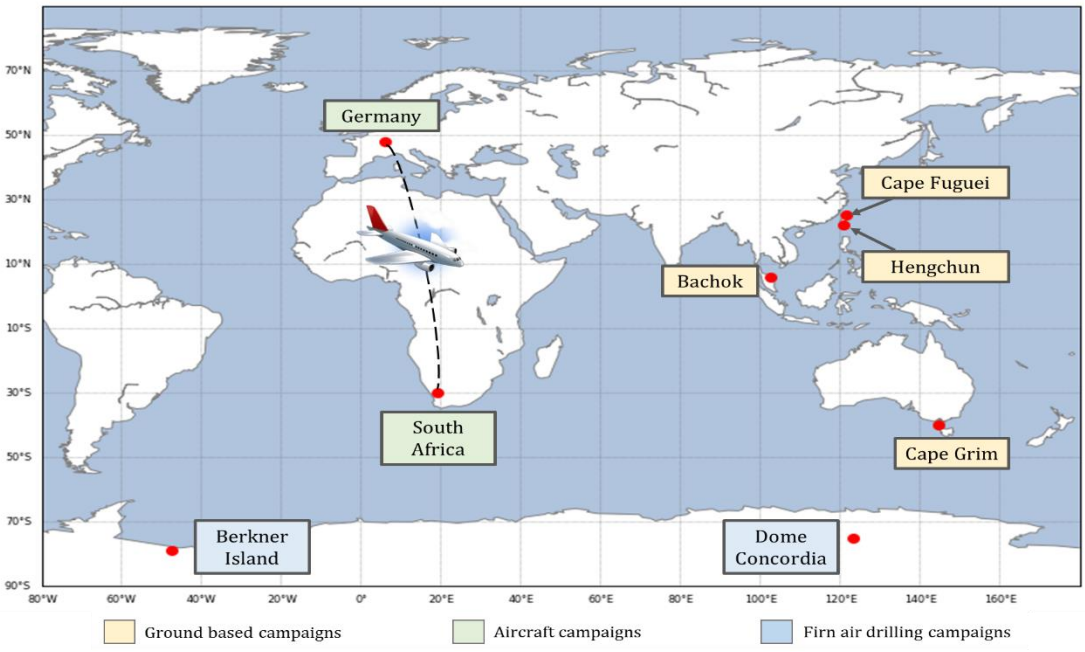

***Figure 2.2**: Map showing the location of sampling stations.*

Table 2.1: *Summary of air sampling campaigns for measuring the short, very short-lived and long lived halogenated gases in this study*

Sampling campaign	Location	Longitude and latitude	Period of sampling	Number of samples	Nature of data
Taiwan	East Asia	Hengchun, 22.0547° N, 120.6995° E, (2013, 2015) Cape Fuguei, 25.297° N, 121.538° E, (2014, 2016)	7 Mar – 5 Apr 2013 11 Mar – 4 Apr 2014 12 Mar – 25 Apr 2015 16 Mar – 29 Apr 2016	2013: 19 2014: 23 2015: 23 2016: 33	Northern Hemisphere ground-based sites
Bachok Marine Research Station	Malaysia, South East Asia	6.009° N, 102.425° E	20 Jan – 5 Feb 2014 19 Nov – 31 Dec 2015 4 – 27 Jan 2016	2014: 28 2015: 23 2016: 17	Tropical ground based site
Cape Grim Baseline Air Pollution Station	Tasmania, Australia	40.41°S, 144.41°E	1978 to 2014	37	Southern Hemisphere ground-based site
Antarctic drilling campaigns	South Pole	Berkner Island 79.04° S, 47.59° W Dome C 75.10° S, 123.35° E	January 2003 January 1999	39	Firn air surface data
CARIBIC Observatory campaign	Germany to South Africa	48 °N-30 °S, 6-19 °E	10 and 11 Feb 2015	15	Commercial aircraft

2.2.1 Taiwan

The atmospheric sampling in Taiwan was carried out in collaboration with the National Central University (NCU) of Taiwan. The aim was to identify compounds emitted from across the East Asian region as well as to establish potential source areas.

There were two sampling stations: Cape Fuguei located on the north-west coast and the Hengchun on the south-west coast (Figure 2.2). In 2013 and 2015, samples were collected in the Hengchun and in 2014 and 2016 samples were collected at Cape Fuguei.

Both sampling stations offers an ideal location to study the Asian outflow. During the springtime, Taiwan experiences winter monsoon wind patterns that are typically predominant over East Asia. These coincide with strong continental outflows of pollution, particularly from mainland China, Korea and Japan (Ou-Yang

et al., 2012). Hence, air masses that pass over the sampling sites in Taiwan should give a good representation of outflow from these areas and are likely to contain halocarbon species emitted from these regions (Gooch, 2016).

2.2.2 Bachok, Malaysia

The measurements of greenhouse gases, ozone depleting substances, and other chemical pollutants were conducted at the atmospheric observation tower built at the Bachok Marine Research Station. The station is situated in the Kelantan province which is located on the east coast of peninsular Malaysia, within 100 m of the water's edge of the South China Sea (Figure 2.2). The station was constructed as part of the Institute of Ocean and Earth Sciences (IOES) at the University of Malaya (UM). The station is extremely well located for studies on the outflow of the rapidly developing Southeast Asian countries.

The Bachok campaigns provided an opportunity to study a number of the tropical processes related to atmospheric chemistry. The aim was to measure a large range of atmospheric trace gases and to conduct meteorological observations from the atmospheric observation tower at the station. The campaign was conducted during the East Asian Winter Monsoon, which provides an opportunity to assess the long-range transport of ozone depleting substances (ODS) during the cold surge event and to explore the influence of weather systems i.e. cold surges towards the variability of chemical composition measured at Bachok.

2.2.3 Cape Grim, Tasmania

Cape Grim is situated in Tasmania, Australia and ideally placed to monitors very clean air which is representative of the mid-latitudes of the Southern Hemisphere. Cape Grim is located in an area with low levels of local industry/pollution and distanced from other land masses. Therefore, the air masses arriving from the south-west over the Southern Ocean can represent some of the cleanest air in the world. Background or baseline atmospheric conditions are classified as being when the wind is from the south-westerly sector and wind speeds are > 15 km h^{-1} (Fraser

et al., 1999). The air sampling was only conducted during baseline atmospheric conditions in order to be representative of background conditions rather than sampling air coming from the landmasses of mainland Australia or Tasmania.

Baseline air samples have been collected approximately three months since 1978 until present and stored at high pressure to form the Cape Grim Air Archive. The Cape Grim Air Archive has underpinned many studies on global emissions of greenhouse and ozone depleting gases, including this study. Cape Grim data have been used extensively in all international assessments of climate change and ozone depletion and in many studies deriving global and regional emissions of carbon dioxide (CO_2), chlorofluorocarbons (CFCs), methane (CH_4), nitrous oxide (N_2O) and synthetic greenhouse gases (SGGs).

2.2.4 Antarctic

In addition to using Cape Grim archive (1978 -2014), it is also possible to derive information about past atmospheric concentrations of gases from air trapped in polar firn. Firn air is air trapped in the open pores of the compacted snow (firn) before it is trapped in ice bubbles. It has been collected and analysed to determine a record of trace gases in the Northern and Southern hemispheres from the early-mid 20th century to the present day.

The air within the firn is still effectively connected to the atmosphere and can mix with other air within the firn via diffusion. Consequently, a smoothed record of atmospheric changes are created and therefore the air at any given depth a is representative of a range of ages (Butler et al., 1999). The main advantage of firn air compared to that trapped within bubbles in ice cores is that a much larger quantities of air can be obtained. Thus, making this method very suited for studying trace gases which are present in too low concentrations to be detected in the small quantities of air extracted from ice cores (Newland, 2013).

In this study, air samples were extracted from deep firn snow during two Antarctic drilling campaigns (Berkner Island and Dome C, see Figure 2.2). The campaigns were conducted as part of the European Union-funded CRYOSTAT project (Cryospheric Studies of Atmospheric Trends in Stratospherically and Radiatively

important gases, http://artefacts.ceda.ac.uk/badc_datadocs/cryostat/). The aim of CRYOSTAT was to undertake the first combined measurements of virtually all significant greenhouse gases (GHGs), ozone-depleting substances (ODSs), and related trace gases in contiguous firn and ice profiles, spanning as much as 200 years, from both the northern and southern polar ice caps.

2.2.5 CARIBIC aircraft measurements

CARIBIC is the acronym for Civil Aircraft for Regular Investigation of the Atmosphere Based on an Instrument Container (CARIBIC project, www.caribic-atmospheric.com). It is an aircraft based scientific project that aims to study and monitor important chemical and physical processes in the upper troposphere and lowermost stratosphere whilst the aircraft travels regularly all over the world. The project utilises a passenger aircraft (Airbus A340-600, operated by Lufthansa) by deploying a container containing equipment for in situ measurements of many types of gases including ozone depleting substances and greenhouse gases.

The air samples used here were collected at regular intervals at altitudes of 10-12 km on a flight between Frankfurt, Germany and Johannesburg, South Africa (Figure 2.2). The samples provide an opportunity to assess recent interhemispheric mixing ratio gradients and their consistency with the inferred tropospheric records of long-lived gases.

2.3 Sample collection and analysis

2.3.1 Sample collection

Air samples from all the surface-based sampling sited were collected in electropolished and/or silco-treated stainless steel gas canisters except for those from CARIBIC. During CARIBIC, aircraft samples are collected in glass flasks using a pumping system. More details on the CARIBIC sampling system can be found in Brenninkmeijer et al. (2007).

For the Antarctic drilling campaigns, the air was pumped directly into stainless steel flasks from the firn using a firn air sampling device. The firn air extraction procedure is described in Martinerie et al. (2009).

2.3.2 Sample analysis

The collected air samples were shipped to University of East Anglia (UEA) where they were analysed for their halocarbon content using gas chromatography–mass spectrometry (GC-MS). A full description of this analytical technique can be found in Oram et al. (2017) and Laube et al. (2016).

For firn air samples, it is important to highlight that the firn air samples provide concentration depth profiles of trace gases. To convert the concentration depth profiles into atmospheric trends of trace gases a combination of firn diffusion modelling (i.e. how much a gas can diffuse at a given depth in the firn) and atmospheric modelling is used (Figure 2.3) . The firn modelling was done by Patricia Martinerie and detailed descriptions on the firn modelling can be found in Martinerie et al. (2009).

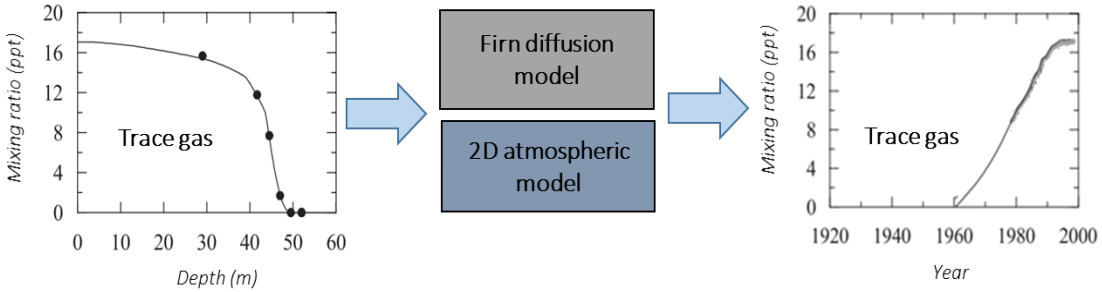

Figure 2.3: Left panel: *Observations (filled circles) and modelled depth profile (solid line) for the trace gases of interest.* ***Central panel:*** *Firn diffusion modelling was combined with 2-D atmospheric chemical models to determine the trends of the trace gases of interest.* ***Right panel:*** *Atmospheric record of trace gases of interest (black line).*

Source : Adapted from Sturrock et al. (2002) and Martinerie et al. (2009)

2.4 Atmospheric chemistry models

The concentrations of chemical species in the atmosphere are affected by four general types of processes i.e. emissions, transport, chemistry and deposition. Using numerical tools called chemical transport models (CTMs), the four processes can be represented and simulated to describe the spatial and temporal variability of chemical species in the atmosphere. The simulations are done by solving the continuity equations for mass conservation of the species in the atmosphere (Brasseur et al., 2017).

This study used two types of models i.e. 3-D Numerical Atmospheric-dispersion Modelling Environment (NAME) and the 2-D global model (Figure 2.1). This section is aimed to introduce both models, starting with the 3-D model (Section 2.4.1) and followed by the 2-D global model (Section 2.4.2). Each section provides the overview of the models, general features and the model setup and simulations specifically to study short, very short-lived gases and long-lived gases.

2.4.1 Introduction to 3-D Numerical Atmospheric-dispersion Modelling Environment (NAME)

2.4.1.1 Model description

2.4.1.1.1 Overview

The 3-D Numerical Atmospheric-dispersion Modelling Environment (NAME) is a model developed by the UK Meteorology Office. NAME was originally designed as an emergency-response nuclear accident model. The development was in response to the widespread dispersion of the radioactive cloud from the Chernobyl power-plant accident in 1986. Since then, NAME has been continuously developed and used in a wide range of atmospheric dispersion events including nuclear accidents, volcanic eruptions, chemical accidents, smoke from fires, odours, airborne animal diseases, as well as the provision of routine air quality forecasts, policy support activities and scientific research (Jones et al., 2007).

NAME is essentially a Lagrangian atmospheric dispersion model. In comparison to the conventional Lagrangian trajectory model which tracks movement of an individual particle, the Lagrangian dispersion model is more accurate because it simulates the complex movement of large number of particles. On top of that, Lagrangian dispersion model provides a very realistic representation of transport in the planetary boundary layer (PBL) (the lowest portion of the atmosphere (from surface to about 1 to 2 km high)) because it incorporates the turbulence, an important feature in the PBL (Fleming et al., 2012).

NAME is designed to predict the atmospheric dispersion of air masses by calculating the air mass pathways and footprints. The motion of particles is governed by two components i.e. mean winds and turbulence (Stohl, 1998). When running the model, the air masses spread in a diffusive fashion, in which background air is mixed into the air masses by turbulent processes.

2.4.1.1.2 Model structure and physical processes

The basic infrastructure of NAME model, its flow processes and core features are summarised and briefly described in Figure 2.4 and Table 2.2. The physical processes within NAME, input and output data are also presented and are discussed in detail in the following sections.

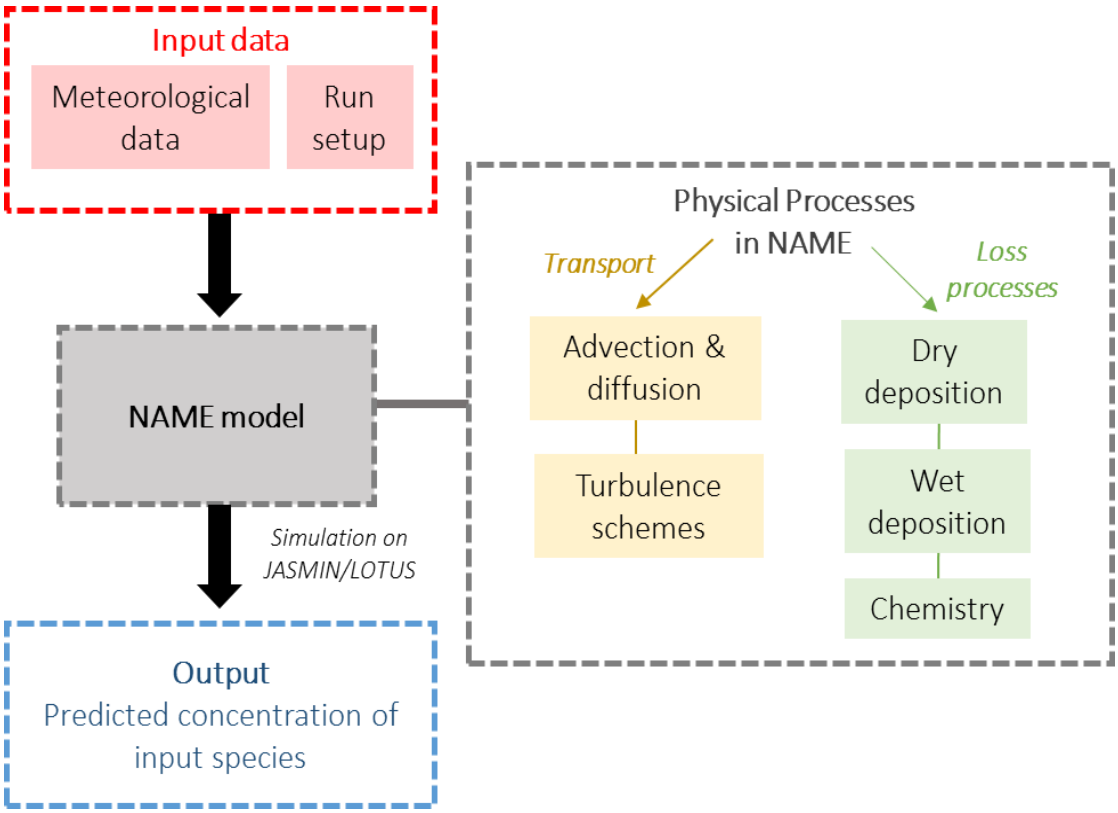

Figure 2.4: *A general scheme of NAME structure showing the flow processes starting from input data (in red), NAME model (in grey) and finally, the model output (in blue). Also shown are the physical processes that are represented within NAME (white box with grey dashed line).*

Table 2.2: *Overview of the core NAME characteristics and features.*

Basic infrastructure		
1	Model domain	Local, regional and global scale, as specified by the user • Local (~10^2 m to ~10 km) • Regional (~10 km to ~10^2 km) • Global (~10^2 km to global)
2	Horizontal resolution	Latitude-Longitude (standard or with a rotated pole); UK National Grid; Polar Stereographic projections; Transverse Mercator projections
3	Vertical resolution	Height (above ground or above sea level); pressure; flight levels in ICAO standard atmosphere; height-based and pressure-based hybrid systems (used by NWP models)
4	Temporal scales	Minutes to years
5	Temporal coverage	• Forecast runs (out to 6 days ahead for global; 36 hours for UK) • Analysis runs (hours to multi-year simulations) • Re-analysis data sets available back to 1957 • 'Forwards' and 'backwards' run modes
6	Technical characteristic	Programming language: Fortran 95
Physical processes		
1	Advection and diffusion	Random-walk techniques
2	Turbulence schemes	Turbulence and meander scales treated independently within the boundary layer
3	Dry deposition	• General scheme based on surface resistance / deposition velocity • Land surface dependent scheme for certain gaseous species
4	Wet deposition	Rain out ('in-cloud' removal) and wash out ('below-cloud' removal by rain impaction)
5	Chemistry	Comprehensive sulphur/nitrogen/hydrocarbon chemistry scheme based on global atmospheric chemistry model STOCHEM
Meteorological data		
1	Numerical weather prediction (NWP) Meteorology	Three-dimensional gridded data parameters from Met Office Unified Model (MetUM): UK (1.5 km) to Global (25 km). ECMWF forecast and reanalysis products (ERA-40 , ERA-Interim)
2	Topography	Uses orography from driving NWP meteorological model(s)
Output data		
1	Model outputs	Two-dimensional fields; vertical cross-sections; location-specific time series; particle trajectory information; model diagnostics
2	Output quantities	• Standard dispersion quantities i.e. air concentration, • Meteorological and flow variables • Gridded chemistry fields • Other quantities: particle numbers, travel times, plume depth, etc.
3	Statistical processing	Time integrating

Source: Adapted from NAME User Guide (Jones, 2015)

NAME is capable of representing numerous physical processes involved in the release of particles, their transport, evolution and removal from the atmosphere (Figure 2.4). The transport and dispersion of particles during the simulation is predominantly governed by a random walk turbulence scheme. The turbulence scheme is one of the physical process represented in NAME. Importantly, NAME incorporate effect of turbulent mixing processes in the atmosphere, and their parameterisation in NAME, was described. Turbulence can be described as a chaotic or irregular flow/ motion or air which are unpredictable. Such turbulent flows or eddies caused air parcels to move so that properties such as momentum and potential temperature are mixed across the boundary layer. Particles move with the resolved wind described by the meteorology plus a random component to represent the effects of atmospheric turbulence (Jones et al., 2007).

The particles in the model atmosphere can be removed via loss processes. This includes wet and dry wet deposition and dry deposition, gravitational settling, radioactive processes, chemical/biological agent decay and resuspension of sand and sea salt.

Both the physical and loss processes in NAME can be controlled and selected by user depending on the objective of the simulation.

2.4.1.2 Model setup and input data requirement

Prior running the model, two type of data were required i.e. the meteorological data and run setup (red boxes in Figure 2.4). The latter determined the version of meteorological data required for NAME to run.

i. Meteorological data

The meteorological input is a time varying 3-dimensional description of meteorological parameters output each time step from the Met Office Numerical Weather Prediction (NWP) model. The NWP model outputs a standard set of meteorological parameters from the operational forecast system in different ranges of resolutions and domains and they are available from 1999 until present (see Table 2.3 for examples). Depending on the date of interest, there are various versions of datasets available for NAME. A standard set of meteorological parameters can currently be read by NAME such as U, V, W component of winds, temperature, specific humidity and pressure (see Davies et al. (2005) for more information). The calculation begins by incorporating a vast amount of observational data at three hourly intervals into the forecast system. This process is continuously repeated to produce a three-dimensional analysis of the state of the atmosphere defined by meteorological variables.

Table 2.3: *Example of the NWP from Met Office Global NWP Models used in this study*

Dates	Met Definition Name	Grid resolution
30/04/2013 - 15/07/2014	UMG Mk7	0.35° longitude by 0.23° latitude
15/07/2014 - 25/08/2015	UMG Mk8	0.23° longitude by 0.16° latitude
25/08/2015 - present	UMG Mk9	0.23° longitude by 0.16° latitude

Note: UMG = Unified Model Global.

ii. Run setup

In general, the model is setup depending on the type of run to be performed (e.g. forward or backward run), the modelling domain and the temporal scales. For example, if NAME was used to calculate backward trajectories starting from a measurement site e.g. Taiwan for each day in October 2015, the 'Backwards' option was specified in the input file setup. The meteorological data i.e. Met Definition Name should satisfy the spatial and temporal coverage of interest. In this case, the

Met Definition Name called UMG Mk9 (Table 2.3) was selected as it covers the global NWP data from 25/08/2015 to present.

For this thesis, NAME was primarily run backward in time to simulate the history of particles that arrive at two measurement sites i.e. Bachok and Taiwan (Table 2.4).

Table 2.4: *Model setup to run NAME for measurement campaigns in Bachok and Taiwan*

Setup requirements	**Bachok**	**Taiwan**
Receptor site coordinate	6.009° N, 102.425° E	Hengchun, 22.0547° N, 120.6995° E, (2013, 2015) Cape Fuguei, 25.297° N, 121.538° E, (2014, 2016)
Sampling period. Version of meteorology and topography data are noted in parentheses	• 20 Jan – 5 Feb 2014 (UMG Mk7) • 19 Nov – 31 Dec 2015 (UMG Mk8) • 4 – 27 Jan 2016 (UMG Mk9)	• 7 Mar – 5 Apr 2013 (UMG Mk6) • 11 Mar – 4 Apr 2014 (UMG Mk7) • 12 Mar – 25 Apr 2015 (UMG Mk8) • 16 Mar – 29 Apr 2016 (UMG Mk9) *Note: UMG = Unified Model Global*
Type of run	Backward run	
Number of particle released	30,000	
Travel time	12 days	
Species category	Inert tracer	
Output request	Air concentration/ particle density	

Once the information required for the model setup have been identified, the relevant input data (files or scripts) need to be prepared prior to running the NAME. There are five files or scripts required for each NAME run (Table 2.5).

Table 2.5: *Description of input files/scripts required for NAME back-run*

Name of file/scripts	Description
Daily Script. scr	• The script automatically repeats the same basic run for every day over N years. For example, if backward trajectories need to be conducted each day in the month of October 2015 at Bachok, the scripts automatically executed the run each day in October 2015 simultaneously with one single command line.
Input template.txt	• This is an input file template comprising of various parameters for a set of daily NAME back runs from one site. • This input file can be specified by the user according to their needs e.g. the location of the receptor for back trajectory calculations, the modelling domain or the number of days for these trajectories.
MetDeclarations	• This module specifies the version and references the directory storing the NWP met data files.
MetRestore_JASMIN.ksh	• This is a script designed to run with NAME on the JASMIN platform and restores an archived UM met data file from the NAME-JASMIN met archive
SourceTermAndOutputRequests.txt	• This template specifies the format of source and output according to the user's requirement. • This source information specifies whether the run is for a single species or a complex mixture of many species, a simple single point source or a complex collection of multiple sources. • The output information specifies how long the simulation should be (e.g. 5 days or 12 days) and the altitude height to output the footprint (e.g. 0-100m and 0-16 km)

2.4.1.3 Model simulations

The NAME simulations were performed on the JASMIN/LOTUS platform. JASMIN is a scientific data analysis environment infrastructure that deploys a High Performance Computing (HPC) facility to supports a wide range of scientific workflows across environmental science domains, primarily to those that handle big data. JASMIN is managed and delivered by the UK Science and Technology Facilities Council (STFC) Centre for Environmental Data Archival (CEDA). LOTUS on the other hand is a group of physical machines that provides the processing component of JASMIN. LOTUS enables efficient scheduling of larger data analysis tasks across nodes in the cluster (Lawrence et al., 2013).

Once all the five input files and scripts in Table 2.5 were ready, the script **Daily Script. scr** was run via the command line in JASMIN/LOTUS, the input template **Input template.txt** was copied and forms the basic structure of the input file. The values/information given for certain variables in the script were then copied into that input file. NAME also reads the meteorological data stored in **MetRestore_JASMIN.ksh** and, behind the scenes, the meteorological module (**MetDeclarations**) sets up the corresponding version of meteorological data required for that run. Once the command is executed, a job ID is prompted, indicating that the job has been submitted to LOTUS. NAME then reads the input files and perform the runs. The output of the run is defined by the information specified in **SourceTermAndOutputRequests.txt.**

In general, NAME back-runs are performed for 12 days backward calculations for batches of 30,000 inert particles from 0-100 m above the surface of measurement site. The trajectories were calculated using three-dimensional meteorological fields produced by the UK Met Office's Numerical Weather Prediction tool, the Unified Model (UM). At the end of the 12 days travel time, NAME produced a gridded time integrated particle density also known as footprints of where the air sampled during the campaigns had previously been close to the Earth's surface.

2.4.1.4 Model output

The output of the NAME back-run is often called air history maps or footprints that describe where the air masses at a receptor at any given time has travelled over the duration of the model run. Examples of NAME footprints are shown in Figure 2.5. This output is useful in identifying the origins of an air parcel and possible contributory sources for pollution to that air parcel. On the other hand, NAME can be requested to output a particle density in a particular grid cell. In this thesis, the time integrated particle density units are used to describe NAME trajectories on a grid. The particle density can be expressed in the form of integrated over time. For example, each particle emitted at the start of the run was attributed by a mass of 1 gram. Therefore, if *n* particles each with a mass of 1 gram are (a) located in a certain grid cell for 15 minutes (900 seconds) time step, and (b) if *V* is the volume of the grid cell, the particle density can be interpreted as follows (Equation 2.1):

***Equation* 2.1 :**

$$\text{Time integrated particle density per grid cell (g s m}^{-3}) = \frac{\text{n(g) x 900 (s)}}{V\ (\text{m}^{-3})}$$

n is equal to the mass of all the particles in the grid cell in grams (g).

2.4.1.5 Post processing of model output

In this thesis, the NAME footprints can be utilised in four ways in order to meet the following objectives i.e.

i. To identify the possible source regions
ii. To quantify the contribution of possible sources regions in (i)
iii. To derive modelled mixing ratios of CO for estimating the emission of short and very short lived gases
iv. To investigate the influence of meteorological factors on the variability of measured compounds.

The description on each way of utilizing NAME footprints are presented in the Sections 2.4.1.5.1 to 2.4.1.5.4.

2.4.1.5.1 Identification of possible source regions

The NAME footprints tell us about the dispersion of the air masses and the pathways of the air particles. As the air particles travelled, they passed over countries that could have emitted chemical species which would then be transported to the sampling site (Gooch, 2016).

The identification of possible source regions of our compound of interest was done by assessing the monthly NAME footprints i.e. the sum of individual footprint generated for each day during each month of sampling. Figure 2.5 provides the examples of the sum of individual footprints for the month of November 2015 generated for Bachok and month of March 2014 generated for Taiwan. The sum of the NAME footprints provide an overview of the dispersion of the air masses and possible countries that might contribute to air masses that arrived in Bachok and Taiwan.

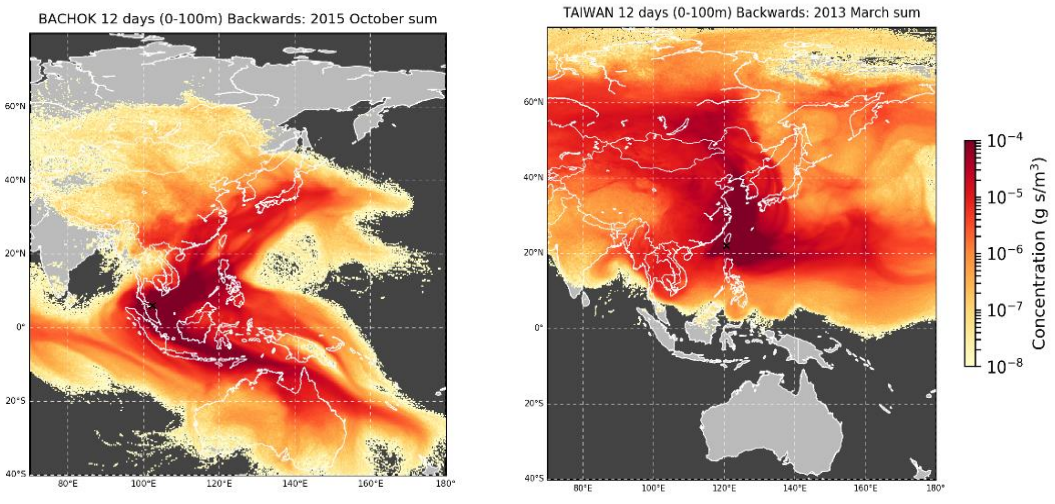

(a) (b)

Figure 2.5: *Example of NAME footprints for (a) Bachok and (b) Taiwan. Each sampling site is denoted by a black cross mark.*

The potential source locations were divided according to the countries that the air particles passed over (Figure 2.6). Since this region is quite complex i.e. comprised of many islands/land masses and ocean, it is much convenient to divide the area via political division. This is because each country is comprised of unique economic activities or sectors which could give different type of emission sources.

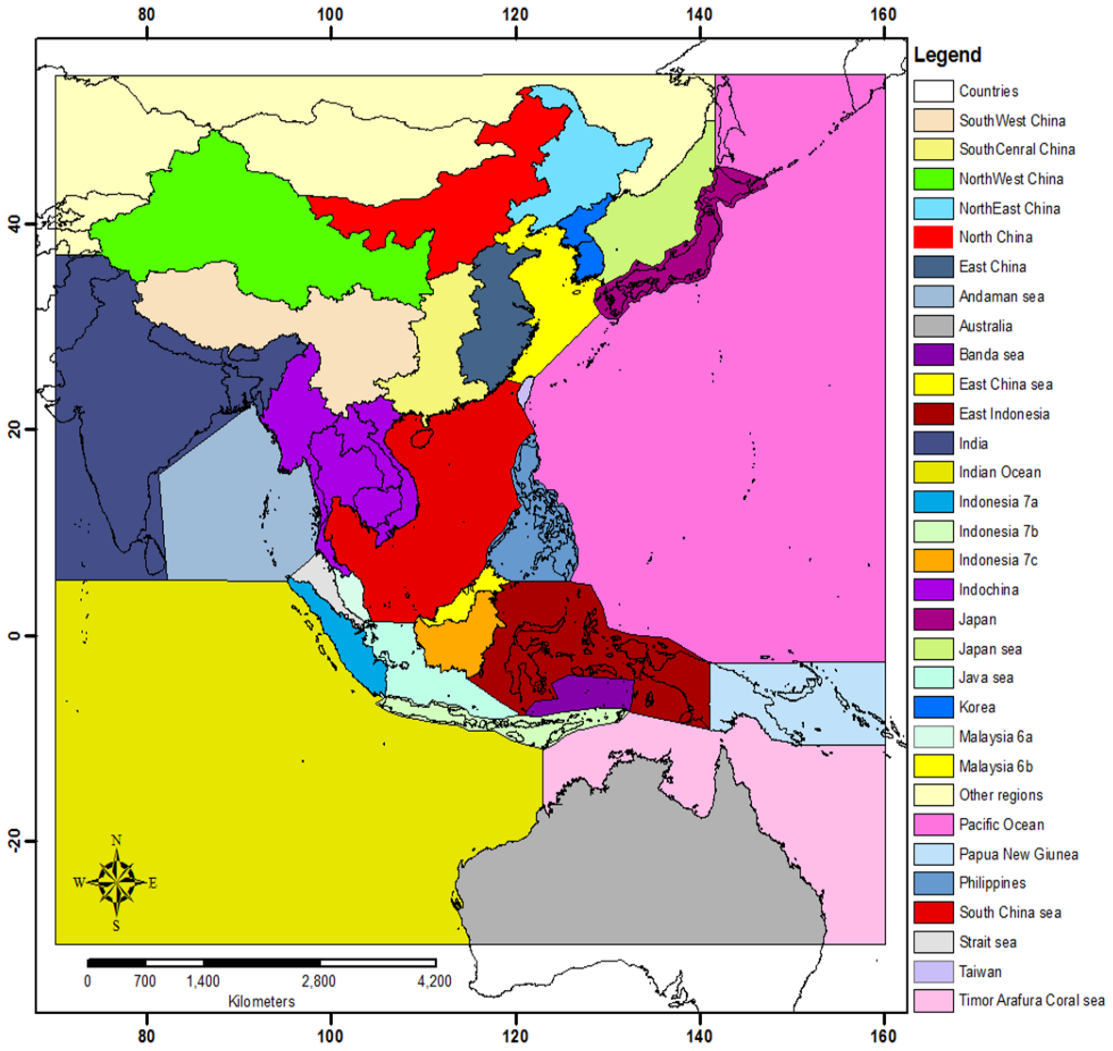

Figure 2.6: *The geographical sector map for Bachok and Taiwan which depicts the possible source locations for the air masses sampled during each campaign, assessed from analysis of the NAME footprints.*

Upon completion of the identification of possible source locations, the next step was to quantify the contribution of each source locations. Quantifying source locations contribution was intended to aid in the explanation of enhanced mixing ratios of

chemical species. This was done by performing particle distribution analysis which were described in detail in the next section (Section 2.4.1.5.2).

2.4.1.5.2 Quantifying the contribution of possible sources regions

The next step was to quantify the contribution of each source location to aid in the explanation of enhanced mixing ratios of chemical species as observed at the sampling sites. The analysis was started done by dividing the area into countries identified in Section 2.4.1.5.1 using shapefiles generated from ArcGIS and then extracting the time integrated particle density (g s m^{-3}) for each region. The process comprised of two steps:

a. Creating gridded shapefiles

Shapefiles can be described as the geometrical feature that define the regions/countries. First, the world map was to be downloaded from the Nature Earth website (http://www.naturalearthdata.com/downloads/) and uploaded into QGIS software and the countries of interest are selected and modified manually.

A shapefile is created by inputting coordinates (latitude + longitude) into a corresponding mapping / Geographic Information System (GIS) program, which converts spatial information into a graphical representation, such as a map with plotted GPS points. The geometry and location of each feature or 'shape' is plotted, stored as a set of coordinates and represented as points, lines or polygons (areas).
This created a .txt file listing all the shapefiles to be used for the analysis.

The next step was to create a grid of the shapefile using a Python codes in order to match the grid of the shapefile with the gridded NAME output. In this code, a technique called pickling was used which essentially converted

the python object structure (shapefiles) into byte streams that create a grid for each shapefile for each region of interest. The gridded shapefiles was kindly generated by Marios Panagi and Zoe Fleming from University of Leicester.

b. Process of counting the particles by extracting the NAME output in each shapefile created in (a).

Another Python code was used to create a master grid of the shapefiles using the information stored (pickled) in the previous code which is then matched to the NAME output data. So, think of it as now we have the shapefiles grid and the NAME grid overlaying. Then we calculated the particles over each region for every 3 hourly NAME outputs using that information.

Finally, the output of the particle distribution analysis (in g s m^{-3}) were compared with the time-series of chemical species measured during the campaigns in order to explain their variations and identify potential major source locations.

2.4.1.5.3 Estimating emission of VSLSs using modelled mixing ratios of carbon monoxide

The purpose of estimating the emissions of short and very short lived gases was to identify where the emissions were coming from and what category of emissions contributed towards the variability of VSLSs measured at Bachok and Taiwan. The NAME particle distribution analysis conducted in Section 2.4.1.5.2 can potentially link the NAME particle densities for possible source regions with the variability of measured mixing ratios of species of interest, but is limited in quantifying the emission strength.

The emission strength of a trace gas emitted by each source region was estimated using (a) NAME footprints and (b) an emission inventory for the chemical tracer. The NAME output was in a form of a time-integrated particle density (g s m^{-3}). A slight modification of this unit enabled the contribution of different source locations and different emission sectors towards the concentration of a trace gas measured at measurement site to be calculated.

This study has selected carbon monoxide (CO) as a chemical tracer because CO is commonly used as a tracer of anthropogenic emissions. Its lifetime of 1–2 months is long enough to track pollution plumes on intercontinental scales, yet short enough to provide enhancements with respect to background. Also, the emission inventory of CO is considered to be relatively well established which thereby provides confidence in the derived emission estimates.

The inventory of industrial and combustion CO emissions was taken from the Representative Concentration Pathway 8.5 (RCP 8.5) (van Vuuren et al., 2011; Riahi et al., 2011; Granier et al., 2011) for the year 2010. RCP 8.5 contains estimated emissions of CO and any other compound up to 2100. The emissions were estimated based on assumptions about economic activity, energy sources, population growth and other socio-economic factors. More information and access to the database can be found on the RCP 8.5 website (http://tntcat.iiasa.ac.at:8787/RcpDb/dsd?Action=htmlpage&page=welcome).

i. Files required

Three input files in netcdf format are required to calculate the modelled mixing ratio of CO. The files and descriptions of each file are presented in Table 2.6 below:

Table 2.6: *Description of input files/scripts required to calculate the modelled mixing ratios of CO*

No.	Type of file	Description
1	Monthly NAME output file.nc	File containing monthly NAME output i.e. particle density (g s m^{-3}) generated from backward simulation. This file has 3 hourly time resolution and are separated by vertical grid.
2	NAME area grid file.nc	File containing the area of grid cell (m^2). It consists of an array of grid cells referenced by rows (305 latitude) and columns (209 longitude) of numbers. This file become the model domain with grid resolution of 0.5625◦ longitude by 0.375◦ latitude.
3	Emission datasets.nc	File containing CO emission values for industrial activities (combustion and processing) ($kgm^{-2}s^{-1}$). The inventory of industrial and combustion carbon monoxide (CO) emissions are taken from the Representative Concentration Pathway 8.5 (RCP 8.5) and are taken for the year 2010. The grid resolution are 0.5◦ longitude by 0.5◦ latitude. The dataset can be downloaded from the RCP 8.5 website (http://tntcat.iiasa.ac.at:8787/RcpDb/dsd?Action=htmlpage&page=welcome).

ii. Pre-Calculation

Prior to performing the calculation, the monthly NAME output file need to be prepared and the emission dataset need to be downloaded and processed. Noted that the NAME backward simulation produced daily output file in a text format. For this analysis, the monthly NAME output file in a netcdf format are required. To do so, all the daily files for our month of interest need to be converted to a netcdf format and summed to produce a monthly NAME output file. For example, to combine all daily outputs file in January 2014 (Total files = 31), the following pre-processing procedure were required:

1. First, each NAME daily output file for January 2014 was converted from text format to netcdf format using a python script on JASMIN. Running the **Fazrin_txt_to_nc_Test.sh** on JASMIN executed the **NAME2NetCDF_incload_V1.py** script. The location for these files are as follows:

   ../../../group_workspaces/jasmin/name/cache/users/fazrinhanif/ **Fazrin_txt_to_nc_Test.sh**

   ../../../group_workspaces/jasmin/name/cache/users/fazrinhanif/Python_script/**NAME2NetCDF_incload_V1.py**

2. Then, the Climate Data Operator (CDO) cat was used to concatenate all 31 daily netcdf files to generate the monthly output file called 'January2014.nc'.

cdo cat Fields_grid1_C1_T1_20140101_pd_100.nc Fields_grid1_C1_T1_20140102_pd_100.nc Fields_grid1_C1_T1_20140103_pd_100.nc Fields_grid1_C1_T1_20140104_pd_100.nc Fields_grid1_C1_T1_20140105_pd_100.nc Fields_grid1_C1_T1_20140106_pd_100.nc Fields_grid1_C1_T1_20140107_pd_100.nc Fields_grid1_C1_T1_20140108_pd_100.nc Fields_grid1_C1_T1_20140109_pd_100.nc Fields_grid1_C1_T1_20140110_pd_100.nc Fields_grid1_C1_T1_20140111_pd_100.nc Fields_grid1_C1_T1_20140112_pd_100.nc Fields_grid1_C1_T1_20140113_pd_100.nc Fields_grid1_C1_T1_20140114_pd_100.nc Fields_grid1_C1_T1_20140115_pd_100.nc Fields_grid1_C1_T1_20140116_pd_100.nc Fields_grid1_C1_T1_20140117_pd_100.nc Fields_grid1_C1_T1_20140118_pd_100.nc Fields_grid1_C1_T1_20140119_pd_100.nc Fields_grid1_C1_T1_20140120_pd_100.nc

Fields_grid1_C1_T1_20140121_pd_100.nc *Fields_grid1_C1_T1_20140122_pd_100.nc*
Fields_grid1_C1_T1_20140123_pd_100.nc *Fields_grid1_C1_T1_20140124_pd_100.nc*
Fields_grid1_C1_T1_20140125_pd_100.nc *Fields_grid1_C1_T1_20140126_pd_100.nc*
Fields_grid1_C1_T1_20140127_pd_100.nc *Fields_grid1_C1_T1_20140128_pd_100.nc*
Fields_grid1_C1_T1_20140129_pd_100.nc *Fields_grid1_C1_T1_20140130_pd_100.nc*
Fields_grid1_C1_T1_20140131_pd_100.nc January2014.nc

3. Finally, the 'January2014.nc' were re-gridded to match the grid resolution of 0.5625◦ by 0.375◦ in 'area_NAME_grid.nc'. The re-gridded file was called 'January2014_regrid.nc'. The cdo operator remapbil was used to re-grid the data on to mygrid:

   cdo remapbil,mygrid January2014.nc January2014_regrid.nc

iii. Preparing the emission dataset

1. In JASMIN, the cdo command was used to re-grid the gridded 'emission dataset.nc' at a 0.5◦ by 0.5◦ resolution in order to match the grid resolution of 0.5625◦ by 0.375◦ in 'area_NAME_grid.nc'. This was again done using the cdo operator remapbil:

   cdo remapbil,mygrid emission dataser.nc area_NAME_grid.nc

iv. Calculating modelled CO

The next step was to calculate the modelled CO in a python script. First, the Python script called the value of NAME particle density from the 'Monthly NAME output file.nc'. Next, the value for surface area of each grid cell and emission of each grid cell were read by Python from the files 'NAME area grid file.nc' and 'Emission datasets.nc', respectively. An additional step was to convert the concentration unit from mol m^{-3} to part per billion (ppb). The sum of all the grid cells will give the total concentration of modelled CO at the measurement site for each day at 3 hourly resolution. Similar

steps were repeated for each day in the 'Monthly NAME output file.nc'. Finally, a time series of modelled CO can then be derived for comparison with the observational data from Bachok and Taiwan.

2.4.1.5.4 Investigating the influence of meteorological factors

For studying VSLSs in Bachok, an additionally meteorological analysis was conducted in order to (1) characterize the cold surge events (an important meteorological process occurring during the Northeast Monsoon in that region) using a cold surge index and (2) to explore the influence of cold surges towards the variation of observed VSLSs.

For identifying and characterising cold surge events during the boreal winters from 2014 to 2017 within our domain of interest i.e. 2.5°S–7.5°N, 107.5°–117.5°E (Figure 2.7), the cold surge index defined by Chang et al. (2005) was used. A cold surge index is a measure of the strength of the North East Monsoon winds in the South China Sea. The index is chosen as the average 925-hPa meridional wind between 110° and 117.5°E along 15°N, referred as V_{15} in Figure 2.7. According to this definition, a cold surge event happens when the value of this index exceeds -8 m s^{-1}. It is important to note that the definition for the cold surge index in this study uses meridional wind (v-wind), i.e. which the intensity of the north-south component of the wind movement. As such, higher negative values for the cold surge index indicate stronger southward-movement of the cold surge winds.

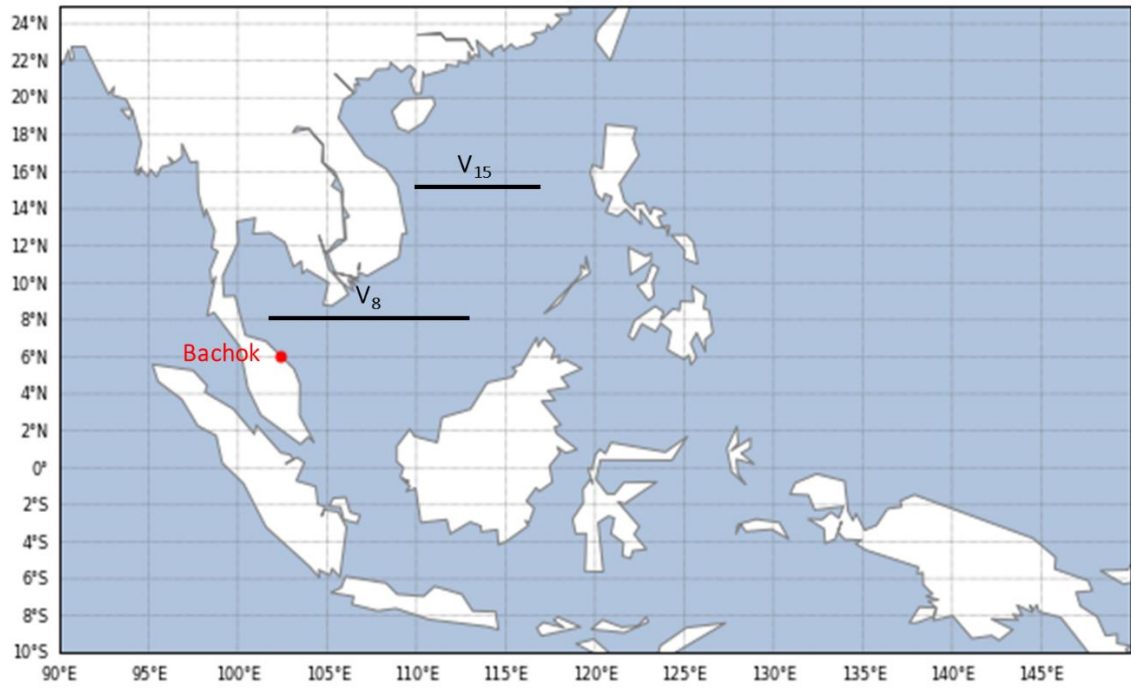

Figure 2.7: *The Bachok Marine Research Station (red) located at 6.07 °N, 102.40 °E. The black horizontal bars are the locations for the cold surge index. V_{15} indicates v at 925 hPa averaged over 110-117.5°E at 15°N. V_8 indicates v at 925 hPa averaged over 102-113°E at 8°N.*

To begin, the meridional wind (v) was downloaded from the ECMWF Public Datasets web interface (http://apps.ecmwf.int/datasets/). The *v* data was selected at 925 hPa pressure level data, which represents the boundary layer conditions but less influenced by local surface processes than the alternative 1000 hPa pressure level (Ashfold et al., 2017). The *v* data was extracted for the periods covered by the dataset (i.e. January to February 2014, November to December 2015 and January 2016) at a horizontal resolution of 0.125° longitude by 0.125° latitude. The time-steps was selected at 00:00, 06:00, 12:00 and 18:00 Universal Time (UT), or approximately 8:00, 14:00, 20:00 and 02:00 local time (LT).

In addition, as I am interested in changes in chemical composition in measurement site which located in the deep tropics, an alternative index is assigned further south and called as V_8. This new index defined the cold surge using the same meridional winds data i.e. at 925 hPa but extracted over 102-113°E at 8°N (Figure 2.7). According to Ashfold et al. (2017), there is no universal definition of a cold surge. Different authors typically use a definition that best suits the geographical scope of their investigation.

For this study, the second location is used based on the following two factors:

(a) I was specifically interested in identifying cold surge events that might bring polluted air masses from the north and its impact towards the chemical compositions further south, i.e. near to our study area in Bachok (6.07 °N, 102.40 °E). Therefore, the latitude of V_8 was chosen to better represent this transport closer to Bachok. Also, I wanted to investigate if there were any differences in meridional wind intensity and the time lags between V_{15} and V_8 in order to evaluate the impact of cold surges on atmospheric composition. The V_{15} index is generally accepted and commonly employed to represent cold surges in climatology (more details in Section 2.4.1.5.4, Chapter 2), whilst the V8 index is an alternative created to represent meridional strong transport near our study area.

(b) The observation of common pathways of northerly winds that arrive at the sampling site at Bachok. This observation was based on the assessment of the pathways of air masses depicted in all NAME footprints generated for each day of sampling. On average, the air masses mainly passed through the second location i.e. between 102-113°E at 8°N.

In this work, the cold surge indexes (V_{15} and V_8) dataset were used to further explore the influence of cold surge events towards the variability of chemical species during the campaigns. This was done by comparing the cold surge indices with the time series of chemical species measured at the sampling sites.

2.4.2 Introduction to the 2-D atmospheric chemistry transport model

2.4.2.1 Model description

2.4.2.1.1 Overview

Two-dimensional global atmospheric chemistry-transport models have often been used to describe the global distribution of trace gases. Use of these models assume that the concentrations of a species are a function of latitude and altitude and do not depend on the longitude (Seinfeld et al., 2006). According to Newland (2013), the mixing time of a species in the troposphere around a latitudinal band is on the order of two to three weeks. Therefore, for the species with a lifetime longer than this, it is a reasonable assumption that within a particular latitude band such a species will be fairly homogeneous and so can be represented by a single model cell.

Originally, the model was developed by Hough (1989) with the focus to investigate the distribution and budgets of ozone precursors and tropospheric ozone distribution, before computational power allowed the development of 3-D models. Since then, the model but with a much simplified chemical mechanism has been used to investigate the global emissions of long lived gases (e.g. Fraser et al., 1999; Reeves et al., 2005; Laube et al., 2010; Sturges et al., 2012; Oram et al., 2012; Laube et al., 2012). This model has been proven to work well for a variety of atmospheric trace gases and so was used in this work for deriving the top-down global annual emissions estimates of the CFC-114 and CFC-114a.

In this study, we used a two-dimensional model to deduce the annual global emissions of CFC-114 and CFC-114a based on the measurements from Cape Grim and firn air in Antarctica. The model allows us to understand the relationship between emission changes and changes in ambient concentration of CFC-114 and CFC-114a.

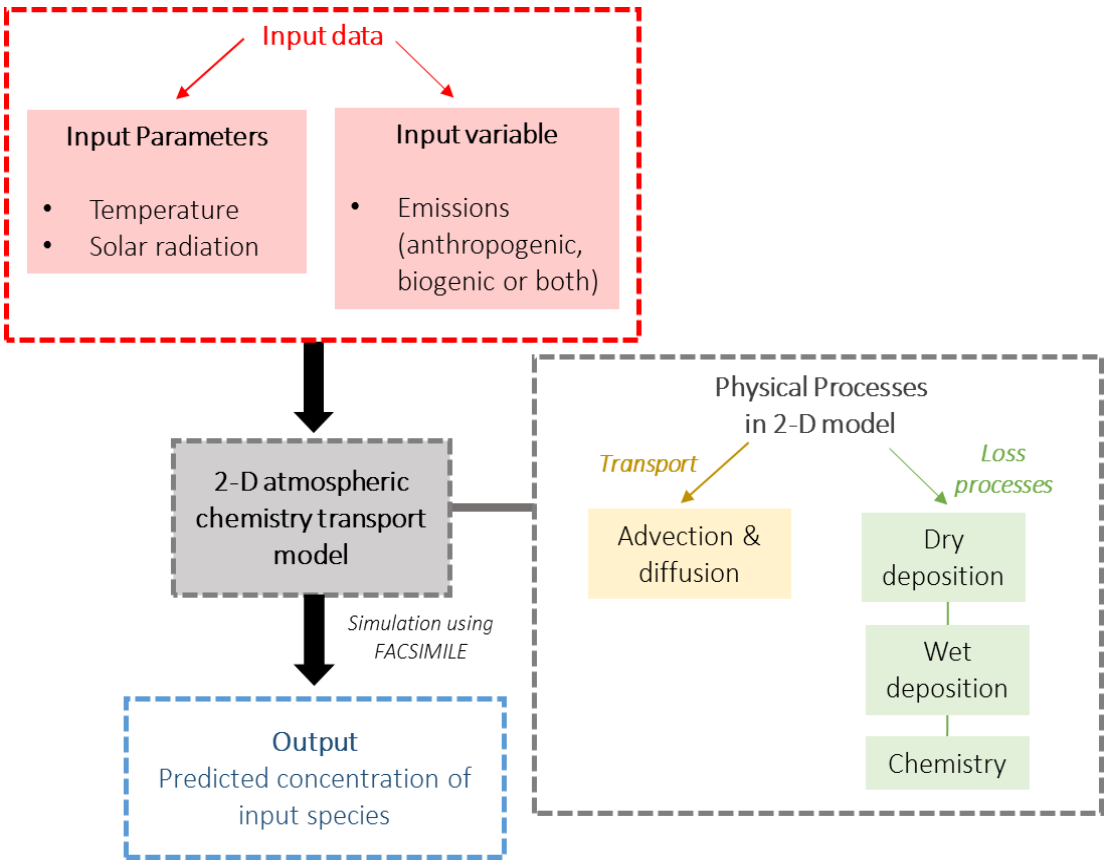

Figure 2.8: *A general scheme for a 2-D chemistry transport model*

2.4.2.1.2 Model structure and physical processes

The model domain stretches from pole to pole and from the surface of the earth to a height of 24 km (Hough 1989). The model comprises of grid boxes which have been divided into 24 equal area, zonally-averaged bands and has 12 vertical layers of 2 km depth. This give a total of 288 cells.

The model used the same latitudinal distribution of emissions as in previous studies of the temporal behaviour and global distribution of other halogenated compounds (Reeves et al., 2005, Oram et al., 2012, Kloss et al., 2014, Laube et al., 2014, Laube et al., 2016). This distribution is based on 95% of emissions originating from industrial activities in the Northern Hemisphere, predominantly from mid-latitudes (in agreement with the work by McCulloch et al. (1994)).Using this latitudinal distribution, the transport scheme of the model has been shown to reproduce the reported global distributions of CFC-11 and CFC-12 to within 5% (Reeves et al.,

2005). Throughout the current model runs, the latitudinal emission distribution has been held constant.

2.4.2.2 Model setup and input data requirement

The model was run using FACSIMILE, a computer programme capable of solving the differential equations encountered in scientific and engineering problems. To simulate the loss process that affect the mixing ratio of CFC-114 and CFC-114a within the model domain, the model was setup to include the photolysis of the individual isomers. For CFC-114, the absorption cross sections are calculated for each grid box as a function of seasonally varying temperature for the wavelengths 200 – 220 nm (Simon et al., 1988). A log-linear extrapolation of the Simon et al. (1988) data, $\log \sigma (\lambda) = -1.8233-0.0913\lambda$ was used to derive the absorption cross sections for longer wavelengths in the range of 222 – 235 nm (Sander et al., 2011). For CFC-114a the absorption data from Davis et al. (2016) were used. The rate coefficients of 1.43×10^{-10} and 1.62×10^{-10} cm^3 $molecule^{-1}$ s^{-1} are applied to the reactions of $O(^1D)$ with CFC-114 and CFC-114a, based on work by Baasandorj et al. (2013) and Baasandorj et al. (2011), respectively. To simulate the stratospheric loss through the upper boundary, the gradient across this boundary is defined to give a diffusive loss from the model domain. The diffusive loss from the top of the model was set by adjusting the mixing ratio of our studied compounds at 25 km (i.e. the boundary conditions) such that they were a fraction (F) of those in the top model box (23 km) (Newland et al., 2013) (for more details see below).

Once the loss processes have been set up, the model was run long enough with constant emission rates for the system to reach a steady state. Steady-state lifetimes refer to a lifetime when the emission and removal rates of a species are equal (Carpenter et al., 2014). The steady-state lifetime (τ) of a species is defined as the ratio of its global atmospheric burden, B (molecules) to its total global loss rate, L (molecules s^{-1}) (Carpenter et al., 2014).

The vast majority of the loss of both CFC-114 and CFC-114a occurs above the height of the model domain so their modelled lifetimes are largely controlled by the values assigned to F. Therefore, we used values of 0.922 and 0.837 for F in order to achieve the steady-state lifetimes of 189 and 102 years for CFC-114 and CFC-114a, respectively, based on the estimates reported in SPARC (2013) and (Carpenter et al., 2014). This is in agreement with the very recently reported lifetime of 105.3 years for CFC-114a, which took into account new UV absorption data (Davis et al., 2016).

2.4.2.3 Model simulations

Model simulations were carried out to reproduce the tropospheric time series of CFC-114 and CFC-114a from the southern hemispheric firn air derived trends (1960 to 2003) and the atmospheric measurements from Cape Grim (1978 to 2014). Where there are discrepancies between these two observational data sets, we favoured the Cape Grim time series, which we have more confidence in,

The model simulations started off by using the published emission estimates using the bottom-up approach by Alternative Fluorocarbon Environmental Acceptability Study (AFEAS). Since 1976, chemical companies that have produced fluorocarbons have participated in an AFEAS survey by voluntarily reporting their production and sales of fluorocarbon (AFEAS, 2009.). AFEAS then compiles all the information and yearly updated emission data are derived. This information is publicly available on the Advanced Global Atmospheric Gases Experiment (AGAGE) website (https://agage.mit.edu/data/afeas-data). The AFEAS emission estimates were calculated by using two types of data set i.e. (i) the time series of data on production and sales by chemical manufactures and (ii) emission functions which represent the timing and rate of halocarbon emission to the atmosphere (Martinerie et al., 2009).

In subsequent model runs, the emission values were adjusted until the concentrations for the surface box of the relevant band agreed with the set of atmospheric measurements at that location. For example, the model derived concentrations of CFC-114 and CFC-114a for (a) the surface box of the band 66.4˚S – 90.0˚S agreed with observations in firn air sites in Antarctic (90˚ from 1960 to 2003 and (b) the surface box of the band 35.7˚S– 41.8˚S agreed with observations in Cape Grim, Tasmania (41˚S) from 1978 to 2014.

This was an iterative process whereby the process of adjusting the emissions for each year was repeated to match the model derived concentrations with the measurements.

2.4.2.4 Model output

The process was completed when the model output from the emissions scenario provided a good fit to the measurements i.e. by eye using plots rather than mathematical fit to the observational data. These modelled mixing ratios were termed as 'best-guess' emission estimates.

2.4.4.1 Derivation of uncertainty ranges of emission estimates

To determine the uncertainty ranges in the emission estimates of CFC-114 and CFC-114a, first an uncertainty in the modelled mixing ratios was calculated based on uncertainties in the model and measurements and the agreement between the model and observed data. This uncertainty was then added to (substracted from) the 'best fit' modelled mixing ratios for Cape Grim to derive upper (lower) uncertainty ranges. Finally, to determine the maximum (minimum) emissions the model was rerun to fit the upper (lower) range using the shortest (longest) estimated lifetimes (following the methodology of Kloss et al. (2014)). The range of lifetimes used for CFC-114 was 153-247 years (SPARC, 2013, Carpenter et al., 2014) and a similar relative range of lifetimes (82–133 years) was assumed for CFC-114a. More details can be found in Laube et al. (2016)

2.5 Summary

This chapter has described and summarised the methodology used to study the atmospheric budgets of gases relevant to climate, with emphasis given on the modelling approach. Two approaches are discussed: (1) 3-D dispersion modelling to determine the impact of different source types and regions on short and very short-lived gases by using two observational datasets generated from the ground-based campaigns in East Asia and South East Asia; (2) 2-D chemistry transport modelling for deriving the emission estimates of long-lived gases using the observational dataset from the Cape Grim firn air campaign in Antarctic. The result and discussion on the model outputs of 3-D model have been split into two chapters which deal separately with chlorinated very short-lived halogenated gases (Chapter 3) and methyl halides (Chapter 4). The 2-D model output are presented and discussed in the chapter of long-lived halogenated gases (Chapter 5).

2.6 References

AFEAS: Production Sales of Fluorocarbons. Alternative Fluorocarbons Environmental Acceptability Study (AFEAS): Production and Sales of Fluorocarbons (last access: 4 March 2015), 2009.

Ashfold, M. J., Latif, M. T., Samah, A. A., Mead, M. I. and Harris, N. R. P.: Influence of Northeast Monsoon cold surges on air quality in Southeast Asia, Atmospheric Environment, 166, 498-509, 10.1016/j.atmosenv.2017.07.047, 2017.

Baasandorj, M., Feierabend, K. J. and Burkholder, J. B.: Rate coefficientsand ClO radical yields in the reaction of $O(^1D)$ with $CClF_2CCl_2F$, CCl_3CF_3, $CClF_2CClF_2$, CCl_2FCF_3, Int. J. Chem. Kinet., 43, 1-9, 2011.

Baasandorj, M., Fleming, E. L., Jackman, C. H. and Burkholder, J. B.: $O(^1D)$ kinetic study of key ozone depleting substancesand greenhouse gases, J. Phys. Chem. A, 117, 275-282, 2013.

Brasseur, G. and Jacob, D. Modeling of Atmospheric Chemistry. Cambridge, Cambridge University Press. 2017

Brenninkmeijer, C. A. M., Crutzen, P., Boumard, F., Dauer, T., Dix, B., Ebinghaus, R., Filippi, D., Fischer, H., Franke, H., Frieβ, U., Heintzenberg, J., Helleis, F., Hermann, M., Kock, H. H., Koeppel, C., Lelieveld, J., Leuenberger, M., Martinsson, B. G., Miemczyk, S., Moret, H. P., Nguyen, H. N., Nyfeler, P., Oram, D., O'Sullivan, D., Penkett, S., Platt, U., Pupek, M., Ramonet, M., Randa, B., Reichelt, M., Rhee, T. S., Rohwer, J., Rosenfeld, K., Scharffe, D., Schlager, H., Schumann, U., Slemr, F., Sprung, D., Stock, P., Thaler, R., Valentino, F., van Velthoven, P., Waibel, A., Wandel, A., Waschitschek, K., Wiedensohler, A., Xueref-Remy, I., Zahn, A., Zech, U. and Ziereis, H.: Civil Aircraft for the regular investigation of the atmosphere based on an instrumented container: The new CARIBIC system, Atmospheric Chemistry and Physics, 7, 18, 4953-4976, 10.5194/acp-7-4953-2007, 2007.

Butler, J. H., Battle, M., Bender, M. L., Montzka, S. A., Clarke, A. D., Saltzman, E. S., Sucher, C. M., Severinghaus, J. P. and Elkins, J. W.: A record of atmospheric halocarbons during the twentieth century from polar firn air, Nature, 399, 6738, 749-755,.

Carpenter, L. J., Reimann, S., Burkholder, J. B., Clerbaux, C., Hall, B. D., Hossaini, R., Laube, J. C. and Yvon-Lewis, S. A. Ozone-Depleting Substances (ODSs) and Other Gases of Interest to the Montreal Protocol, Chapter 1 in Scientific Assessment of Ozone Depletion: 2014, Global Ozone Research and Monitoring Project – Report No. 55. Geneva, Switzerland, World Meteorological Organization.2014

Chang, C. P., Harr, P. A. and Chen, H. J.: Synoptic disturbances over the equatorial South China Sea and western maritime continent during boreal winter, Monthly Weather Review, 133, 3, 489-503, 2005.

Davies, T., M. J. P. Cullen, A. J. Malcolm, M. H. Mawson, A. Staniforth, A. A. White and N. Wood A new dynamical core for the Met Office's global and regional modelling of the atmosphere, Quarterly Journal Of The Royal Meteorological Society, 131, 608, 1759 -1782, 2005.

Davis, M. E., Bernard, F., McGillen, M. R., Fleming, E. L. and Burkholder, J. B.: UV and infrared absorption spectra, atmospheric lifetimes, and ozone depletion and global warming potentials for CCl_2FCCl_2F (CFC-112), CCl_3CClF_2 (CFC-112a), CCl_3CF_3 (CFC-113a), and CCl_2FCF_3 (CFC-114a), Atmospheric Chemistry and Physics, 16, 12, 8043-8052, 10.5194/acp-16-8043-2016, 2016.

Fleming, Z. L., Monks, P. S. and Manning, A. J.: Review: Untangling the influence of air-mass history in interpreting observed atmospheric composition, Atmospheric Research, 104-105, 1-39, 10.1016/j.atmosres.2011.09.009, 2012.

Fraser, P. J., Oram, D. E., Reeves, C. E., Penkett, S. A. and McCulloch, A.: Southern Hemispheric halon trends (1978-1998) and global halon emissions, Journal

of Geophysical Research: Atmospheres, 104, D13, 15985-15999, 10.1029/1999jd900113, 1999.

Gooch, L. J. Atmospheric Halocarbon Measurements with a focus on East and South-East Asia. School of Environmental Sciences, University of East Anglia. PhD.2016

Hough, A. M.: The development of a two-dimensional global tropospheric model-1. The model transport, Atmospheric Environment (1967), 23, 6, 1235-1261, 10.1016/0004-6981(89)90150-9, 1989.

Jones, A. User Guide for Numerical Atmospheric-dispersion Modelling Environment (NAME) UK Met Office.2015

Jones, A., Thomson, D., Hort, M. and Devenish, B. The U.K. Met Office's Next-Generation Atmospheric Dispersion Model, NAME III. Air Pollution Modeling and Its Application XVII. C. Borrego and A.-L. Norman. Boston, MA, Springer US**:** 580-589. 2007

Kloss, C., Newland, M. J., Oram, D. E., Fraser, P. J., Brenninkmeijer, C. A. M., Röckmann, T. and Laube, J. C.: Atmospheric abundances, trends and emissions of CFC-216ba, CFC-216ca and HCFC-225ca, Atmosphere, 5, 2, 420-434, 10.3390/atmos5020420, 2014.

Laube, J. C., Mohd Hanif, N., Martinerie, P., Gallacher, E., Fraser, P. J., Langenfelds, R., Brenninkmeijer, C. A. M., Schwander, J., Witrant, E., Wang, J. L., Ou-Yang, C. F., Gooch, L. J., Reeves, C. E., Sturges, W. T. and Oram, D. E.: Tropospheric observations of CFC-114 and CFC-114a with a focus on long-term trends and emissions, Atmospheric Chemistry and Physics, 16, 23, 15347-15358, 10.5194/acp-16-15347-2016, 2016.

Laube, J. C., Newland, M. J., Hogan, C., Brenninkmeijer, C. A. M., Fraser, P. J., Martinerie, P., Oram, D. E., Reeves, C. E., Röckmann, T., Schwander, J., Witrant, E. and Sturges, W. T.: Newly detected ozone-depleting substances in the atmosphere, Nature Geoscience, 7, 4, 266-269, 10.1038/ngeo2109, 2014.

Lawrence, B. N., Bennett, V. L., Churchill, J., Juckes, M., Kershaw, P., Pascoe, S., Pepler, S., Pritchard, M. and Stephens, A. (2013). Storing and manipulating environmental big data with JASMIN. 2013 IEEE International Conference on Big Data.

Martinerie, P., Nourtier-Mazauric, E., Barnola, J. M., Sturges, W. T., Worton, D. R., Atlas, E., Gohar, L. K., Shine, K. P. and Brasseur, G. P.: Long-lived halocarbon trends and budgets from atmospheric chemistry modelling constrained with measurements in polar firn, Atmospheric Chemistry and Physics, 9, 12, 3911-3934, 10.5194/acp-9-3911-2009, 2009.

McCulloch, A., Midgley, P. M. and Fisher, D. A.: Distribution of emissions of chlorofluorocarbons (CFCs) 11, 12, 113, 114 and 115 among reporting and non-reporting countries in 1986, Atmospheric Environment, 28, 16, 2567-2582, 10.1016/1352-2310(94)90431-6, 1994.

Newland, M. J. Long term trends of halogenated trace gases, hydrocarbons, alkyl nitrates and of the oxidative capacity of the atmosphere, University of East Anglia. Ph.D.2013

Newland, M. J., Reeves, C. E., Oram, D. E., Laube, J. C., Sturges, W. T., Hogan, C., Begley, P. and Fraser, P. J.: Southern hemispheric halon trends and global halon emissions, 1978-2011, Atmospheric Chemistry and Physics, 13, 11, 5551-5565, 10.5194/acp-13-5551-2013, 2013.

Oram, D. E., Ashfold, M. J., Laube, J. C., Gooch, L. J., Humphrey, S., Sturges, W. T., Leedham-Elvidge, E., Forster, G. L., Harris, N. R. P., Mead, M. I., Abu Samah, A., Phang, S. M., Chang-Feng, O. Y., Lin, N. H., Wang, J. L., Baker, A. K., Brenninkmeijer, C. A. M. and Sherry, D.: A growing threat to the ozone layer from short-lived anthropogenic chlorocarbons, Atmospheric Chemistry and Physics, 7, 19, 11929-11941, 2017.

Oram, D. E., Mani, F. S., Laube, J. C., Newland, M. J., Reeves, C. E., Sturges, W. T., Penkett, S. A., Brenninkmeijer, C. A. M., Röckmann, T. and Fraser, P. J.: Long-term tropospheric trend of octafluorocyclobutane (c-C_4F_8 or PFC-318), Atmospheric Chemistry and Physics, 12, 1, 261-269, 10.5194/acp-12-261-2012, 2012.

Ou-Yang, C.-F., Hsieh, H.-C., Wang, S.-H., Lin, N.-H., Lee, C.-T., Sheu, G.-R. and Wang, J.: Influence of Asian continental outflow on the regional background ozone level in northern South China Sea, Atmospheric Environment, 78, 144-253, 2012.

Reeves, C. E., Sturges, W. T., Sturrock, G. A., Preston, K., Oram, D. E., Schwander, J., Mulvaney, R., Barnola, J. M. and Chappellaz, J.: Trends of halon gases in polar firn air: Implications for their emission distributions, Atmospheric Chemistry and Physics, 5, 8, 2055-2064, 2005.

Sander, S. P., Friedl, R. R., Abbatt, J. P. D., Barker, J. R., Burkholder, J. B., Golden, D. M., Kolb, C. E., Kurylo, M. J., Moortgat, G. K., Wine, P. H., Huie, R. E. and Orkin, V. L. Chemical kinetics and photochemical data for use in atmospheric studies, evaluation number 17. JPL Publ. 10-6, 4G-33. Pasadena, USA.2011

Seinfeld, J. H. and Pandis, S. N. Atmospheric chemistry and physics: From air pollution to climate change. Hoboken, New Jersey, John Wiley & Sons, Inc. 2006

Simon, P. C., Gillotay, D., Vanlaethem-Meuree, N. and Wisemberg, J.: Temperature dependence of ultraviolet absorption cross-sections of chlorofluoroethanes, Annales Geophysicae, 6, 3, 239-248, 1988.

SPARC. SPARC Report: Report on the lifetimes of stratospheric ozone-depleting substances, their replacements, and related species. M. edited by: Ko, Newman, P., Reimann, S., and Strahan, S.,. Geneva, Switzerland.2013

Sturrock, G. A., Etheridge, D. M., Trudinger, C. M., Fraser, P. J. and Smith, A. M.: Atmospheric histories of halocarbons from analysis of Antarctic firn air: Major Montreal Protocol species, Journal of Geophysical Research Atmospheres, 107, 24, 10.1029/2002JD002548, 2002.

Chapter 3

Chlorinated very-short-lived substances in East Asia and South East Asia

3.1 Introduction

The success of the Montreal Protocol in phasing out the consumption of ozone-depleting substances has facilitated the gradual healing of the ozone layer. However, recent research has revealed that increasing emissions of chlorinated very-short-lived substances (chlorinated VSLSs) threaten to delay this recovery. VSLSs are defined as trace gases whose local lifetimes are comparable to, or shorter than, interhemispheric transport timescales (Carpenter et al., 2014). Historically, VSLSs were not considered damaging to the ozone layer as they have relatively short atmospheric lifetimes (less than six months) and are not expected to reach the stratosphere in large quantities. Their short lifetimes and corresponding low ozone depletion potentials (ODPs) has led them to be excluded from the Montreal Protocol (Hossaini et al., 2015). However, chlorinated VSLSs, which are mainly anthropogenic in origin, have been found to be increasing (~1.3 ± 0.3 ppt Cl yr^{-1}, 2008–2012) in contrast to the decline of long-lived controlled chlorinated substances (-13.4 ± 0.9 ppt Cl yr^{-1}) over the same period (Carpenter et al., 2014). Increased anthropogenic emissions of VSLSs containing chlorine, particularly from tropical sources, are an emerging issue for stratospheric ozone. The relative contribution of these emissions could become important as levels of ozone-depleting substances (ODSs) controlled under the Montreal Protocol decline (Carpenter et al., 2014). Chapter 1 has provided evidence on the growing emissions of chlorinated VSLSs including how they can be transported from the boundary layer, reach the upper troposphere and potentially pose a threat to the ozone layer in the stratosphere. Therefore, continued research into and monitoring of chlorinated VSLSs are essential to ensure environmental protection against ozone loss. Further observations are also required to understand

the origin of those emissions, especially in the South East Asia and East Asia region, which motivates this present study.

This chapter focuses on the chlorinated VSLSs most widely reported in the background atmosphere, dichloromethane (CH_2Cl_2), trichloromethane ($CHCl_3$), tetrachloroethene (CCl_2CCl_2, shortened to C_2Cl_4), and 1,2-dichloroethane (CH_2ClCH_2Cl). A summary of sources, sinks and atmospheric lifetime of each chlorinated VSLS are presented in Table 3.1. According to Montzka et al. (2011), chlorinated VSLSs are primarily anthropogenic in origin, with the exception of $CHCl_3$. For $CHCl_3$, up to ~50% can be accounted for by anthropogenic sources (Trudinger et al., 2004). The abundances of chlorinated VSLSs in the background atmosphere have been reported by two main surface networks, the Advanced Global Atmospheric Gases Experiment (AGAGE) and the National Oceanic and Atmospheric Administration, U.S. (NOAA). The atmospheric abundance of CH_2Cl_2 increased from 21.7 ppt to 25.1 ppt in 2012 (NOAA, Carpenter et al., 2014). C_2Cl_4 has been found to have decreased in the atmosphere, with an abundance of 1.18 ppt in 2012, 63% lower than when observations began in 1994 (NOAA, Carpenter et al., 2014). For $CHCl_3$, no significant trend has been seen at present. An average annual mole fraction for 2012 was found to be 7.53 ppt (AGAGE, Carpenter et al., 2014). The current background concentrations and longer-term trends of CH_2ClCH_2Cl are unknown since no long-term atmospheric measurements of CH_2ClCH_2Cl have been made or reported for over a decade. Although (1) no current data are available for CH_2ClCH_2Cl and (2) C_2Cl_4 as well as $CHCl_3$ do not exhibit any increases in mixing ratios, their tropospheric abundances need to be monitored to allow assessment of (1) their current and future changes in tropospheric abundance and (2) their contribution to stratospheric chlorine in order to reflect on their impact towards stratospheric ozone depletion. This information is crucial in order to make an informed decision as to whether chlorinated VSLSs should be covered under the Montreal Protocol.

Table 3.1 *Summary of sources, sinks and atmospheric lifetime of each chlorinated VSLS.*

Compound	Sources		Local Lifetime (days) WMO (2014)	Atmospheric sinks
	Anthropogenic	**Natural**		
CH_2Cl_2	• Paint remover • Foam blowing agent • Chemical processes	• Biomass burning • Phytoplankton production	144	Troposphere • Reaction with OH Stratosphere • Photolysis
CH_2ClCH_2Cl	• Polymer • Rubber production	• Biomass burning	65	
$CHCl_3$	• Used in the production of HFC-22	• Biomass burning • Soils such as drained peat land pasture soils or blanket peat bogs	149	
C_2Cl_4	• Dry-cleaning solvent • Metal degreasing		90	

Source: adapted from Carpenter et al. (2014)

This chapter provides an assessment of the abundances of four chlorinated VSLSs in the regions of East Asia and South East Asia. The findings from sampling stations located in Taiwan and Bachok are presented. The overall aim of the multiyear regional measurements was to improve our knowledge on the tropospheric abundances of a wide range of halocarbon compounds including chlorinated VSLSs. Specifically, this chapter aims:

1. To assess the variability of chlorinated VSLSs at both sampling locations and identify any enhancement above background levels for the chlorinated VSLSs.

2. To investigate potential source regions and emission sectors that may contribute towards the variations in chlorinated VSLS levels.

3. To examine the influence of meteorological features in the long-range transport of chlorinated VSLSs to Bachok.

It is important to highlight that the following section will not start off with the typical section on methodology. The methodology for this study is presented in Chapter 2 and is not going to be discussed in detail here. Instead, this chapter will proceed to the presentation and discussion of key findings (Section 3.2). Finally, some conclusions are made and suggestions of further study are given in Section 3.3.

3.2 Results & Discussion

3.2.1 Observation of chlorinated VSLS mixing ratios

3.2.1.1 Taiwan

Overall, CH_2Cl_2 contributed the largest fraction of the total chlorinated VSLSs measured in Taiwan across the four years of measurements, followed by CH_2ClCH_2Cl, $CHCl_3$ and C_2Cl_4 (Table 3.2). Figure 3.1 and Table 3.2 show the four chlorinated VSLS data from Taiwan during the campaigns, which took place between 2013 and 2016. Overall, the mixing ratios of all chlorinated VSLSs exceeded background levels. For instance, the median values of CH_2Cl_2 measured throughout each Taiwan campaign were around a factor of seven to nine greater than the median value of CH_2Cl_2 measured in background air samples (Table 3.2).

The chlorinated VSLSs showed an enhancement of mixing ratios mostly on the same days (examples are labelled (a), (c), (d), (e) and (f) in Figure 3.1). The spikes in mixing ratios of chlorinated VSLSs generally occurred when the NAME footprints showed the air most likely came from the boundary layer over eastern China or the peninsula of Korea (examples are indicated by (a), (d), and (e) in Figure 3.1). The NAME footprints also suggested an influence from Taiwan on the high mixing ratios

of CH_2Cl_2 (examples indicated by (c) and (f)). Whereas when lower mixing ratios were observed, the NAME footprints showed that the air masses still originated from the north but instead travelled between eastern China and the peninsula of Korea, e.g. (b).

Table 3.2: *Summary of the chlorinated VSLS data obtained from measurement campaigns in Taiwan. For comparison, also shown are the approximate median background concentrations and ranges for each chlorinated VSLS in the remote marine boundary layer (MBL), taken from the most recent WMO ozone assessment (Carpenter et al., 2014).*

	2013		2014	
	Median	**Range**	**Median**	**Range**
CH_2Cl_2	239.3	76.8 - 671.8	265.3	77.9 - 741.0
CH_2ClCH_2Cl	118.5	23.7 - 820.1	82.4	17.6 - 290.2
$CHCl_3$	32.9	11.6 - 199.3	35.1	13.8 - 103.2
C_2Cl_4	4.4	1.7 - 16.6	5.5	1.6 - 18.6

	2015		2016		MBL (WMO 2014)[a]	
	Median	**Range**	**Median**	**Range**	**Median**	**Range**
CH_2Cl_2	198.6	59.4 - 536.7	270.7	84.5 - 1203.4	28.4	21.8 - 34.4
CH_2ClCH_2Cl [b]	59.0	12.8 - 355.8	-	-	3.7	0.7-14.5 [c]
$CHCl_3$	28.0	12.7 - 125.1	39.2	14.4 - 149.4	7.5	7.3 - 7.8
C_2Cl_4 [b]	4.3	1.8 - 17.7	-	-	1.3	0.8-1.7

Note:

[a] *The WMO data are a compilation of all reported global measurements up to, and including, the year 2012.*

[b] *CH_2ClCH_2Cl and C_2Cl_4 data were not available for the 2014 and 2016 campaigns.*

[c] *The CH_2ClCH_2Cl MBL data actually date back to the early 2000s. No recent data were reported.*

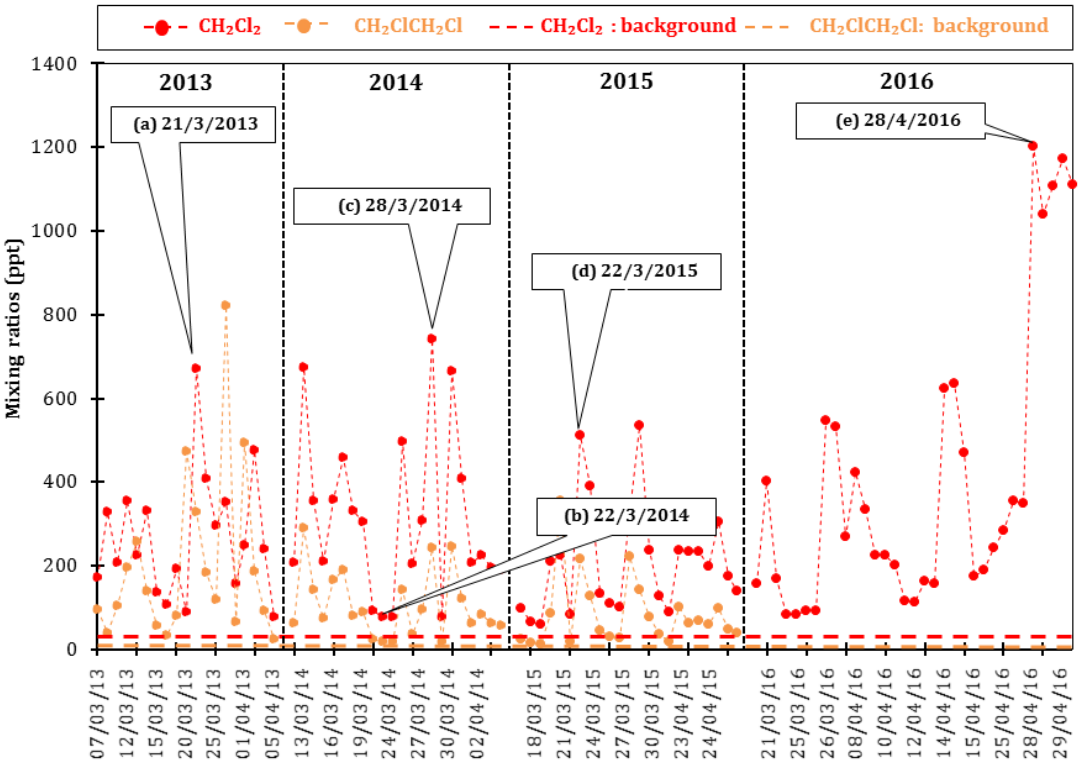
CH2Cl2
CH2ClCH2Cl
CH2Cl2 : background
CH2ClCH2Cl: background
Mixing ratios (ppt)
2013
2014
2015
2016
(a) 21/3/2013
(b) 22/3/2014
(c) 28/3/2014
(d) 22/3/2015
(e) 28/4/2016

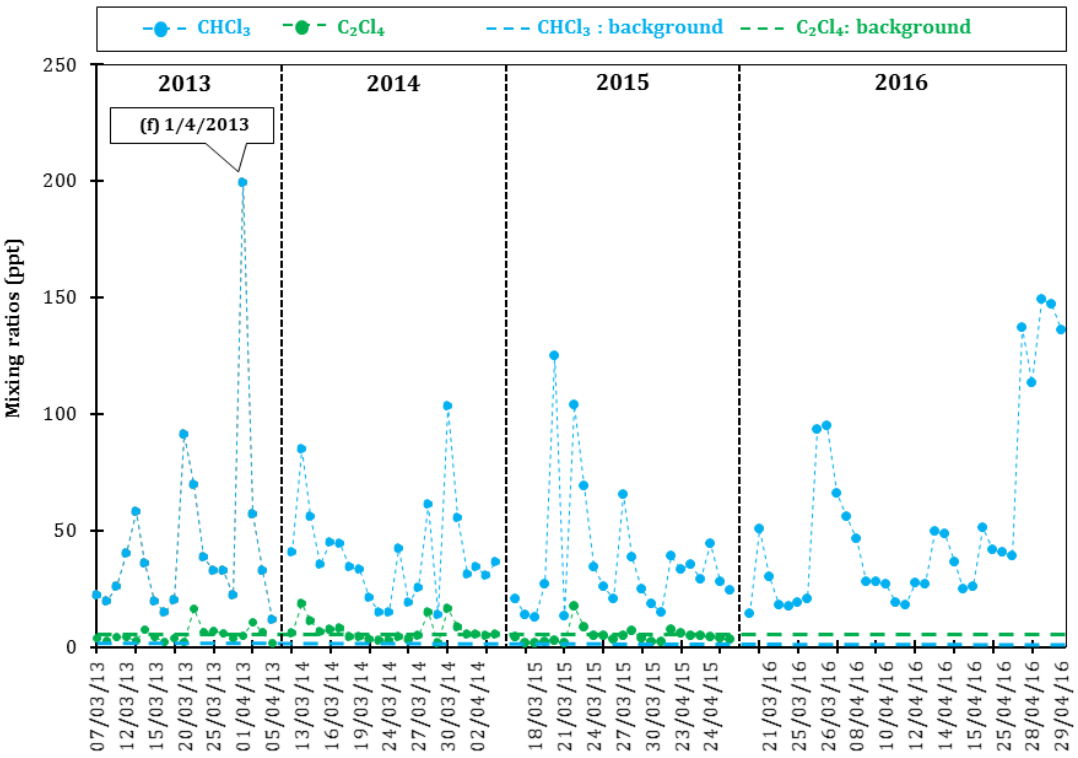
CHCl3
C2Cl4
CHCl3 : background
C2Cl4: background
Mixing ratios (ppt)
2013
2014
2015
2016
(f) 1/4/2013

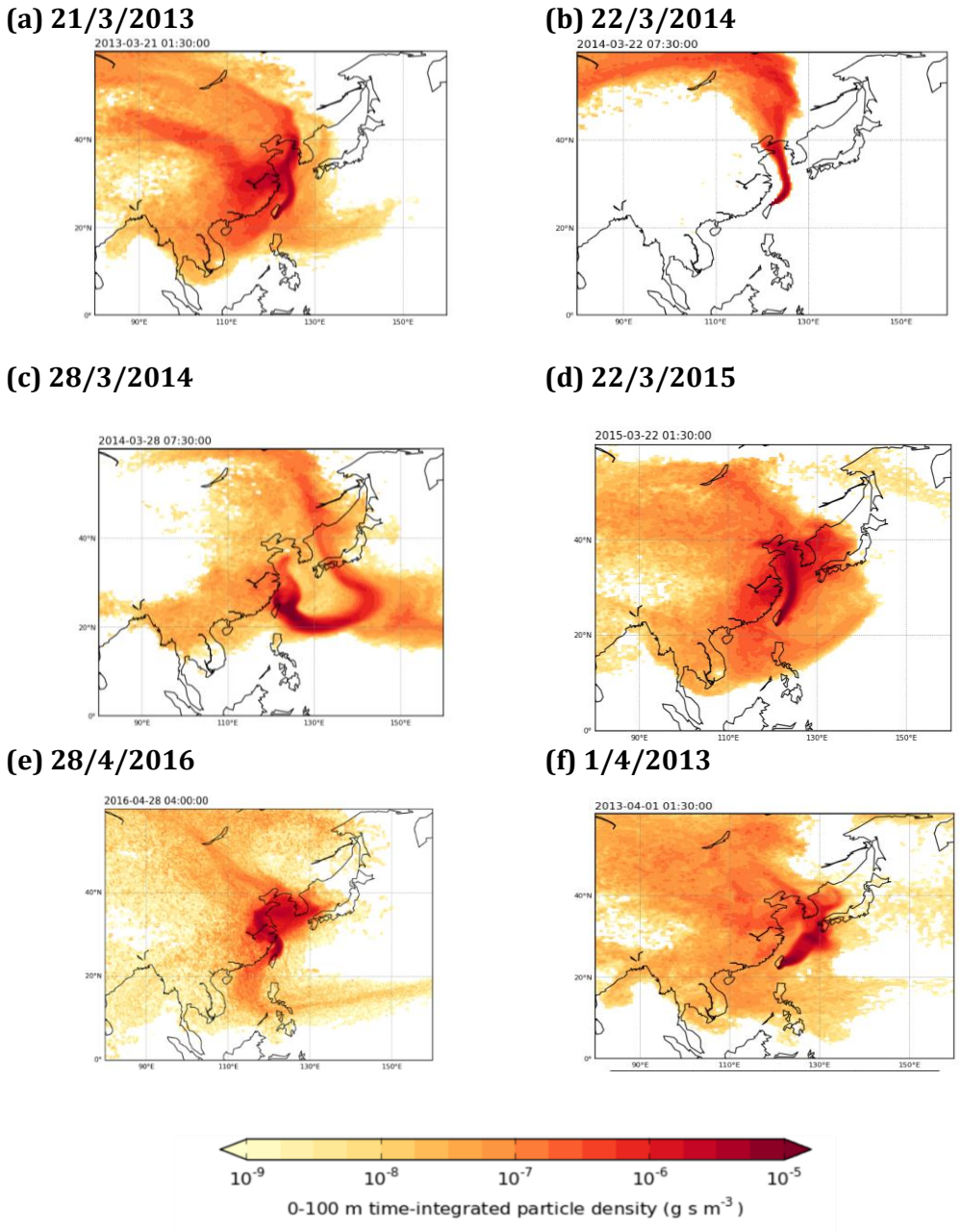

Figure 3.1: Upper panel: *Mixing ratios (ppt) of the four chlorinated VSLSs in 97 air samples collected in Taiwan during campaigns between 2013 and 2016. The approximate median background concentrations for each chlorinated VSLS in the remote marine boundary layer (MBL) in 2012 are represented by the dashed lines. Also shown are examples where the observed mixing ratios of four chlorinated VSLSs were unusually high, indicated by (a), (c), (d), (e) and (f). For comparison, (b) represents a mixing ratio that is much closer to the expected background level.* ***Lower panel, (a) to (f):*** *NAME footprint maps generated from a back-trajectory analysis indicating the likely origin of the air sampled in Taiwan, with the darker colours indicating greater influence. The colour scale is logarithmic and represents the calculated time-averaged concentration within surface layer (0–100 m) during the 12 days prior to the sampling days given a point release in Taiwan.*

3.2.1.2 Bachok

When comparing the contribution of each chlorinated VSLS to total chlorinated VSLSs measured in Bachok, CH_2Cl_2 contributed the largest fraction (~70%) during both campaigns, followed by CH_2ClCH_2Cl, $CHCl_3$ and C_2Cl_4 (Table 3.3).

During both campaigns, in 2013/2014 and 2015/2016, the mixing ratios of the four chlorinated VSLSs were above the background levels (Table 3.3 and Figure 3.2). For example, the median values of CH_2Cl_2 in 2013/2014 and 2015/2016 were 86.1 ppt and 70 ppt, respectively, three and 2.5 times higher than the background value (28.4 ppt, range = 21.8 – 34.4 ppt).

Table 3.3: *Summary of the chlorinated VSLS data obtained from measurement campaigns in Bachok. For comparison, also shown are the approximate median background concentrations and ranges for each chlorinated VSLS in the remote marine boundary layer (MBL), taken from the most recent WMO ozone assessment (Carpenter et al., 2014).*

	1st campaign (2013/2014)		**2nd campaign (2015/2016)**		**MBL (WMO 2014)[a]**	
	Median (ppt)	Range (ppt)	Median (ppt)	Range (ppt)	Median (ppt)	Range (ppt)
CH_2Cl_2	86.1	66.4 - 352.2	70.0	47.4 - 268.0	28.4	21.8 - 34.4
CH_2ClCH_2Cl	40.6[b]	16.4 - 119.5	16.0	8.5 - 78.2	3.7	0.7 - 14.5[c]
$CHCl_3$	15.2	12.8 - 30.5	13.8	9.7 - 35.4	7.5	7.3 - 7.8
C_2Cl_4	2.0	1.6 - 9.5	2.1	1.3 - 7.9	1.3	0.8 - 1.7

Note:
[a] *The WMO data are a compilation of all reported global measurements up to, and including, the year 2012.*

[b] *CH_2ClCH_2Cl was only analysed in 16 of the 28 samples during the 2013/2014 campaign.*

[c] *The CH_2ClCH_2Cl MBL data actually date back to the early 2000s. No recent data were reported.*

Interestingly, some unusual enhancements in the mixing ratios of all chlorinated VSLSs were observed on certain days throughout the campaigns (examples are labelled (a), (c), (d), (e) and (f) in Figure 3.2). It appears that the variation of chlorinated VSLSs measured at Bachok could have been influenced by the pathway along which the air masses had travelled prior to reaching Bachok. For example, the spikes in mixing ratios usually occurred when the NAME footprints showed that the air most likely came from the boundary layer over eastern China, Taiwan or

Indochina at some point prior to reaching Bachok (indicated by (a), (c), (d), (e) and (f) in Figure 3.2). Whereas when lower mixing ratios were observed, the NAME footprints, e.g. (b), showed very little influence from the regions mentioned above. Instead there was more influence from marine sector with the air mass having travelled predominantly over the South China Sea and Pacific Oceans with some influence from the Philippines and Borneo.

Also noticeable is that $CHCl_3$ showed additional high mixing ratios on two more days during the 2013/2014 campaign (labelled (g) and (h) in Figure 3.2). In contrast, the mixing ratios of the three other compounds were low on those two days. The NAME footprints for these two days showed that the air masses that arrived at Bachok were primarily from the South China Sea and not from the potential source region, eastern China. This suggests that the sources of high mixing ratios of $CHCl_3$ on the 31st of January and the 1st of February 2014 were mainly natural, i.e. from marine or perhaps local sources (detailed discussion in Section 3.2.2.2). This further emphasizes that $CHCl_3$ had some different source types to other chlorinated VSLSs on those two days.

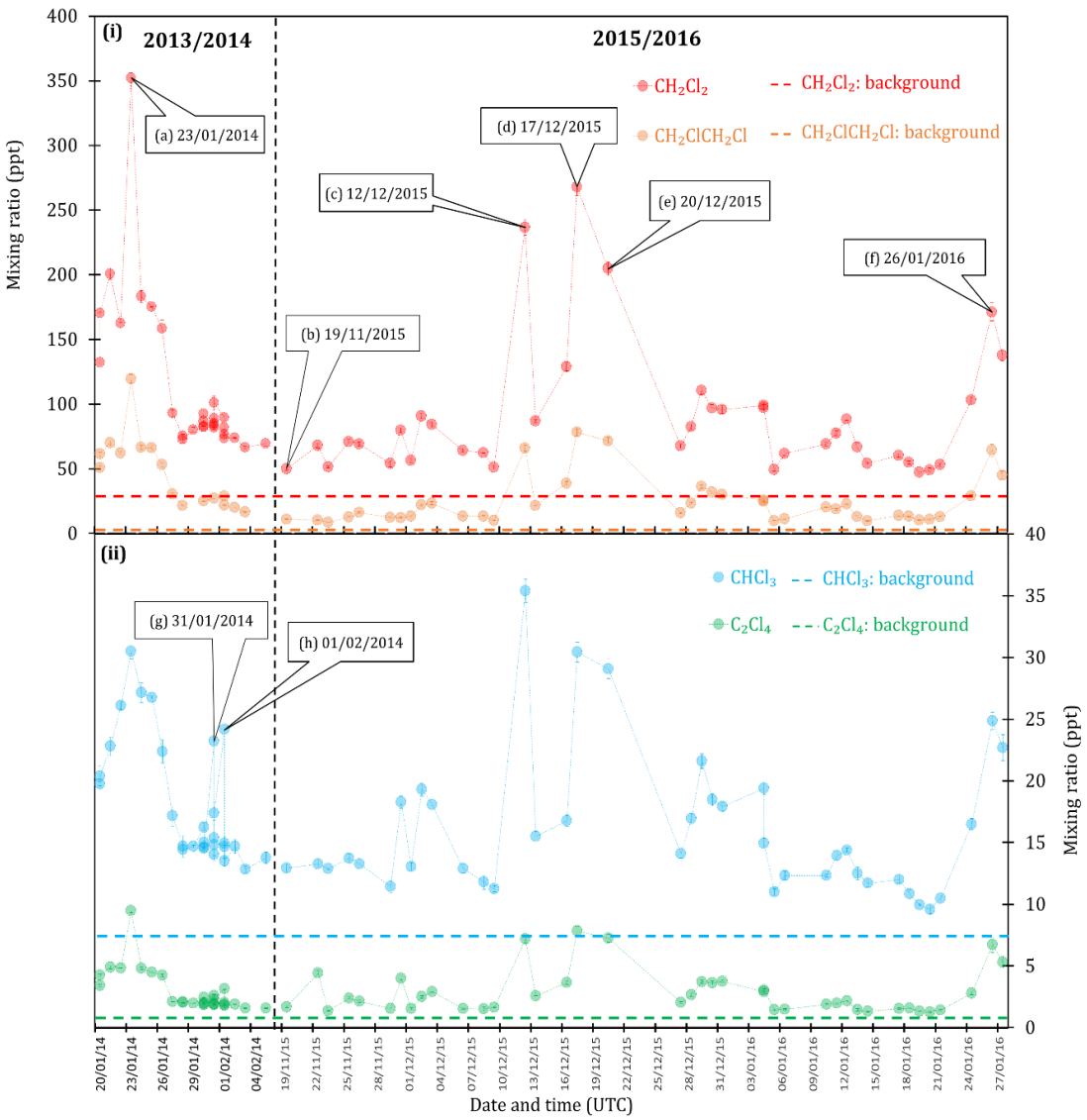
(i)
2013/2014
2015/2016
CH_2Cl_2
CH_2Cl_2: background
CH_2ClCH_2Cl
CH_2ClCH_2Cl: background
(a) 23/01/2014
(b) 19/11/2015
(c) 12/12/2015
(d) 17/12/2015
(e) 20/12/2015
(f) 26/01/2016
Mixing ratio (ppt)
(ii)
$CHCl_3$
$CHCl_3$: background
C_2Cl_4
C_2Cl_4: background
(g) 31/01/2014
(h) 01/02/2014
Mixing ratio (ppt)
Date and time (UTC)

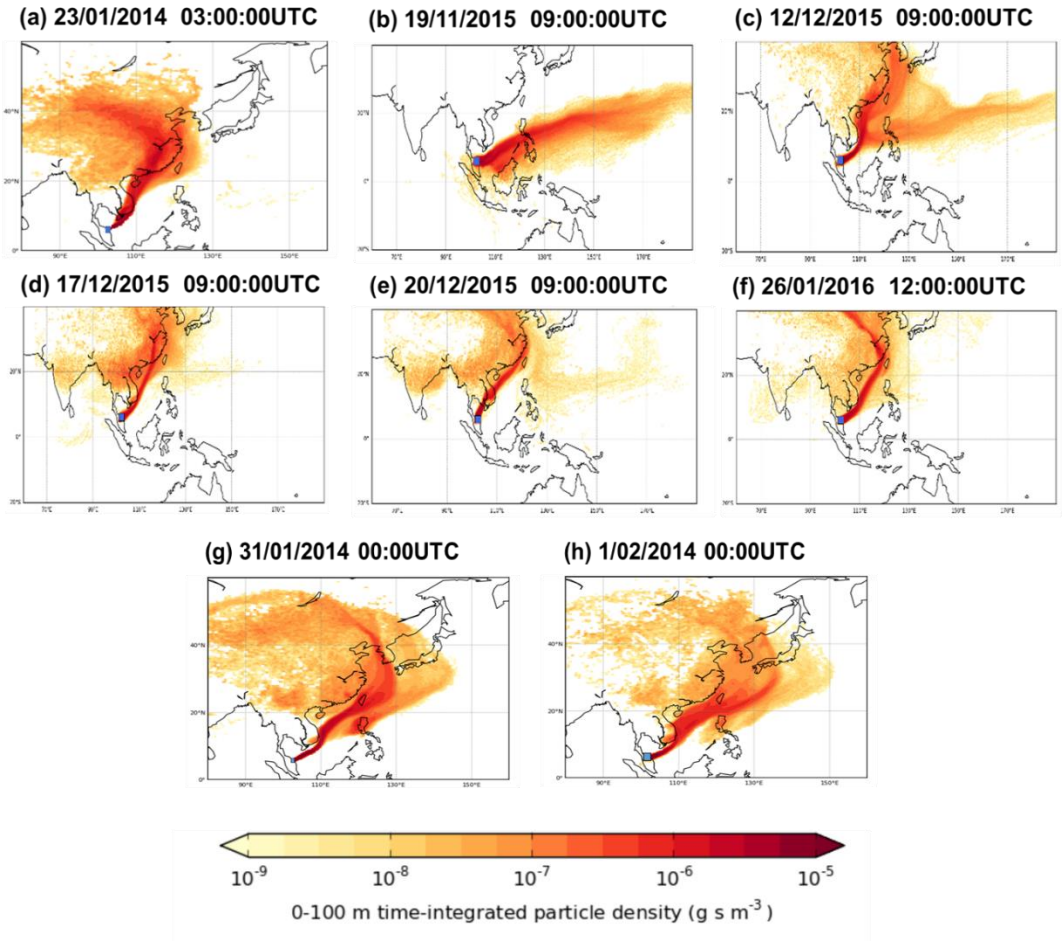

Figure 3.2: Upper panel: *Mixing ratios (ppt) of the four chlorinated VSLSs in 68 air samples collected at Bachok during the Northern Hemisphere winters, 2013/2014 and 2015/2016. The approximate median background concentrations for each chlorinated VSLS in the remote marine boundary layer (MBL) in 2012 are represented by the dashed lines. Also shown are the examples where the observed mixing ratios of the four chlorinated VSLS were unusually high, indicated by (a), (c), (d), (e), (f), (g) and (h). For comparison, (b) represents a mixing ratio that is much closer to the expected background level.* ***Lower panel, (a) to (f):*** *NAME footprint maps generated from a back-trajectory analysis indicating the likely origin of the air sampled at Bachok, with the darker colours indicating greater influence. The colour scale is logarithmic and represents the calculated time-averaged concentration within surface layer (0–100 m) during the 12 days prior to the sampling days given a point release at Bachok.*

3.2.1.3 Synthesis

The mixing ratios of the chlorinated VSLSs generally exceeded background levels in both Taiwan and Bachok, demonstrating a widespread regional enhancement. The mixing ratios were often higher in Taiwan than Bachok, indicating that Taiwan is located relatively closer to major source regions. By examining the NAME footprints, some preliminary conclusions were drawn on the possible origins of the compounds, especially when the mixing ratios were extraordinarily high. The NAME footprints suggested the influence of the China region towards the air masses that arrived in Bachok and Taiwan when the mixing ratios were extraordinarily high. China is an Article 5 country under the Montreal Protocol, meaning it is still allowed to produce and use some halocarbons under the terms of the Protocol and its Amendments (Shao et al., 2011). Therefore, the elevated mixing ratios of chlorinated VSLSs above background levels in Taiwan could have been due to appreciable emissions of chlorinated VSLSs from extensive industrial use in China that were then transported to Taiwan. The emission sources in China could also have been responsible for the higher median concentrations in Bachok, these being higher than the global median. The lifetime of these chlorinated VSLSs means that they will persist for several weeks and so will be mixed into the regional background air. The lower observed concentrations of chlorinated VSLSs in Bachok compared to Taiwan is consistent with China being the main source for chlorinated VSLS in this region. Additionally, dilution, i.e. mixing with background air, could be the main reason for the reduced concentrations of chlorinated VSLSs in Bachok as they have had time to mix from emission to detection.

Although the high mixing ratios of chlorinated VSLSs above the background level as observed in Bachok may reflect a substantial contribution from Chinese industrial emissions, nonindustrial sources may also be present in the region and could affect the observed mixing ratios of chlorinated VSLSs. All chlorinated VSLSs except C_2Cl_4 can originate from nonindustrial sources, mainly biomass burning and oceanic sources (Leedham et al., 2015). That Bachok is located in a maritime area with oceanic source regions nearby and that biomass burning is widespread in the tropics suggest the potential influence of nonindustrial sources towards the variations in chlorinated VSLSs.

It is also highly likely that the peak concentrations of chlorinated VSLS in Bachok were influenced by meteorological conditions. Previous literature has suggested that the observed enhancements in mixing ratios of several trace gases in the region were caused by rapid meridional transport, in the form of "cold surges", from the relatively polluted East Asian land mass. For instance, using trajectory calculations and observations for one Northern Hemisphere winter, Ashfold et al. (2015) showed that cold surges could rapidly (over a few days) transport polluted air masses from East Asia to tropical Southeast Asia. Oram et al. (2017) and Adcock et al. (2018) presented further measurements and model results that demonstrated the likely importance of this mechanism for transporting large quantities of several chlorinated compounds that could deplete ozone from East Asian emission sources to the tropics. However, the influence of cold surges towards atmospheric composition is still unclear. There are several studies (e.g. Liu et al. (2003), Wang et al. (2016)) that have investigated the relationship between cold surges and atmospheric composition away from tropics. Nevertheless, little information is available on the importance of cold surge for the tropics. This will be discussed in detail in Section 3.2.4 in which a quantitative approach is employed in order to test if enhancements of mixing ratios of chlorinated VSLS in Bachok coincide with the occurrence of cold surge events.

3.2.2 Interspecies correlations of chlorinated VSLS

It is known that measured chlorinated VSLSs do not all originate from the exactly the same sources (Table 3.1). However, the temporal patterns of all compounds throughout the whole campaign periods both in Taiwan (Figure 3.1) and Bachok (Figure 3.2) seem comparable which suggests that the compounds are co-emitted, or at least coming from same source location(s). In this section, interspecies correlation analysis was performed to identify if any connection exists between the four measured chlorinated VSLSs. The strengths of the relationships were measured using the Spearman correlation coefficients (R) that inform on how strongly two variables are related to each other. The R value varies between 0 and 1 with a perfect correlation represented by an R value of 1. High levels of correlation will indicate combined emissions or source locations.

The interspecies correlations of four chlorinated VSLSs in air samples measured in Taiwan and Bachok are discussed in Section 3.2.2.1 and Section 3.2.2.2, respectively.

3.2.2.1 Taiwan

Figure 3.3 shows the correlation plots between CH_2Cl_2 and other chlorinated VSLSs. The interspecies correlations for the other three compounds (CH_2ClCH_2Cl, $CHCl_3$ and C_2Cl_4) are presented in the form of correlation matrices (Table 3.4). In most cases, CH_2Cl_2 correlated significantly with all chlorinated VSLSs throughout the multiyear campaigns.

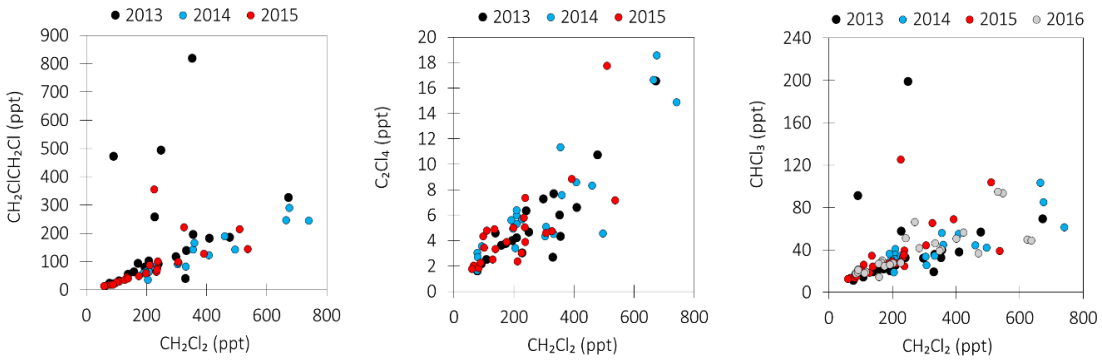

Figure 3.3: *Interspecies correlations between CH_2Cl_2 and other chlorinated VSLSs, CH_2ClCH_2Cl (left panel), C_2Cl_4 (centre panel) and $CHCl_3$ (right panel) during multiyear campaigns in Taiwan.*

Table 3.4 *Correlation matrices for three chlorinated VSLSs, CH_2ClCH_2Cl, $CHCl_3$ and C_2Cl_4 measured in Taiwan. The value presented is the correlation coefficient (R). Correlations that are significant ($p<0.05$) are in bold font.*

	2013			
	CH_2Cl_2	**CH_2ClCH_2Cl**	**$CHCl_3$**	**C_2Cl_4**
CH_2ClCH_2Cl	**0.55**		**0.92**	0.44
$CHCl_3$	**0.53**	**0.92**		**0.46**
C_2Cl_4	**0.79**	0.44	**0.46**	
No. of data points	19	19	19	19

	2014			
	CH_2Cl_2	**CH_2ClCH_2Cl**	**$CHCl_3$**	**C_2Cl_4**
CH_2ClCH_2Cl	**0.96**		**0.88**	**0.84**
$CHCl_3$	**0.87**	**0.88**		**0.94**
C_2Cl_4	**0.79**	**0.84**	**0.94**	
No. of data points	22	22	22	22

	2015			
	CH_2Cl_2	**CH_2ClCH_2Cl**	**$CHCl_3$**	**C_2Cl_4**
CH_2ClCH_2Cl	**0.94**		**0.93**	**0.64**
$CHCl_3$	**0.88**	**0.93**		**0.75**
C_2Cl_4	**0.77**	**0.64**	**0.75**	
No. of data points	23	23	23	23

A reasonable overall correlation suggests that on the whole, the main sources of chlorinated VSLS were co-located. However, some significant outliers (Figure 3.4) provide an insight into other possible locations that may only be a source of one of the compounds. For example, during the 2013 campaign, there are four samples [denoted by (a),(b), (c) and (d)] where the points are above the CH_2Cl_2 and CH_2ClCH_2Cl regression plot (Figure 3.4 (a), left panel), with three of them with particularly high mixing ratios for CH_2ClCH_2Cl. Another example is during the 2015 campaign (Figure 3.4 (b), right panel) in which there are three high values for CH_2ClCH_2Cl [denoted by (e) and (f)] identified above the regression plot. All six outliers from Taiwan [labelled (a) to (f) in Figure 3.4 (a)] and five outliers from Bachok [labelled (a) to (f) except (c) in Figure 3.4 (b)] showed high mixing ratios of CH_2ClCH_2Cl and $CHCl_3$ but the mixing ratios of CH_2Cl_2 in the same samples were low. Therefore, it is speculated that the outliers were from samples that had different air mass origins compared to the majority of the samples collected during the Taiwan campaigns.

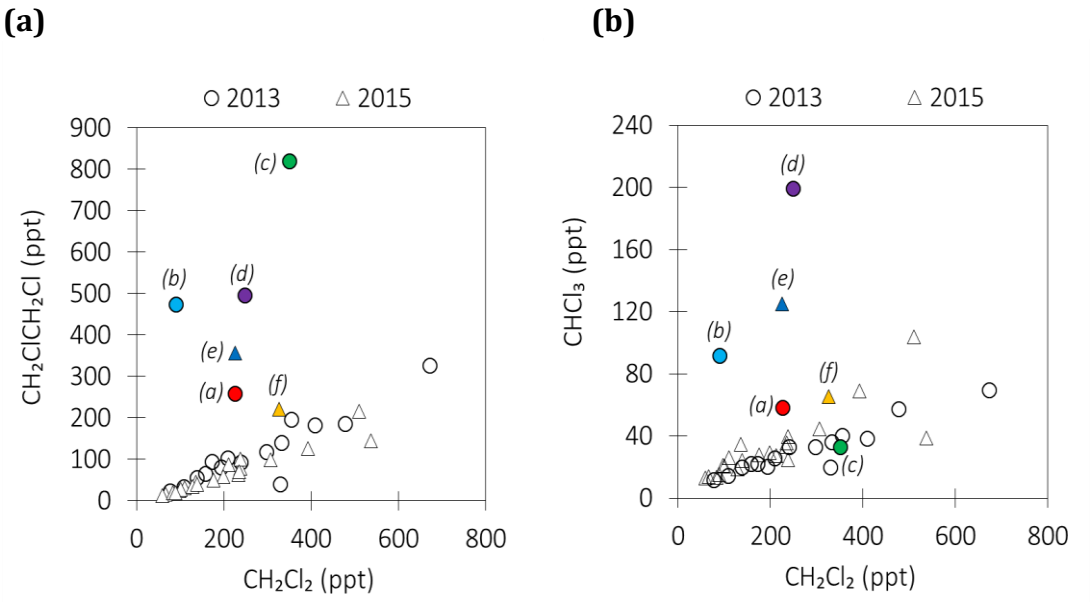

Figure 3.4: (a) *Correlation plot of CH_2Cl_2 and CH_2ClCH_2Cl with a focus on the six outliers in samples collected in 2013 (circles) and 2015 (triangles).* ***(b):*** *Correlation plot of CH_2Cl_2 and $CHCl_3$ with a focus on the six outliers in samples collected in 2013 (circles) and 2015 (triangles).*

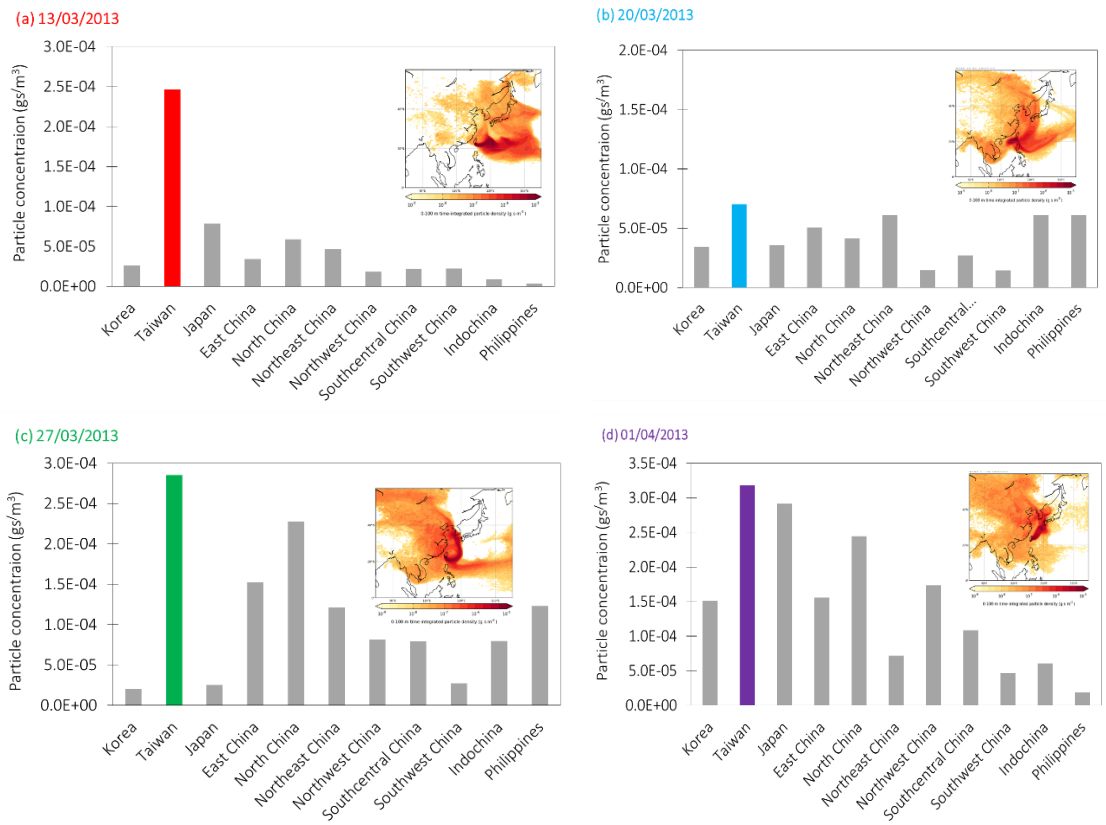

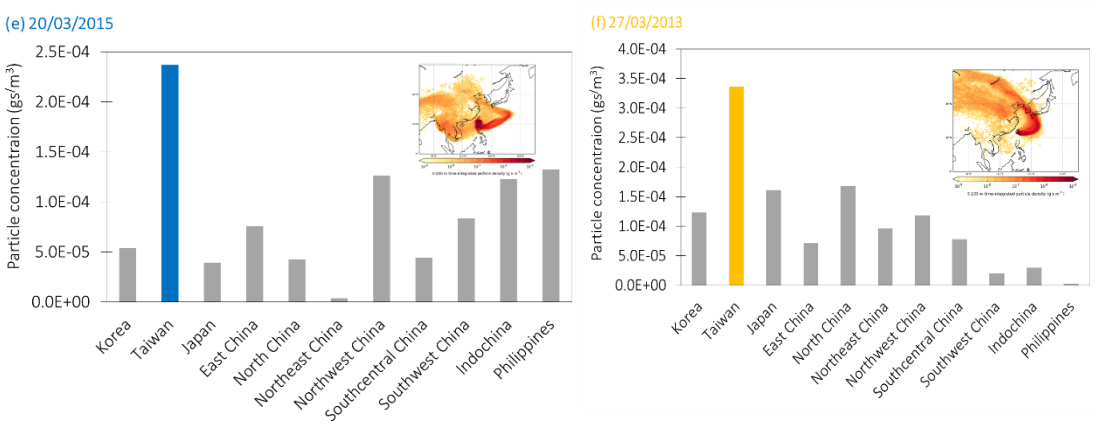

Figure 3.5: *Particle concentration analysis to assess the air masses that have resided over different regions during the 12 days prior to sampling with an insert of NAME footprints to give an overview of the origin of air masses for the six affected samples identified in Figure 3.4.*

To investigate the origin of the air masses of the six samples, the individual NAME footprints for all affected samples were examined and a particle concentration analysis conducted to assess the air masses that have resided over different regions during the 12 days prior to sampling. This is to assess to what extent those regions influenced the sampled air. The results of the analysis are shown in Figure 3.5.

In general, these six samples were collected when the air masses had spent a significant portion of the previous 12 days over Taiwan, which suggests the source of the high concentrations of both the CH_2ClCH_2Cl and $CHCl_3$ [denoted by (a), (b), (d), (e) and (f) in Figure 3.4(a) and (b)] may have been of local origin. Interestingly, the sample collected on 27 March 2013 [denoted by (c) in Figure 3.4 (b)] showed very high concentrations of CH_2ClCH_2Cl but low concentrations of $CHCl_3$. The main origin of the air mass for that particular sample [(Figure 3.5(c)] appears to have been Taiwan, which suggests that Taiwanese air masses might be sources of CH_2ClCH_2Cl but not $CHCl_3$.

To summarise, all six samples demonstrated (1) the influence of local sources i.e. Taiwanese and (2) less influence from East China unlike the majority of the samples collected from Taiwan in 2013 and 2015.

3.2.2.2 Bachok

Recall that in Section 3.2.1.2, the mixing ratios of $CHCl_3$ in air samples collected on the 31st January 2014 and the 1st February 2014 (Figure 3.2) were high in comparison to the other three measured chlorinated VSLSs. Whilst all air samples collected in Bachok were taken between 12 noon and 6 pm local time, the two samples collected on the 31st January 2014 and the 1st February 2014 were collected at 8.00 am local time.

This means that those two samples were collected when air originated from the land prior moving to the sea as part of the local land-sea breeze effect. The NAME particle concentration analysis demonstrated in Figure 3.6 shows that there is a diurnal pattern in the NAME particles concentrations over the Peninsula Malaysia land area, with higher values during the night and early morning. This means that there is a greater influence of emissions from the land on the samples collected at the site at this time. The high concentrations of $CHCl_3$ found in these samples could result from various natural or local sources such as tropical terrestrial emissions and biomass burning. The latter might be possible as on certain days of the campaigns fires were started by local people to burn residential rubbish.

Since the Bachok campaigns aimed to investigate long-range transport to the tropics, we are more interested in samples in which the air has travelled across the South China Sea with less mixing with local sources. Hence, in this section, I have decided to exclude the two samples in my analysis and made several assumptions: (1) the air travels across the South China Sea; and (2) all chlorinated VSLSs are emitted in the same general location but not necessarily from the same point sources.

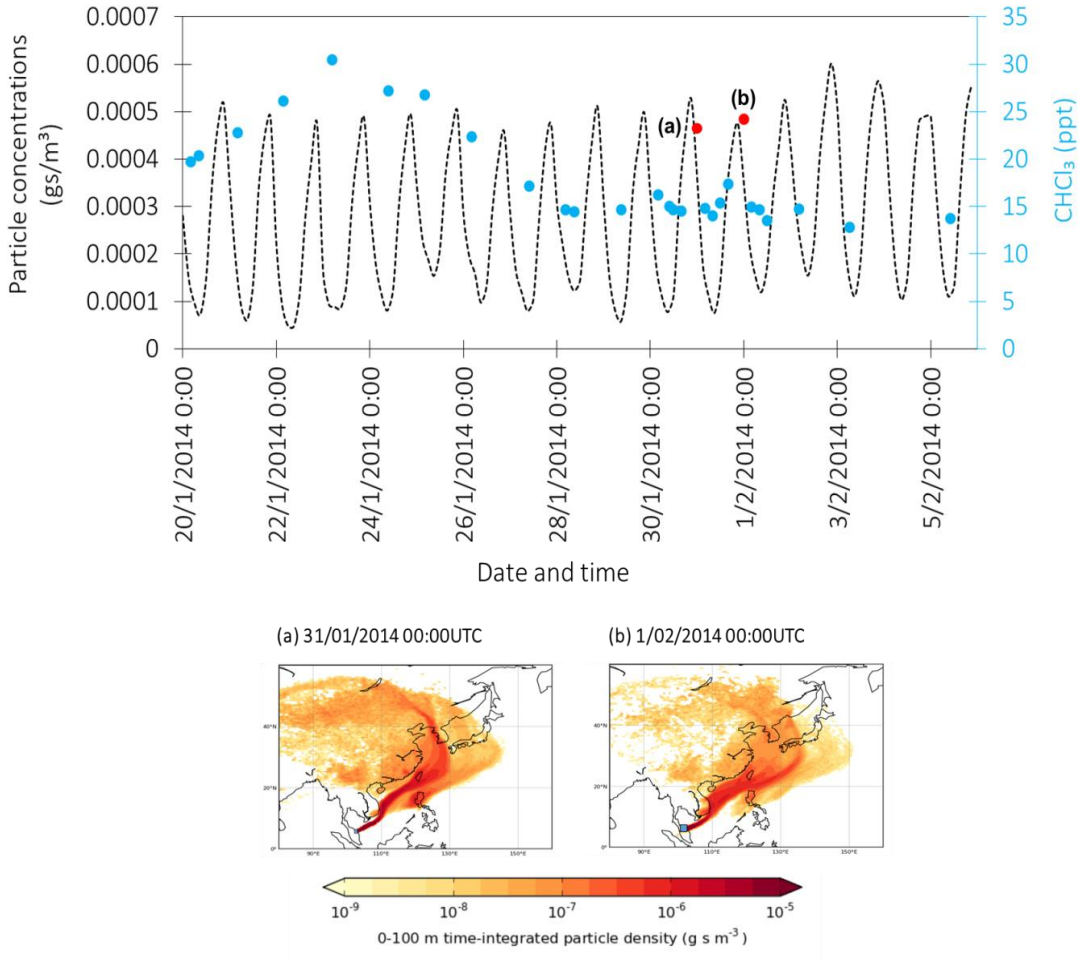

Figure 3.6: Upper panel: *The diurnal pattern of concentrations of particles (g s/m^3) for air masses arriving in Bachok during the 2013/2014 campaign (dashed lines). Higher values indicated a greater influence of emissions from the land (i.e. Bachok) rather than marine emissions. Also presented are the mixing ratios of $CHCl_3$ (ppt), represented by blue circles. The times on the x-axis are in UTC (Local time = UTC + 8 hours).* ***Lower panel:*** *NAME footprints indicating the origin of air masses for samples collected on (a) 31st January 2014 and (b) 1st February 2014. Both samples demonstrate unusually high mixing ratios of $CHCl_3$ (red circles).*

The results of the interspecies correlation show that there were very good correlations ($R > 0.8$, $p < 0.05$) between all four measured chlorinated VSLSs (Figure 3.7, Table 3.5). This could possibly be because the air masses that transported the chlorinated VSLSs to Bachok originated or travelled across the same regions and so the chlorinated VSLSs are very likely to have similar source emissions.

(a)

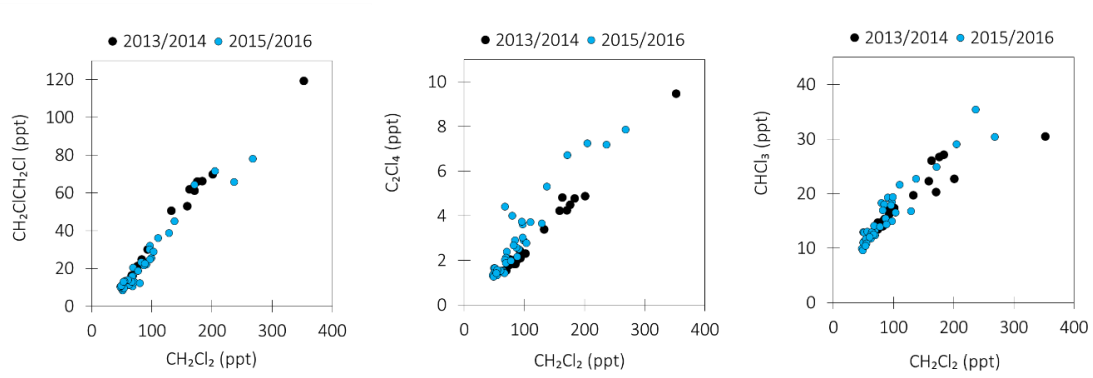
2013/2014
2015/2016
CH2ClCH2Cl (ppt)
CH2Cl2 (ppt)
C2Cl4 (ppt)
CHCl3 (ppt)

(b)

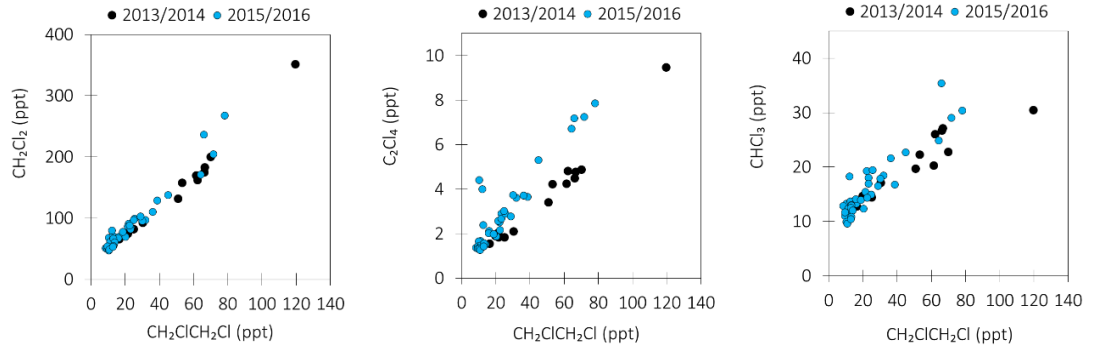
2013/2014
2015/2016
CH2Cl2 (ppt)
CH2ClCH2Cl (ppt)
C2Cl4 (ppt)
CHCl3 (ppt)

(c)

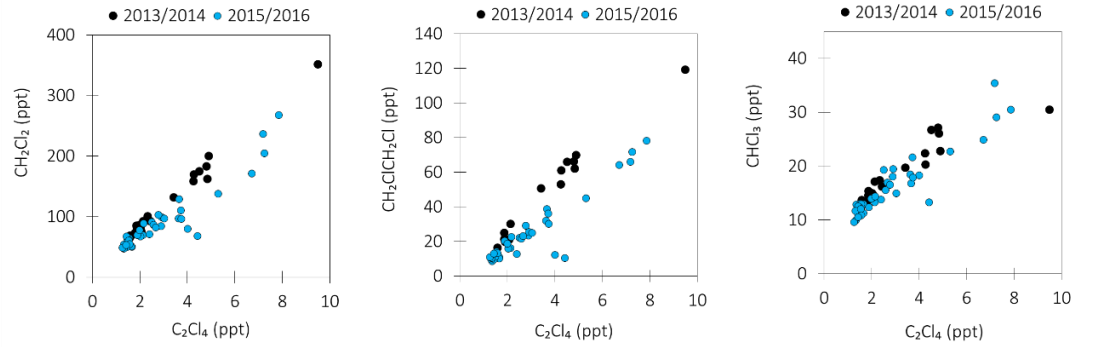
2013/2014
2015/2016
CH2Cl2 (ppt)
C2Cl4 (ppt)
CH2ClCH2Cl (ppt)
CHCl3 (ppt)

(d)

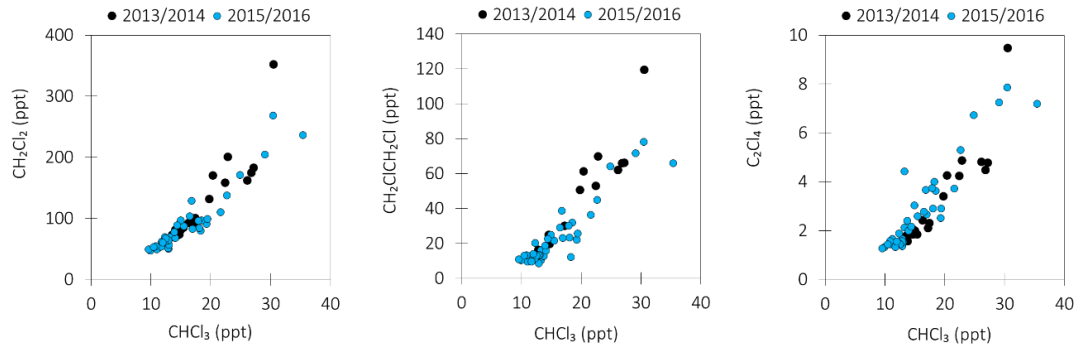

Figure 3.7: *Interspecies correlation of chlorinated VSLSs measured at Bachok. (a) Correlation between CH_2Cl_2 and other chlorinated VSLSs – CH_2ClCH_2Cl (left panel), C_2Cl_4 (centre panel) and $CHCl_3$ (right panel) during the Northern Hemisphere winter 2013/2014 and 2015/2016. (b), (c), (d) The same as (a), but for interspecies correlations of CH_2ClCH_2Cl, C_2Cl_4 and $CHCl_3$ with other chlorinated VSLSs.*

Table 3.5 *Correlation matrices for three chlorinated VSLSs, i.e. CH_2ClCH_2Cl, $CHCl_3$ and C_2Cl_4 measured in Bachok. The value presented is the correlation coefficient (R). Correlations that are significant ($p<0.05$) are in bold font.*

	2013/2014			
	CH_2Cl_2	**CH_2ClCH_2Cl**	**$CHCl_3$**	**C_2Cl_4**
CH_2ClCH_2Cl	**1.00**		**0.94**	**0.95**
$CHCl_3$	**0.94**	**0.93**		**0.90**
C_2Cl_4	**0.85**	**0.95**	**0.90**	
No. of data points	26	26	26	26

	2015/2016			
	CH_2Cl_2	**CH_2ClCH_2Cl**	**$CHCl_3$**	**C_2Cl_4**
CH_2ClCH_2Cl	**0.93**		**0.93**	**0.79**
$CHCl_3$	**0.93**	**0.84**		**0.90**
C_2Cl_4	**0.90**	**0.90**	**0.90**	
No. of data points	40	40	40	40

3.2.2.3 Synthesis

Overall, there were good correlations between all species from both Taiwan and Bachok, indicating that they were emitted from the same general location. Therefore, in the subsequent analysis rather than looking at individual species, only CH_2Cl_2 will be used as an example.

Interestingly, the presence of some significant outliers from the interspecies correlations of chlorinated VSLSs observed in Sections 3.2.2.1 and 3.2.2.2 provide an insight into other possible locations of the sources of the measured compounds. In this study, I have looked at the outliers to try to better understand the sources of these compounds. I demonstrated that the affected samples had significantly different air mass origins from the majority of the samples. The affected samples were influenced by local point sources, which caused the correlation coefficient to change slightly. For example, the correlation coefficients for the Taiwan data vary from year to year and were not as strong as for Bachok. Taiwan samples were expected to be better correlated than Bachok due to the fact that Taiwan is located closer to the source region, i.e. East China (based on the NAME footprints). But this is not the case when the samples were strongly influenced by local Taiwanese sources.

3.2.3 Identification and quantification of possible geographical source region(s) of chlorinated VSLSs

To understand the variations in the chlorinated VSLSs' mixing ratios, the recent histories of the air masses that arrived at the measurement sites needed to be assessed. For that purpose, analyses of the NAME footprints and their relative particle concentrations have been conducted to investigate the possible origins and paths of the particles which arrived at the station during the sampling periods. This exercise was especially important when the mixing ratios were extraordinarily high.

The 2013–2016 measurement campaigns in Taiwan were conducted during the springtime (March to May), the season in which the strongest Asian continental outflow was observed. The monthly NAME footprints demonstrate that during that period, the winter monsoon airflow usually drives Asian continental outflow originating in inland China to the Pacific Ocean (Figure 3.8). The footprints covered various regions north of the tropics which meant that emissions from any of these regions may have impacted air reaching the Taiwanese stations during the periods of campaigns.

(a) 2013 campaign

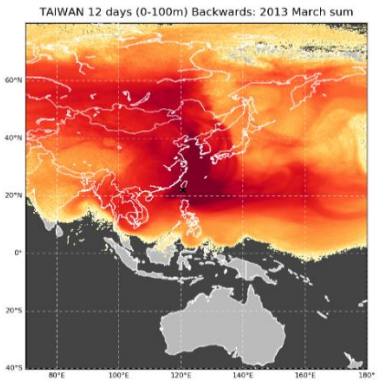

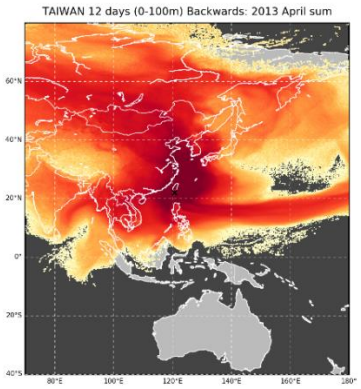

(b) 2014 campaign

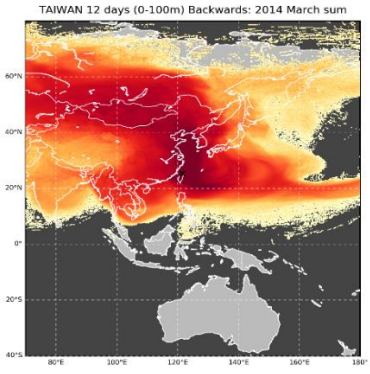

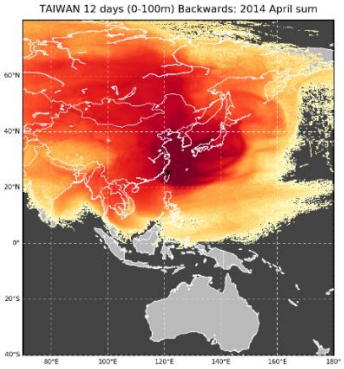

(c) 2015 campaign

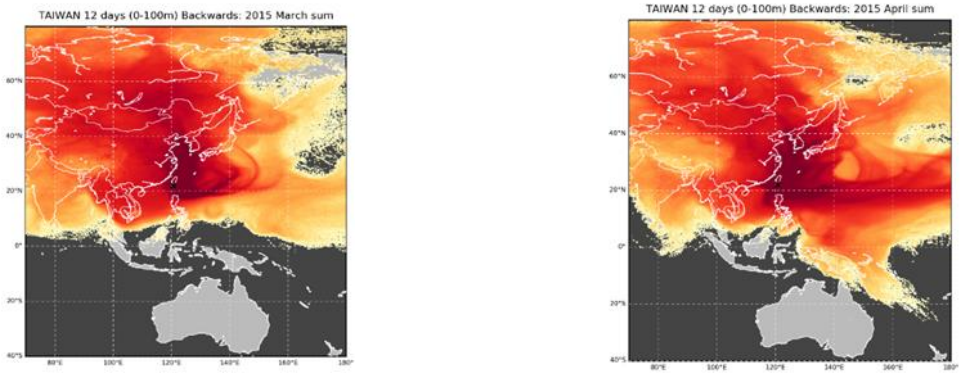

(d) 2016 campaign

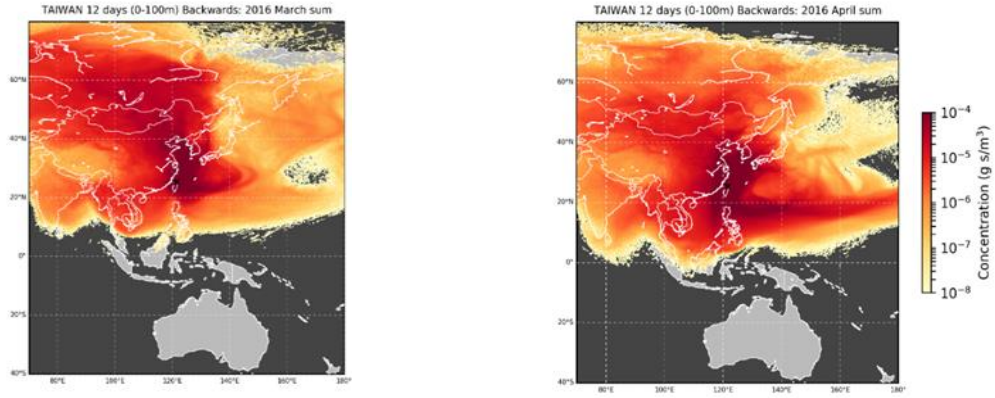

Figure 3.8: *The monthly sum of the NAME footprints for each month are a combination of the daily NAME footprints for each month during the Taiwan campaigns in 2013, 2014, 2015 and 2016. The twelve-day air mass history footprints were calculated for three hourly periods and these have been integrated into monthly footprints. The sum of the NAME footprints provides an overview on the dispersion of the air masses and possible countries that might contribute emissions to air masses that arrived in that particular month.*

The measurement campaigns in Bachok were conducted during the Northern Hemisphere winter months (November to February). The first campaign was from the 20th January 2014 to the 5th February 2014. The second campaign was conducted from the 19th November 2015 to the 27th January 2016. During that period of sampling, the air flow was generally dominated by south-eastward movement of cold air in the high-pressure Siberian-Mongolian High. This is evident in the monthly NAME footprints during the campaign periods 2013/2014 and 2015/2016 (Figure 3.9), where the cold air then passed the East Asia region and travelled to the northern South China Sea and as far as the tropics.

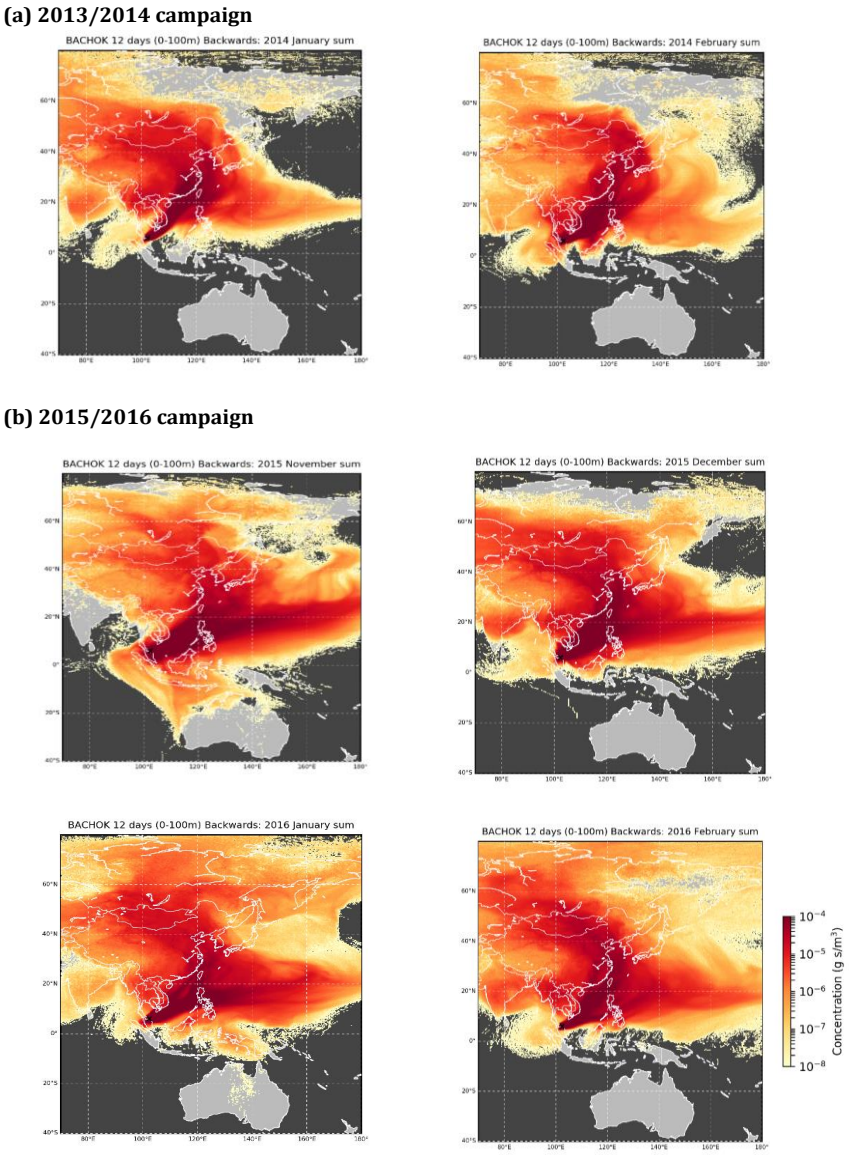

Figure 3.9 *The monthly NAME footprints for the Bachok campaigns in 2013/2014 and 2015/2016. The twelve-day air mass history footprints were calculated for three hourly periods and these have been integrated into monthly footprints. The sum of the NAME footprints provides an overview on the dispersion of the air masses and possible countries that might contribute emissions to air masses that arrived in that particular month.*

All trajectories in their twelve-day journey passed over a combination of countries. Figure 3.8 and 3.9 show the NAME footprints covering various countries which mean that emissions from any of these countries may have impacted air reaching the Taiwan and Bachok stations during the periods of campaigns. The geographical sector map for Bachok and Taiwan that depicts the possible source locations for the air masses sampled during each campaign assessed from analysis of the NAME footprints can be found in Figure 2.6 in Chapter 2, Section 2.4.1.5.1.

Asian countries can be divided into sub-regions according to the classification system of the 2017 United Nations Population Division (United Nations, 2007). This exercise was important since China is a big country comprising six provinces. Although China belongs to the East Asian region, all its six sub-regions have been clustered into a separate region called "China" in this study (Table 3.6). The segregation of China from East Asia also enabled the conduction of more detailed analyses to determine whether regions apart from East China contribute to the variations in the mixing ratios of chlorinated VSLSs.

***Table 3.6**: Classification of Asian countries by sub-region.*

China	East Asia	South East Asia	Oceanic regions
• East China • South West China • South Central China • North East China • North China • North West China	• Taiwan • Korea • Japan	• Malaysia • Indochina • (Thailand, Cambodia, Laos, Vietnam) • Philippines • Indonesia	• East China Sea • Japan Sea • South China Sea • Pacific Ocean

3.2.3.1 Taiwan

As mentioned in Section 3.2.2, the mixing ratios of CH_2Cl_2 correlated well with other chlorinated VSLSs, suggesting that they shared common sources or source regions. Therefore, an understanding of the influences of potential regions on the CH_2Cl_2 mixing ratio variation would also shed some light on the potential sources of other chlorinated VSLSs measured in this work.

The mixing ratio of CH_2Cl_2 can be regarded as extremely high when it is consistently more than 300 ppt (i.e. almost ten times higher than the background levels). These samples containing extremely high CH_2Cl_2 were mainly influenced by continental air masses, especially from the China (East China) and East Asia regions (Figure 3.10). When lower mixing ratios were observed (< 300 ppt), contributions from continental air masses reduced. In this situation, the oceanic regions showed a strong influence on the air masses, primarily from the East China Sea and the Pacific

Ocean. Likewise, the samples collected between 2014 and 2016 inclusive also had similar findings (i.e. air masses of continental origin gave rise to CH_2Cl_2 mixing ratios of over 300 ppt). Evidently, low mixing ratios reflect greater oceanic influence.

(a) 2013

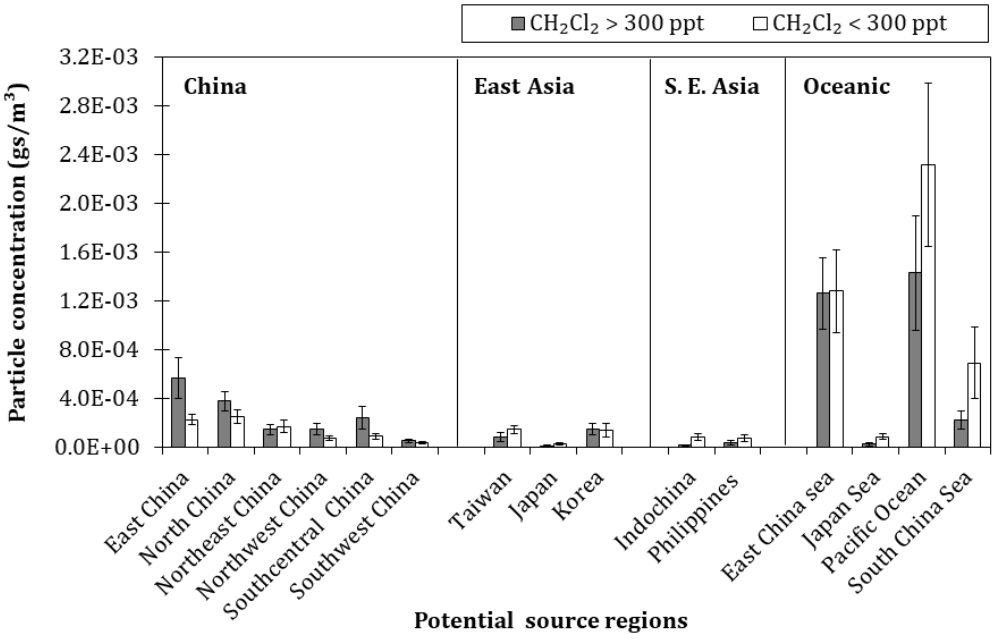

(b) 2014

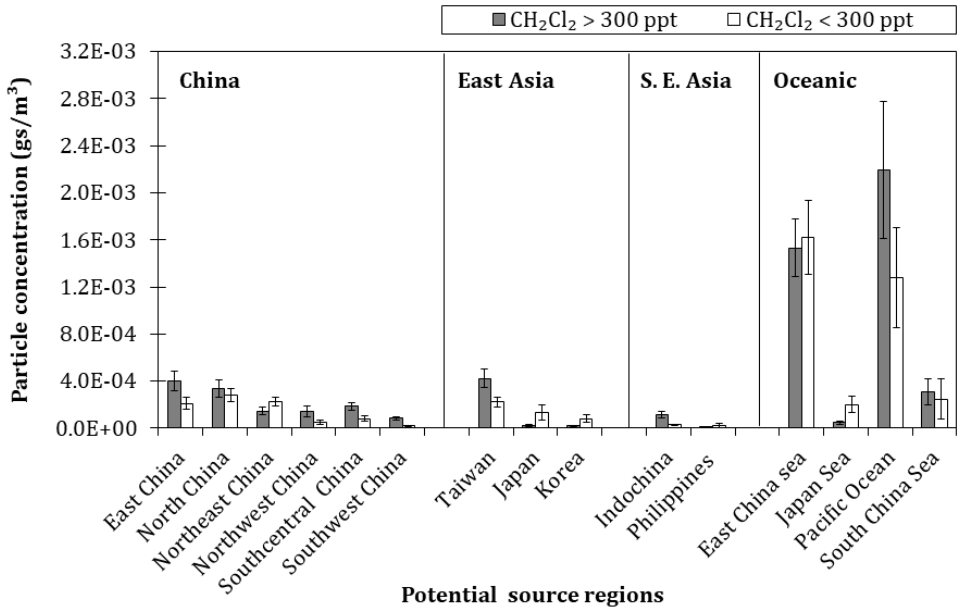

(c) 2015

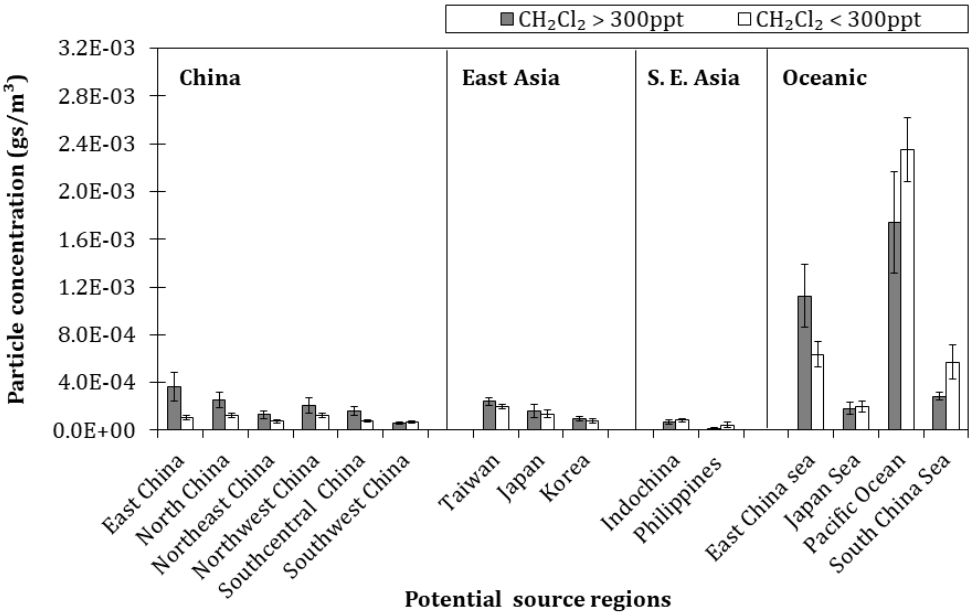

(d) 2016

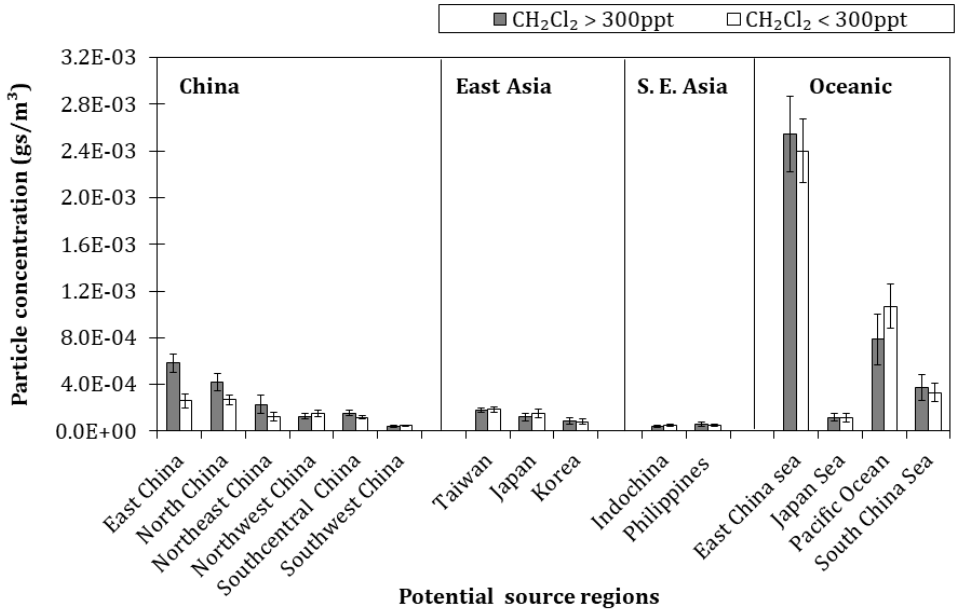

Figure 3.10 *The mean particle concentrations (g s/m^3) from potential source regions during the 2013 to 2016 campaigns in Taiwan.*

3.2.3.2 Bachok

In the Bachok campaigns, CH_2Cl_2 mixing ratios that were consistently above 130 ppt were regarded as extremely high. On average, the high CH_2Cl_2 mixing ratios in 2013/2014 were influenced by air masses that originated from the oceanic regions (especially from the South China Sea). Air masses from East China and Indochina also had an effect on CH_2Cl_2 mixing ratios that were in excess of 130 ppt, even though the mean particle concentrations were not as high as those which were influenced by air masses from the oceanic regions [Figure 3.11 (a)]. When the CH_2Cl_2 mixing ratios were low, the influence of air masses from terrestrial regions (e.g. China and Indochina) and oceanic regions (e.g. South China Sea and Pacific Ocean) decreased and increased respectively. Clearly, the air masses have very minimal contact with East Asia regions i.e. Taiwan, Japan and Korea, suggesting that the East Asia regions do not contribute to the variation of CH_2Cl_2 and other chlorinated VSLSs at Bachok. Evidently, all the observations during the 2013/2014 campaign were similar to those of the 2015/2016 campaigns [Figure 3.11 (b)].

(a) 2013/2014

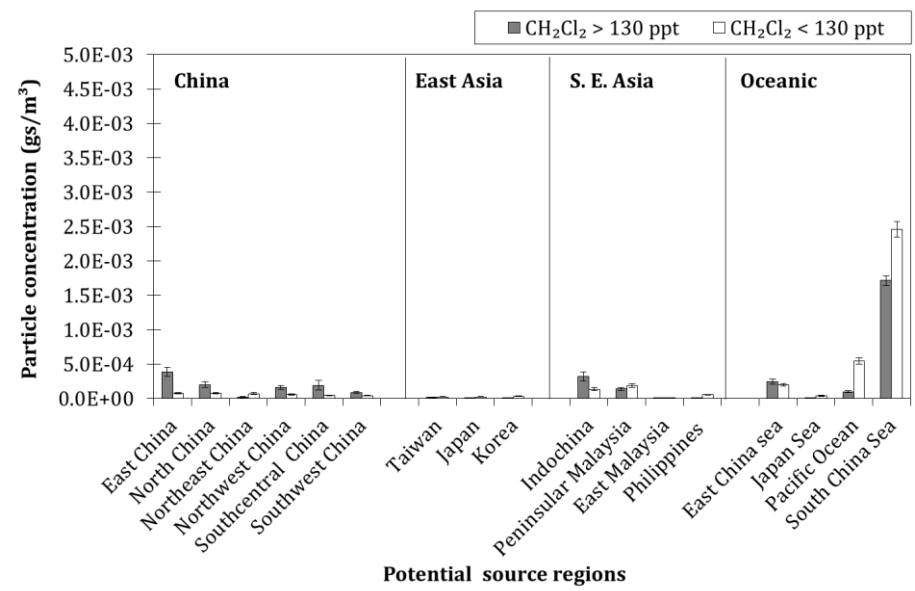

(b) 2015/2016

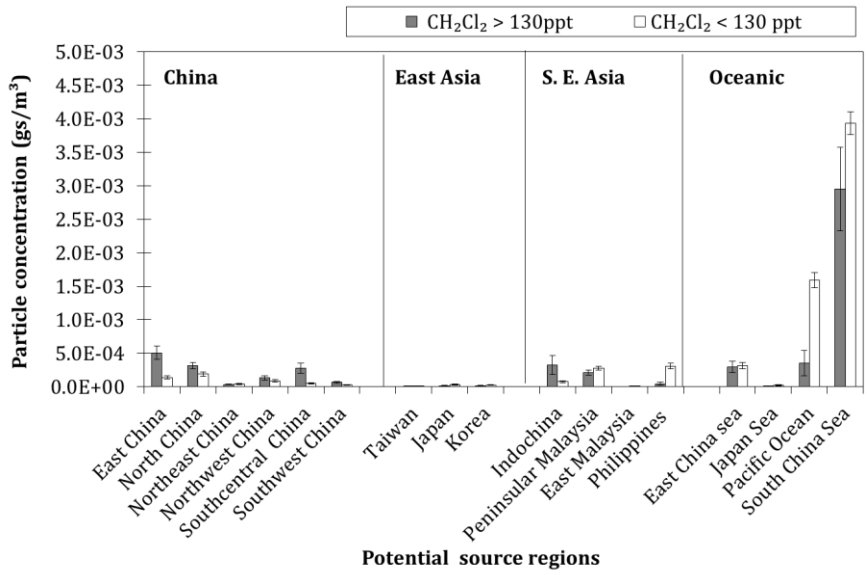

Figure 3.11: *The mean relative particle concentrations (g s/m^3) from potential source regions during the (a) 2013/2014 and (b) 2015/2016 campaigns in Bachok.*

3.2.3.3 Synthesis

The East Asia region has always been known to have the potential to act as a source of chlorinated VSLSs due to rapid industrialization in the region. This means various trace gases including chlorinated VSLSs could be emitted by the industrial sector in substantial concentrations to the atmosphere. The findings from this work are consistent with recent publications (e.g. Ashfold et al. (2015), Hossaini et al. (2017), Oram et al. (2017)) and provide further evidence that the East Asia region is responsible for the emission of chlorinated VSLSs.

Overall, the analysis conducted in this section suggests China to be the main source region of CH_2Cl_2 observed at both Taiwan [Table 3.7 (a)] and Bachok [Table 3.7(b)]. The fact that there are strong observed correlations between CH_2Cl_2 and the other observed chlorinated VSLSs suggests China is also a strong source of other observed chlorinated VSLSs.

Table 3.7: (a) *Association of particle concentrations (g s/m^3) from potential source regions with the observed mixing ratios of CH_2Cl_2 in Taiwan. The values indicate the Spearman correlation coefficients, R. Significant correlations (p < 0.05) are in bold font.*

Sub-regions	Potential regions	2013	2014	2015	2016
China	1. East China	0.33	**0.60**	**0.73**	**0.92**
	2. North China	**0.43**	0.22	0.39	0.08
	3. Northeast China	0.40	-0.23	**0.56**	0.14
	4. Northwest China	0.28	0.57	-0.13	-0.01
	5. Southcentral China	0.27	**0.58**	**0.66**	0.41
	6. Southwest China	0.22	**0.66**	0.01	0.20
East Asia	7. Taiwan	-0.11	0.24	0.21	-0.07
	8. Japan	-0.26	-0.14	**0.53**	0.03
	9. Korea	0.18	-0.01	0.62	0.31
South East Asia	10. Indochina	-0.27	**0.49**	-0.01	0.00
	11. Philippines	-0.19	0.10	0.03	0.06
Oceanic regions	12. East China sea	0.39	0.39	**0.68**	0.13
	13. Japan Sea	-0.20	-0.10	**0.59**	0.41
	14. Pacific Ocean	-0.36	0.12	-0.25	-0.07
	15. South China Sea	-0.41	0.15	0.07	0.10

Table 3.7: (b) *Association of particle concentrations (g s/m^3) from potential source regions with the observed mixing ratios of CH_2Cl_2 in Bachok. The values indicate the Spearman correlation coefficients, R. Significant correlations (p < 0.05) are in bold font.*

Sub-regions	Potential regions	2013/2014	2015/2016
China	1. East China	**0.87**	**0.68**
	2. North China	**0.61**	**0.56**
	3. Northeast China	-0.49	0.49
	4. Northwest China	**0.86**	**0.61**
	5. Southcentral China	**0.82**	**0.80**
	6. Southwest China	**0.76**	**0.70**
East Asia	7. Taiwan	0.14	**0.47**
	8. Japan	-0.86	0.20
	9. Korea	-0.61	**0.44**
South East Asia	10. Indochina	0.34	**0.50**
	11. Peninsula Malaysia	-0.05	-0.22
	12. East Malaysia	0.42	-0.53
	13. Philippines	-0.50	-0.65
Oceanic regions	14. East China sea	**0.47**	**0.46**
	15. Japan Sea	-0.90	0.38
	16. Pacific Ocean	-0.70	-0.57
	17. South China Sea	-0.57	-0.57

At this stage, it is challenging to pinpoint which industrial sector(s) were responsible for emitting the chlorinated VSLS and if the emissions were from single or multiple industrial applications. The challenge arises due to limited knowledge of Chinese emissions and a lack of official usage reports to regulating bodies (Gooch, 2016). However, there are known sources of chlorinated compounds in East China that could be associated with chlorinated VSLSs.

A recent study by Oram et al. (2017) reported that emissions of CH_2Cl_2, $CHCl_3$ and C_2Cl_4 could be connected with the manufacturing of HCFC-22. Production of HCFC-22 requires $CHCl_3$ as a feedstock, with more than 99% of the $CHCl_3$ made being used to produce HCFC-22. Like any other manufacturing process that produces chloromethanes, manufacturing $CHCl_3$ leads to the inevitable co-production of CH_2Cl_2 and co-production of C_2Cl_4 (3-5%). The production ratios of CH_2Cl_2:$CHCl_3$ vary within the range of 30:70 to 70:30, depending on the individual plant. The chloromethane plants in China represent 60% of global production and, in 2015, China produced approximately 600 kt of HCFC-22 (Nolan Sherry Associates, 2015). Much of the Chinese HCFC-22 production caters for the growing demand in developing countries for HCFC-22 which is used as a replacement for CFCs. Given the significant production of HCFC-22 in China and the fact that most HCFC-22 factory clusters are known to be located on the eastern coast of China, specifically in the Shangdong, Jinagsu, Shejian and Sichuan provinces (Stohl et al., 2010), it is probable that HCFC-22 plants in East China contribute significantly towards the elevated chlorinated VSLSs detected over the Asia region.

As for CH_2ClCH_2Cl, the increased atmospheric emissions in this region could be due to the large use of CH_2ClCH_2Cl in vinyl chlorine manufacturing, the precursor of polyvinyl chloride (PVC). China is the world's largest producer of PVC, accounting for 27% of global production in 2009 (DCE, 2018). Production has increased rapidly in recent years (14% per year over the period 2000–2009; DCE, 2018), which could potentially have led to increased atmospheric emissions of CH_2ClCH_2Cl (Oram et al., 2017). Since most of the industry is located in the eastern coast of China (Adcock et al., 2018), this further explains the good correlations observed between variations of measured CH_2ClCH_2Cl with air mass particle concentrations from the East Asia region.

It is interesting to note that other Chinese regions, e.g. Southcentral China, also have a significant influence on the variation of chlorinated VSLSs measured in Bachok and Taiwan. Significant correlation between particles from Southcentral China and chlorinated VSLSs could be due to the industrial sector in that region. There are several HCFC-22 plants located in Southcentral China (Stohl et al., 2010) which could contribute towards emissions of CH_2Cl_2, $CHCl_3$ and C_2Cl_4.

The findings also demonstrate the significant effect of other regions such as Indochina towards the variation of measured VSLSs, in particular in Bachok during 2015/2016 campaign. Another source of chlorinated VSLSs such as CH_2Cl_2 and $CHCl_3$ is biomass burning. Previous literature reports that higher chlorinated compounds such as CH_2Cl_2 and $CHCl_3$ are emitted during incomplete combustion (Lobert et al., 1999). Indochina is known as one of the main regions in the tropics where biomass burning is extensive (Huang et al., 2016) and we suspect that this could influence the variability of measured chlorinated VSLSs. However, due to the uncertainty in the contribution of biomass burning (Simmonds et al., 2006) and insufficient data available within the scope of this study, verification of this theory was challenging.

3.2.4 Influence of cold surges at Bachok

3.2.4.1 Northeast monsoon winds and cold surges

Prior to investigating the influence of cold surges on the variation of observed chlorinated VSLSs, it is essential to understand the features of the monsoon winds that affected the South East Asia region during the period of the campaigns. In order to characterise the northerly winds and identify cold surge events, two type of indices have been employed, the meridional wind, v at 15°N and v at 8°N (more details in Section 2.4.1.5.4, Chapter 2). The former index is generally accepted and commonly employed to represent cold surges in climatology, whilst the latter index

is an alternative created to represent strong meridional transport near our study area.

Comparison between time series of v at 15°N and 8°N are presented in Figure 3.12. Notice that v at 15°N is often much larger than at 8°N. For example, between the 23rd and 25th January 2016, the maximum value of v at 15°N reached -18 m s^{-1} in comparison to v at 8°N which reached -12 m s^{-1}. Also notice that during that same period, high values of v at 15°N occurred earlier than those at 8°N. In fact, throughout all the campaigns (a) the magnitude of v at 15°N was often larger than at 8°N and (b) the changes in v at 15°N often preceded similar changes to v at 8°N. This is to be expected because the meridional wind data tracks the intensity of the north-south component of the wind with higher negative values indicating the southward-moving component of the winds. Also, the fact that there is a time lag between v at 15°N and v 8°N is because the air is moving to the south and any variations in wind speed will reach 15°N before 8°N. Nevertheless, the differences in meridional wind intensity and the time lags between the two indices were not significant ($p > 0.05$). This suggests that the choice of v at 15°N and v at 8°N would not significantly change our overall conclusions. Therefore, I have decided to focus on v at 8°N rather that the v at 15°N for the subsequent analysis as the index best suits the geographical scope of our investigation.

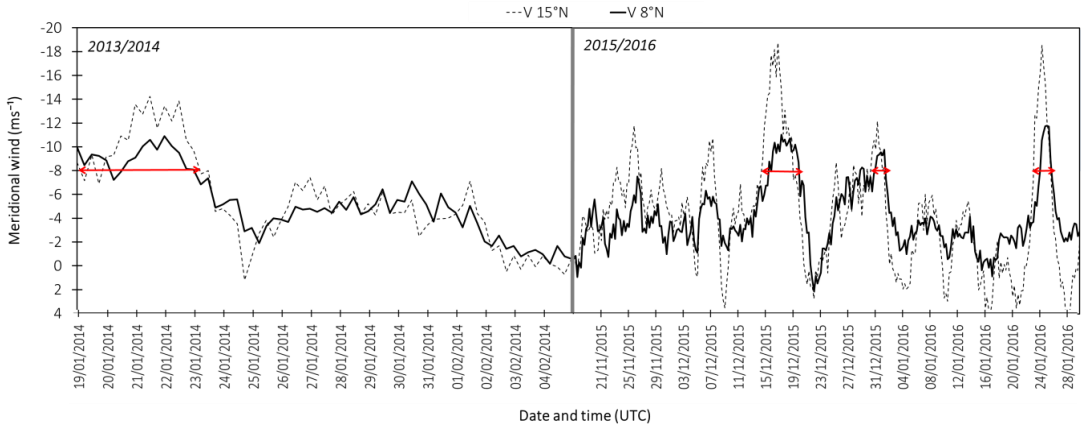

Figure 3.12: *Time series of averaged 925-hPa meridional wind extracted at 8°N (solid dark line) and 15°N (dashed line) during the Bachok campaigns in 2013/2014 (left-hand panel) and 2015/2016 (right-hand panel). The red arrows highlight the periods of the cold surge events i.e. when both v at 8°N and v at 15°N are < -8 m s^{-1}.*

The intensity of the northerly winds in Figure 3.12 can be classified based on the categories of the northerly winds defined by Chang et al. (2005) and Ashfold et al. (2017) and the results are presented in Figure 3.13. Strong winds are defined as v at 8°N < -8 m s^{-1}, weak winds are defined as v at 8°N > -4 m s^{-1} and moderate winds are defined as wind speed between the two limits, -4 m s^{-1} < v at 8°N < -8m s^{-1}.

During the 2013/2014 campaign (19th January to 5th February 2014), the weak winds occurred 38% of the time, strong or cold surge winds 16% of the time and moderate winds 46% of the time (Figure 3.13). For the 2015/2016 campaign (19th November 2015 to 27th January 2016) the corresponding values for weak, strong and moderate winds were 31%, 12% and 58% of the time. During both campaigns the northerly wind is mostly moderate, i.e. 4 m s^{-1} < v at 8°N <-8 m s^{-1}. Yet, cold surge events (i.e. when v at 8°N < -8 m s^{-1}) are common during Northeast monsoon seasons. During the 2013/2014 winter, the early part of the campaign demonstrated the occurrence of cold surge events (denoted by red arrows in Figure 3.12). This is evident when v at 8°N is less than -8 m s^{-1} between 19th January and 23th January 2014. During 2015/2016, the occurrence of cold surges can be seen more often in comparison to 2013/2014. Some examples can be seen: (1) between 15th December to 20th December 2015, (2) 31st December 2015 to 1st January 2016 and (3) 24th January to 26th January 2016. Comparison between the two campaigns showed that the frequency of cold surges in 2015/2016 was three times more than in 2014/2015 (Figure 3.13). This was because the 2014/2015 campaign was later in the winter season after most of the cold surge events had occurred. The cold surge event in 2013/2014 lasted around five days whilst in 2015/2016 cold surges occurred regularly and lasted around three days.

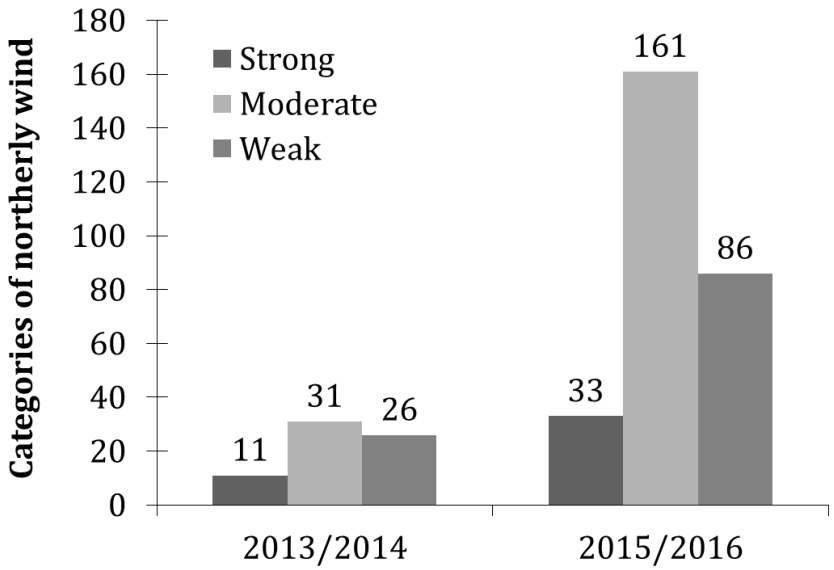

Figure 3.13: *Categories of northerly wind i.e. v at 8°N during campaigns in 2013/2014 and 2015/2016. The numbers in each bar indicate the total number of strong, average and weak winds. Strong winds are defined as v at 8°N < -8 m s^{-1}, weak winds are defined as v at 8°N > -4 m s^{-1} and moderate winds are defined as wind speed between the two limits, i.e. -4 m s^{-1} < v at 8°N < -8 m s^{-1}.*

3.2.4.2 Cold surges and atmospheric composition

Figure 3.14 shows the comparison between the cold surge index and the time series of CH_2Cl_2. There are some indications that a relationship exists between the magnitude of the northerly wind component and the mixing ratio of CH_2Cl_2. An example would be the sample collected on 17th December 2015, when one of the highest mixing ratios of CH_2Cl_2 was recorded during 2015/2016 campaign and it coincided with a cold surge event (v = -9.4 m s^{-1}). This finding suggests the possible connection between cold surges and regional atmospheric compositions.

However, the direct relationship between CH_2Cl_2 mixing ratios and cold surges is not always the case. For example, during the 2013/2014 campaign, a cold surge was detected on the 22nd January 2014 when v = -11 m s^{-1}. The mixing ratio of CH_2Cl_2 was only recorded to be around 150 ppt but interestingly, the CH_2Cl_2 mixing ratios on the next day were found to be 353 ppt which was unusually high. This implies that there may have been a lag between the time when the strong northerly winds

were experienced near Bachok and the transport of air polluted with CH_2Cl_2 from further away.

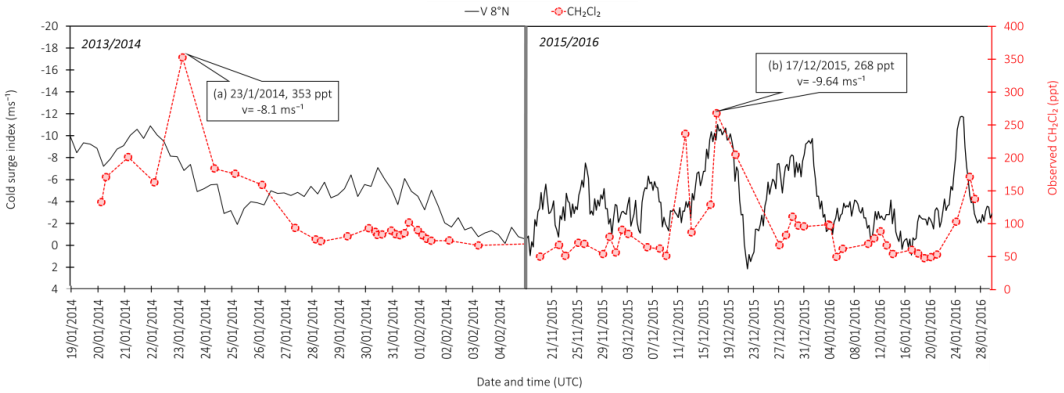

Figure 3.14: *Time series of the meridional winds, v at 8°N (black solid line) versus CH_2Cl_2 (ppt) (red circles) observed at Bachok during campaigns in 2013/2014 (left panel) and 2015/2016 (right panel). (a) and (b) are examples of samples that have high mixing ratios of CH_2Cl_2 (ppt) that coincide with v values lower than -8 m s^{-1}.*

To further understand the relationship between the variation of CH_2Cl_2 mixing ratios and northerly winds speeds, the correlation coefficients were computed as shown in Table 3.8 and summarised in Figure 3.15.

During the 2013/2014 campaign, CH_2Cl_2 mixing ratios significantly correlated with the northerly winds that occurred one to five days before the sampling date. This is consistent with the high mixing ratios of CH_2Cl_2 on 23rd January 2014 being linked to the cold surge that happened a day before. During the 2015/2016 campaign, CH_2Cl_2 mixing ratios were found to correlate significantly with the northerly winds on the day of sampling and up to two days before sampling. These findings suggest that cold surges can lead to increased CH_2Cl_2 mixing ratios at Bachok during the following few days.

Table 3.8: *Slope and correlation coefficient, R, values for correlation between mixing ratios of CH_2Cl_2 (ppt) and meridional wind at 8°N from the day of sampling (T) to seven days before sampling. For example, T-1 represents one day before the sampling day.*

v at 8°N ($m\ s^{-1}$)	2013/2014			2015/2016		
	Slope	R	p value	Slope	R	p value
T	-13.59	0.26	0.005413	-8.90	0.20	**0.004211***
T-1	-17.79	0.39	**0.000421***	-13.03	0.43	**0.000005***
T-2	-18.24	0.52	**0.000015***	-8.89	0.19	**0.004418***
T-3	-20.49	0.56	**0.000004***	-5.33	0.08	0.083463
T-4	-22.55	0.56	**0.000004***	0.98	0.00	0.780228
T-5	-16.30	0.44	**0.000121***	0.05	0.00	0.989367
T-6	-10.41	0.22	0.012455	-2.44	0.01	0.476217
T-7	-10.01	0.18	0.024096	3.60	0.03	0.292329

** $p < 0.05$*

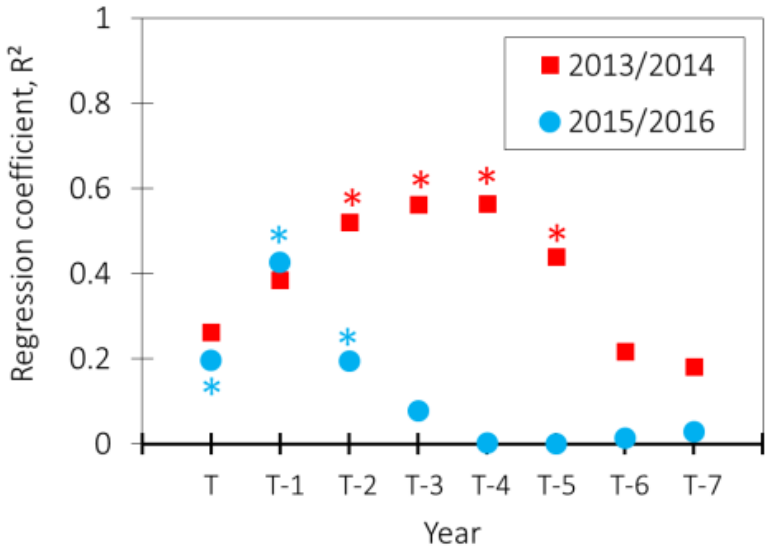

Figure 3.15*: Summary of the correlation between mixing ratios of CH_2Cl_2 (ppt) and meridional wind at 8°N during the sampling day (T) and days before sampling. For example, T-1 represents one day before the sampling day.*

The relationships between CH_2Cl_2 mixing ratios and meridional wind speeds at 8°N four days prior to sampling (T-4) for 2013/2015 and one day prior to sampling (T-1) for 2015/2016 (Figure 3.16) suggest that during a cold surge event, i.e. when the meridional wind speeds at 8°N are above the threshold (8 ms^{-1}), the CH_2Cl_2 mixing ratios are reasonably likely to exceed 150 ppt at Bachok in the following days. A

comprehensive analysis with more datasets is required to more robustly to evaluate the impact of cold surges on atmospheric composition.

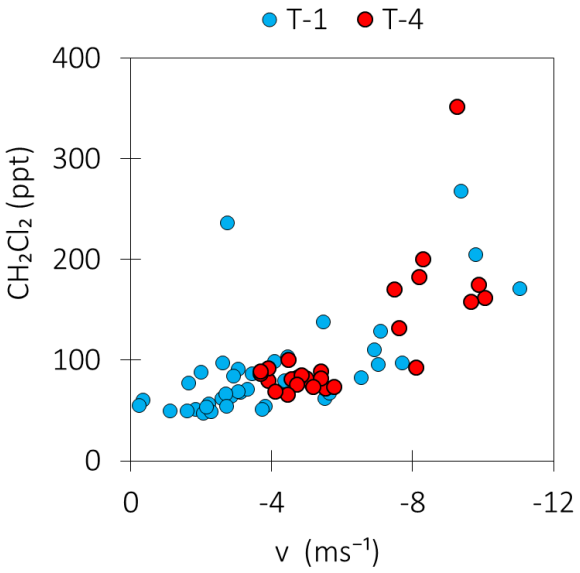

Figure 3.16: *Correlation between CH_2Cl_2 mixing ratios (ppt) with meridional wind at 8°N four days prior to sampling (T-4) for 2013/2014 (blue circles) and meridional wind at 8°N one day prior to sampling (T-1) during 2015/2016 (red circles).*

3.2.4.3 Synthesis

In this analysis, it was shown that cold surges have a significant impact on the variability of chlorinated VSLSs at Bachok. The cold surge events are typical synoptic disturbances that occur in this region. They are manifested by the rapid south-eastward movement of cold air in the high-pressure Siberian-Mongolian High, passing through East Asia and terminating south of China (Chang et al., 2005). The findings provide further evidence of the potential of cold surges to rapidly transport chlorinated VSLSs from mainland China to the tropics, which is in agreement with other studies that have reported the impact of cold surges on other ozone-depleting substances (e.g. Adcock et al. 2018 and Oram et al. 2017) and ozone (e.g. Ashfold et al. 2017) in Southeast Asia. Although the first evidence of cold surges during Bachok campaign has been demonstrated (e.g. Oram et al. 2017), this work for the first time used the cold surge index to define cold surges (this index is generally used in climatology) which strengthens understanding of the relationship between cold surges and the variability of chlorinated VSLSs.

Additionally, the findings from two years of campaigning have confirmed that cold surges can occur regularly throughout the winter periods and can last for several days. The occurrences of cold surge events in 2013/2014 were not as regular as in 2015/2016 due to the stronger winds were less observed in 2013/2014 (Section 3.2.4.1) compared to 2015/2016. Also, the period of the 2013/2014 campaign was much shorter and later than the 2015/2016 campaign, which means that the occurrence of cold surges cannot be fully observed in comparison to 2015/2016 campaign. On the other hand, the winter 2015/2016 was known as an El Nino winter. Studies by Inness et al. (2015) and Hou et al. (2016) have found that year-to-year variations in O_3 in the tropical boundary layer are linked to El Nino-Southern Oscillation (ENSO), which modifies chemical and transport processes, and drives changes in emissions of O_3 precursors. Also, in most other parts of South East Asia, pollutant levels are higher during El Nino winters (Ashfold et al., 2017). Therefore, the frequency and duration of future campaigns should be consistent and increased if possible in order to (1) evaluate that the year-to year variation in cold surge activity and (2) investigate how the influence of cold surges on the variation of atmospheric composition in this region can be affected by El Nino-Southern Oscillation (ENSO).

3.2.5 Effect of emission sources on chlorinated VSLS mixing ratio

This section looks into the influences of various emission sectors on the mixing ratios of chlorinated VSLS at Taiwan and Bachok with the purpose of identifying the likely key sources of chlorinated VSLS emissions.

As described in Chapter 2, carbon monoxide (CO) surface emission data from the representative concentration pathways (RCPs) were used along with the NAME footprints to estimate the modelled CO mixing ratios. The modelled CO mixing ratios were compared with the chlorinated VSLS mixing ratios at the measurement sites. The details of the method are provided in Chapter 2 (Section 2.4.1.5.3).

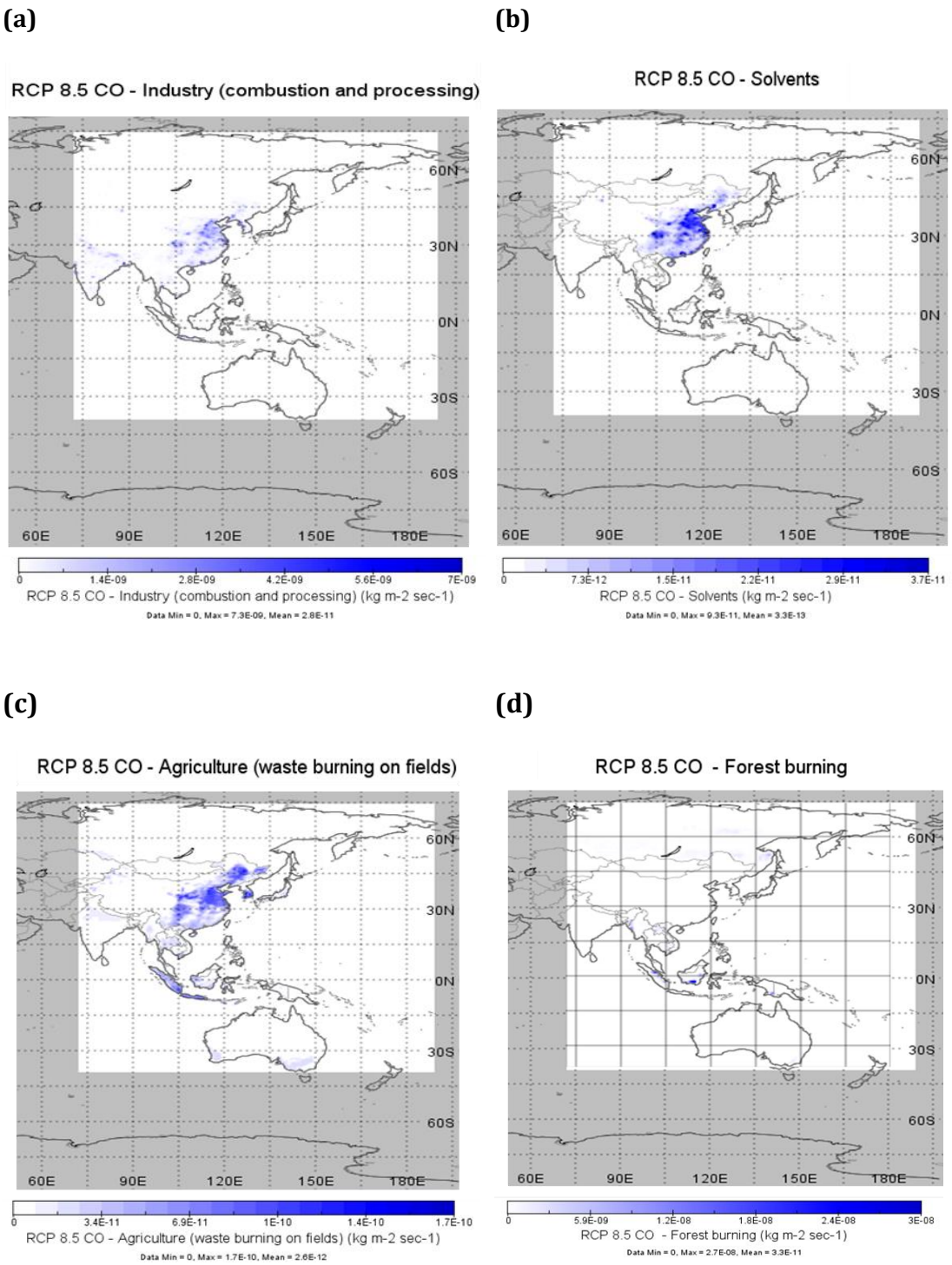

Figure 3.17: *Potential and relevant emission sectors of chlorinated VSLSs. The distribution of carbon monoxide (CO) emissions (kgm^{-2} s^{-1}) for 2010 due to* ***(a)*** *industry (combustion and processing),* ***(b)*** *solvents,* ***(c)*** *agriculture (waste burning on fields) and* ***(d)*** *forest burning. The white area represents the location of study region also known as the model domain (approximately bounded by 75 – 185 ˚E and 10 ˚S – 45 ˚N). The inventories of carbon monoxide (CO) emissions were taken from Representative Concentration Pathway 8.5 (2010) to derive modelled CO to estimate the emissions of chlorinated VSLSs.*

CO emissions inventories are divided into four categories of emission sectors i.e. industry (combustion and process), solvent production, agriculture (waste burning on fields), and forest burning (Figure 3.17). These types of emission sectors were chosen since they were most likely to represent the emission sources of chlorinated VSLSs.

3.2.5.1 Taiwan

The results of the correlation analysis between modelled CO derived from each emission sector and CH_2Cl_2 are presented in Figure 3.18. There was a significant correlation (*R > 0.5, p > 0.05)* between the observed CH_2Cl_2 and modelled CO from industrial, solvent production and agricultural emissions in 2013, 2014, 2015 and 2016 (Table 3.9). The correlations between CH_2Cl_2 were all quite similar with industry, solvents and agricultural burning. Interestingly the slopes of the correlations were very different, i.e. there were very different emission ratios of CO:CH_2Cl_2. This reflects the much larger amounts of CO emitted from industry. Looking at the emission distributions from these sectors (Figure 3.17), they are fairly similar which implies that these emission sectors are largely co-located. On the other hand, the correlations between CH_2Cl_2 and modelled CO due to forest burning were found to be insignificant throughout the four campaigns, suggesting a minimal contribution of forest burning towards the variability of chlorinated VSLSs in Taiwan.

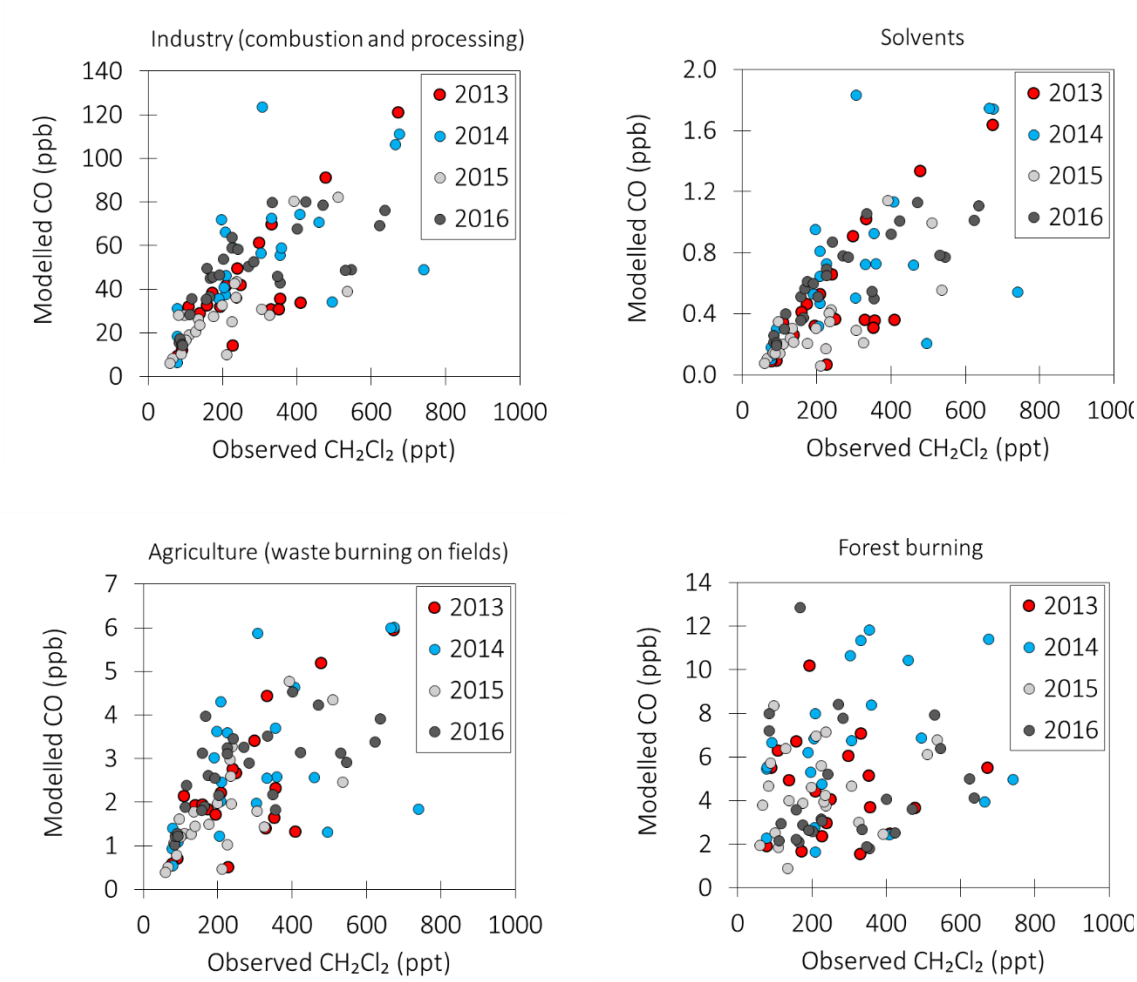

Figure 3.18: *Correlations of the modelled CO from various emission sectors with CH_2Cl_2 (ppt) measured at Taiwan from 2013 to 2016. The modelled CO (ppb) is due to emissions occurring within the timescale of the backward trajectories i.e. 12 days.*

Table 3.9: *Association of modelled CO mixing ratios derived from various emission types with the observed mixing ratios of CH_2Cl_2 in Taiwan. The values indicate the Spearman correlation coefficients (R). Significant correlations ($p < 0.05$) are in bold.*

Emission type	2013	2014	2015	2016
1. Industry (combustion and processing)	**0.64**	**0.63**	**0.79**	**0.86**
2. Solvent	**0.56**	**0.57**	**0.64**	**0.77**
3. Agriculture (waste burning on fields)	**0.49**	**0.51**	**0.74**	**0.80**
4. Forest burning	-0.11	0.32	0.18	0.02

Also, the high CH_2Cl_2 mixing ratios (> 300 ppt) corresponded to high contributions of modelled CO from various sectors [Figure 3.19 (a)]. In contrast, when the mixing ratios of CH_2Cl_2 were low (< 300 ppt), the contribution of modelled CO also decreased. These observations were similar to those for the 2014, 2015 and 2016 campaigns [Figure 3.19 (b–d)].

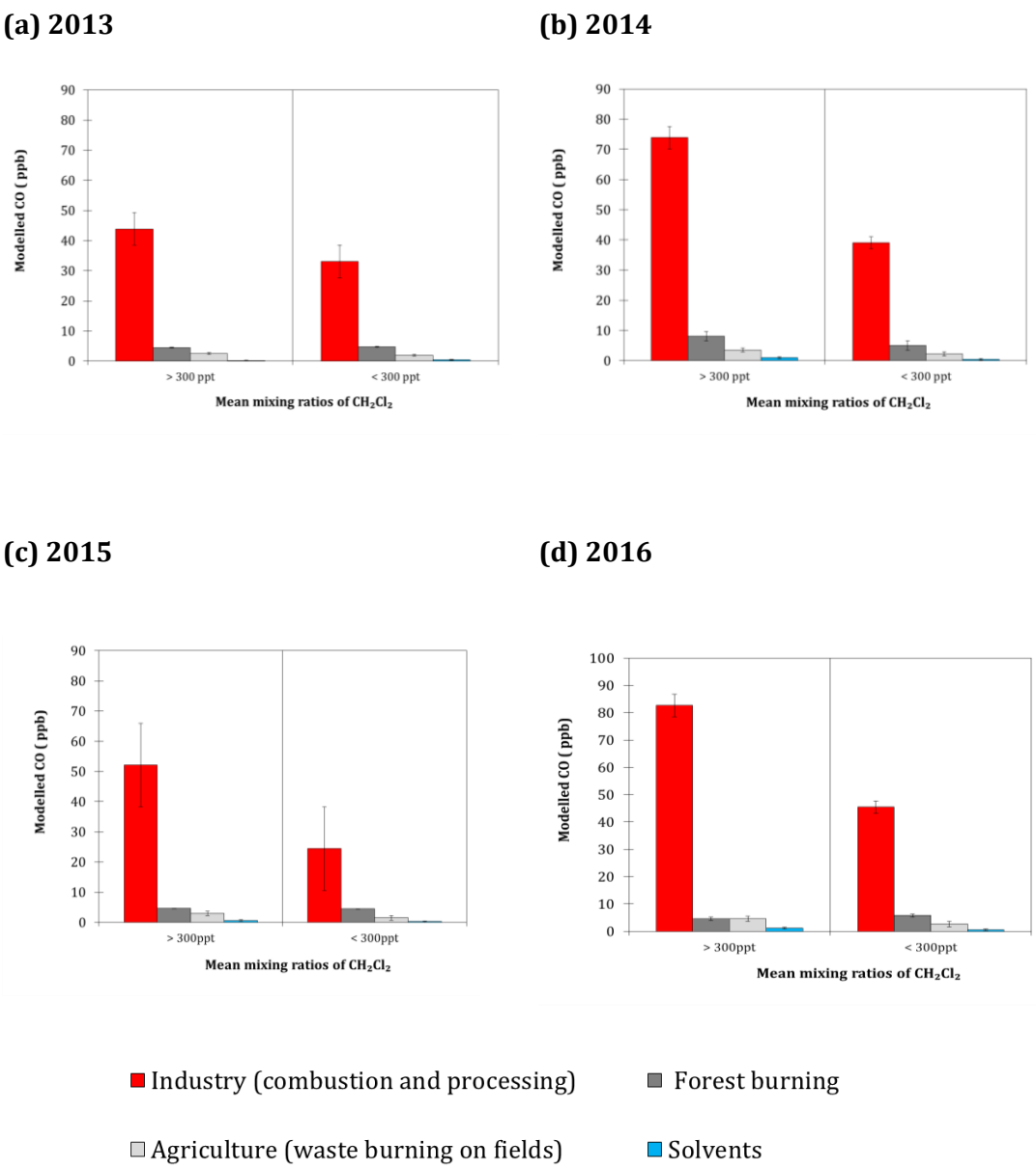

Figure 3.19 *Comparison between modelled CO (ppb) from various emission sectors with high (> 300 ppt) and low (< 300 ppt) mixing ratios of CH_2Cl_2 in Taiwan between 2013 and 2016. The modelled CO mixing ratio is accounted for by various emissions within the timescale of the backward trajectories (i.e. 12 days prior to the observations).*

Overall, the variation of CH_2Cl_2 observed in Taiwan from 2013 to 2016 has been influenced by emissions due to industry (combustion and processing), the solvent industry and biomass emissions (i.e. agriculture burning).

3.2.5.2 Bachok

The results of the correlation analysis between modelled CO due to each emission sector and chlorinated VSLSs are presented in Figure 3.20 and Table 3.10. For both the 2013/2014 and the 2015/2016 campaign, the modelled CO due to emissions from industrial, solvents and agriculture (waste burning on fields) were significantly correlated ($R > 0.69, p > 0.05$) with observed CH_2Cl_2 at Bachok. On the other hand, the correlation between modelled CO due to forest burning emissions and observed CH_2Cl_2 was found to be insignificant in the 2013/2014 campaign but significant in the 2015/2016 campaign.

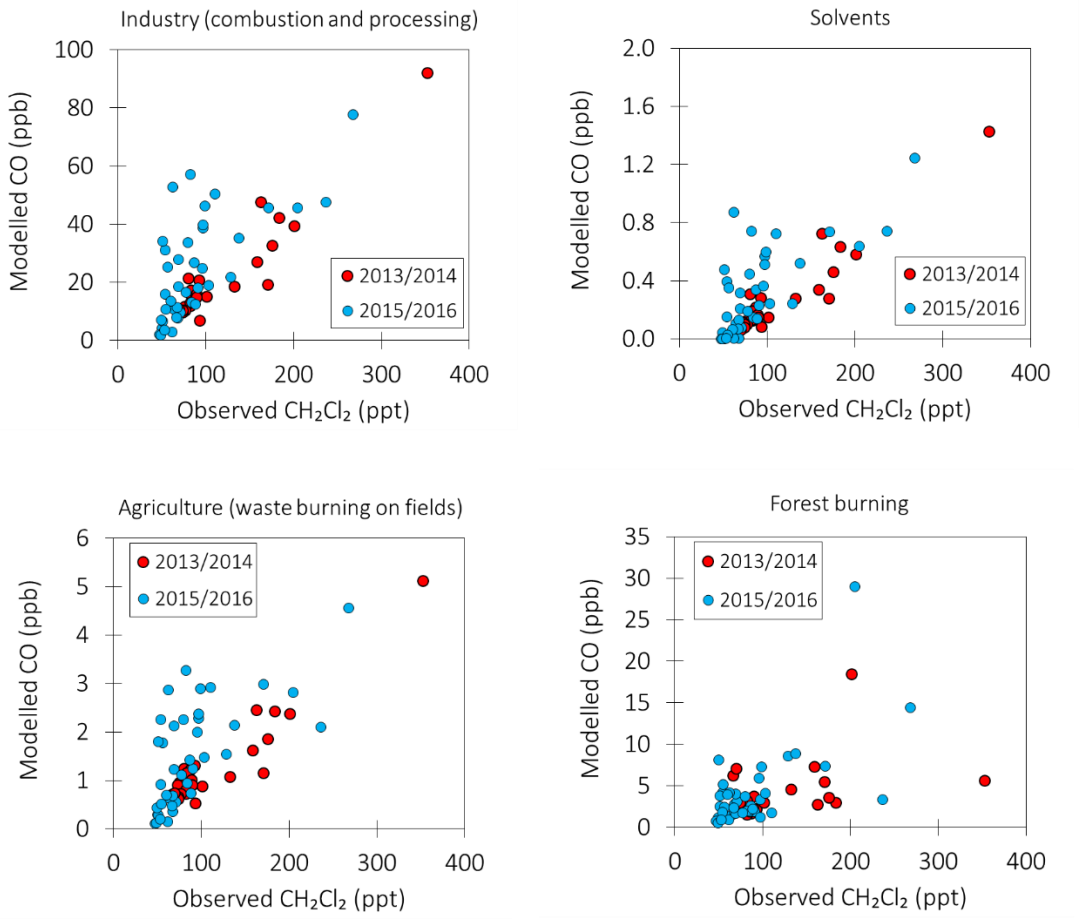

Figure 3.20: *Correlation of the modelled CO with CH_2Cl_2 (ppt) measured at Bachok in the winters of 2013/2014 and 2015/2016. The modelled CO (ppb) is due to emission sectors occurring within the timescale of the backward trajectories i.e. 12 days.*

Table 3.10: *Association of modelled CO mixing ratios derived from various emission types with the observed mixing ratios of CH_2Cl_2 in Bachok. The values indicate the Spearman correlation coefficients (R). Significant correlations ($p < 0.05$) are in bold.*

Emission type	2013/2014	2015/2016
1. Industry (combustion and processing)	**0.80**	**0.69**
2. Solvent	**0.83**	**0.71**
3. Agriculture (waste burning on fields)	**0.71**	**0.70**
4. Forest burning	0.27	**0.45**

Figure 3.21 (a) shows that the high CH_2Cl_2 mixing ratios (> 130 ppt) corresponded to the high contribution of modelled CO from various sectors. In contrast, when the mixing ratios of CH_2Cl_2 were low (< 130 ppt), the contribution of modelled CO also decreased. These observations were similar to those of the 2015/2016 campaign [Figure 3.21 (b)]. Interestingly, when high CH_2Cl_2 mixing ratios were recorded in the

2015/2016 campaign, much higher contributions of forest burning towards the modelled CO were observed. This was not the case during 2013/2014 campaign.

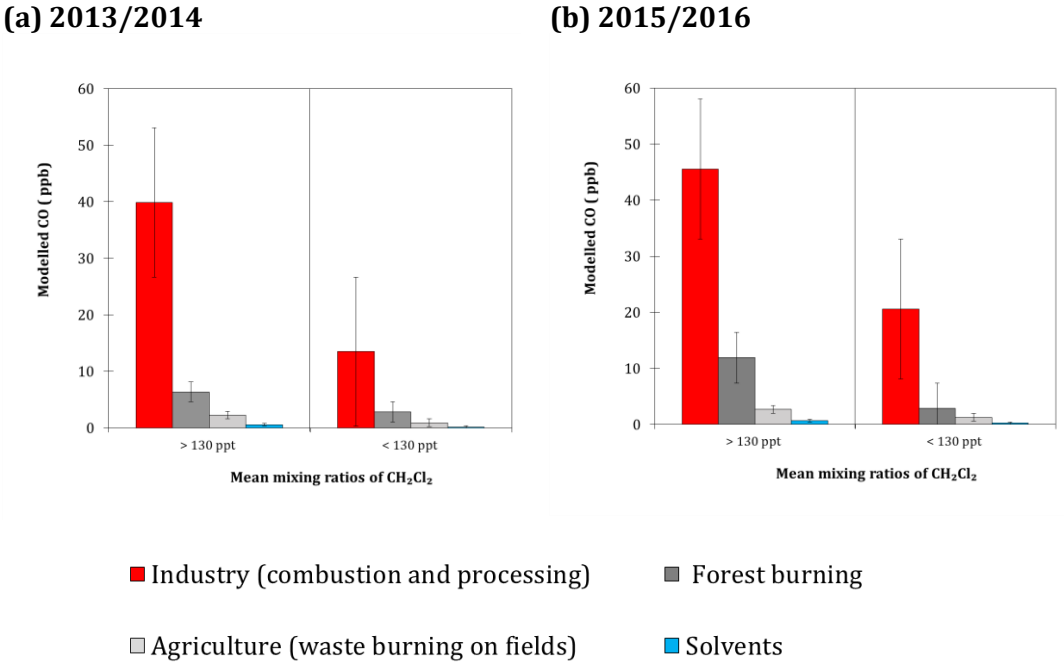

Figure 3.21: *Comparison between modelled CO (ppb) from various emission sectors with high (> 130 ppt) and low (< 130 ppt) mixing ratios of CH_2Cl_2 in Bachok during 2013/2014 and 2015/2016. The modelled CO mixing ratio is accounted for by various emissions within the timescale of the backward trajectories (i.e. 12 days prior to the observations).*

3.2.5.3 Synthesis

Within the domain of our study area, the results showed that chlorinated VSLSs were likely to be emitted from anthropogenic sources, i.e. they were probably related to industrial activity that is mainly located in the mid-latitudes (north of 20˚N) and especially from East China, the region where most of these industrial emissions are located (as per suggested in Section 3.2.3.3). The findings are consistent with recent publications (e.g. Ashfold et al. (2015), Hossaini et al. (2017), Oram et al. (2017)) that suggest and provide evidence that rapid industrialization especially in China is responsible for the growing emission of chlorinated VSLSs.

The modelled CO was well correlated with observed CH_2Cl_2 in both Taiwan and Bachok, suggesting that combustion and processing from industrial sectors were likely to be related to the emissions of CH_2Cl_2 and other chlorinated VSLSs. It seems unlikely that chlorinated VSLSs were direct products of industrial combustion. Thus, the chlorinated VSLSs measured in this work most probably originated from an industrial process or processes producing or involving chlorinated VSLSs. Chlorinated VSLSs could be associated with the production of HFC and HCFC, which is likely responsible for the increased emissions of chlorinated VSLSs in recent years (Campbell et al., 2005, Hossaini et al., 2017).

On the other hand, since CH_2Cl_2 mixing ratios correlated well with CO from the solvent industry, it can be suggested that some emissions of CH_2Cl_2 were due to its continuing use as a common solvent in various applications which include use in metal cleaning/degreasing, paint removal, and use by the pharmaceutical industry for preparing drugs. It is also used as blowing agent in production of foam plastics. This is also the case for CH_2ClCH_2Cl and C_2Cl_4 which have been predominantly used as solvents in the dry-cleaning industry (McCulloch et al., 1996, Montzka et al., 2011).

Although a significant contribution is shown to be from industrial sources, emissions of VSLSs could also be from biomass burning. Both the Taiwan and Bachok data in this section have highlighted that the variability of CH_2Cl_2 can be significantly related not only to anthropogenic sources but also nonindustrial sources i.e. from agriculture (waste burning on fields) in the mid-latitudes. Field burning of crop residues is common both in rural agricultural regions and peri-urban areas in China as it is a method used to control weeds and clear agricultural combustible waste inexpensively (Chen et al., 2017). Interestingly, the 2015/2016 Bachok data showed that biomass burning in the region south of 20^0N could have also been a potential emitter of chlorinated VSLSs. This could be true since a substantial part of biomass burning activities occur in tropical regions and thus may be the dominant trace gas source in these areas with otherwise only relatively small manmade emissions (Andreae, 1991). However, little information is known on the contribution of biomass burning as a potential emission source.

Although it is evident from this analysis that chlorinated VSLSs are consistently associated with emissions from industry and biomass burning, it is still uncertain as

to the exact the mechanism or pathway that leads the chlorinated VSLSs to being emitted to the atmosphere. This work was restricted to a limited number of compounds and further investigation (e.g. correlations with other tracers) may enable detailed source pinpointing and provide concrete conclusions as to the possible emission sources of each gas.

3.3 Conclusions

The mixing ratios of the chlorinated VSLSs generally exceeded the global background values in both Taiwan and Bachok demonstrating a widespread regional enhancement. For both campaigns, CH_2Cl_2 was more abundant, followed by CH_2ClCH_2Cl, $CHCl_3$ and C_2Cl_4. The NAME trajectory and the particle concentration analysis showed that higher mixing ratios events were associated with continental air masses, especially from the region of East Asia. This also explained why the mixing ratios of chlorinated VSLSs showed more variation and often higher mixing ratios in Taiwan than Bachok as Taiwan is located closer to major source regions. This study demonstrates that the enhancement of chlorinated VSLSs in East and Southeast Asia most probably originates from anthropogenic sources related to industries in the mid-latitudes, primarily in East China. CH_2Cl_2, CH_2ClCH_2Cl and $CHCl_3$ could be associated with the production of HFC and HCFC. As for CH_2ClCH_2Cl, the increase in atmospheric abundances in this region could be due to the large use of CH_2ClCH_2Cl in vinyl chlorine manufacturing, the precursor of polyvinyl chloride (PVC). Interestingly, biomass burning could also potentially contribute towards the variability of the measured chlorinated VSLSs. However, ground-based measurements, which can provide strong evidence to support the rationale that biomass burning activities have extensive influences towards chlorinated VSLSs, remain limited. Hence, it is necessary to carry out more investigations, especially in the South East Asia region, to further understand the impact of biomass burning towards chlorinated VSLSs. More studies at different times of the year could also be helpful to compare how different seasons affect the variability of chlorinated VSLSs.

In addition, the findings provide further evidence that the observed enhancements in chlorinated VSLS mixing ratios are caused by rapid meridional transport, in the

form of “cold surges”, from the relatively polluted East Asian land mass to the tropics. This work for the first time used the cold surge index to define cold surges (this index is generally used in climatology) which strengthened understanding of the relationship between cold surges and the variability of chlorinated VSLSs.

Overall, this work has suggested that the sources of chlorinated very-short-lived substances (VSLSs) may just be co-located with emission activities generated from industry, solvent production, waste burning on agricultural fields found in the regions of East Asia and South East Asia. The fact that both regions contain various sources of chlorinated VSLSs suggests the importance of the regions as potential emitters of chlorinated VSLSs to the atmosphere. This highlights the importance of conducting further regional studies not only as few measurements have been made so far but also the proximity of this region to prevalent deep convection, which increases the chance of pollutants emitted from here being transported into the stratosphere and impacting the ozone layer.

3.4 References

Adcock, K. E., Reeves, C. E., Gooch, L. J., Leedham Elvidge, E. C., Ashfold, M. J., Brenninkmeijer, C. A. M., Chou, C., Fraser, P. J., Langenfelds, R. L., Mohd Hanif, N., O'Doherty, S., Oram, D. E., Ou-Yang, C. F., Phang, S. M., Samah, A. A., Röckmann, T., Sturges, W. T. and Laube, J. C.: Continued increase of CFC-113a mixing ratios in the global atmosphere: emissions, occurrence and potential sources, Atmospheric Chemistry and Physics, 18, 7, 4737-4751, 10.5194/acp-18-4737-2018, 2018.

Andreae, M. O. Biomass burning: its history, use, and distribution and its impact, Global Biomass Burning: Atmospheric, Climatic, and Biospheric Implications [JS Levine (Ed.)]. Cambridge, MA, MIT Press.1991

Ashfold, M. J., Latif, M. T., Samah, A. A., Mead, M. I. and Harris, N. R. P.: Influence of Northeast Monsoon cold surges on air quality in Southeast Asia, Atmospheric Environment, 166, 498-509, 10.1016/j.atmosenv.2017.07.047, 2017.

Ashfold, M. J., Pyle, J. A., Robinson, A. D., Meneguz, E., Nadzir, M. S. M., Phang, S. M., Samah, A. A., Ong, S., Ung, H. E., Peng, L. K., Yong, S. E. and Harris, N. R. P.: Rapid transport of East Asian pollution to the deep tropics, Atmospheric Chemistry and Physics, 15, 6, 3565-3573, 10.5194/acp-15-3565-2015, 2015.

Campbell, N., Shende, R., Bennett, M., Blinova, O., Derwent, R., McCulloch, A., Yamabe, M., Shevlin, J. and Vink, T.: HFCs and PFCs: Current and future supply, demand and emissions, plus emissions of CFCs, HCFCs and halons, Safeguarding the Ozone Layer and the Global Climate System, Issues Related to Hydrofluorocarbons and Perfluorocarbons, IPCC/TEAP Special Report, 404-436, 2005.

Carpenter, L. J., Reimann, S., Burkholder, J. B., Clerbaux, C., Hall, B. D., Hossaini, R., Laube, J. C. and Yvon-Lewis, S. A. Ozone-Depleting Substances (ODSs) and Other Gases of Interest to the Montreal Protocol, Chapter 1 in Scientific Assessment of Ozone Depletion: 2014, Global Ozone Research and Monitoring Project – Report No. 55. Geneva, Switzerland, World Meteorological Organization.2014

Chang, C. P., Harr, P. A. and Chen, H. J.: Synoptic disturbances over the equatorial South China Sea and western maritime continent during boreal winter, Monthly Weather Review, 133, 3, 489-503, 2005.

Chen, J., Li, C., Ristovski, Z., Milic, A., Gu, Y., Islam, M. S., Wang, S., Hao, J., Zhang, H., He, C., Guo, H., Fu, H., Miljevic, B., Morawska, L., Thai, P., Lam, Y. F., Pereira, G., Ding, A., Huang, X. and Dumka, U. C.: A review of biomass burning: Emissions and impacts on air quality, health and climate in China, Science of The Total Environment, 579, 1000-1034.

DCE (2018). "Dalian Commodity Exchange website, PVC product guide."

Gooch, L. J. Atmospheric Halocarbon Measurements with a focus on East and South-East Asia. School of Environmental Sciences, University of East Anglia. PhD.2016

Hossaini, R., Chipperfield, M. P., Montzka, S. A., Leeson, A. A., Dhomse, S. S. and Pyle, J. A.: The increasing threat to stratospheric ozone from dichloromethane, Nature Communications, 8, 15962, 10.1038/ncomms15962, 2017.

Hossaini, R., Chipperfield, M. P., Saiz-Lopez, A., Harrison, J. J., Von Glasow, R., Sommariva, R., Atlas, E., Navarro, M., Montzka, S. A., Feng, W., Dhomse, S., Harth, C., Mühle, J., Lunder, C., O'Doherty, S., Young, D., Reimann, S., Vollmer, M. K., Krummel, P. B. and Bernath, P. F.: Growth in stratospheric chlorine from short-lived chemicals not controlled by the Montreal Protocol, Geophysical Research Letters, 42, 11, 4573-4580, 10.1002/2015GL063783, 2015.

Hou, X., Zhu, B., Fei, D., Zhu, X., Kang, H. and Wang, D.: Simulation of tropical tropospheric ozone variation from 1982 to 2010: The meteorological impact

of two types of ENSO event, Journal of Geophysical Research: Atmospheres, 121, 15, 9220-9236, 2016.

Huang, W. R., Wang, S. H., Yen, M. C., Lin, N. H. and Promchote, P.: Interannual variation of springtime biomass burning in Indochina: Regional differences, associated atmospheric dynamical changes, and downwind impacts, Journal of Geophysical Research: Atmospheres, 121, 17, 2016.

Inness, A., Benedetti, A., Flemming, J., Huijnen, V., Kaiser, J., Parrington, M. and Remy, S.: The ENSO signal in atmospheric composition fields: emission-driven versus dynamically induced changes, Atmospheric Chemistry and Physics, 15, 15, 9083-9097, 2015.

Leedham, E. C., Oram, D. E., Laube, J. C., Baker, A. K., Montzka, S. A., Humphrey, S., O'Sullivan, D. A. and Brenninkmeijer, C. A. M.: Increasing concentrations of dichloromethane, inferred from CARIBIC air samples collected 1998-2012, Atmospheric Chemistry and Physics, 15, 4, 1939-1958, 10.5194/acp-15-1939-2015, 2015.

Liu, H., Jacob, D. J., Bey, I., Yantosca, R. M., Duncan, B. N. and Sachse, G. W.: Transport pathways for Asian pollution outflow over the Pacific: Interannual and seasonal variations, Journal of Geophysical Research: Atmospheres, 108, D20, 2003.

Lobert, J. M., Keene, W. C., Logan, J. A. and Yevich, R.: Global chlorine emissions from biomass burning: Reactive chlorine emissions inventory, Journal of Geophysical Research: Atmospheres, 104, D7, 8373-8389, 1999.

McCulloch, A. and Midgley, P. M.: The production and global distribution of emissions of trichloroethene, tetrachloroethene and dichloromethane over the period 1988–1992, Atmospheric Environment, 30, 4, 601-608, 1996.

Montzka, S., Reimann, S., O'Doherty, S., Engel, A., Krüger, K. and Sturges, W. Ozone-depleting substances (ODSs) and related chemicals, World Meteorological Organization. 2011

Nolan Sherry Associates. Review of Anthropogenic Emissions of Certain Potentially Stratospheric Ozone Depleting Substances: Asia. United Kingdom.2015

Oram, D. E., Ashfold, M. J., Laube, J. C., Gooch, L. J., Humphrey, S., Sturges, W. T., Leedham-Elvidge, E., Forster, G. L., Harris, N. R. P., Mead, M. I., Abu Samah, A., Phang, S. M., Chang-Feng, O. Y., Lin, N. H., Wang, J. L., Baker, A. K., Brenninkmeijer, C. A. M. and Sherry, D.: A growing threat to the ozone layer from short-lived anthropogenic chlorocarbons, Atmospheric Chemistry and Physics, 7, 19, 11929-11941, 2017.

Shao, M., Huang, D., Gu, D., Lu, S., Chang, C. and Wang, J.: Estimate of anthropogenic halocarbon emission based on measured ratio relative to CO in the Pearl River Delta region, China, Atmospheric Chemistry and Physics, 11, 10, 5011-5025, 10.5194/acp-11-5011-2011, 2011.

Simmonds, P., Manning, A., Cunnold, D., McCulloch, A., O'Doherty, S., Derwent, R., Krummel, P., Fraser, P., Dunse, B. and Porter, L.: Global trends, seasonal cycles, and European emissions of dichloromethane, trichloroethene, and tetrachloroethene from the AGAGE observations at Mace Head, Ireland, and Cape Grim, Tasmania, Journal of Geophysical Research: Atmospheres, 111, D18, 2006.

Stohl, A., Kim, J., Li, S., O'Doherty, S., Mühle, J., Salameh, P. K., Saito, T., Vollmer, M. K., Wan, D., Weiss, R. F., Yao, B., Yokouchi, Y. and Zhou, L. X.: Hydrochlorofluorocarbon and hydrofluorocarbon emissions in East Asia determined by inverse modeling, Atmospheric Chemistry and Physics, 10, 8, 3545-3560, 10.5194/acp-10-3545-2010, 2010.

Trudinger, C. M., Etheridge, D. M., Sturrock, G. A., Fraser, P. J., Krummel, P. B. and McCulloch, A.: Atmospheric histories of halocarbons from analysis of Antarctic firn air: Methyl bromide, methyl chloride, chloroform, and dichloromethane, Journal of Geophysical Research: Atmospheres, 109, D22, n/a-n/a, 10.1029/2004JD004932, 2004.

United Nations (2007). "United Nations Population Division: World Population Prospect: The 2017 Revision." Retrieved 24 September 2018.

Wang, Z., Liu, X. and Xie, X.: Effects of strong East Asian cold surges on improving the air quality over mainland China, Atmosphere, 7, 3, 10.3390/atmos7030038, 2016.

Chapter 4

Methyl Halides in East Asia and South East Asia

4.1 Introduction

The atmospheric mixing ratios of many halogenated substances have declined and stabilised. This was in view of the reduction in anthropogenic halocarbon contributions to ozone loss as a result of their production limits as per the Montreal Protocol (Montzka et al., 2018). Hence, the relative influence of naturally-produced halogenated substances towards the future chemistry of the stratospheric ozone becomes ever more significant (Gebhardt et al., 2008). The predominant natural sources of stratospheric chlorine and bromine are methyl chloride (CH_3Cl) (17%) and methyl bromide (CH_3Br) (50%) respectively (Carpenter et al., 2014).

The mean global surface mixing ratio of CH_3Cl in 2012 was 540 ppt (range = 537.1 – 542.2 ppt). Also, the abundance of CH_3Cl had declined since the previous WMO assessment in 2008 (~546 ppt). Similarly, a declining trend was observed in the mean global surface mixing ratio of CH_3Br (7 ppt in 2012 vs ~7.4 ppt in 2008) (Carpenter et al., 2014). Unlike the majority of the halogenated substances mentioned in Chapter 3, both aforementioned methyl halides are mainly of natural origin, and thus their atmospheric abundances are less influenced by anthropogenic emissions. Their largest sink reaction is that with hydroxyl radicals (OH). Table 4.1 summarises the current understanding of the sources and sinks of both gases.

Table 4.1: *Sources and sinks of atmospheric CH_3Cl and CH_3Br*

	Source type	Source range (Gg/year)		Sink type	Sink range (Gg/year)	
		Best estimates	Range		Best estimates	Range
CH_3Cl	**Natural sources**					
	1. Oceans	700	510 – 910	1. OH reaction	2832	2470 3420
	2. Terrestrial sources			2. Loss to soil	1058	664 – 1482
	• Tropical and subtropical plants, Tropical dead leaves	2040	1430 – 2650	3. Loss in ocean	370	296 – 445
	• Mangroves	12		4. Loss in stratosphere	146	
	• Salt marshes	85	11 – 12			
	• Fungus	145	1.1 – 170			
	• Wetlands	27	128 – 162			
	• Rice paddies	3.7	5.5 – 48			
	• Shrub lands	15	2.7 – 4.9			
	• Rapeseed	n.q.	9 – 21			
			n.q.			
	3. Biomass burning (open field burning)	355	142 – 569			
	Anthropogenic sources					
	Coal combustion	162	29 – 295			
	• Waste incineration					
	• Industrial processes					
	Total	**3658**		**Total**	**4406**	
CH_3Br	**Natural sources**					
	1. Oceans	32	22 – 44	1. OH reaction	56	48 – 63
	2. Terrestrial sources	n.q.	n.q.	2. Loss to soil	30	19 – 41
	• Tropical and subtropical plants, Tropical dead leaves	n.q.	n.q.	3. Loss in ocean	33	20 – 44
	• Mangroves	1.3	1.2 – 1.3	4. Loss in stratosphere	4	
	• Salt marshes	7	0.6 – 14			
	• Fungus	2.2	1 – 5.7			
	• Wetlands	0.6	0.1 – 1.3			
	• Rice paddies	0.7	0.1 – 1.7			
	• Shrub lands	0.7	0.5 – 0.9			
	• Rapeseed	5.1	4.0 – 6.1			
	3. Biomass burning (open field burning)	17	7 – 27			
	Anthropogenic sources					
	1. Leaded gasoline	0 – 3				
	2. Fumigation – QPS	7.4	6.9 – 7.8			
	3. Fumigation – non-QPS	2.5	1.7 – 3.5			
	Total	**84**		**Total**	**123**	

Note : n.q. = not quantified, QPS = Quarantine and pre-shipment *Source : adapted from Carpenter et al. (2014)*

Overall, CH_3Cl and CH_3Br have several common sources, namely oceans, terrestrial sources (mangroves, fungi, salt marshes, wetlands, rice fields, and shrublands) as well as biomass burning (indoor biofuel use and open field burning). CH_3Cl also originates from sources that do not generate CH_3Br. These include tropical and subtropical terrestrial sources (e.g. plants and/or their degraded materials) as well as coal combustion (i.e. from waste incineration and industrial activities). Likewise, CH_3Br has its unique sources (i.e. terrestrial sources like rapeseed, leaded gasoline, and fumigation activities).

Despite the comprehensive measures previously taken to quantify the sources and sinks of both gases, the sinks of CH_3Cl and CH_3Br still outweigh the sources, and the budgets of both gases remain unbalanced (Gebhardt et al. (2008), Hu (2012), Carpenter et al. (2014). Previous studies (e.g. Yokouchi et al. (2000), Yokouchi et al. (2002), Lee-Taylor et al. (2005), Blei et al. (2010)) have proposed several tropical terrestrial sources of CH_3Cl and CH_3Br apart from the oceans and biomass burning. However, the sparseness of these methyl halides measurements has resulted in huge uncertainties over the nature and strengths of the tropical sources (Gebhardt et al., 2008). With regards to the global CH_3Br budget, its sinks seem to outweigh the sources, thereby suggesting the existence of an underestimated or still-unknown (tropical) source (Gebhardt et al., 2008). The source–sink imbalance might also be attributable to an underestimation of the atmospheric lifetime of CH_3Br (Reeves, 2003). It is estimated that both naturally-occurring gases contribute up to 25% of the stratospheric halogen loading, and that this value will exceed 50% by 2050 (WMO, 2007). For that reason, further investigations on the origins of the missing sources are required. Also, the atmospheric abundance of said gases should be continuously monitored. Likewise, further understanding of their life cycles is important for the development of additional global policies and regulations pertaining to ozone-depleting substances (Simmonds et al., 2004).

This chapter explores the abundances of CH_3Cl and CH_3Br in East Asia and South East Asia. Specifically, the Taiwan and Bachok observational datasets are interpreted in order to:

1. Assess the variability of methyl halides at both sampling locations and to identify the presence of above-background levels of the same.

2. Investigate the potential sources regions and types of emissions that can contribute to the variations of the levels of methyl halides.

It is important to highlight that the following section will not start off with the typical methodology section. Since the methodology of this study has already been presented in Chapter 2, it will not be discussed in detail here. Instead this chapter will directly proceed to the presentation and discussion of the key findings (Section 4.2). Conclusions and suggestions of further studies are put forward in Section 4.3.

4.2 Results & Discussion

4.2.1 Mixing ratios of methyl halides

4.2.1.1 Taiwan

Figure 4.1 shows the mixing ratios of CH_3Cl and CH_3Br in Taiwan during campaigns from 2013 to 2016. Overall, the mixing ratios of both exceeded their background atmospheric mixing ratios. For instance, the mean atmospheric mixing ratios of CH_3Cl during the said timeframe were 37.9% to 71.1% greater than the global mean value of 540 ppt. As for the mixing ratios of CH_3Br, the mean was 2 to 3 times greater than the global mean value (7 ppt) (Table 4.2).

Evidently, the mixing ratios of CH_3Cl and CH_3Br throughout the campaigns were highly variable. Both gases appeared to be enhanced simultaneously [examples are labelled by (a), (b), (c), and (d) in Figure 4.1]. The NAME footprints showed that the

spikes in the methyl halide mixing ratios were associated with the occurrence of continental air masses which mainly originated from the boundary layer over eastern China [examples are indicated by (a), (c), and (d) in Figure 4.1]. Additionally, the high mixing ratios of methyl halides were influenced by Taiwan itself [an example is indicated by (b)]. When lower mixing ratios were observed, the NAME footprints [as denoted by (e)] showed that the air masses still originated from the north, with minimal contact with inland regions such as China and Taiwan.

Table 4.2: *Summary of data on methyl halides obtained during measurement campaigns in Taiwan*

	2013		**2014**		**2015**		**2016**		**Global surface mixing ratio** [a]
	Mean (ppt)	Range (ppt)	Mean (ppt)	Range (ppt)	Mean (ppt)	Range (ppt)	Mean (ppt)	Range (ppt)	Mean (ppt)
CH_3Cl	924.0	756.4 – 1237	744.5	576.5 – 1086.8	770.3	640.9 – 1091.4	826.4	670.8 – 1326.4	540
CH_3Br	22.5	15.8 – 48.8	15.3	8.9 – 25.2	13.4	8.7 – 20.6	17.1	10.5 – 34	7

Note:

[a] *The global surface mean mole fraction of CH_3Cl and CH_3Br were determined by the NOAA and AGAGE global networks in 2012 (Carpenter et al. (2014))*

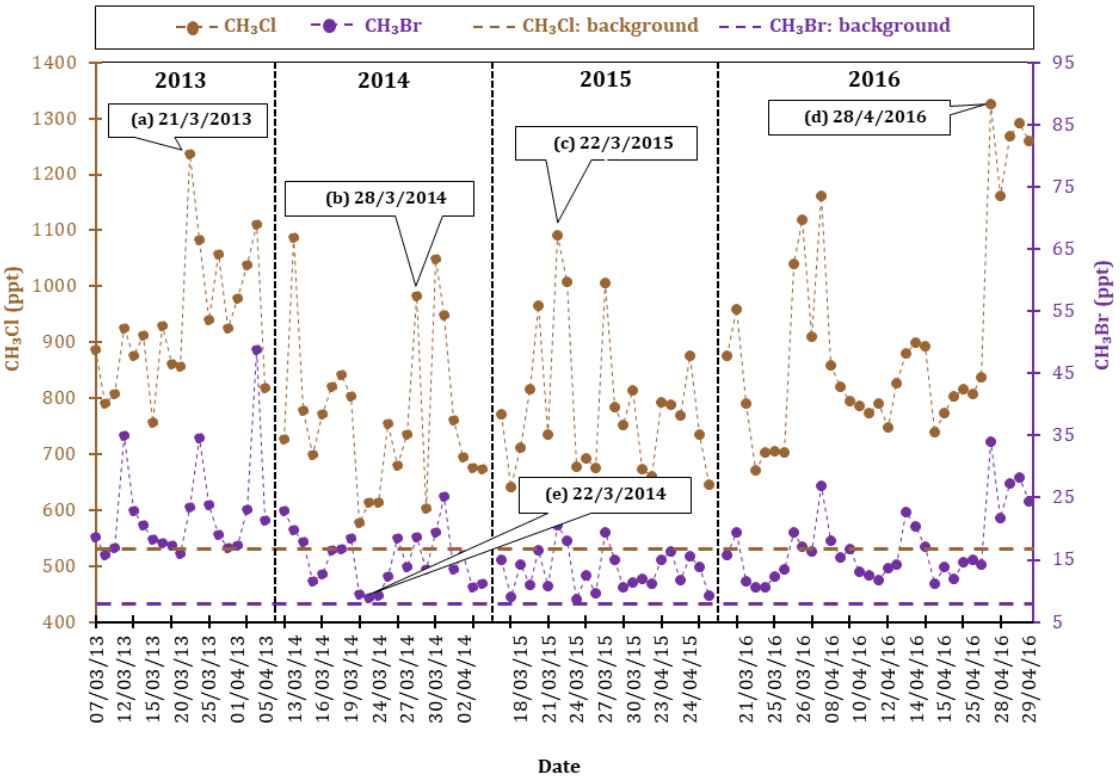

(a) 21/3/2013 01:30:00 UTC

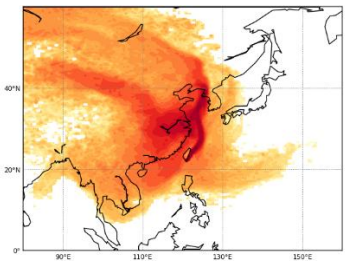

(b) 28/3/2014 07:30:00 UTC

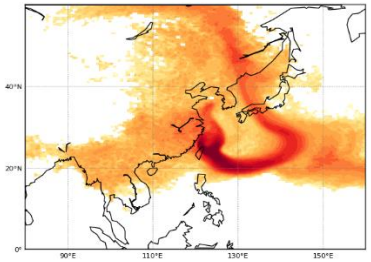

(c) 22/3/2015 01:30:00 UTC

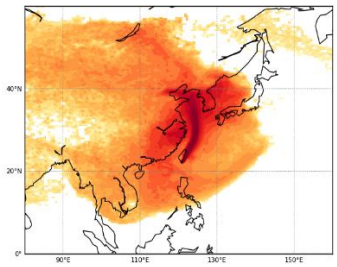

(d) 28/4/2016 04:00:00 UTC

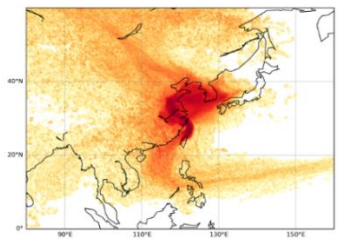

(e) 22/3/2014 07:30:00 UTC

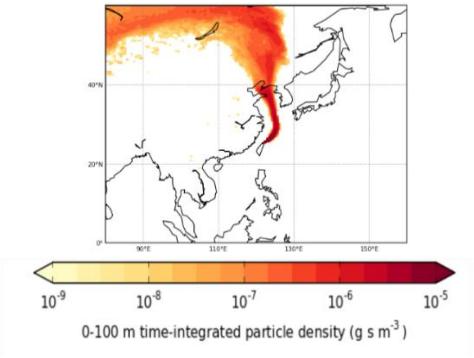

Figure 4.1: Upper panel: *Mixing ratios (ppt) of the methyl halides in air samples collected in Taiwan in 2013, 2014, 2015 and 2016. The global surface mean mixing ratios for each methyl halide in 2012 are represented by the dashed lines. Also shown are the examples where the observed mixing ratios of methyl halides are unusually high, indicated by (a), (b), (c) and (d). For comparison, (e) represents a mixing ratio that is much closer to the global surface mean mixing ratio of each methyl halide.* ***Lower panel:*** *NAME footprint maps generated from a back-trajectory analysis indicating the likely origin of the air sampled in Taiwan, with the darker colours indicating greater influence. The colour scale is logarithmic and represents the calculated time-averaged concentration within surface layer (0–100 m) during the 12 days prior to the sampling days given a point release in Taiwan. The NAME footprints for samples when the air masses have influence from the potential source regions, e.g. East China, are indicated by (a), (b), (c), and (d), whilst (e) is a NAME footprint of air that was less affected by potential source regions.*

4.2.1.2 Bachok

During both the 2013/2014 and 2015/2016 campaigns, the mixing ratios of the methyl halides were already higher than their global surface mean mixing ratios (Table 4.3, Figure 4.2). Specifically, the mean values of CH_3Cl in 2013/2014 and 2015/2016 were 778.5 ppt and 709 ppt respectively, which were 44% and 31% higher than that of the global value (540 ppt). In terms of CH_3Br, the mean values were 11.6 ppt and 9.7 respectively, which were 65% and 39% higher than the global value of 7 ppt.

Table 4.3: *Summary of data on methyl halides obtained during measurement campaigns in Bachok*

	1st campaign (2013/2014)		**2nd campaign (2015/2016)**		**Global surface mixing ratio [a]**
	Mean (ppt)	Range (ppt)	Mean (ppt)	Range (ppt)	Mean (ppt)
CH_3Cl	778.5	592.8 – 1574.1	709	612.1 – 1017.7	540
CH_3Br	11.6	8.1 – 20.8	9.7	7.6 – 15.0	7.0

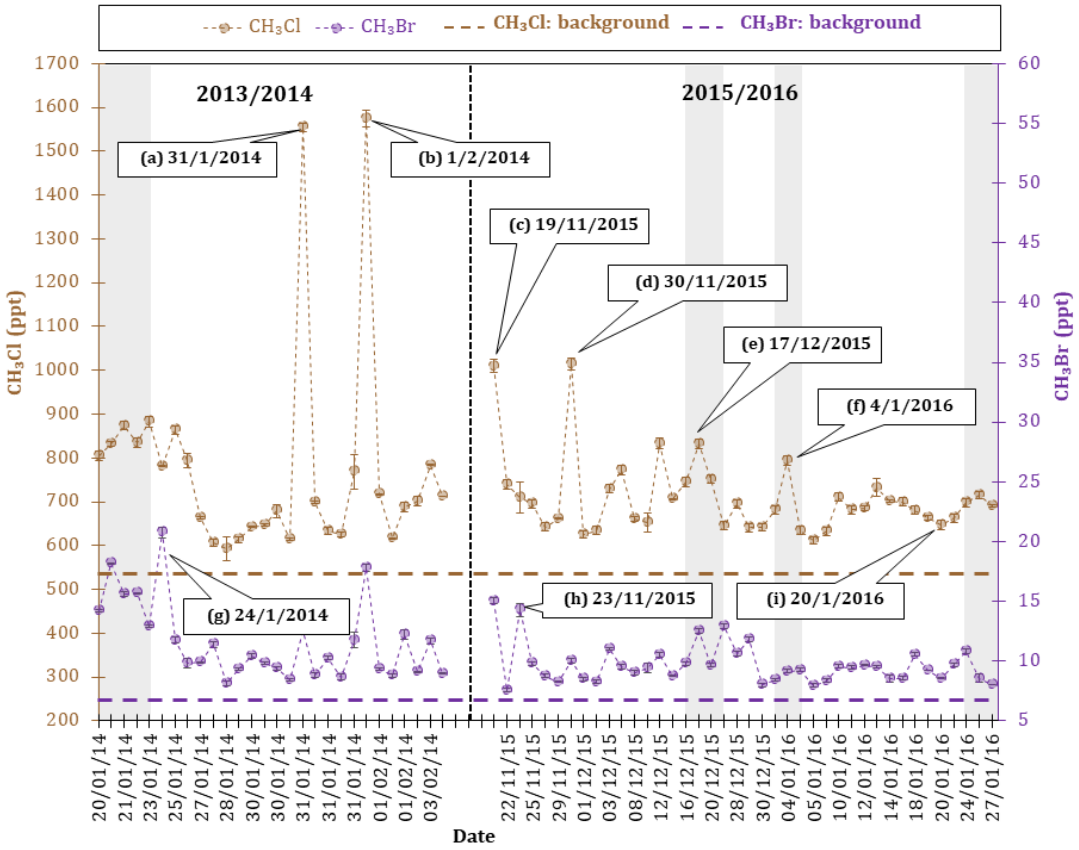

(a) 31/01/2014 00:00 UTC

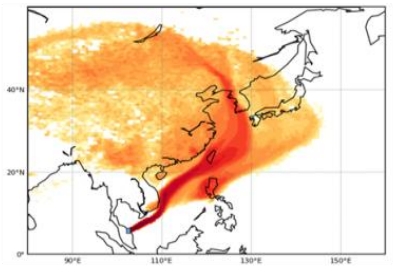

(b) 1/2/2014 00:00 UTC

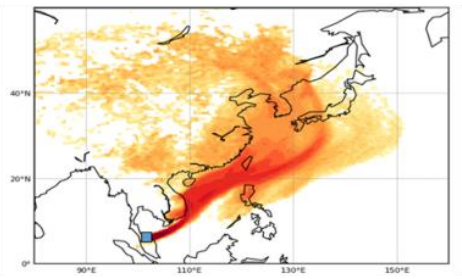

(c) 19/11/2015 09:00 UTC

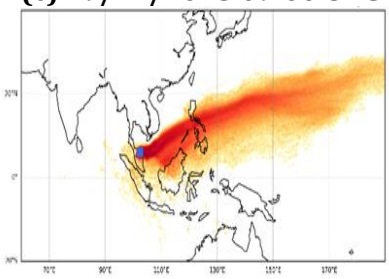

(d) 30/11/2015 09:00 UTC

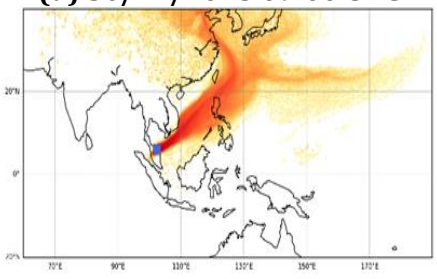

(e) 17/12/2015 09:00 UTC

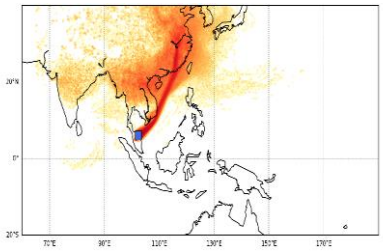

(f) 4/1/2016 03:00 UTC

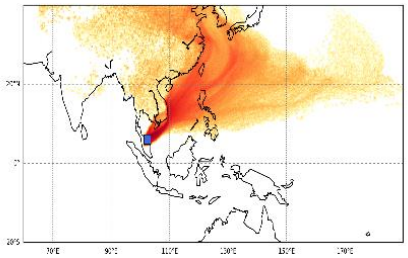

(g) 24/1/2014 10:30 UTC

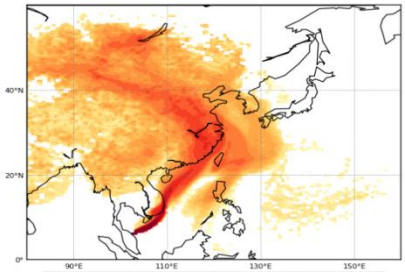

(h) 23/11/2015 09:00 UTC

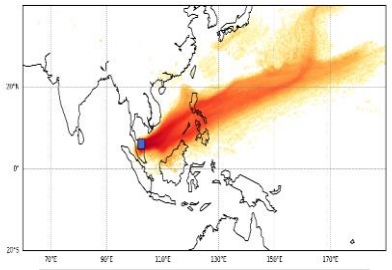

(i) 20/1/2016 09:00 UTC

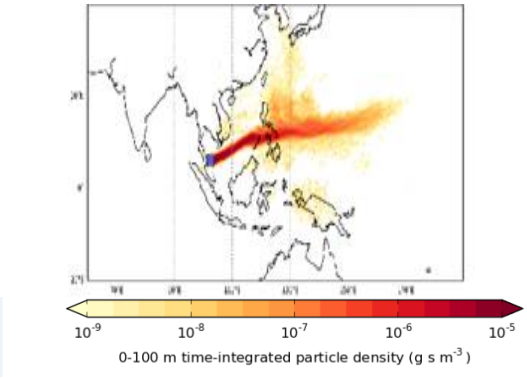

Figure 4.2: Upper panel: *Mixing ratios (ppt) of the methyl halides in air samples collected in Bachok during the Northern Hemisphere winters, 2013/2014 and 2015/2016. The global surface mean mixing ratios of each methyl halide in 2012 are represented by the dashed lines. Also shown is the period of cold surge events (grey shaded regions). This is to highlight that differences in meteorological conditions affect the variation of methyl halides. The examples where the observed mixing ratios of methyl halides were unusually high are also shown, indicated by (a) to (h). For comparison, (i) represents a mixing ratio much closer to the global surface mean mixing ratio for each methyl halide.* ***Lower panel:*** *NAME footprint maps generated from a back-trajectory analysis indicating the likely origin of the air sampled in Bachok, with the darker colours indicating greater influence. The colour scale is logarithmic and represents the calculated time-averaged concentration within surface layer (0–100 m) during the 12 days prior to the sampling days given a point release in Bachok.*

In addition, some enhancements in the mixing ratios of methyl halides were observed on certain days during the campaigns. For example, spikes in the mixing ratios of CH_3Cl and CH_3Br were seen on two days of the 2013/2014 campaign [labelled by (a) and (b)] and five days of the 2015/2016 campaigns [denoted by (c) to (f)]. In all seven instances of elevated methyl halide mixing ratios, the air masses had some contact with continental and oceanic regions as per the NAME footprints. Also, the footprints showed that the mixing ratios had a certain degree of dependence on the amount of contact of air masses with the terrestrial sector. The fact that the air substantially dispersed within the marine sector supports the notion that the compounds could be primarily of marine origin. This suggests that the oceanic production of halocarbons is mostly related to biological processes or reactions that make use of decaying organic matter (Gebhardt et al., 2008).

Interestingly, the mixing ratio enhancements on 31 January and 1 February 2014 were substantial for CH_3Cl but slight for CH_3Br. As stated in Section 3.2.2.2 in Chapter 3, the samples collected on both these days were influenced by the land-sea breeze effect, which meant that the air originated from Bachok (i.e. the land) and, to a lesser extent, the marine sector. The high mixing ratios of methyl halides were unlikely to be attributed to the industrial sources in light of the fact that Bachok is a rural area with very minimal industry. Therefore, the high concentrations of both methyl halides could come from various natural or local sources such as tropical tree emissions and biomass burning. The latter might be possible because on certain days of the campaigns, fires were started by locals to burn residential rubbish.

Apart from the seven days on which the mixing ratios were increased, there were isolated spikes in the mixing ratio of CH_3Br on two additional days – i.e. 24 January 2014 and 23 November 2015 [labelled by (g) and (h) respectively]. In other words, the mixing ratios of CH_3Br on both days were elevated relative to its background values by a much greater percentage amount than were those of CH_3Cl. On 24 January 2014, the spike corresponded with the arrival of air that most likely originated from the boundary layer over eastern China, as per the NAME footprint map. However, the NAME footprint map of 23 November 2015 showed very little influence from the terrestrial regions and the eastern China region as depicted by (h). Rather, the influence of the marine sector was greater; the air mass predominantly originated from the South China Sea and the Pacific Ocean, with

some from the Philippines and Borneo. Overall, the different air mass origins on those two days suggests that the cause of the elevated CH_3Br mixing ratios but not CH_3Cl mixing ratios in Bachok could have been caused by anthropogenic sources on one day and natural sources on another.

4.2.1.3 Synthesis

The methyl halide mixing ratios at Taiwan and Bachok were generally higher than the background levels, demonstrating widespread regional enhancement. As the mixing ratios in Taiwan were slightly higher and more variable than those in Bachok, the site in Taiwan was likely to be located relatively closer to the major source regions. With reference to the NAME footprints, some preliminary conclusions of the possible origins and emission histories of the compounds could be drawn, especially when the mixing ratios were extraordinarily high. Overall, the air masses spent more time over the South China Sea during the campaigns, which implied that oceanic sources had an effect on the observed concentrations. However, the NAME footprints depicted in Figure 4.2 suggested that East Asian and South East Asian sources were also responsible for the high concentrations of methyl halides in Taiwan and Bachok. In Section 4.2.3, the influences of potential regions on the variations of the mixing ratios of the methyl halides are further investigated and quantified.

Although the high mixing ratios of methyl halides above the background level as observed in Bachok may reflect a substantial contribution from Chinese industrial emissions, natural or nonindustrial sources present in the region may affect the observed mixing ratios of methyl halides. Both CH_3Cl and CH_3Br predominantly originate from natural sources, mainly biomass burning and oceanic sources. Bachok is located in a maritime continent, a tropical site with both oceanic and terrestrial sources nearby, along with frequent biomass burning. This suggests that the abovementioned sources could possibly contribute towards the variations of methyl halides.

It was also highly likely that the peak concentrations of methyl halides in Bachok were influenced by meteorological conditions. One cold surge was detected during

the earlier part of the 2013/2014 campaign, while two more were detected in the middle of the 2015/2016 campaign (denoted by grey shaded regions in Figure 4.2). Coincidently, during these cold events, the mixing ratios of the methyl halides were enhanced, suggesting that the unusual enhancements in the mixing ratios of methyl halides in such regions were caused by unusually strong northerly winds in the form of "cold surges". Therefore, rapid meridional transports are likely to act as an important mechanism for transporting large quantities of these short-lived chlorinated compounds, with the capacity to deplete stratospheric O_3, from East Asian emission sources to Bachok and other locations near the tropics (Ashfold et al., 2017).

The findings from this work were found to be consistent with Ashfold et al. (2015), who showed that during a Northern Hemisphere winter, cold surges could, over a few days, rapidly transport polluted air masses from East Asia to tropical South East Asia. In summary, it is evident from this work that meteorological conditions, e.g. cold surges, can influence the variability of the measured methyl halides. However, since (a) a handful of cold surges were detected during the campaigns and (b) as there are still few studies (e.g. Liu et al. (2003) and Wang et al. (2016)) on the importance of cold surges in the tropics, further observations are required to investigate the influence of cold surges on the atmospheric compositions of the said substances in such regions.

4.2.2 Interspecies correlations of methyl halides

In this section, the outcomes of interspecies correlation analyses are presented to shed some light on the potential sources of methyl halides in Taiwan and Bachok. The initial analysis was performed to identify the presence of connections between CH_3Cl and CH_3Br. A similar analysis was also performed for methyl halides and other chlorinated VSLSs – e.g. dichloromethane (CH_2Cl_2), which represents a chlorinated VSLS of predominantly anthropogenic origin, as well as chloroform ($CHCl_3$), which arises from both anthropogenic and natural sources (more details in Chapter 3). The interspecies correlations are discussed in Sections 4.2.2.1 and 4.2.2.2 respectively.

4.2.2.1 Taiwan

In general, the mixing ratios of CH_3Cl correlated well with CH_3Br ($R > 0.6$) in most years, although a slightly lower correlation coefficient was observed in 2013 [Table 4.4(a)]. The mixing ratios of CH_3Cl also correlated very well ($R > 0.6$) with CH_2Cl_2 over multiple years. The same ($R > 0.6$) was true for CH_3Cl versus $CHCl_3$ in 2014, 2015, and 2016 as well, but not in 2013 [Table 4.4 (a)). Meanwhile, CH_3Br correlated well with CH_2Cl_2 in 2014, 2015 and 2016 but not in 2013 [Table 4.4 (b)]. CH_3Br also correlated with CH_3Cl in all four years [Table 4.4 (b)]. Evidently, the correlations had year-to-year variations. This was probably due to the sampling of air from different source regions which in turn were very likely to have different source signatures.

Table 4.4: *Interspecies correlations of mixing ratios between (a) CH_3Cl with other compounds, and (b) CH_3Br with other compounds in Taiwan during campaigns from 2013 to 2016. The values indicate the Spearman correlation coefficients (R). Correlations that are significant ($p<0.05$) are in bold font.*

(a) CH_3Cl versus other species

	2013	2014	2015	2016
CH_3Br	**0.62**	**0.75**	**0.78**	**0.92**
CH_2Cl_2	**0.63**	**0.91**	**0.65**	**0.90**
$CHCl_3$	**0.49**	**0.81**	**0.65**	**0.87**
No. of data points	19	22	23	33

(b) CH_3Br versus other species

	2013	2014	2015	2016
CH_3Cl	**0.62**	**0.75**	**0.78**	**0.92**
CH_2Cl_2	**0.52**	**0.65**	**0.55**	**0.90**
$CHCl_3$	0.28	**0.61**	**0.63**	**0.81**
No. of data points	19	22	23	33

It is noteworthy that in 2013, the correlation between CH_3Cl and CH_3Br had a R value that was lower (0.62) than those of other years (range: 0.75 – 0.92) (Table 4.4, Figure 4.3). To identify the cause of the change in the correlation strength, the correlation plots were examined for the presence of significant outliers. Also, individual NAME footprints and outcomes of the NAME particle concentration analysis were used to provide further insight on the origins of the air masses of the

affected samples. In Figure 4.3 (a), there was a point below the CH_3Cl and CH_3Br regression plot which denoted a high mixing ratio of CH_3Cl but low mixing ratio of CH_3Br [denoted by (a)]. This outlier corresponded to the sample collected on 21 March 2013, when the air masses had some influence from the East Asian region (China, Taiwan, and Korea). Apart from minimal contributions from Taiwan and Korea, it is interesting to note that some influence from Indochina was also seen on that day.

Comparisons were also made against the data points that showed high mixing ratios of CH_3Cl and CH_3Br. One such point corresponded to the samples taken on 4 April 2013, when the air masses were under a greater influence from oceanic regions rather than continental sites (especially China) [Figure 4.3 (a) and (b)]. The contradictory origins of air masses on 21 March 2013 and 4 April 2013 suggested that (1) continental air masses, especially those from East Asia, had a more significant impact on the mixing ratio of CH_3Cl than that of CH_3Br, as well as (2) the air masses from South East Asia, especially Indochina, contributed more to the high mixing ratios of CH_3Cl. Overall, CH_3Cl correlated well with CH_3Br in most years, indicating that they were very likely to arise from similar source emissions.

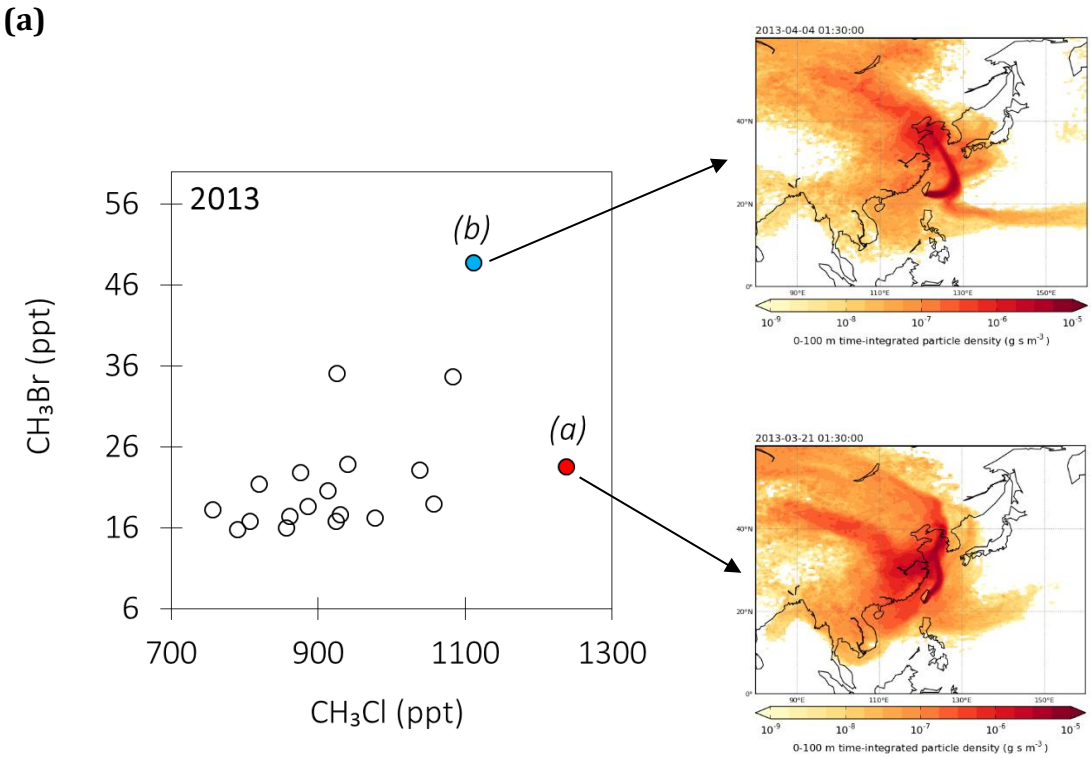

(b)

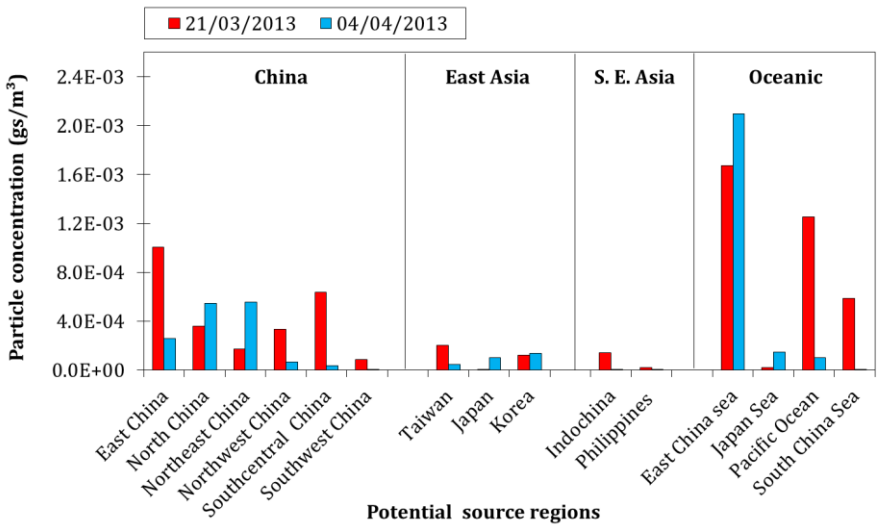

Figure 4.3: *The correlation between CH_3Cl and CH_3Br in which the R value was low in comparison to the R values recorded for other years. The NAME footprints and the results of the particle concentration analysis are presented to understand the source of air masses for affected samples.*

Interestingly, the mixing ratios of CH_3Cl and CH_3Br correlated very well ($R > 0.7$) in 2014, 2015, and 2016; the regression slope was also relatively constant during this period (Figure 4.4). Hence, these findings suggest that their different lifetimes did not have a significant effect on their ratios.

Also, it is noted that when there were good interspecies correlations ($R > 0.5$), the correlation coefficients between CH_3Cl and other compounds (i.e. CH_2Cl_2 and $CHCl_3$) were always higher than those of CH_3Br against CH_2Cl_2 and $CHCl_3$. This implies a possible link between the sources of CH_3Cl with those of CH_2Cl_2 and $CHCl_3$.

4.2.2.2 Bachok

A good correlation ($R = 0.7$) was observed between CH_3Cl and CH_3Br in 2013/2014, highlighting that they could have shared similar source type(s) or region(s) (Table 4.5). CH_3Cl also correlated well ($R > 0.6$) with other chlorinated VSLSs (i.e. CH_2Cl_2 and $CHCl_3$) [Table 4.5(a)], which suggested that the variability in the mixing ratios

of CH_3Cl during the 2013/2014 campaign could have been influenced by mixed sources or similar source regions. Meanwhile, CH_3Br also correlated well with $CHCl_3$ (R = 0.58) and CH_2Cl_2 (R = 0.61) [Table 4.5(b)].

In 2015/2016, some degree of correlation was seen between CH_3Cl and other species, although these values were slightly lower than those of 2013/2014 [Table 4.5(a)]. This was also the case with the correlation coefficients between CH_3Br and other species [Table 4.5(b)]. The significant year-to-year variations in the correlation coefficients could probably be attributed to the different transport pathways taken by the air masses prior to reaching Bachok. During the 2015/2016 campaigns, the air masses might not have traversed the same regions that emitted significant quantities of methyl halides. The differing source regions in each year were very likely to contain different source signatures or ratios.

Table 4.5: *Interspecies correlations of mixing ratios of (a) CH_3Cl with other compounds, and (b) CH_3Br with other compounds in Bachok during the 2013/2014 and 2015/2016 campaigns. The values indicate the Spearman correlation coefficients (R). Correlations that are significant ($p<0.05$) are in bold font.*

(a) CH_3Cl versus other species

	2013/2014	2015/2016
CH_3Br	**0.70**	0.42
CH_2Cl_2	**0.64**	0.31
$CHCl_3$	**0.65**	0.36
No. of data points	26	40

(b) CH_3Br versus other species

	2013/2014	2015/2016
CH_3Cl	**0.70**	0.42
CH_2Cl_2	**0.61**	0.13
$CHCl_3$	**0.58**	0.18
No. of data points	26	40

4.2.2.3 Synthesis

In the Taiwan campaigns, the mixing ratios of CH_3Cl and CH_3Br had very good correlations in 2014 (R = 0.75), 2015 (R = 0.78), and 2016 (R = 0.92). Also, the gradients in Figure 4.4 (a) were relatively constant from year to year. Similarly, a good correlation (R = 0.70) existed between CH_3Cl and CH_3Br in Bachok during the 2013/2014 campaign [Table 4.5, Figure 4.4 (b)]. These findings suggest that the compounds' different lifetimes did not have a significant effect on their ratios.

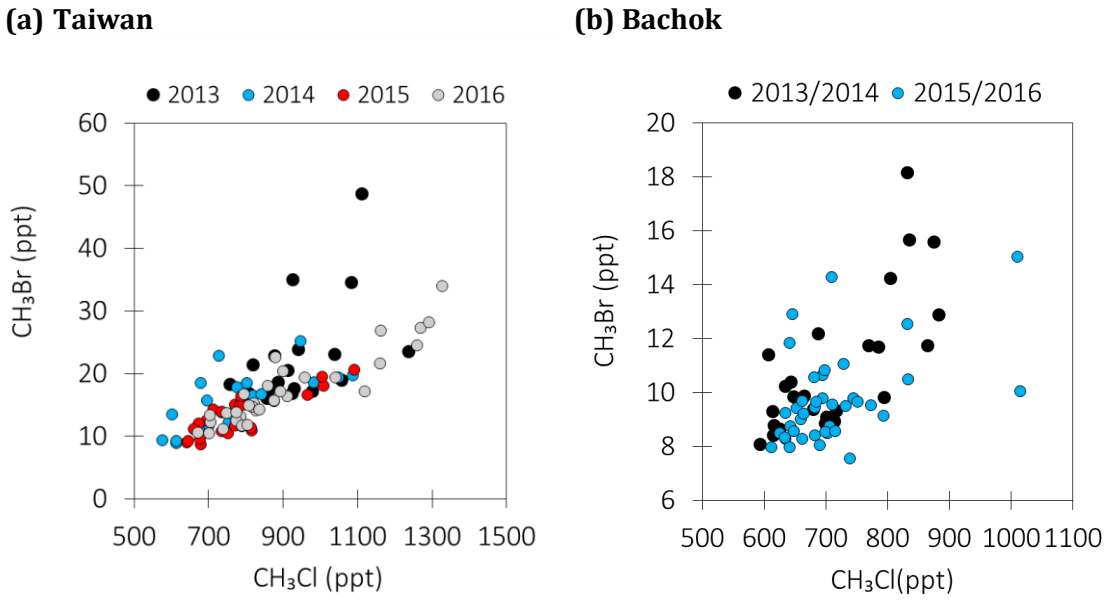

Figure 4.4: *The correlation plots for CH_3Br and CH_3Cl during multiyear campaigns in (a) Taiwan and (b) Bachok.*

Additionally, when good interspecies correlations were observed (R > 0.5), the correlation coefficients of CH_3Cl with CH_2Cl_2 and $CHCl_3$ were always higher than those of CH_3Br with the same compounds. This suggests the presence of a significant link between the sources of CH_3Cl with those of CH_2Cl_2 and $CHCl_3$.

The lack of correlation between CH_3Cl and CH_2Cl_2 during 2015/2016 campaign in Bachok was probably caused by potentially minimal influences of anthropogenic sources from East China. The same was also true for CH_3Br versus CH_2Cl_2 in 2015/2016. In contrast, CH_3Br had some degree of correlation with CH_2Cl_2 in the

2013/2014 campaign, which implied that East China was a potential source of emissions. However, in all cases, the correlations were not significant ($p > 0.05$), which highlighted that the methyl halides in Bachok did not predominantly originate from anthropogenic sources. Instead, natural or nonindustrial sources – oceans, biomass burning, and tropical vegetation – could have been the chief contributors to the variability in the mixing ratios of methyl halides in Bachok, which would also explain the consistent elevation of their mixing ratios above their global surface mean mixing ratio.

4.2.3 Identification and quantification of possible geographical source region(s) and source type(s) of methyl halides

4.2.3.1 Potential geographical source region(s)

To understand the variations in the methyl halide mixing ratios, the recent histories of the air masses that arrived at the measurement sites needed to be assessed. For that purpose, analyses of the NAME footprints and their relative particle concentrations have been conducted to investigate the possible origins and paths of the particles which arrived at the station during the sampling periods. This exercise was especially important when the mixing ratios were extraordinarily high.

Over the twelve days prior to sampling, the trajectories of all particles traversed a combination of countries. Figure 4.5 shows examples of NAME footprints which covered various countries. In other words, the emissions from any of these countries could have had an impact on the air which arrived at the Taiwan and Bachok stations during the campaign periods. The geographical sector map for Bachok and Taiwan which depicts the possible source locations for the air masses sampled during each campaign, assessed from analysis of the NAME footprints, can be found in Figure 2.6 in Chapter 2, Section 2.4.1.5.1.

(a) Taiwan campaign in March 2016 **(b) Bachok campaign in February 2016**

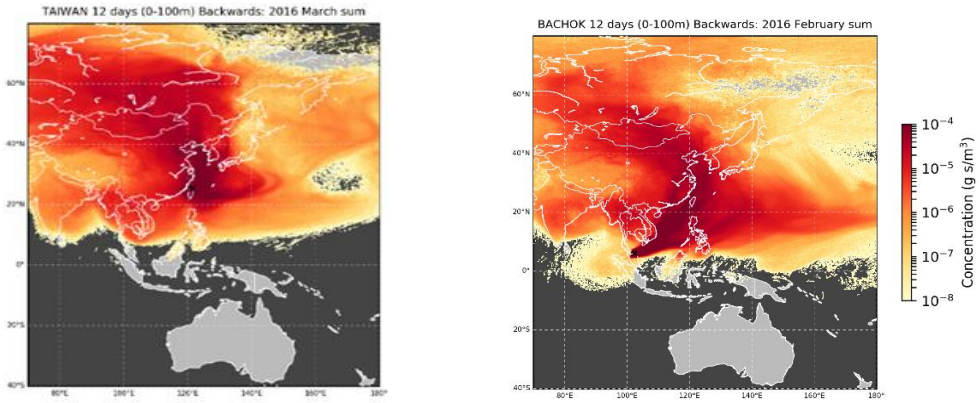

Figure 4.5: *Examples of the monthly sum of the NAME footprints in (a) Taiwan and (b) Bachok. The sum of NAME footprints is a combination of the daily NAME footprints that provides an overview on the dispersion of the air masses and possible countries that may contribute emissions to the air masses that arrived in that particular month.*

The relevant countries can be divided into sub-regions according to the classification system of the 2017 United Nations Population Division (United Nations, 2007). This exercise was important since China is a big country comprising six provinces. Although China belongs to the East Asian region, its six sub-regions have been clustered into a separate region called "China" in this study (Table 4.6). The segregation of China from East Asia enabled more detailed analyses to determine whether regions apart from East China contribute to the variations in the methyl halide mixing ratios.

Table 4.6: *Classification of Asian countries by sub-region*

China	East Asia	South East Asia	Oceanic regions
• East China • South West China • South Central China • North East China • North China • North West China	• Taiwan • Korea • Japan	• Malaysia • Indochina (Thailand, Cambodia, Laos, Vietnam) • Philippines • Indonesia	• East China Sea • Japan Sea • South China Sea • Pacific Ocean

4.2.3.1.1 Taiwan

As mentioned in Section 4.2.2.1, the mixing ratios of CH_3Cl correlated well with those of CH_3Br, thereby suggesting that they shared common sources or source regions. Therefore, an understanding of the influences of potential regions on the CH_3Cl mixing ratio variation would also shed some light on the potential sources of CH_3Br.

The mixing ratio of CH_3Cl can be regarded as extremely high when it is consistently more than 900 ppt (i.e. almost double the global surface mixing ratio). Overall, eleven out of the nineteen samples obtained in 2013 had very high CH_3Cl mixing ratios. From these, nine of the samples contained high mixing ratios of CH_3Br (above 20 ppt). These samples were mainly influenced by the air masses which originated from oceanic regions, especially the East China Sea and the Pacific Ocean. Concurrently, the influences of continental air masses were also seen, especially from China (East China), Korea and Taiwan (Figure 4.6). When low mixing ratios were observed (< 900ppt), contribution of continental air masses reduced. This time much influence was seen coming from the oceanic regions. Likewise, the samples collected between 2014 and 2016 inclusive also had similar findings (i.e. air masses of continental origin gave rise to CH_3Cl mixing ratios of over 900 ppt). Evidently, low mixing ratios reflect greater oceanic influence.

(a) 2013

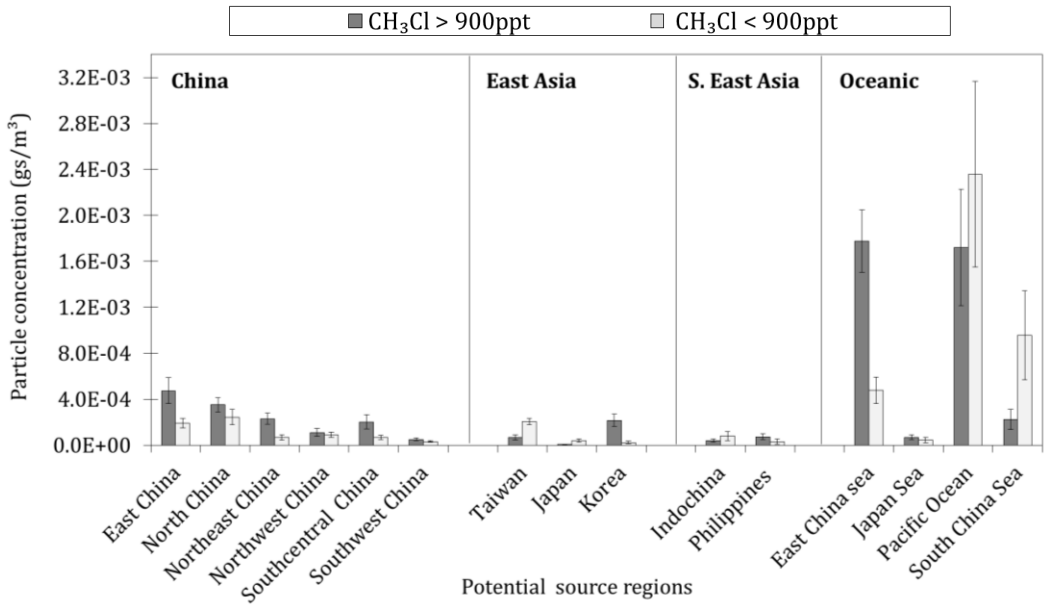

(b) 2014

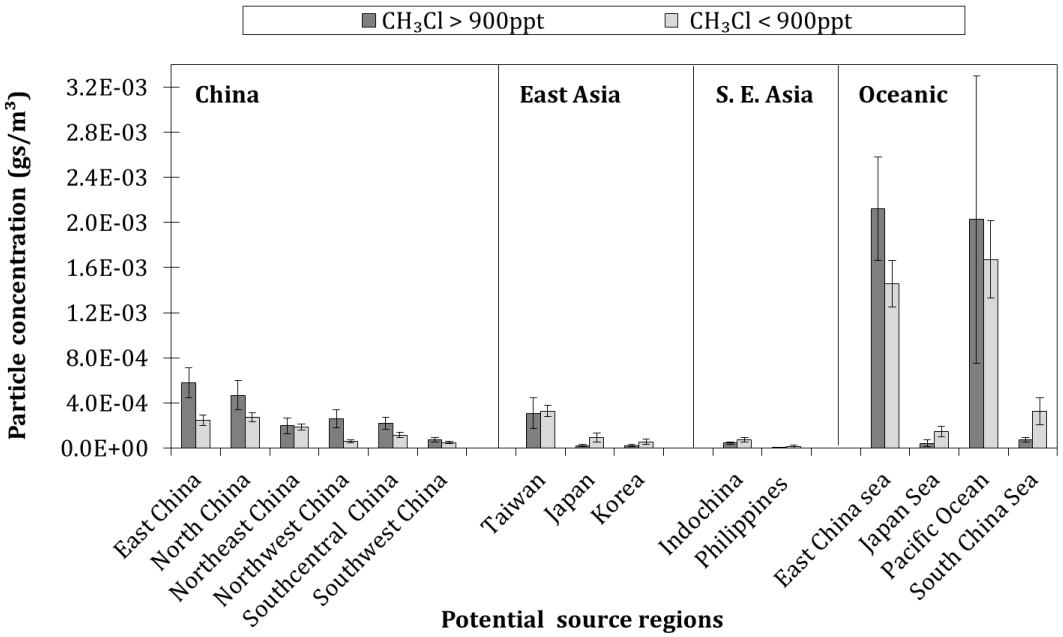
CH3Cl > 900ppt
CH3Cl < 900ppt
Particle concentration (gs/m3)
3.2E-03
2.8E-03
2.4E-03
2.0E-03
1.6E-03
1.2E-03
8.0E-04
4.0E-04
0.0E+00
China
East Asia
S. E. Asia
Oceanic
East China
North China
Northeast China
Northwest China
Southcentral China
Southwest China
Taiwan
Japan
Korea
Indochina
Philippines
East China sea
Japan Sea
Pacific Ocean
South China Sea
Potential source regions

(c) 2015

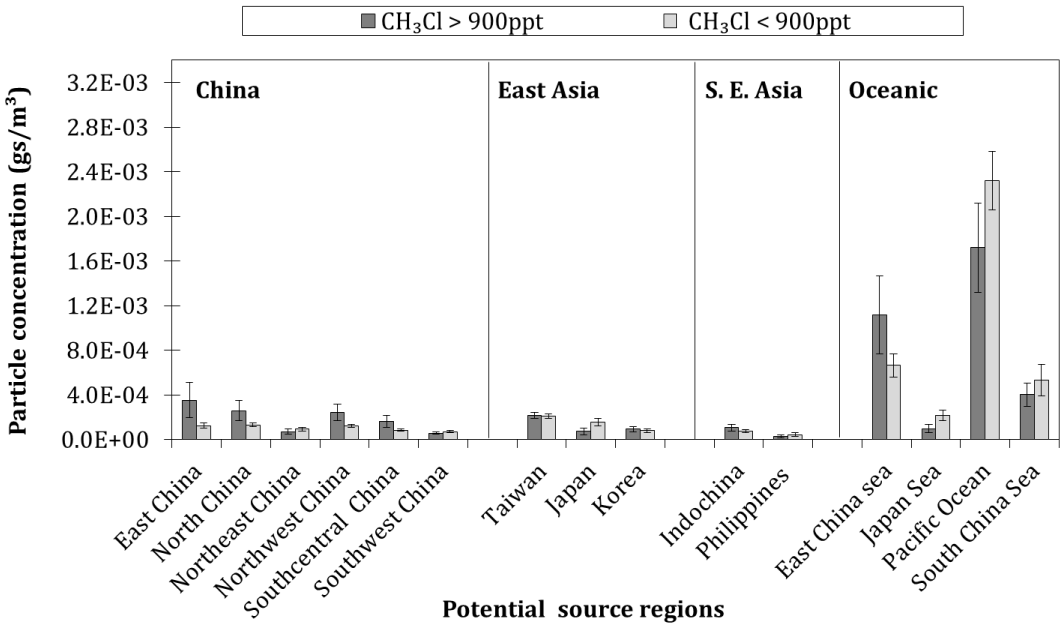
CH3Cl > 900ppt
CH3Cl < 900ppt
Particle concentration (gs/m3)
3.2E-03
2.8E-03
2.4E-03
2.0E-03
1.6E-03
1.2E-03
8.0E-04
4.0E-04
0.0E+00
China
East Asia
S. E. Asia
Oceanic
East China
North China
Northeast China
Northwest China
Southcentral China
Southwest China
Taiwan
Japan
Korea
Indochina
Philippines
East China sea
Japan Sea
Pacific Ocean
South China Sea
Potential source regions

(d) 2016

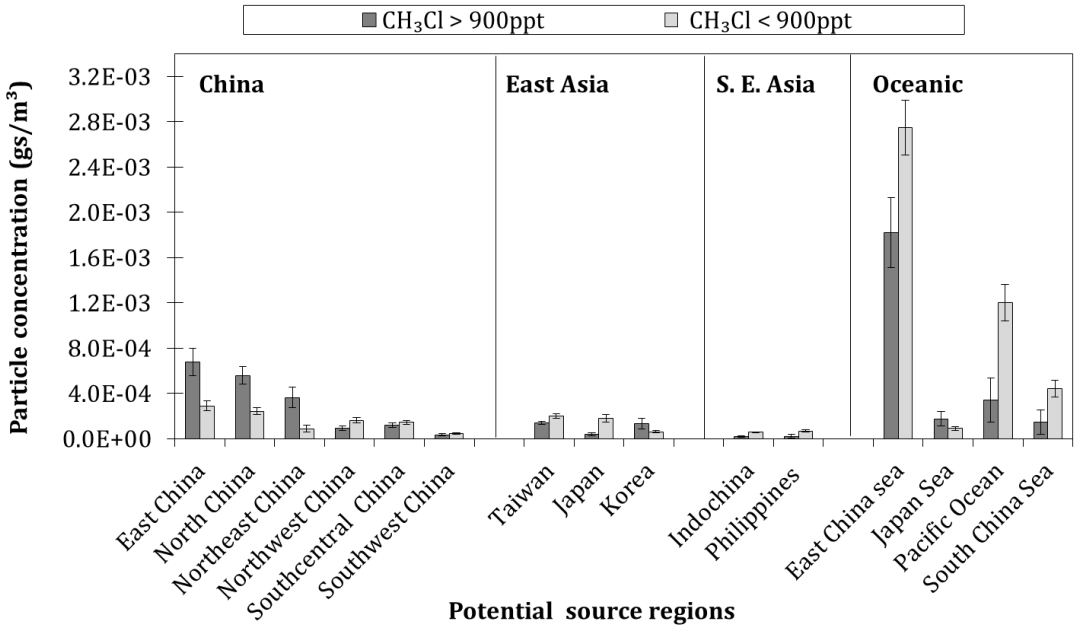

Figure 4.6 *The mean particle concentration (g s/m^3) from potential source regions during campaigns in Taiwan from 2013 to 2016.*

4.2.3.1.2 Bachok

In the Bachok campaigns, CH_3Cl mixing ratios which were above 800 ppt could be regarded as extremely high. Meanwhile, CH_3Br mixing ratios which exceeded 11 ppt were considered to be high. On average, the high CH_3Cl mixing ratios in 2013/2014 were influenced by air masses that originated from the oceanic regions (especially the South China Sea). Air masses from East China and Indochina also had an effect on CH_3Cl mixing ratios that were in excess of 800 ppt, even though the mean particle concentrations were not as high as those which were influenced by air masses from the South China Sea [Figure 4.7 (a)]. When the CH_3Cl mixing ratios were low, the influence of air masses from terrestrial regions (e.g. China and Indochina) and oceanic regions (e.g. South China Sea and Pacific Ocean) decreased and increased respectively. Evidently, these observations were similar to those of the 2015/2016 campaigns [Figure 4.7 (b)]. It is interesting to note that the mean particle concentrations in the oceanic regions during the 2015/2016 campaign were much higher than that of the 2013/2014 campaign. Specifically, air masses from the South China Sea had a high CH_3Cl mixing ratio of 3.8×10^{-3} g s/m^3 in 2015/2016, which was almost double the value in 2013/2014 (1.7×10^{-3} g s/m^3).

(a) 2013/2014

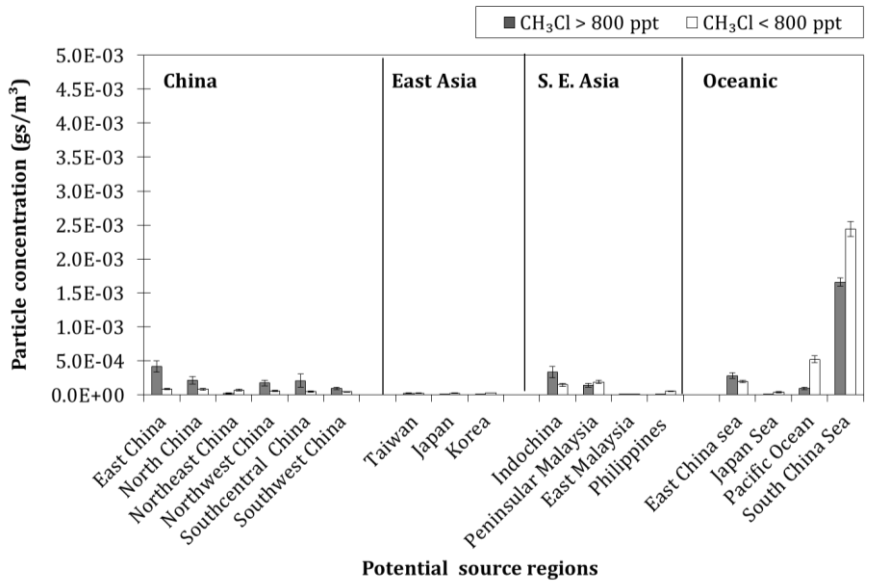

(b) 2015/2016

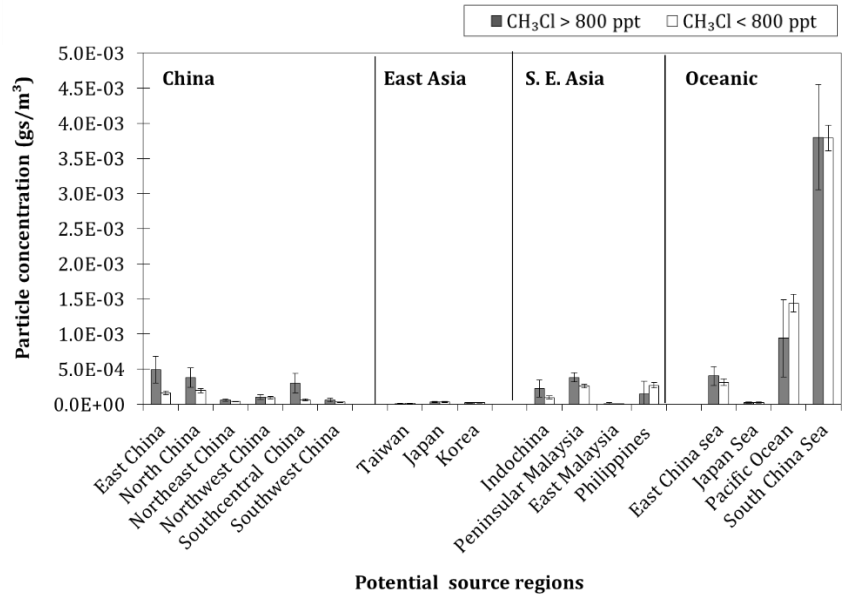

Figure 4.7: *Mean particle concentrations (g s/m^3) from potential source regions during 2013/2014 and 2015/2016 campaigns in Bachok.*

During the 2013/2014 campaign, there were two days in which the CH_3Cl mixing ratios were unusually high (Section 4.2.1.2). On 31 January and 1 February 2014, the aforementioned ratios were 1554 and 1574 ppt respectively – around three times higher than the global surface mean mixing ratio (540 ppt) and almost two times

higher than the threshold of high CH_3Cl mixing ratios (above 800 ppt) recorded during both 2013/2014 and 2015/2016 campaigns (Figure 4.2). The mixing ratios of CH_3Br were also elevated on these days, but their magnitudes were not as outstanding compared those of CH_3Cl. As mentioned in Section 4.2.1.2, the samples taken on these days were influenced by the land-sea breeze effect, which meant that the air masses spent more time over the land (Peninsular Malaysia) rather than the sea. Similar magnitude CH_3Cl mixing ratios, i.e. as high as 1500 ppt, have also been detected at Cape Hedo, Okinawa, Japan (26.9^0N, 128.3^0E) on a calm night (Yokouchi et al., 2000). A possible reason for this occurrence was the immense production of CH_3Cl in the island's surrounding coastal waters (marine bioactivity). However, Moore et al. (1996) suggest that the emission of CH_3Cl was not only related to marine bioactivity and coastal waters; instead, land sources of CH_3Cl might also have been responsible for the increase. Bachok district in the state of Kelantan is a rural area whose primary economic activity is tobacco and kenaf plantations. Other agrarian activities in Kelantan include the production of rice and rubber (Farren et al., 2019). Those activities could be potential emitters of methyl halides. Since the unusually high CH_3Cl mixing ratios were recorded on the two days when the air masses spent more time over Peninsular Malaysia, the occurrence could be related to the biogenic emission which is released by many kinds of terrestrial plants (Zimmerman et al., 1979; Yokouchi et al., 1981).

Overall, with reference to the influence of continental air masses, unusually high mixing ratios of particle concentrations were also observed in air masses coming from Peninsular Malaysia (Figure 4.8). This was contrary to the fact that high mixing ratios of CH_3Cl always corresponded to continental air masses which came from East China (Figure 4.7). Therefore, there was a good chance that the air masses sampled on those two days had spent a significant portion of time at Bachok. In other words, the outlier CH_3Cl mixing ratio peaks recorded on those two days were likely to be affected by local activities in Bachok.

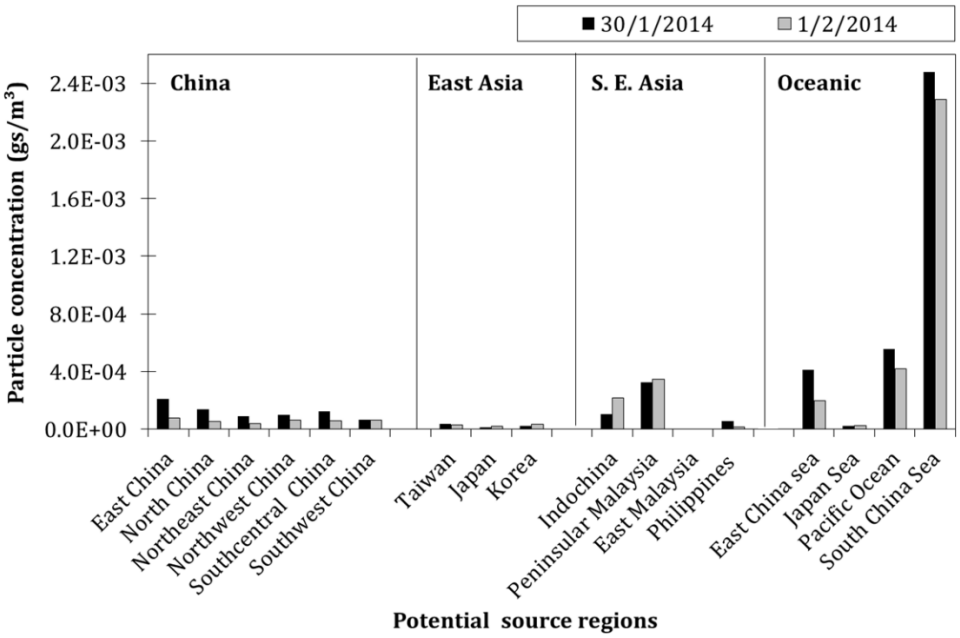

Figure 4.8: *Mean particle concentrations (g s/m^3) of samples collected on 31 January and 1 February 2014.*

4.2.3.2 Potential source type(s)

This section examines the influences of various emission sectors on the mixing ratios of methyl halides at Taiwan and Bachok with the purpose of identifying the likely key sources of methyl halide emissions.

As described in Chapter 2, carbon monoxide (CO) surface emission data from the representative concentration pathways (RCPs) were used along with the NAME footprints to estimate the modelled CO mixing ratios. The modelled CO mixing ratios were compared with the methyl halide mixing ratios at the measurement sites. The details of the method are provided in Chapter 2 (Section 2.4.1.5.3).

The CO emission inventories were divided into seven emission sectors: (1) industry (combustion and processing), (2) surface transportation, (3) agriculture (waste burning in fields), (4) waste (landfills, waste water, waste incineration), (5) forest burning, (6) grassland burning, as well as (7) agriculture (animals, rice, soil). These types of emission sectors were chosen since they most likely represented the sources of methyl halide emissions (as described in Table 4.1, Section 4.1).

4.2.3.2.2 Taiwan

Table 4.7 presents the Spearman correlation coefficients (R) for the association of the modelled CO mixing ratios (which were derived from various emission categories) with the mixing ratios of CH_3Cl and CH_3Br. This analysis aimed to assess the extent to which these categories of emissions influenced the mixing ratios of methyl halides in the air masses that arrived at Taiwan and Bachok. Doing so would shed some light on the potential source(s) of methyl halides.

Table 4.7: *Association of modelled CO mixing ratios derived from various emission types with the observed mixing ratios of (a) CH_3Cl and (b) CH_3Br in Taiwan. The values indicate the Spearman correlation coefficients (R). Correlations that are significant ($p < 0.05$) are in bold.*

(a)

Emission type	2013	2014	2015	2016
1. Industry (combustion and processing)	**0.59**	**0.72**	**0.47**	**0.82**
2. Surface transportation	**0.51**	0.34	**0.47**	**0.48**
3. Agriculture (waste burning on fields)	**0.51**	**0.59**	0.34	**0.80**
4. Waste (landfills, waste water, incineration)	0.14	0.04	0.22	0.27
5. Forest burning	0.09	0.29	0.34	0.05
6. Grassland burning	0.13	0.24	0.37	0.17
7. Agriculture (animals, rice, soil)	**0.47**	0.21	-0.03	0.02

(b)

Emission type	2013	2014	2015	2016
1. Industry (combustion and processing)	0.40	**0.55**	**0.49**	**0.85**
2. Surface transportation	0.28	0.39	0.41	**0.60**
3. Agriculture (waste burning on fields)	0.33	0.42	0.38	**0.74**
4. Waste (landfills, waste water, incineration)	0.05	-0.10	0.24	0.34
5. Forest burning	-0.21	-0.04	0.12	0.34
6. Grassland burning	-0.01	-0.09	0.22	0.03
7. Agriculture (animals, rice, soil)	0.15	0.20	0.04	0.02

The results showed that the modelled CO mixing ratios, which were derived from industries (combustion and processing), surface transportation, and agriculture (waste burning in fields), correlated significantly with multiple years' CH_3Cl mixing ratios, particularly in 2013 and 2016 [Table 4.7 (a)]. In 2014, significant correlations were observed between CH_3Cl mixing ratios with the modelled CO derived from industries (combustion and processing) and agriculture (waste burning in fields). In 2015, modelled CO derived from industries (combustion and processing) and surface transportation correlated significantly with mixing ratios of CH_3Cl.

As for CH_3Br [Table 4.7 (b)], the mixing ratios mainly correlated with modelled CO mixing ratios that were derived from industries (combustion) from 2014 until 2016. Unlike CH_3Cl, much stronger and significant correlations between CH_3Br mixing ratios and modelled CO derived from surface transportation and agriculture (waste burning in fields) were only seen in 2016.

Interestingly, the plot patterns in Figure 4.9 imply that there were highly similar geographical distributions of three significant emissions of modelled CO (i.e. industry (combustion and processing), surface transportation and agriculture (waste burning in fields)). As these emission sectors are largely co-located, it is challenging to determine the exact source(s) of methyl halides.

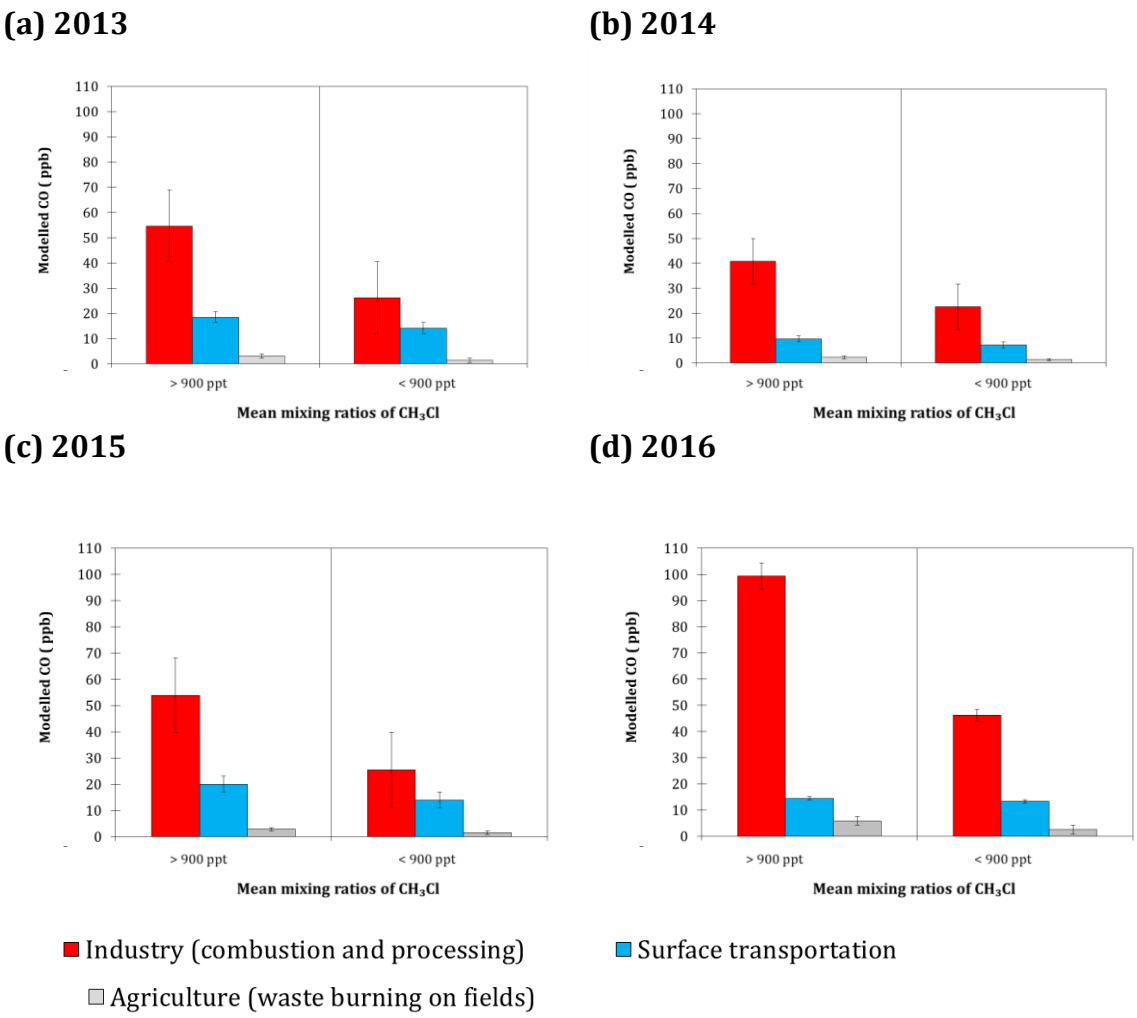

Figure 4.9: *Comparison between modelled CO (ppb) from various emission sectors with high (> 900 ppt) and low (< 900 ppt) mixing ratios of CH_3Cl in Taiwan between 2013 and 2016. The modelled CO mixing ratio is accounted for by various emissions within the timescale of the backward trajectories (i.e. 12 days prior to the observations).*

4.2.3.2.2 Bachok

In the 2013/2014 campaigns, significant correlations were observed between the mixing ratios of CH_3Cl and the modelled mixing ratios of CO that were derived from all emission types except for waste (landfills, waste water, incineration) and agriculture (animals, rice, soil) [Table 4.8 (a)]. However, the strengths of the correlations reduced during 2015/2016 campaigns; significant correlations were observed only between the mixing ratios of CH_3Cl and modelled CO mixing ratios that were derived from forest burning.

Similarly, for CH_3Br, the 2013/2014 mixing ratios correlated significantly with the modelled mixing ratios of CO that were derived from all emission types except for

waste (landfills, waste water, incineration) and agriculture (animals, rice, soil) [Table 4.8 (b)]. In contrast, no significant correlations were observed between the mixing ratios of CH_3Br and the modelled CO mixing ratios that were derived from any of the sectors during the 2015/2016 campaigns.

Table 4.8: *Association of modelled CO mixing ratios derived from various emission types with the observed mixing ratios of (a) CH_3Cl and (b) CH_3Br in Bachok. The values indicate the Spearman correlation coefficients (R). Correlations that are significant ($p < 0.05$) are in bold.*

(a)

Emission type	2013/2014	2015/2016
1. Industry (combustion and processing)	**0.51**	0.12
2. Surface transportation	**0.61**	0.21
3. Agriculture (waste burning on fields)	**0.41**	0.10
4. Waste (landfills, waste water, incineration)	-0.37	0.22
5. Forest burning	**0.71**	**0.44**
6. Grassland burning	**0.61**	0.16
7. Agriculture (animals, rice, soil)	n.a	0.14

(b)

Emission type	2013/2014	2015/2016
1. Industry (combustion and processing)	**0.48**	0.03
2. Surface transportation	**0.51**	0.11
3. Agriculture (waste burning on fields)	**0.43**	0.01
4. Waste (landfills, waste water, incineration)	-0.46	0.10
5. Forest burning	**0.40**	0.13
6. Grassland burning	**0.47**	-0.06
7. Agriculture (animals, rice, soil)	n.a.	-0.12

Note: n.a. = data not available

The plot patterns in Figure 4.10 imply highly similar geographical distributions of the five significant emissions of modelled CO (i.e. Industry (combustion and processing), surface transportation, agriculture (waste burning in fields), forest burning and grassland burning). As these emission sectors are largely in the same region, the exact sources of the methyl halides measured in Bachok are hard to specify.

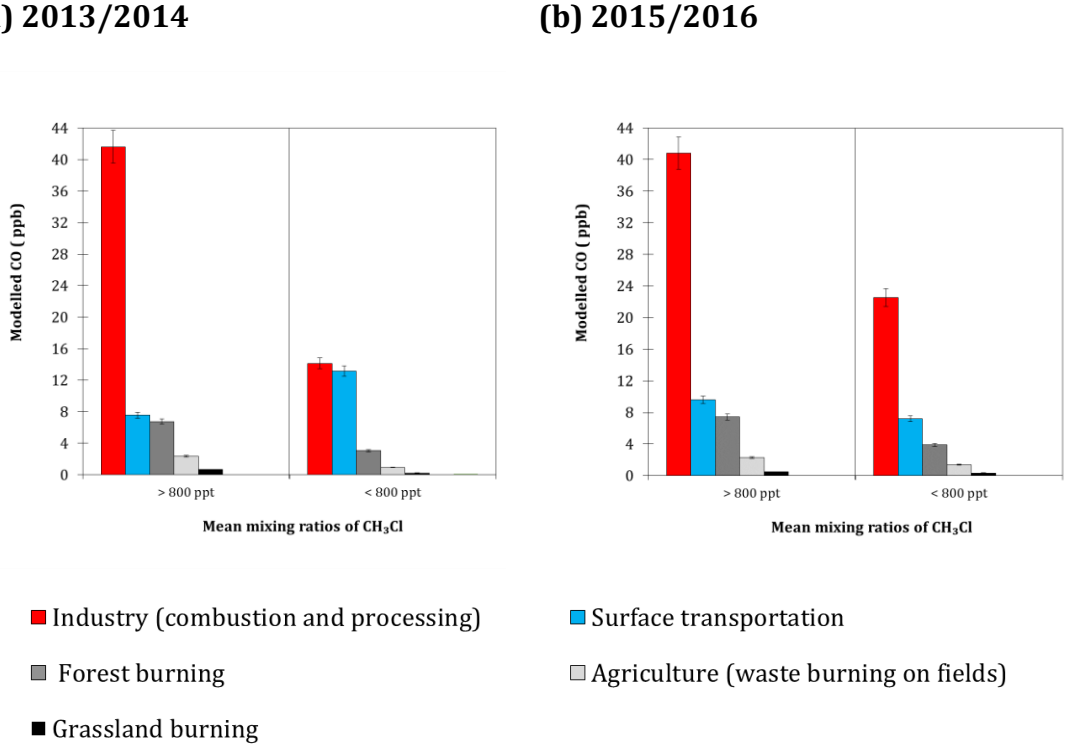

Figure 4.10: *Comparison between modelled CO (ppb) from significant emission sectors with high (> 800 ppt) and low (< 800 ppt) mixing ratios of CH_3Cl in in Bachok during the 2013/2014 and 2015/2016 campaigns. The modelled CO mixing ratio is accounted for by various emissions within the timescale of the backward trajectories (i.e. twelve days prior to the observations).*

4.2.3.3 Synthesis

Methyl halides are predominantly of natural origin, with little influence from anthropogenic sources. Therefore, significant natural sources and probably some anthropogenic sources around Taiwan and Bachok should have affected the variability of the measured methyl halide mixing ratios. Overall, when high mixing ratios of methyl halides in both Taiwan and Bachok (CH_3Cl > 800 ppt, CH_3Br > 11 ppt) were observed (Section 4.2.3.1), air masses were found to be predominantly from oceanic regions, with some influence from continental regions (i.e. China, East Asia, and South East Asia). In contrast, when low mixing ratios of methyl halides were recorded (CH_3Cl < 800 ppt, CH_3Br < 11 ppt), the involvement of oceanic regions was much more profound, and the influence of continental air masses reduced.

However, when looking at the correlation between potential source regions and methyl halides in Taiwan (Table 4.9), significant multiyear correlations were shown between CH_3Cl mixing ratios and the continental air masses, such as from East China. Whilst for CH_3Br, correlations between the mixing ratios and Southcentral China were found to be significant. There were also some significant correlations observed between methyl halides and oceanic regions (e.g. East China Sea and Japan Sea), but only for certain years.

Table 4.9: *Association of particle concentration (g s/m^3) from potential source regions with the observed mixing ratios of (a) CH_3Cl and (b) CH_3Br in Taiwan. The values indicate the Spearman correlation coefficients (R). Correlations are significant ($p < 0.05$) is when $R > 0.5$.*

(a)

Sub-regions	Potential regions	2013	2014	2015	2016
China	1. East China	0.31	**0.63**	**0.40**	**0.86**
	2. North China	0.25	0.29	0.09	0.19
	3. Northeast China	**0.71**	-0.18	0.25	0.20
	4. Northwest China	0.01	**0.67**	0.10	-0.08
	5. Southcentral China	0.32	**0.69**	0.40	0.31
	6. Southwest China	0.23	**0.75**	0.24	0.09
East Asia	7. Taiwan	-0.17	0.19	0.28	-0.14
	8. Japan	0.04	-0.17	-0.03	-0.14
	9. Korea	**0.46**	0.02	0.26	0.39
South East Asia	10. Indochina	-0.03	**0.52**	0.31	-0.11
	11. Philippines	-0.02	0.19	0.34	-0.11
Oceanic regions	12. East China sea	**0.74**	0.38	**0.43**	0.06
	13. Japan Sea	0.26	-0.12	0.16	**0.42**
	14. Pacific Ocean	-0.25	0.09	-0.09	-0.12
	15. South China Sea	-0.39	0.23	0.33	-0.07

(b)

Sub-regions	Potential regions	2013	2014	2015	2016
China	1. East China	-0.13	**0.45**	0.37	**0.86**
	2. North China	0.25	0.20	0.21	-0.03
	3. Northeast China	0.40	-0.18	0.17	0.13
	4. Northwest China	-0.04	0.49	0.02	-0.17
	5. Southcentral China	-0.19	**0.60**	**0.48**	**0.42**
	6. Southwest China	-0.20	0.59	0.07	0.16
East Asia	7. Taiwan	-0.17	0.20	0.29	-0.01
	8. Japan	-0.08	-0.11	0.01	0.02
	9. Korea	0.31	0.03	0.33	**0.42**
South East Asia	10. Indochina	-0.41	0.38	0.12	0.04
	11. Philippines	-0.11	0.19	0.30	0.01
Oceanic regions	12. East China sea	0.23	0.17	0.52	0.20
	13. Japan Sea	0.01	0.04	0.21	**0.51**
	14. Pacific Ocean	-0.22	0.18	-0.08	-0.03
	15. South China Sea	-0.33	0.28	0.19	0.06

For Bachok, significant correlations were consistently found between both methyl halides and continental air masses from East China, Northwest China, Southcentral China, Southwest China and Indochina (Table 4.10). This was the case for 2013/2014 campaign but not during 2015/2016. Unlike during the Taiwan campaign, no significant correlations were observed between mixing ratios of methyl halides and oceanic regions, suggesting that the variability of methyl halides observed in Bachok was mainly influenced by the air masses from continental regions.

Table 4.10: *Association of particle concentration (g s/m^3) from potential source regions with the observed mixing ratios of (a) CH_3Cl and (b) CH_3Br in Bachok. The values indicate the Spearman correlation coefficients (R). Correlations are significant ($p < 0.05$) is when $R > 0.5$.*

(a)

Sub-regions	Potential regions	2013/2014	2015/2016
China	1. East China	**0.58**	0.16
	2. North China	0.17	0.08
	3. Northeast China	-0.73	0.07
	4. Northwest China	**0.54**	0.07
	5. Southcentral China	**0.52**	0.20
	6. Southwest China	**0.45**	0.05
East Asia	7. Taiwan	-0.06	-0.11
	8. Japan	-0.63	0.07
	9. Korea	-0.74	0.01
South East Asia	10. Indochina	**0.82**	0.32
	11. Peninsular Malaysia	0.13	0.26
	12. East Malaysia	0.25	-0.18
	13. Philippines	-0.68	-0.01
Oceanic regions	14. East China sea	0.16	-0.01
	15. Japan Sea	-0.69	0.03
	16. Pacific Ocean	-0.81	-0.04
	17. South China Sea	-0.64	0.01

(b)

Sub-regions	Potential regions	2013/2014	2015/2016
China	1. East China	**0.59**	0.02
	2. North China	0.38	-0.24
	3. Northeast China	-0.43	0.00
	4. Northwest China	**0.58**	-0.25
	5. Southcentral China	**0.52**	0.05
	6. Southwest China	**0.47**	-0.03
East Asia	7. Taiwan	-0.06	-0.06
	8. Japan	-0.59	-0.05
	9. Korea	-0.61	0.00
South East Asia	10. Indochina	**0.47**	0.14
	11. Peninsular Malaysia	-0.17	0.11
	12. East Malaysia	0.14	0.05
	13. Philippines	-0.63	0.08
Oceanic regions	14. East China sea	0.28	0.04
	15. Japan Sea	-0.60	-0.11
	16. Pacific Ocean	-0.64	0.00
	17. South China Sea	-0.61	-0.04

Overall, the analyses of the impact of potential source regions' surface properties on the variations of the measured methyl halide mixing ratios have suggested that continental air masses were consistently the main source. China (mainly East China) contributed the most to the atmospheric methyl halides. The mixing ratios of methyl halides strongly correlated with air masses which originated from East China, thereby suggesting that East China was the main source region of the atmospheric methyl halides at Taiwan and Bachok. This is plausible because East China is the most populated and developed part of the country in view of the more habitable physical geographical conditions of East China relative to mid- and west-China (which mostly comprise mountains and deserts with extreme weather). Therefore, areas in East China rapidly develop and are immensely industrialised to accommodate the high population density. Therefore, it is likely that industries, surface transportation, and agriculture (waste burning in fields) in East China are also the main sources of methyl halides in East Asia. On another note, the particle concentration analysis revealed contributions from other sub-regions of China. This could have been due to the northern origin of the air due to the prevailing direction of wind at the time of year the samples were collected. Thus, all the sampled air masses probably have spent a significant portion of time in China, even though they did not pick up any methyl halides emissions apart from those from East China. Hence, this could explain the better correlation of methyl chloride with air masses from East China but not with other sub-regions of China.

On the other hand, influences from other industrial regions were also noted (i.e. East Asian countries such as Korea; and South East Asian regions, especially Indochina). Indochina is less industrialised in comparison with other East Asian regions; its economic activities were primarily dependent on agriculture and farming. However, since Indochina is known to be one of the main tropical regions where biomass burning is extensive (Huang et al., 2016), it is suspected that biomass burning could have influenced the variability of measured mixing ratios of methyl halides. However, owing to the lack of data which would have befitted the scope of this study, verification of this theory is challenging.

On the other hand, the mixing ratios of CH_3Cl and CH_3Br in both Taiwan and Bachok significantly correlated with modelled CO mixing ratios that were derived from three emission categories, industries (combustion and processing), surface transportation, and agriculture (waste burning in fields). Among the three emission categories, agriculture (waste burning on fields) is a known source of both gases. These findings were consistent with studies that have shown that biomass burning is a major source of methyl halides (Lobert et al., 1993, Andreae et al., 2001, Mead et al., 2008). Agricultural residues include (1) all leaves, straw, and husks left in the field after harvest; (2) hulls and shells removed during crop-processing at the mills; (3) animal dung (Yevich et al., 2003). Burning of agricultural waste in fields was mainly conducted to prepare the fields for new planting or harvesting seasons (Mead et al., 2008). It has been reported that methyl halides – CH_3Cl, CH_3Br, and CH_3I – were predominantly released during the smouldering of a fire, probably due to the reaction between methanol and HCl which is catalysed by the glowing char surfaces or radical reactions in the flames (Reinhardt et al., 1995, Andreae et al., 2001). However, since the agricultural emission ratios of $CO:CH_3Cl$ and $CO:CH_3Br$ were lower than those of industries and surface transportation, the predominant source of the methyl halides at both stations was unlikely to be agriculture (waste burning in fields). Industrial sources could emit more CH_3Cl than CH_3Br (Carpenter et al., 2014). The main industrial process that gave rise to CH_3Cl emissions is coal combustion (waste incineration and industrial activities). Some of the chlorine in coal is released in the form of CH_3Cl during combustion, and it is expected that some of the chlorine in the municipal waste employed the same chemical pathway (McCulloch et al., 1999).

On top of the abovementioned three emission sectors, two additional sectors i.e. forest burning and grassland burning have been found to be significantly correlated with mixing ratios of methyl halides in Bachok, suggesting that both nonindustrial emissions potentially contribute towards the variation of methyl halides measured in Bachok, but not in Taiwan. On the other hand, the significant correlations seen between mixing ratios of methyl halides in Taiwan and oceanic regions could also suggest the contribution of marine sources towards the variability of methyl halides. However, in the oceans (seawater), numerous physical, chemical, and biological processes could be summarised into a single effect. Taking

into account the limitations of the relatively sparse datasets in this study, the identification of the exact production pathways of methyl halides in the oceanic regions remain challenging. Nevertheless, there are several possible ways by which oceans became the contributor of atmospheric methyl halides in this region. One of these is mostly linked to phytoplankton bloom. This was mostly true for CH_3Br in light of the evidence that CH_3Br can be produced by both macroalgal and phytoplankton species in the oceans (Baker et al., 2001). Although the trace gases were all related to phytoplankton, the production mechanisms of each specific gas are complex and some are still unclear (Zhai et al., 2018). However, both compounds were most probably directly released from phytoplankton (Gebhardt et al., 2008).

4.3 Conclusions

In Taiwan and Bachok the mixing ratios of the methyl halides generally exceeded the global background values, thereby demonstrating widespread regional enhancements. In all campaigns, methyl chloride was much more abundant than methyl bromide. Strong contributions of these compounds by air masses which originated from the continental regions implied that such regions predominantly influenced the observed methyl halide concentrations. The NAME trajectories and particle concentration analyses showed that the events of higher mixing ratios were associated with continental air masses, especially those from East Asia. This also explained the greater variations in the methyl halide mixing ratios and frequently higher methyl halide mixing ratios at Taiwan relative to Bachok indicating that Taiwan is located relatively closer to major source regions. Cold surges and the land-sea breeze also had important effects on the variation of the methyl halide mixing ratios.

To summarise, there were two main possible shared sources of methyl halides at Taiwan and Bachok, namely (1) Industry (combustion and processing) and (2) agriculture (waste burning on fields). Additionally, (1) forest burning and grassland burning emissions were suspected to also contribute to the methyl halide variations, especially at Bachok and (2) oceanic emissions potentially influence the variability of methyl halides in Taiwan.

This work suggests that emissions from industry, waste burning on agricultural fields, forest burning, grassland burning and marine in the region of East Asia and South East Asia may be co-located with the sources of methyl halides. These regions are important due to fact that both regions have various potential sources of methyl halides. Therefore, there is a need for further regional studies not only due to the lack of measurements made so far but also the proximity of these regions to the inter-tropical convergence zones (ITCZs) – a region of prevailing deep convections which increases the chances of the methyl halides being transported to the stratosphere.

4.4 References

Andreae, M. O. and Merlet, P.: Emission of trace gases and aerosols from biomass burning, Global biogeochemical cycles, 15, 4, 955-966, 2001.

Ashfold, M. J., Latif, M. T., Samah, A. A., Mead, M. I. and Harris, N. R. P.: Influence of Northeast Monsoon cold surges on air quality in Southeast Asia, Atmospheric Environment, 166, 498-509, 10.1016/j.atmosenv.2017.07.047, 2017.

Ashfold, M. J., Pyle, J. A., Robinson, A. D., Meneguz, E., Nadzir, M. S. M., Phang, S. M., Samah, A. A., Ong, S., Ung, H. E., Peng, L. K., Yong, S. E. and Harris, N. R. P.: Rapid transport of East Asian pollution to the deep tropics, Atmospheric Chemistry and Physics, 15, 6, 3565-3573, 10.5194/acp-15-3565-2015, 2015.

Baker, J., Sturges, W., Sugier, J., Sunnenberg, G., Lovett, A., Reeves, C., Nightingale, P. and Penkett, S.: Emissions of CH_3Br, organochlorines, and organoiodines from temperate macroalgae, Chemosphere-Global Change Science, 3, 1, 93-106, 2001.

Blei, E., Hardacre, C. J., Mills, G. P., Heal, K. V. and Heal, M. R.: Identification and quantification of methyl halide sources in a lowland tropical rainforest, Atmospheric Environment, 44, 8, 1005-1010.

Carpenter, L. J., Reimann, S., Burkholder, J. B., Clerbaux, C., Hall, B. D., Hossaini, R., Laube, J. C. and Yvon-Lewis, S. A. Ozone-Depleting Substances (ODSs) and Other Gases of Interest to the Montreal Protocol, Chapter 1 in Scientific Assessment of Ozone Depletion: 2014, Global Ozone Research and Monitoring Project – Report No. 55. Geneva, Switzerland, World Meteorological Organization.2014

Farren, N. J., Dunmore, R. E., Mead, M. I., Nadzir, M. S. M., Samah, A. A., Phang, S.-M., Sturges, W. T. and Hamilton, J. F.: Chemical Characterisation of Water-soluble Ions in Atmospheric Particulate Matter on the East Coast of Peninsular Malaysia, Atmospheric Chemistry and Physics, 19, 3, 1537-1553, 10.5194/acp-19-1537-2019, 2019.

Gebhardt, S., Colomb, A., Hofmann, R., Williams, J. and Lelieveld, J.: Halogenated organic species over the tropical South American rainforest, Atmospheric Chemistry and Physics, 8, 12, 3185-3197, 2008.

Hu, L. The role of the ocean in the atmospheric budgets of methyl bromide, methyl chloride and methane, Texas A & M University.2012

Huang, W. R., Wang, S. H., Yen, M. C., Lin, N. H. and Promchote, P.: Interannual variation of springtime biomass burning in Indochina: Regional differences, associated atmospheric dynamical changes, and downwind impacts, Journal of Geophysical Research: Atmospheres, 121, 17, 2016.

Lee-Taylor, J. and Redeker, K.: Reevaluation of global emissions from rice paddies of methyl iodide and other species, Geophysical Research Letters, 32, 15, 2005.

Liu, H., Jacob, D. J., Bey, I., Yantosca, R. M., Duncan, B. N. and Sachse, G. W.: Transport pathways for Asian pollution outflow over the Pacific: Interannual and seasonal variations, Journal of Geophysical Research: Atmospheres, 108, D20, 2003.

Lobert, J. M. and Warnatz, J.: Emissions from the combustion process in vegetation, Fire in the Environment, 13, 15-37, 1993.

McCulloch, A., Aucott, M. L., Benkovitz, C. M., Graedel, T. E., Kleiman, G., Midgley, P. M. and Li, Y. F.: Global emissions of hydrogen chloride and chloromethane from coal combustion, incineration and industrial activities: Reactive Chlorine Emissions Inventory, Journal of Geophysical Research: Atmospheres, 104, D7, 8391-8403, 1999.

Mead, M., Khan, M., White, I., Nickless, G. and Shallcross, D.: Methyl halide emission estimates from domestic biomass burning in Africa, Atmospheric Environment, 42, 21, 5241-5250, 2008.

Montzka, S. A., Dutton, G. S., Yu, P., Ray, E., Portmann, R. W., Daniel, J. S., Kuijpers, L., Hall, B. D., Mondeel, D., Siso, C., Nance, J. D., Rigby, M., Manning, A. J., Hu, L., Moore, F., Miller, B. R. and Elkins, J. W.: An unexpected and persistent increase in global emissions of ozone-depleting CFC-11, Nature, 557, 7705, 413-417, 10.1038/s41586-018-0106-2, 2018.

Reeves, C. E.: Atmospheric budget implications of the temporal and spatial trends in methyl bromide concentration, Journal of Geophysical Research: Atmospheres, 108, D11, 2003.

Reinhardt, T. E. and Ward, D. E.: Factors affecting methyl chloride emissions from forest biomass combustion, Environmental Science & Technology, 29, 3, 825-832, 1995.

Simmonds, P., Derwent, R., Manning, A., Fraser, P., Krummel, P., O'doherty, S., Prinn, R., Cunnold, D., Miller, B. and Wang, H.: AGAGE observations of methyl bromide and methyl chloride at Mace Head, Ireland, and Cape Grim, Tasmania, 1998–2001, Journal of Atmospheric Chemistry, 47, 3, 243-269, 2004.

United Nations (2007). "United Nations Population Division: World Population Prospect: The 2017 Revision . ." Retrieved 24 September 2018.

Wang, Z., Liu, X. and Xie, X.: Effects of strong East Asian cold surges on improving the air quality over mainland China, Atmosphere, 7, 3, 10.3390/atmos7030038, 2016.

WMO. Scientific Assessment of Ozone Depletion: 2006, Chapter 8: Halocarbon Scenarios, ODPs ans GWPs, Global Ozone Research and Monitoring Project - Report No. 50. Geneva, Switzerland, World Meteorological Organization**:** 8.1–8.39.2007

Yevich, R. and Logan, J. A.: An assessment of biofuel use and burning of agricultural waste in the developing world, Global biogeochemical cycles, 17, 4, 2003.

Yokouchi, Y., Ikeda, M., Inuzuka, Y. and Yukawa, T.: Strong emission of methyl chloride from tropical plants, Nature, 416, 6877, 163, 2002.

Yokouchi, Y., Noijiri, Y., Barrie, L. A., Toom-Sauntry, D., Machida, T., Inuzuka, Y., Akimoto, H., Li, H. J., Fujinuma, Y. and Aoki, S.: A strong source of methyl chloride to the atmosphere from tropical coastal land, Nature, 403, 295, 10.1038/35002049, 2000.

Zhai, X., Zhang, H.-H., Yang, G.-P., Li, J.-L. and Yuan, D.: Distribution and sea-air fluxes of biogenic gases and relationships with phytoplankton and nutrients in the central basin of the South China Sea during summer, Marine Chemistry, 200, 33-44, 2018.

Chapter 5

Atmospheric emission estimates of CFC-114 and CFC-114a

The research presented in this chapter has been published in Laube et al. (2016). My main contribution to the published work was to run two types of models to generate outputs for the interpretation of CFC-114 and CFC-114a observational data. I used a 2-D global model to derive the 'top-down' emissions of CFC-114 and CFC-114a. The output was used to generate Figures 5.5 to 5.11. In addition, I have used a second model, the 3-D NAME dispersion model, to perform back-trajectory analyses and I generated the footprints (presented in Figure 5.14) for identification of the possible source regions of measured species in Taiwan. During the development of the manuscript for Laube et al. (2016), I provided material in the form of a literature review for Section 1 and I also wrote Section 2.5 on emission modelling.

5.1 Introduction

Anthropogenic trace gases, particularly chlorofluorocarbons (CFCs), emitted into our atmosphere have had a substantial influence on the Earth's climate system. It has been recognised since the mid-1970s that CFCs are strong greenhouse gases that can significantly impact radiative forcing, as well as being substances that contribute towards stratospheric ozone depletion (Hodnebrog et al., 2013). Due to the absence of significant tropospheric loss process, CFCs remain in the atmosphere long enough to reach the stratosphere. In the stratosphere, they are eventually broken down and release reactive chlorine, which destroys ozone (Rowland et al., 1975). The impact of CFCs was first recognised in the atmosphere with the discovery of the Antarctic ozone hole (Farman et al., 1985). As a result, great attention was given to regulating

CFCs and other halogenated compounds, which subsequently had galvanized the interest of scientists and policy makers, and prompted unprecedented international action i.e. establishment of the Montreal Protocol in 1987. This protocol was created with the mission to regulate halogenated gases in developed and developing countries for the protection of the ozone layer via controlling of the global production and consumption of ODSs (Derwent et al., 1998). The enforcement and subsequent amendments of the Montreal Protocol on Substances that Deplete the Ozone Layer (1989) have resulted in the successful phase-out of CFC production and consumption in industrialised and developing nations by 2010 (apart from relatively minor critical-use exemptions). Consequently, the abundance of most documented CFCs in the atmosphere have started to decline (Montzka et al., 1996, Rigby et al., 2013, Carpenter et al., 2014, Laube et al., 2014, UNEP, 2014).

One compound has received little attention in the literature and has been understudied to date, namely CFC-114 ($C_2Cl_2F_4$). It is categorised under the minor CFCs, along with CFC-115 and CFC-13, since its industrial applications are not as extensive as major CFCs (e.g. CFC-11, CFC-12 & CFC-113). Therefore, the amount of information on its atmospheric trends and emissions are limited relative to the major CFCs, which are well documented. In this study, our particular interest is to differentiate between CFC-114 ($CClF_2CClF_2$) and its asymmetric isomeric form CFC-114a (CF_3CCl_2F). Previously, published atmospheric long-term measurements have represented the sum of both CFC-114 ($CClF_2CClF_2$) and its isomer CFC-114a (CF_3CCl_2F).

CFC-114 was first used in industrial application in the 1930s as an aerosol propellant, as a foam blowing agent and in large centrifugal chillers and heat pumps (Fisher et al., 1993). The application of CFC-114 also was reported in the enrichment of uranium (EIA, 1996). Minor remaining uses of CFC-114 were for cooling processes e.g. in naval vessels (Andersen et al., 2007). Like other CFCs, the application of CFC-114 in various industries was assumed to be safe to the environment due to its unique characteristics e.g. good chemical stability, low toxicity, non-flammable, low gas phase thermal conductivity, low production cost, low corrosiveness during use, low toxicity (IPCC, 2000, UNEP, 2012). As a result of the Montreal Protocol regulations, HFCs were introduced as alternatives for CFCs,

one of these being HFC-134a an alternative to CFC-114 in chillers. CFC-114a has reportedly been used in the production of HFC-134a (Banks et al., 1994).

The major loss process of CFCs occurs in the stratosphere, via two reactions i.e. photolysis by ultraviolet radiation and reaction with excited-state atomic oxygen, $O(^1D)$. For CFC-114 and CFC-114a, the dominant loss process is the former, with the latter thought to be responsible for 25% of its total stratospheric loss (Liang et al., 2008). Additionally, as CFC-114a has two chlorine atoms on the same carbon, CFC-114a is more prone to photolysis than CFC-114, making the lifetime of CFC-114a much shorter in comparison to CFC-114 (Oram, 1999). The total atmospheric steady-state lifetimes of CFC-114 and CFC-114a are currently estimated to be ~189 and ~102 years respectively (Burkholder et al., 2013, Carpenter et al., 2014, Davis et al., 2016).

Both isomers have almost identical boiling points (3.5^0C) which make them difficult to separate and analyse chromatographically. Also, the similarity of their mass spectra complicates even their separate detection with mass spectrometric techniques (Oram, 1999). Therefore, published atmospheric long-term measurements have been assumed to represent the sum of both isomers. The contribution of CFC-114a was reported to be ~10% of the sum of isomers and has remained constant to date (Carpenter et al., 2014).

The earliest reported atmospheric measurement of CFC-114 was in the 1990s. At that time, the observed concentration in northern hemisphere mid-latitudes and Antarctica was around 15 pptv and 14 pptv, respectively (Chen et al., 1994). The global mixing ratios are updated regularly in the WMO Scientific Assessments of Ozone Depletion. Reimann et al. (2004) reported that atmospheric abundances of CFC-114 had stabilised with no upward trend of tropospheric abundances of CFC-114 observed at Jungfraujoch, a high-altitude station in Switzerland. Moreover, the study of Chan et al. (2006) found no substantial emissions from the heavily industrialised region of the Pearl River Delta in China.

None of these studies distinguishes between the two isomeric forms of CFC-114. The first attempt to distinguish between the two isomeric forms of CFC-114 was made by Lee (1994), followed by Oram (1999) who reported the first tropospheric

measurements of the individual isomers in the southern hemisphere and their individual emission estimates from 1978-1995. Findings by Oram (1999) showed that the mixing ratios of CFC-114 and CFC-114a were 16.5 ppt and 1.75 ppt at the end of the record. Importantly, this work provided crucial input to the WMO ozone assessments, that is the fraction of CFC-114a relative to CFC-114 has increased from 6.5% to 10.7% over the same period and assumed to remain constant until now.

Previous studies have shown that historical trends for CFC-114 or the sum of CFC-114 and CFC-114a can also be reconstructed using firn data. The first attempt was made by Sturrock et al. (2002) who used inverse firn modelling techniques constrained with firn air data from an Antarctic site (Law Dome) and air archive data from an observatory at Cape Grim, Australia (40.7^0 S, 144.7^0E; Oram, 1999), to reconstruct a CFC-114 + CFC-114a atmospheric trend. They concluded that southern hemispheric concentrations were negligible before 1960. Their firn air-based data (calibration first reported in Prinn et al. (2000)) were compared with University of East Anglia (UEA) data of CFC-114 (fully separated from CFC-114a) from Cape Grim on an earlier UEA calibration scale (Lee, 1994) and a calibration difference (factor of 0.94, constant over time) was found. The second attempt was made by Martinerie et al. (2009). They used Alternative Fluorocarbons Environmental Acceptability Study (AFEAS) emissions and an atmospheric chemistry model to calculate atmospheric trends that were compared to firn data at five sites from Antarctica and Greenland using a forward firn modelling approach. They concluded that the AFEAS-emissions-based trend, which gave significant atmospheric concentrations before 1960, is inconsistent with the firn and atmospheric data-based trend from Sturrock et al. (2002) and that the Sturrock et al. (2002) trend is more consistent with their northern hemispheric firn data than the AFEAS-based trend. The firn data used in Martinerie et al. (2009) are a combination of UEA CFC-114 measurements at North GRIP, Berkner Island and Dome C (earlier calibration scale) and NCAR CFC-114 + CFC-114a measurements at Devon Island, North GRIP and Dronning Maud Land.

5.1.1 Objective and specific aims of this chapter

Global networks of measurement stations routinely monitor the atmospheric concentrations of many ODSs and greenhouse gases. Therefore, those measurement dataset are very valuable for use in conjunction with atmospheric models to establish historical records of the global emissions of ODSs and greenhouse gases. This work takes advantage of the improved measurement since the first CFC-114 and CFC-114a measurement in the 1990s. This advancement provides us the opportunity to evaluate and update the abundances, temporal and emissions of the isomers. The specific aims of this research are:

1. To use the atmospheric measurements and modelling to estimate CFC-114 and CFC-114a emissions. Two types of air measurement dataset have been used to constrain the 2-D atmospheric chemistry transport model. The measurement sources include (a) air samples collected directly from the atmosphere in Cape Grim, Tasmania from 1978 until 2014 and (b) air trapped in polar firn at two Antarctic drilling sites (Berkner Island and Dome C), covering the period of 1960 to 2003. The usage of both datasets represent the longest historical record of CFC-114 and CFC-114a.

2. To compare our derived 'top-down' emissions to 'bottom-up' estimates by industry in order to verify the usage of CFC-114 and CFC-114a reported by industry.

3. Ultimately, this work aims to demonstrate whether or not emissions continue to fall as required under the Montreal Protocol or are there any persisting emissions to the atmosphere.

5.2 Methodology

The overview of the model, general features and the model setup have been introduced in Section 2.4.2 on Chapter 2. This section focuses on the types of model simulations used to derive the emission estimates of both isomers.

5.2.1 Derivation of emission estimates of CFC-114 and CFC-114a

Essentially, the emissions in the model were adjusted until the concentrations for the surface box of the relevant band agreed with the set of atmospheric measurements at that location. This was an iterative process whereby the process of adjusting the emissions for each year was repeated to improve the fit of the model output with the measurements. The process was completed when the model output from the emissions scenario provided a good fit (done by eye using plots) to the measurements. A similar approach has been used in previous studies e.g. Newland et al. (2013), Kloss et al. (2014), Laube et al. (2014).

In this study, three types of model runs have been carried out to estimate the emission of both CFC-114 and CFC-114a. Table 5.1 summarised the respective model runs and the type of observational dataset used to constrain the model.

Table 5.1 *Model runs used to derive the emission estimates of CFC-114 and CFC-114a*

Name of run	Descriptions
Run A	• This was done by adjusting the annual emissions until the model derived concentrations for the surface box of the band 35.7˚S– 41.8˚S agreed with observations in Cape Grim, Tasmania (41˚S) from 1978 to 2014.
Run B	• This was done by adjusting the annual emissions until the model derived concentrations for the surface box of the band 66.4˚S – 90.0˚S agreed with observations in firn air sites in Antarctic (90˚S from 1960 to 2003). • This is because the measurement of air in the firn directly provides information on past evolution prior to available atmospheric records. The firn air measurements can be used as an extension of the records of CFC-114 and CFC-114a measured in situ at Cape Grim and in the Cape Grim archive • The past abundances of both isomers have been reconstructed from the deep polar firn which provide a natural archive of atmospheric composition up to about century back in time.
Run C	• A combination of the southern hemispheric firn air derived trends (1960 to 2003) and the atmospheric measurements from Cape Grim (1978 to 2014) are used to constrain the model. • This combination of two datasets allows (a) extension of the emissions estimates derived from Cape Grim, which we have more confidence in, backwards based on the firn trend prior to 1978 and (b) reconstruction of the longest histories and emissions of CFC-114 and CFC-114a going back to the early use of both gases in the industry. • This was done by adjusting the annual emissions to match the firn air-derived pre -1978 trends (within the constraint from the mixing ratio uncertainty ranges of the firn air record (dashed lines in Figure 5.4)) up to 1978 and then to fit the Cape Grim-derived record from 1978 onwards.

a) Comparison between observed and modelled mixing ratios

The model output from Run A, B and C are presented in Figure 5.1, Figure 5.2 and Figure 5.3 & 5.4, respectively. Here, the modelled mixing ratio for Run A, Run B and Run C was compared to observed concentrations at (a) Cape Grim, Tasmania (41˚S) (b) firn air sites in Antarctic (90˚) and (c) both Cape Grim, Tasmania (41˚S) and Antarctic (90˚), respectively.

In general, the CFC-114 and CFC-114a modelled mixing ratio generated from Run A (Figure 5.1) and Run B (Figure 5.2) agreed well with the measured mixing ratio observed in each sampling site. For Run C, the model run was successful in matching the pre-1978 modelled mixing ratio within the constraint from the mixing ratio uncertainty ranges of the firn air record (Figure 5.3a and 5.4a). The model fit however would have a significant impact towards the exact temporal shape of the pre-1978 emission record. This is discussed further in Section 5.2.5.4 (b). On the other hand, the modelled concentrations from Run C gave excellent agreement with the Cape Grim-derived record from 1978 onwards (Figure 5.3b and 5.4b).

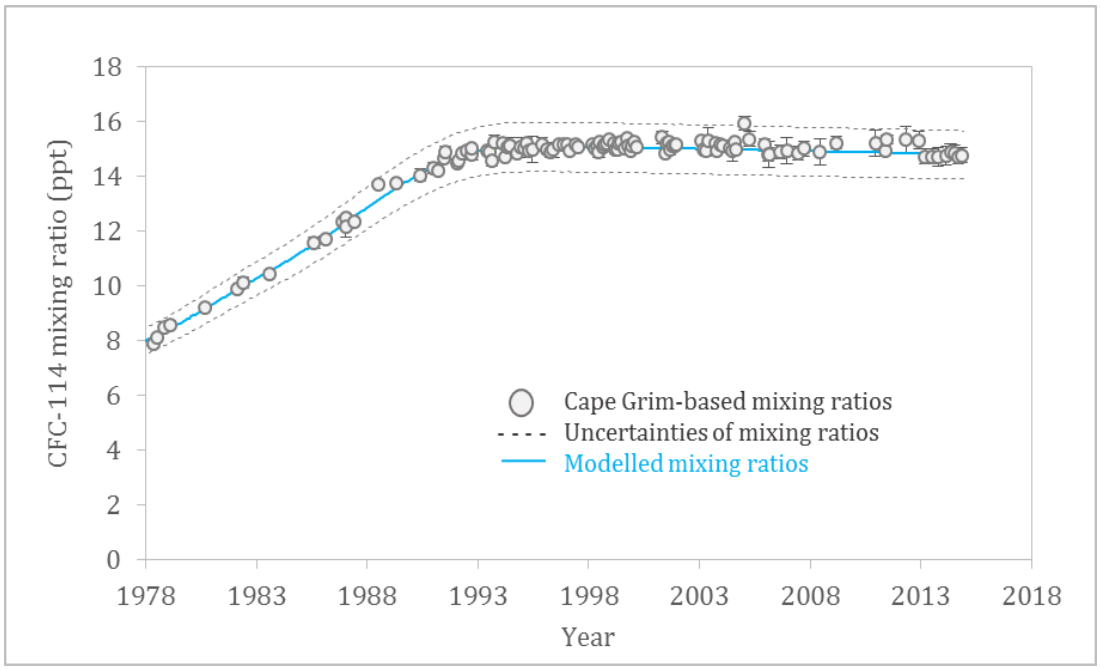

(a)

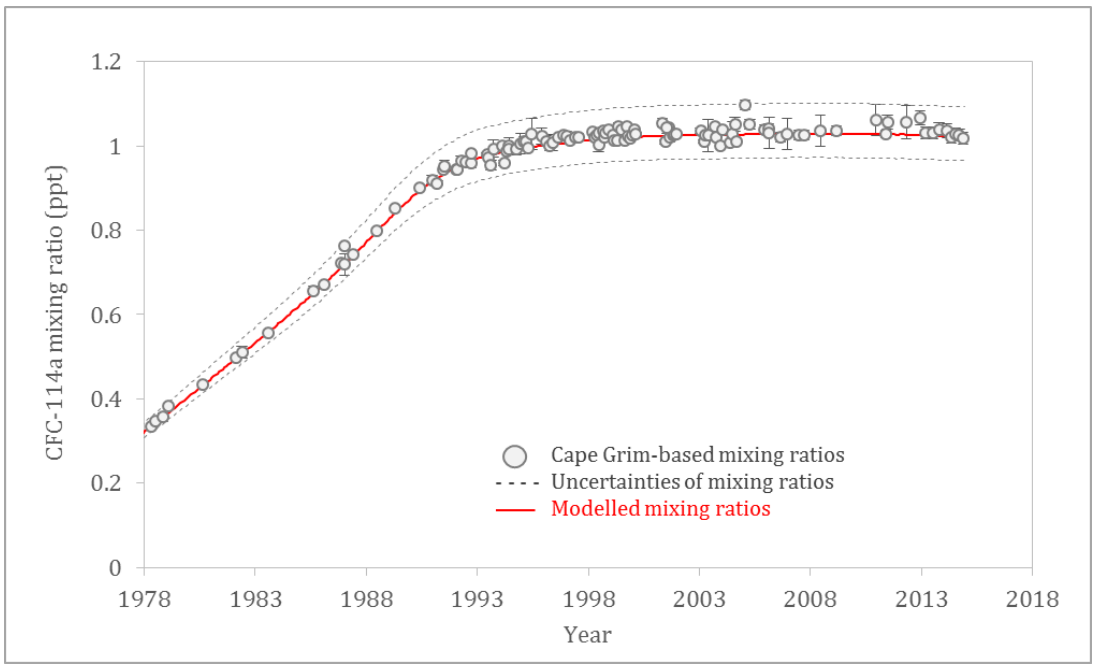

(b)

Figure 5.1: *Output of run A. (a) CFC-114 and (b) CFC-114a modelled and observed mixing ratios at Cape Grim (1978 – 2014)*

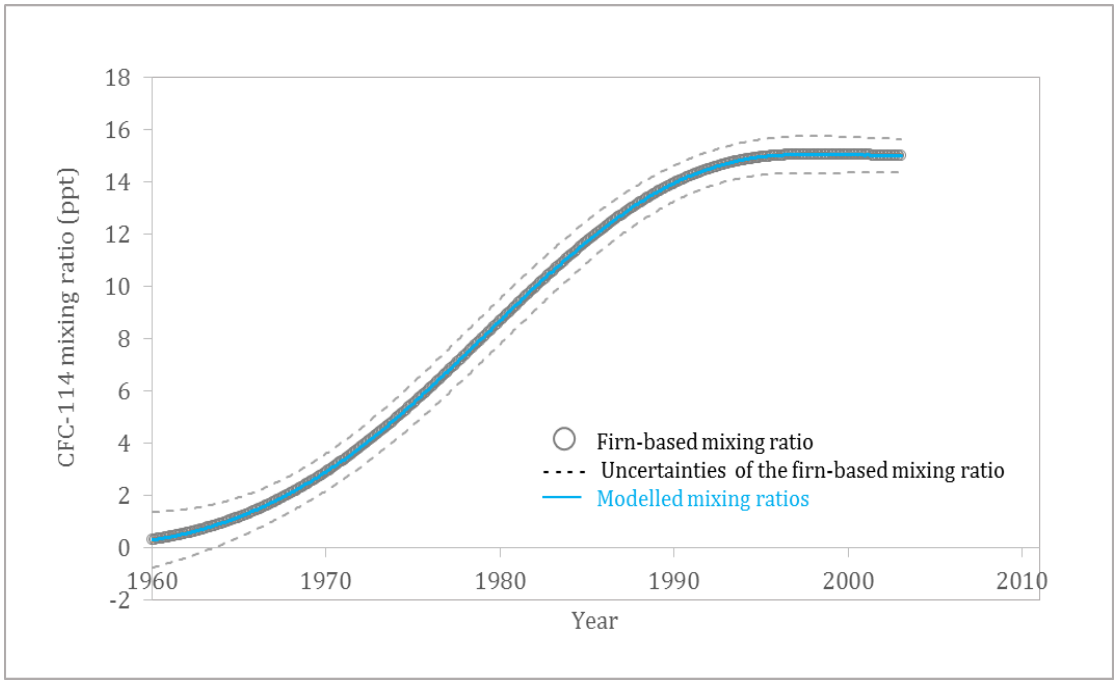

(a)

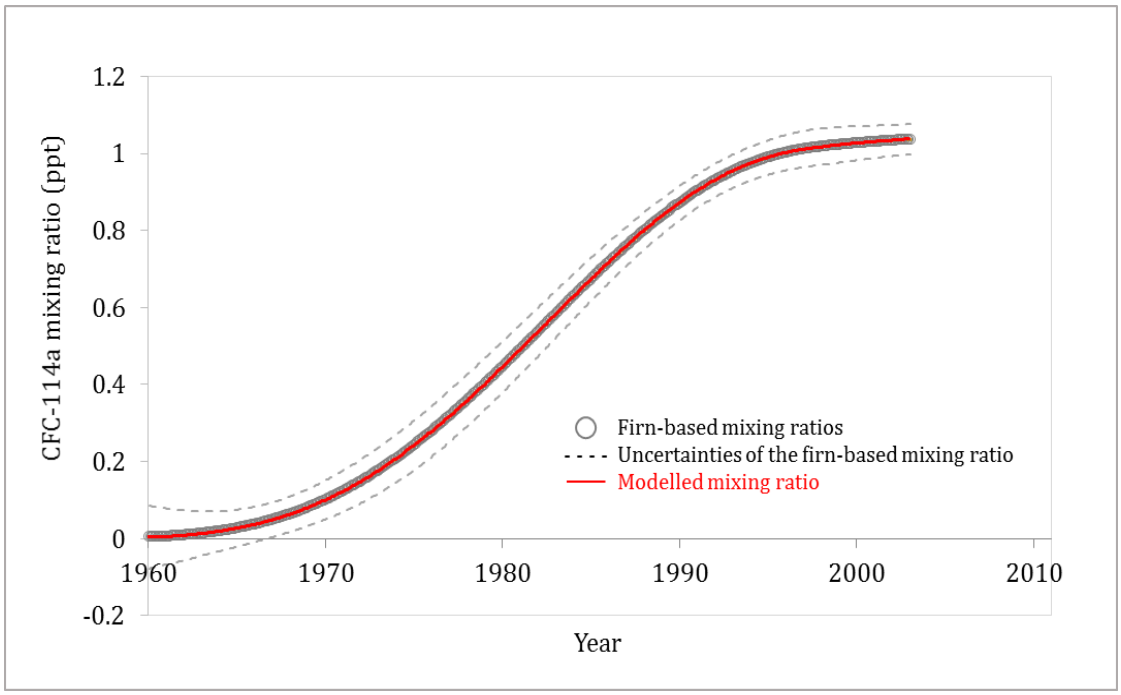

(b)

Figure 5.2: *Output of Run B. (a) CFC-114 and (b) CFC-114a modelled and observed mixing ratios from firn-based record (1960-2003)*

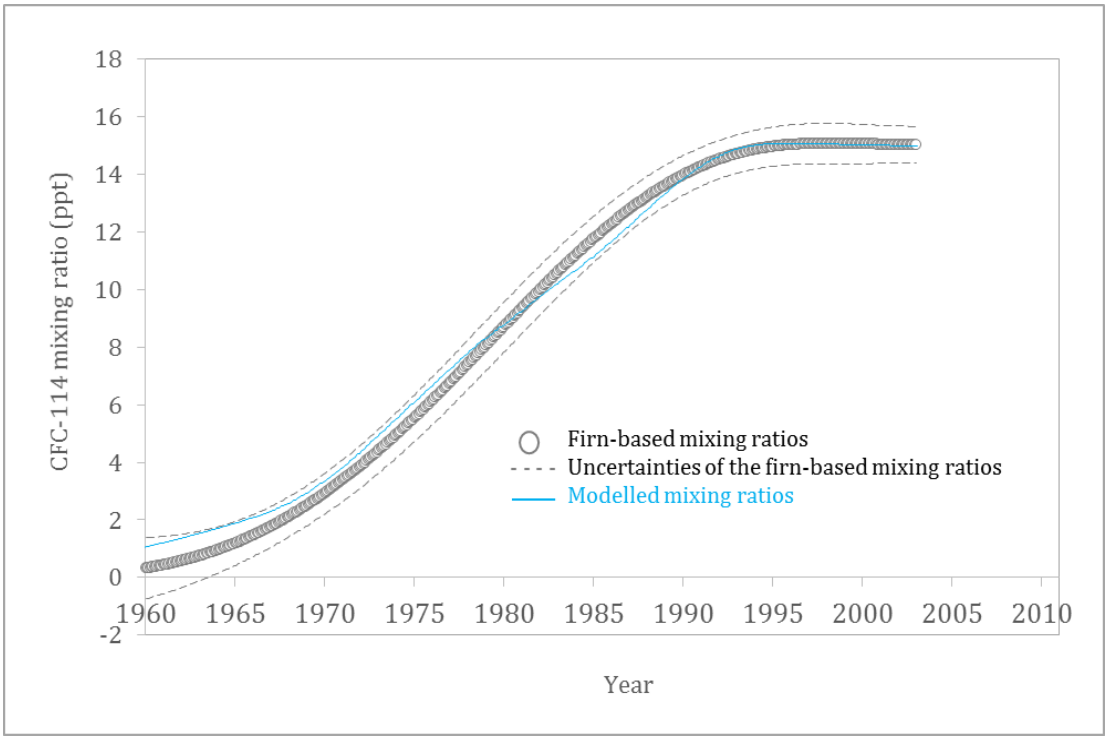

(a)

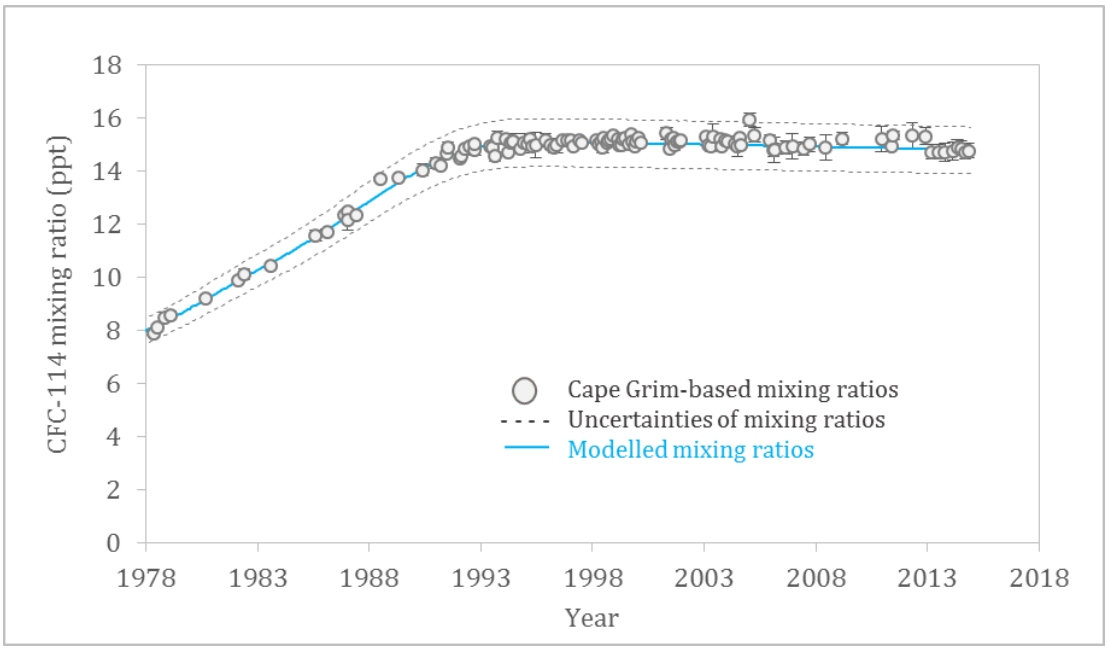

(b)

Figure 5.3: *Output of Run C. Mixing ratio time series of CFC-114 at the (a) latitude of Antarctic and (b) Cape Grim. Circle represent the measured mixing ratios within their respective limits. Solid line (blue) showed the model fits used to determine the best fit emission.*

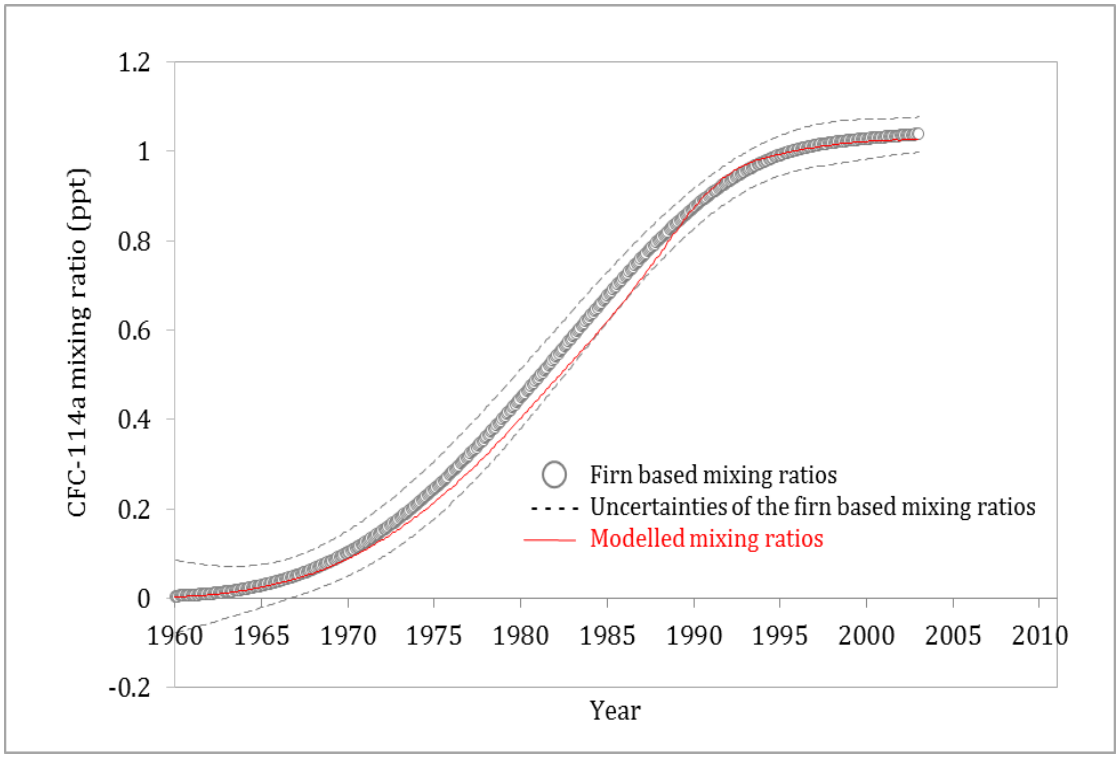

(a)

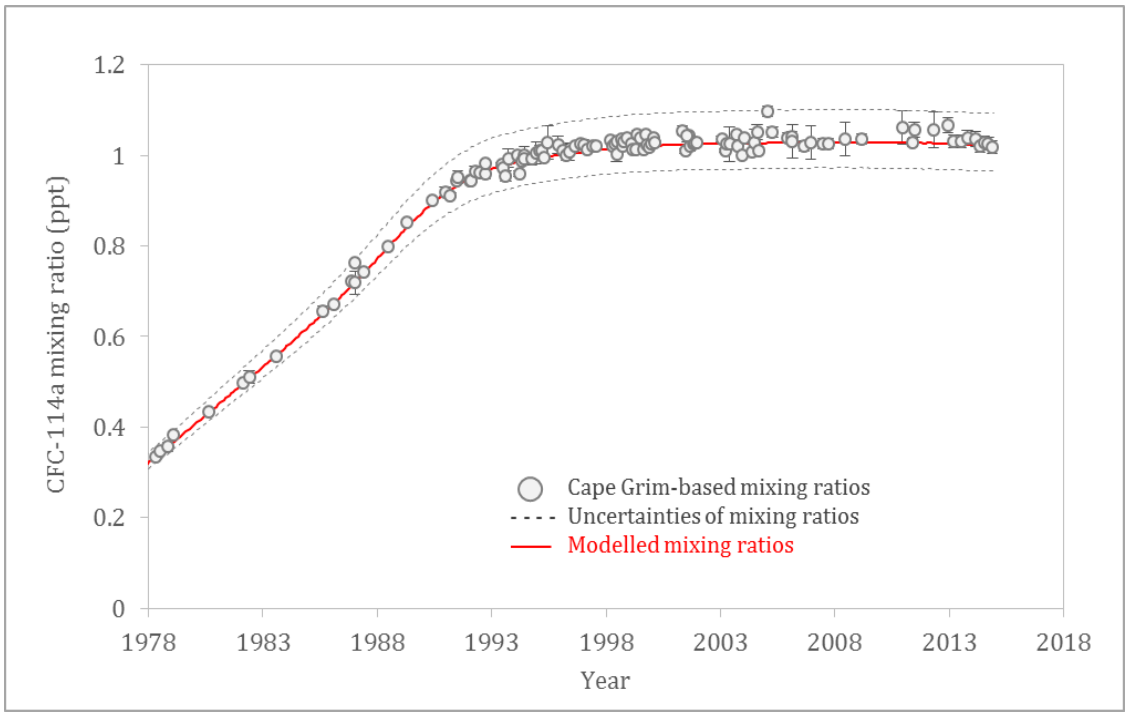

(b)

Figure 5.4: *Output of Run C. Mixing ratio time series of CFC-114a at the (a) latitude of Antarctic and (b) Cape Grim. Circle represent the measured mixing ratios within their respective limits. Solid line (red) showed the model fits used to determine the best fit emission scenarios.*

b) Emission estimates derived by fitting the Cape Grim and firn-based records

The emission estimates derived by performing Run A and Run B are presented in Figure 5.5. Despite the firn derived atmospheric mixing ratio records fitting those observed at Cape Grim well for the overlap period within the uncertainties (Figure 5.5), it is apparent in Figure 5.5 that both Run A and Run B lead to a slightly different emission trends. For example, the curvature for emissions derived purely from the atmospheric records derived from the firn air data (dotted lines in Figure 5.5), are smoothed out and the timings for the emission to reach their maximum values are much earlier compared to the emissions derived purely from the Cape Grim records (solid lines in Figure 5.5). This illustrates the limitations of that methodology when relying on data from only two sites. Emission estimates strongly depend on the annual growth rates, and thus small discrepancies between the curvature of the firn derived trends and the Cape Grim-based atmospheric records translate into large changes in the estimated emissions. The limited accumulation rate of the two firn sites used here prevents a high temporal resolution of the respective record and results partly in smoothing and partly in a shift of the timing of the derived maximum emissions. However, the total emissions estimated from the firn record are 530 Gg (range: 505 to 557 Gg, period from 1960 to 2003), which agrees very well with those from the Cape Grim-based trend over the same period, as well as the AFEAS data (see Section 5.3.2) when including emissions reported from 1934 onwards.

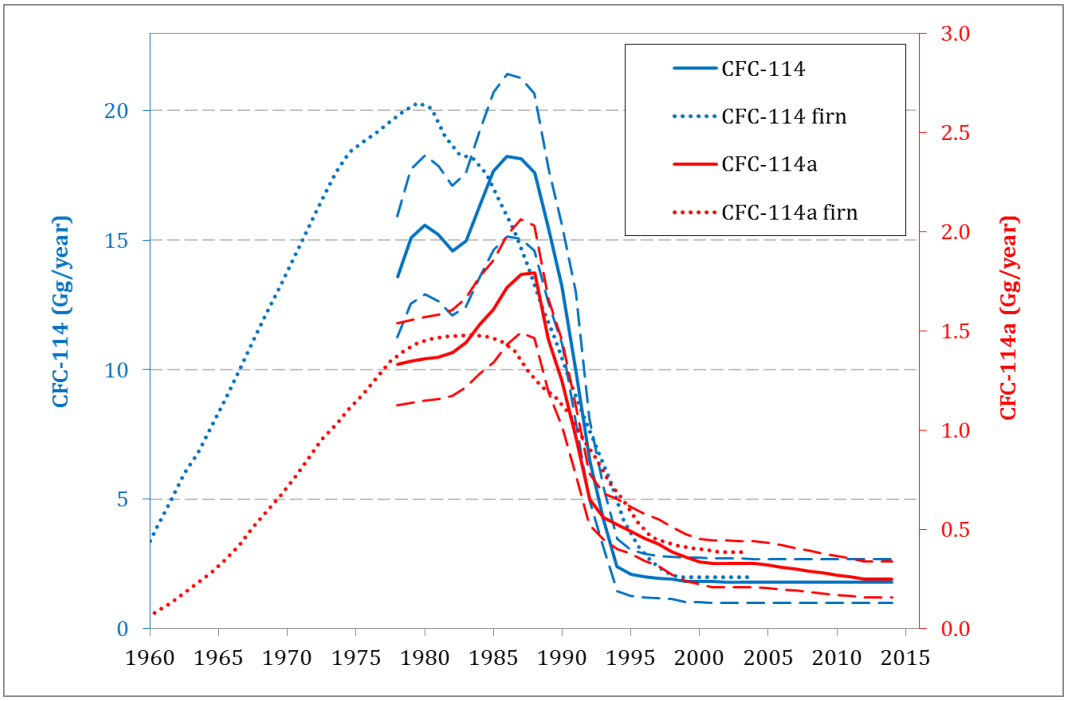

Figure 5.5: *Global emissions of CFC-114 and CFC-114a derived from Cape Grim observations (solid lines) (Run A) with uncertainties represented by dashed lines. The dotted lines represent emissions derived from firn air data (Run B).*

Figure 5.6 shows the results of Run C (Table 5.1), which was successful in matching the firn-derived pre-1978 trend (within the uncertainty range of the firn-based mixing ratio) and the Cape Grim-derived record from 1978 onwards. The exact temporal shape of this pre-1978 emission record is very uncertain as the uncertainty range in the firn air-derived mixing ratios allows a large range of growth rates and therefore emission scenarios.

Overall, it can be concluded that the good agreement between the model runs based on the measured mixing ratios at Cape Grim and the measurements in the firn suggests that the two datasets can be used together to give the longest historical record of the atmospheric mixing ratios of CFC-114 and CFC-114a. Also, the near-complete emission records derived from our observation-based approach would be extremely useful when comparing with bottom-up inventory-based emission estimates. This is discussed further in Section 5.3.3.

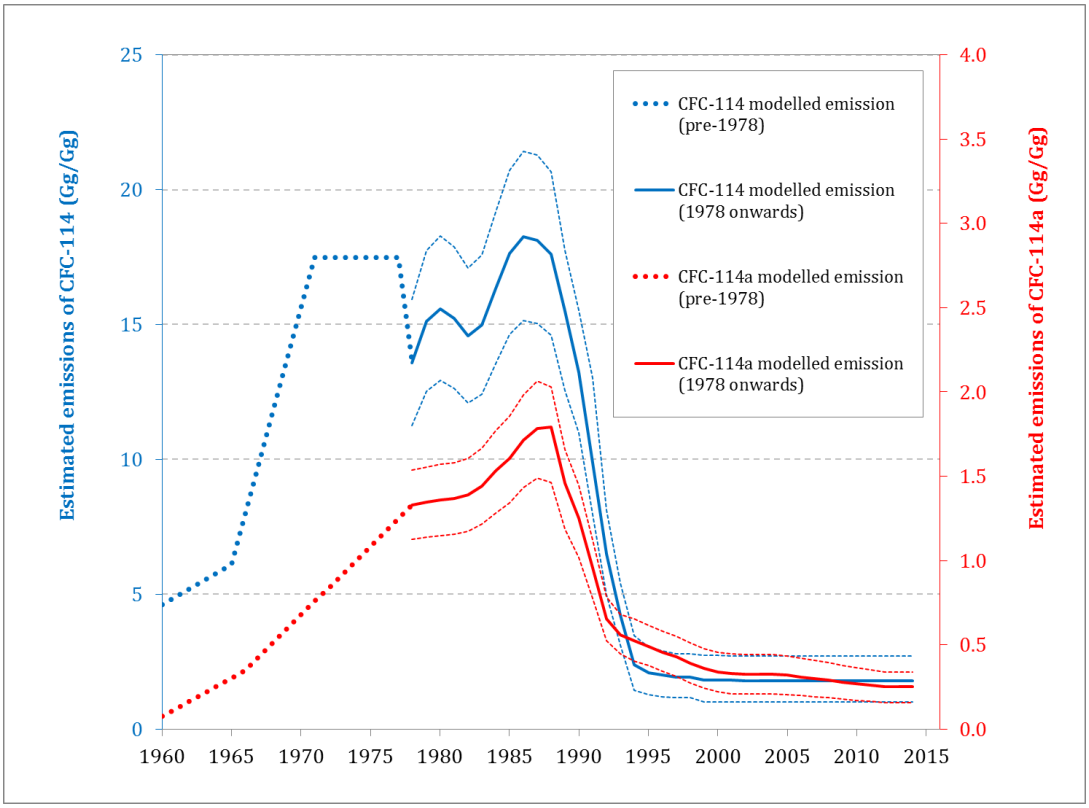

Figure 5.6: *Global emissions of CFC-114 (blue) and CFC-114a (red) derived from Cape Grim observations (solid lines) with uncertainties represented by dashed lines (Run C). The dotted lines represent emissions derived from firn-derived pre-1978 trend (within the uncertainty range of the firn-based mixing ratio).*

5.3 Results & Discussions

The outline of this section is as follows. Firstly, the results from long-term trend and emission estimates for each individual isomers (Section 5.3.1.1 and 5.3.1.2) are presented, followed by discussion on the results in Section 5.3.1.3 and 5.3.1.4. In Section 5.3.2, the top-down emission estimates for both isomers derived from this study are compared and discussed with bottom-up estimates by AFEAS. In order to relate the emission estimates derived in this work to a wider context, the results from aircraft-based observations and samples collected in East Asia I are demonstrated and discussed in Section 5.3.3.

5.3.1 Long-term tropospheric trends and estimated global annual emission of CFC-114 and CFC-114a

The atmospheric abundances of any long-lived gas is indicative of its cumulated emissions into the atmosphere (Laube et al., 2016). Therefore this section attempts to relate the CFC-114 and CFC-114a atmospheric records and their emission estimates in order to understand their long term changes in the atmosphere. The long-term atmospheric records of CFC-114 and CFC-114a from 1960 to 2014 was provided from both firn and Cape Grim air archives. Analysis of the composition of unpolluted air samples extracted from deep firn snow at two Antarctic sites (1960-2012) and collected in Cape Grim, Tasmania (1978 and 2014) has allowed the identification and quantification of CFC-114 and CFC-114a in the atmosphere. The merging of both records has allow an acquisition of a near-complete record of both isomers since their initial production and release in the 1930s (Laube et al., 2016). In this section, for each isomer, both atmospheric abundance and emission estimates are shown in the same figure and examined at the same time.

5.3.1.1 CFC-114

At the beginning of the record i.e. in 1960s, the atmospheric abundances for CFC-114 were extremely low and then they increased rapidly until late 1970s (Figure 5.7). This can be explained by looking at the emission estimates of CFC-114 from Run C which was done by matching the model to the firn trends prior to 1978 and to the Cape Grim observations after 1978. The pre-1978 emission had to be reasonably substantial to explain the accelerating abundance of CFC-114 during that period. However, the exact temporal shape of our pre-1978 emission record is very uncertain, due to the the large uncertainty range in the firn air-derived mixing ratios (Laube et al., 2016). From 1978 until the 1990s, further steady increase in atmospheric abundances in both air archives (firn and Cape Grim) were found, followed by weakening in growth. The derived emissions rose from 1978 until 1990s, reaching a maximum value of at 18.2 Gg yr^{-1} in 1986. The atmospheric

abundances of CFC-114 stopped increasing around 1993, which is consistent with a substantial decline in emissions in the mid-1990s. It is noteworthy that it can take on the order of a year for the gases such as CFC-114 that are emitted primarily in the northern hemisphere to reach to southern hemisphere, the location of the observed trends.

At the end of our record, CFC-114 is the fourth most abundant CFC in the atmosphere, although its mixing ratios are substantially lower than the three others (CFC-11=236.3, CFC-12=524.4 and CFC-113=73.8 ppt, NOAA global average in 2012, Carpenter et al., 2014). Its average mixing ratios decreased at a rate of 0.01 ppt yr^{-1} between 2008 and 2014. This is in agreement with Carpenter et al. (2014), who reported an average decrease of 0.01 ppt yr^{-1} between 2008 and 2012.

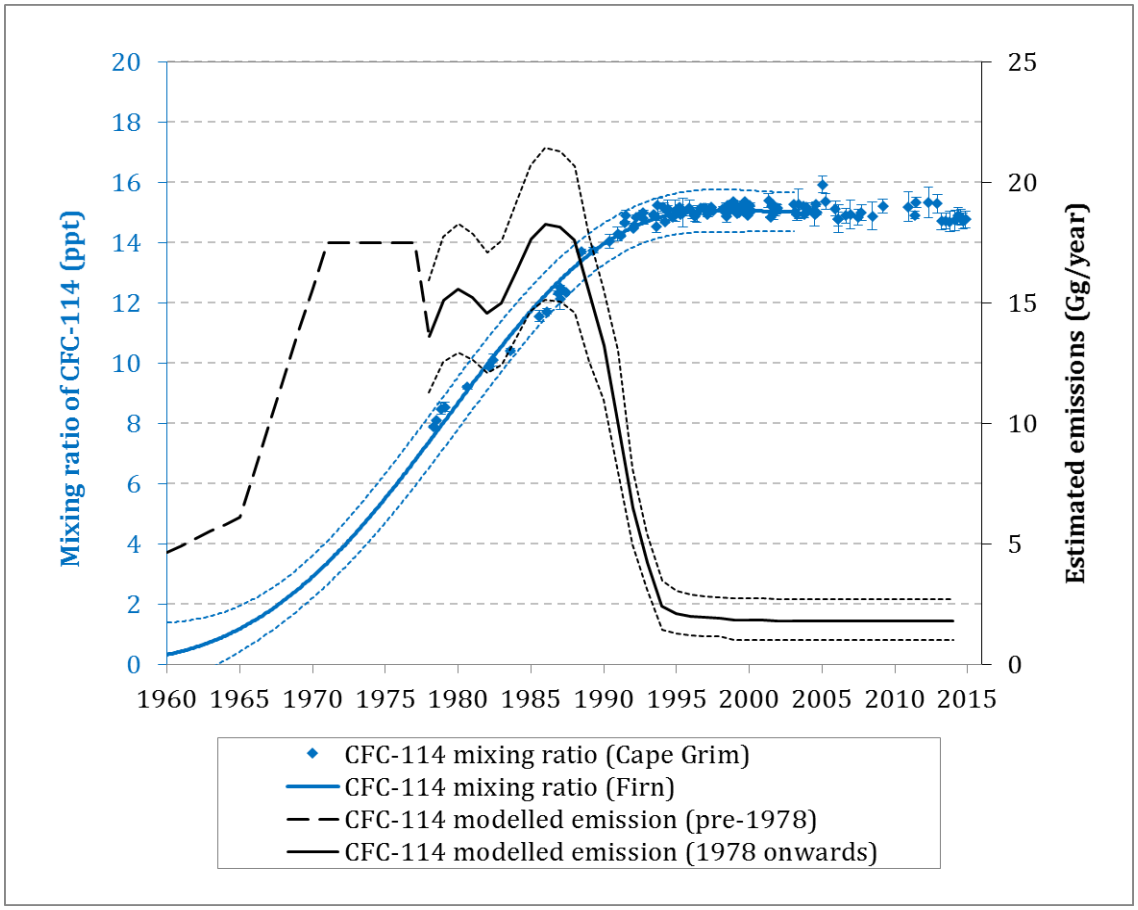

Figure 5.7: *CFC-114 observed mixing ratios derived from two Antarctic firn air profiles (1960-2012) and at Cape Grim (1978 and 2014). The estimated global annual emission of CFC-114 from Run C which was based on matching the model to the firn trends prior to 1978 to the Cape Grim observations after 1978.*

5.3.1.2 CFC-114a

Similar to CFC-114, the atmospheric abundances of CFC-114a were very low in the 1960s but continued to rapidly increase until 1990s, followed by weakening in growth (Figure 5.8). This is consistent with the CFC-114a emissions which were extremely small in the 1960s, rapidly increase until they reach a peak in 1988 at 1.79 Gg yr^{-1} before substantially decline and stopped in the mid-1990s. The mixing ratio of CFC-114a continued to increase until around 2000 whilst the emissions continue to decline and reach to 0.25 Gg yr^{-1} in 2014. At the end of our record, CFC-114a is found to be the seventh most abundant CFC in the atmosphere, after CFC-115 and CFC-13, its growth rate not turning negative until 2008 with a subsequent average decrease of 0.001 ppt yr^{-1}.

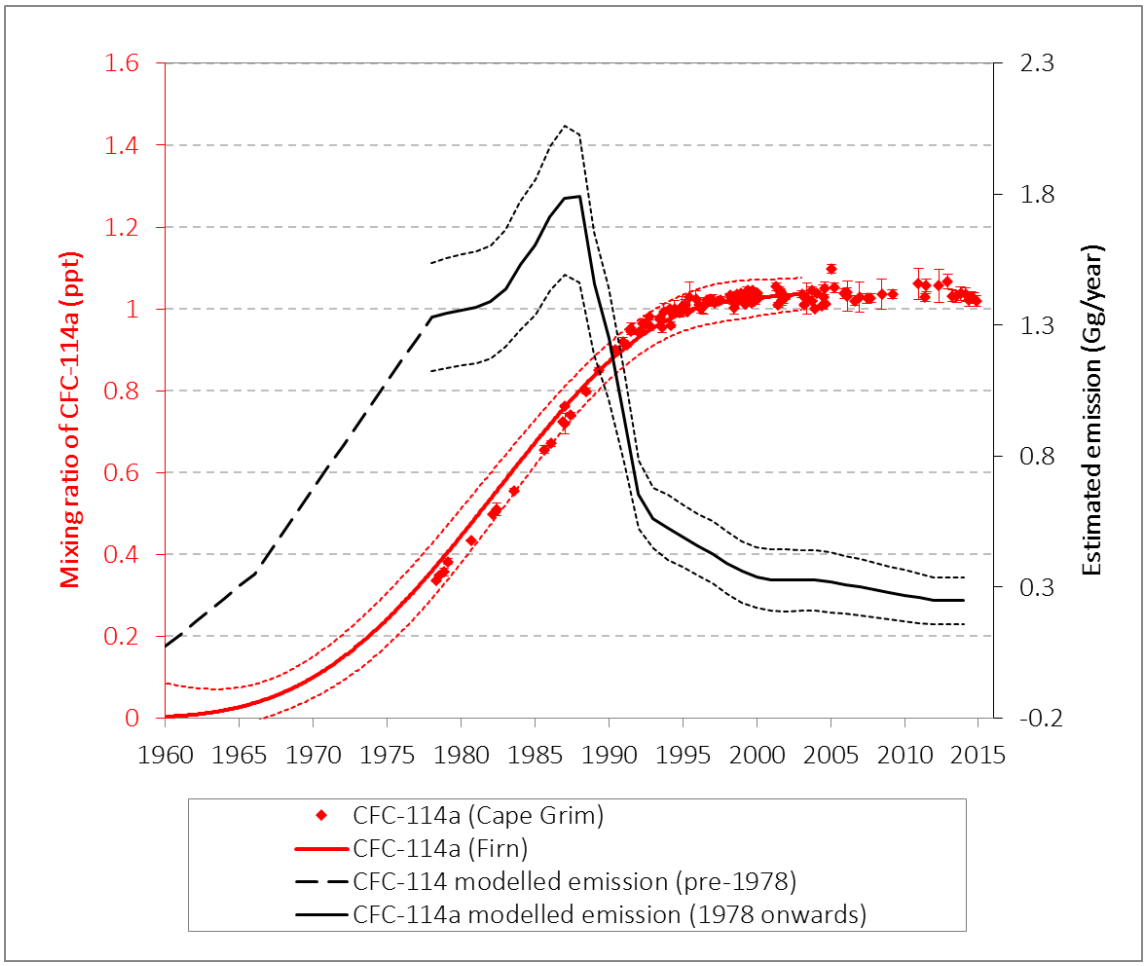

Figure 5.8: *CFC-114a observed mixing ratios derived from two Antarctic firn air profiles (1960-2012) and at Cape Grim (1978 and 2014). The estimated global annual emission of CFC-114a derived by matching the pre-1978 firn-based emissions (within the uncertainty range of the firn-based mixing ratio) to the Cape Grim-based emission record in 1978.*

5.3.1.3 Synthesis

Figure 5.9 compares the changing atmospheric abundances of CFC-114 and CFC-114a from 1960 to 2014. Prior to 1960, the atmospheric abundances of both isomers were negligible (<0.3 ppt). The firn air archive indicate that both compounds are entirely anthropogenic, as they are not detectable in air dated from before the 1960s.

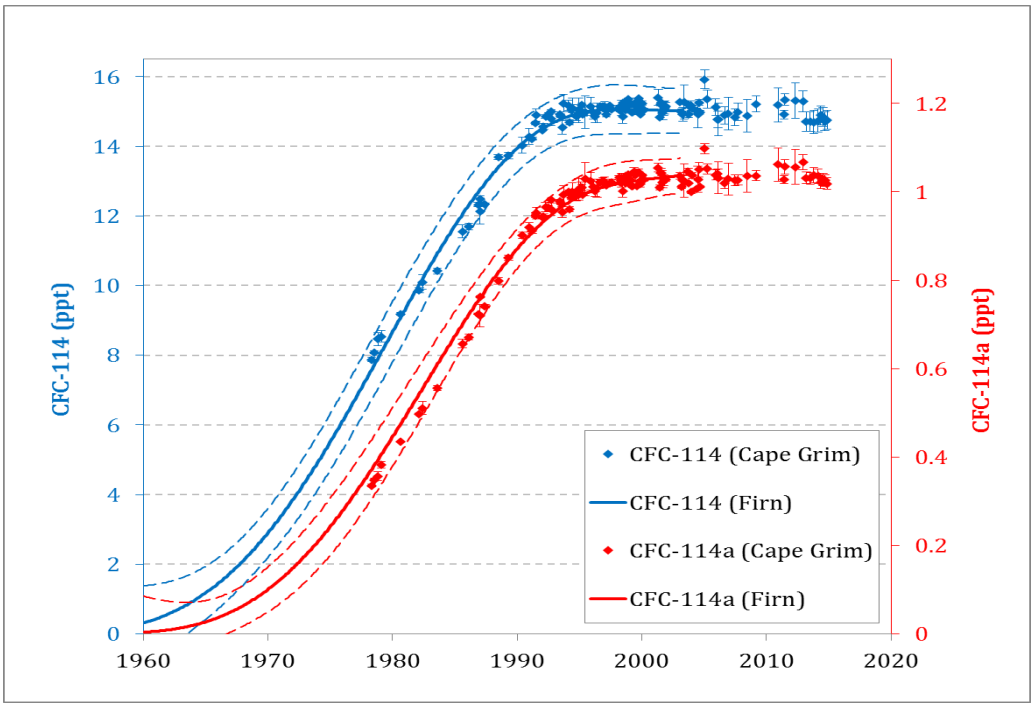

Figure 5.9: *Mixing ratios of CFC-114 and CFC-114a as measured in air samples collected at Cape Grim, Australia, between 1978 and 2014 (diamonds) and derived from Antarctic firn air profiles (lines). Uncertainties are 1σ standard deviations for Cape Grim data and a combination of the former and a firn modelling uncertainty for the latter (shown as dashed lines).*

Our Cape Grim record also demonstrates that the mixing ratio of CFC-114 has doubled from 7.9 to 14.8 ppt whilst the mixing ratio of CFC-114a trebled from 0.35 to 1.03 ppt, between 1978 and 2014. Owing to their long atmospheric lifetimes (CFC-114 = ~189 years, CFC-114a = ~102 years), both isomers still persist in the atmosphere but were no longer increasing significantly at the end of record in 2014. In 2012, the average atmospheric abundances of CFC-114 and CFC-114a at Cape Grim were 15.2±0.3 and 1.05±0.01 ppt respectively. This means that our result

agrees well with the combined mixing ratio of 16.33 ppt given in Carpenter et al. (2014) at this point in time.

5.3.1.4 Ratio of mixing ratios and ratio of emissions of CFC-114a and CFC- 114a

The previous sections have highlighted that some significant differences are identified between CFC-114 and CFC-114a in terms of the long-term tropospheric trends and the estimated global annual emission. For example:

i. The mixing ratios of CFC-114 stabilise a bit earlier at around 1993 whilst for CFC-114a, the mixing ratio continued to increase until it stabilised around 2000. This suggests a difference in the source of emissions although both isomers.

ii. Throughout our Cape Grim record, the fraction of CFC-114a mixing ratio relative to that of CFC-114 increased from 4.3% to 6.9% over the 37-year period, which is inconsistent with the ~10% contribution of CFC-114a to the sum of the isomers has been assumed constant reported in the previous assessments.

Therefore, to further discuss and understand those dissimilarities, the ratio of mixing ratios and ratio of emissions (i.e. CFC-114a/CFC-114) is presented as percentages.

For this study, the information on ratios is useful in various ways i.e.

i. To quantify the connection of CFC-114 and CFC-114a and calculate the contribution of CFC-114a to the sum of isomers (CFC-114 + CFC-114a). This also allow us to compare with the current ~10% assumption used in previous assessment

ii. To evaluate whether the ratio of mixing ratio or emission is constant or changing over number of years. The evolution of the ratio will shed light on the budget of both isomers.

CFC-114 and CFC-114a are always thought to be emitted as a mixture because both isomers have same molecular mass and similar physicochemical properties e.g. boiling point (Oram, 1999). In theory, they should have approximate similar emission rate and undergo similar environmental fate process which then reflects their relative abundances in the atmosphere (Tobiszewski et al., 2012). However that is not the case due to their different atmospheric lifetimes. This is obvious when comparing the pre-1991 ratio of mixing ratio of CFC-114a/CFC-114 with their ratio of emission.

First, let us begin by observing our Cape Grim record from 1978 to 1991 (Figure 5.10). The CFC-114a / CFC-114 ratio of mixing ratios increased rapidly from 4% in 1978 to around 7% by 1991. However, that is not the case for their ratio of emissions, which remained nearly constant at around 9% over the same period. It would be expected that if CFC-114 and CFC-114a were emitted in a constant ratio, they will reach steady state at the same time (if they have similar lifetimes) and hence the ratio of mixing ratios should be constant too. However, their relative atmospheric abundances also depend on the lifetime of the isomers.

The lifetime of CFC-114a (102 years) is much shorter in comparison to CFC-114 (189 years). Therefore, with a constant emission during 1978 to 1991, the rate of growth of CFC-114a would be expected to be slower. However, that is not happening but instead the CFC114a/CFC-114 ratio of mixing ratios increases. This may seem odd at first but what this telling us is that prior to 1978, more CFC-114 must have being emitted relative to 114a and that caused CFC-114 to already be closer to its steady state. This is apparent when looking at the low ratio of emissions prior to 1978 (solid green line in Figure 5.10). This is confirmed when looking at the ratio of the mixing ratios in both the Cape Grim record and the firn-based record that give less than 4.5%. This finding could point to change in manufacturing process or a partly independent source(s).

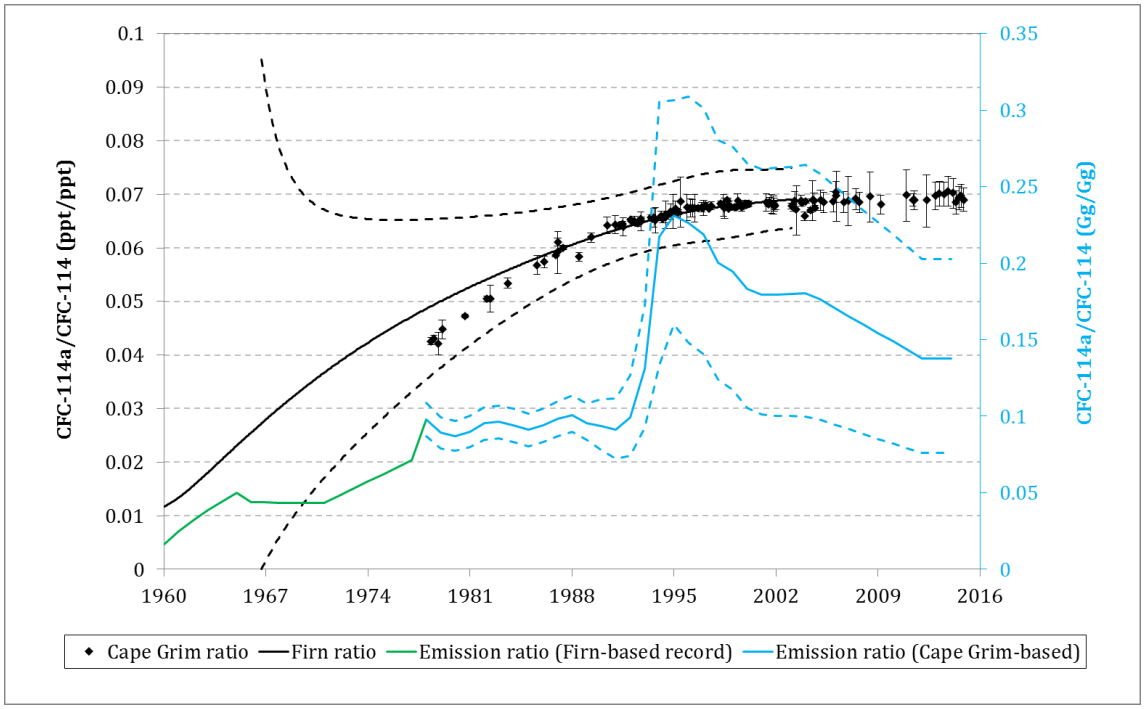

Figure 5.10: *CFC-114a / CFC-114 ratio of mixing ratios at Cape Grim (left axis, black diamonds) and derived from Antarctic firn (left axis, black line), as well as the ratio of their emissions derived from these observations (right axis, green and blue line).*

From 1991 to around 1995, a sharp increase of CFC-114a emissions was found relative to those of CFC-114. While emissions of both isomers decrease substantially throughout the 1990s, those of CFC-114a decline much more slowly. The isomeric emission ratio (Figure 5.9) only starts to decrease again after CFC-114 emissions stop declining in 1996. In contrast to CFC-114, emissions of CFC-114a continue to decline until 2010. This could perhaps be due to the aforementioned involvement of pure CFC- 114a in the production of HFC-134a (Banks et al., 1994). Interestingly, the abundance of HFC-134a started increasing in the atmosphere in the early 1990s (Montzka et al., 1996b; Oram et al., 1996) as it replaced CFCs predominantly in mobile air conditioning. However, our CFC-114a emission data suggest that it is not an impurity in all the HFC-134a produced as emissions of the latter continue to increase to date (Carpenter et al., 2014). CFC-114a is only an intermediate in one of the pathways to synthesise HFC-134a. Our CFC-114a emission data are consistent with two possible scenarios, i.e. (a) emissions of CFC-114a as an impurity in HFC-134a produced via that pathway, as well as (b) emissions at the HFC-134a production level.

On the other hand, the fraction of CFC-114a mixing ratio relative to that of CFC-114 increased from 4.3% to 6.9% over the 37-year period (Figure 5.10). An important implication of these findings is that (i) the 10% contribution of CFC-114a which has been assumed in Carpenter et al. (2014) and previous WMO/UNEP ozone assessments appears to have been an overestimate and (ii) the contribution of CFC-114a to the sum of the isomers differs from the current tacit assumption used in previous assessment that both isomers have been largely co-emitted and that their atmospheric concentration ratio has remained approximately constant (~10%) in time.

5.3.2 Comparison with bottom-up emission

Comparison between our observation-based top-down emission estimates with the bottom-up inventory-based bottom-up estimates by the Alternative Fluorocarbons Environmental Acceptability Study (AFEAS) are presented in (Figure 5.11). The bottom-up emission estimates by AFEAS are available from 1934 until 2003. No estimates are available after 2003 because the companies responding to AFEAS represented a small and diminishing fraction of global CFC production (less than 16% in 2004) which lead to no CFC data being sought or reported (AFEAS, 2009.). In contrast, my top-down emission estimates based on Cape Grim observation start and end later, i.e. from1978 until 2014. Therefore, I rely on the firn-derived emission estimates prior to 1978 (Run C). It is noteworthy to highlight that the emissions of CFC-114 and CFC-114a are not reported separately by AFEAS, but instead as the sum of isomers. Therefore, I combined our derived emission of CFC-114 with CFC-114a (Figure 5.11).

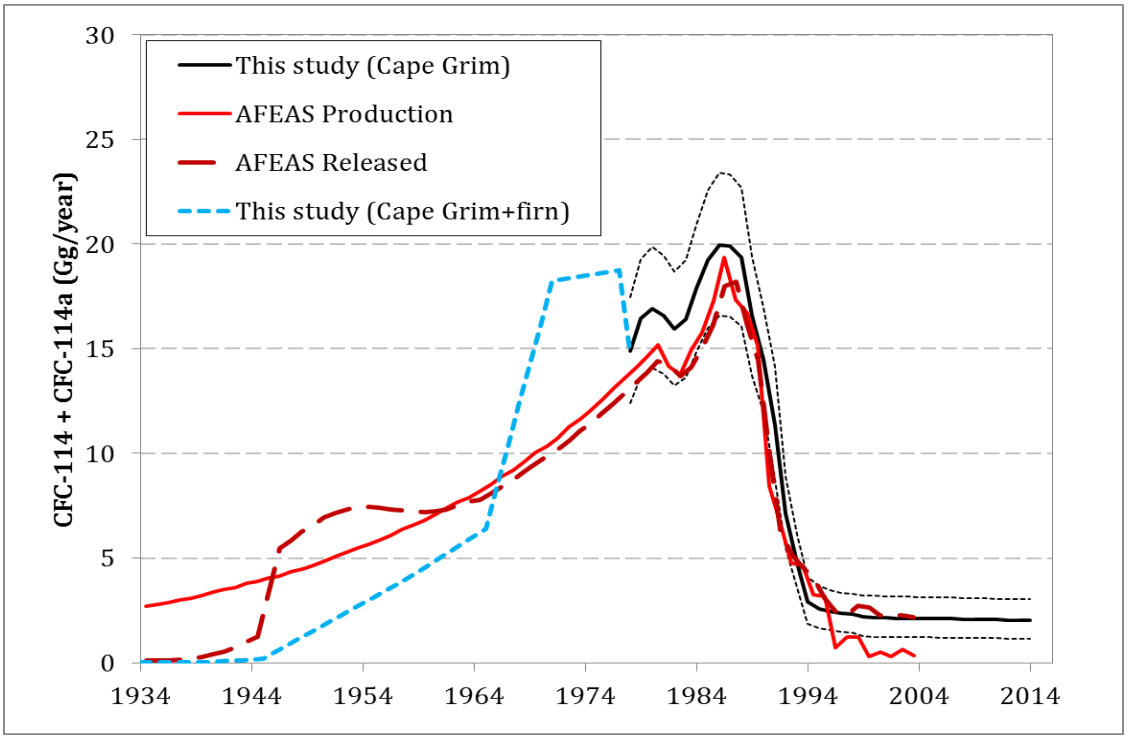

Figure 5.11: *Atmospheric observation-based top-down emissions of the sum of CFC-114 and CFC-114a (black line with black dashed lines representing uncertainty ranges) in comparison with bottom-up emissions from the AFEAS inventory (in red). The dashed blue line represents the firn derived emissions.*

There are noticeable difference between our best estimates of the sum of CFC-114 and CFC-114a and AFEAS estimates, particularly during the pre-1978 period. For example, the temporal shape of our top-down estimated emissions from 1934 to 1978 is different from the emission estimates derived by AFEAS. As previously mentioned in Section 5.2.5.4, the uncertainties in firn air-derived mixing ratios allow a large range of growth rates and therefore cause the exact temporal shape of our emission record to be extremely uncertain (Laube et al., 2016). However, it can be deduced that our estimated pre-1978 cumulative emissions for the sum of the isomers are 6% lower than the AFEAS emission estimates, although the difference between the two estimates is insignificant ($p>0.05$). In addition, timing of the emission estimated by AFEAS is somewhat inconsistent with our derived emission estimates. For example, in the late 1940s, AFEAS emissions increased rapidly to more than 5 Gg yr^{-1} while our estimated emission is extremely lower during 1940s. Our derived emissions only reached more than 5 Gg yr^{-1} in early 1960s. Another example is also observed during the period of 1960 to 1978 whereby a high

emission is observed using our top-down approach while that is not the case for the emission estimates by AFEAS, although this difference is insignificant.

From 1978 until early 1990s, both emission estimates agree reasonably well within the uncertainty range of the Cape Grim record. From 1990 to 1993 our emissions were significantly higher than the AFEAS data (Figure 5.11). It should be noted that, while no uncertainties are given in the AFEAS database, there are considerable uncertainties related to bottom-up methods, which are difficult to quantify. This especially applies to the timing of the release to the atmosphere. Differences between the two emission data sets (release data for AFEAS) reach up to 4.5 Gg yr^{-1} in 1991, but this discrepancy all but disappears after 1993. Both data sets also agree that emissions decreased rapidly and stabilised between 2.0 and 2.3 Gg yr^{-1} from 2000 onwards, demonstrating the success of the Montreal Protocol. Cumulative emissions from our top-down approach reach 537 Gg in 2003 (uncertainty range from 436 to 627 Gg) and agree very well with both AFEAS production and release figures between 1934 and 2003, which have been reported at 520 and 511 Gg respectively (AFEAS, 2009). The aforementioned discrepancy in the early part of the record may therefore originate from pre-1960 production which was released to the atmosphere later than predicted by AFEAS.

For the post-2003 part, a substantial amount of CFC-114 (containing a fraction of CFC-114a) is believed to have been in "banks". Although CFCs are no longer being produced, they are still being released to the atmosphere from existing "CFCs bank''. That is, the stockpile of CFCs which remain unused in old and long- lived equipment and yet to be either released or destroyed. The "CFCs bank'' are calculated by subtracting the specific estimates of the cumulative emission from the estimates of cumulative production (Newland, 2013). Interestingly, the AFEAS database itself does not fully reflect this in their emissions as only 8.8 Gg remained "unreleased" to the atmosphere in 2003. If current emissions are from existing equipment, then such a small "bank" is not consistent with current persisting emissions of 1.80 Gg yr^{-1} (range: 1.0 to 2.7 Gg yr^{-1}) of CFC-114 and 0.25 Gg yr^{-1} (range: 0.18 to 0.32 Gg yr^{-1}) of CFC-114a in 2014, giving cumulative emissions for those 11 years of 23 Gg (13 to 34 Gg).

5.3.3 Possible sources of CFC-114 and CFC-114a

Emission of trace gases are mainly originated from the Northern Hemisphere. Most industrialised countries are located in the Northern Hemisphere, which is why trace gases of predominantly anthropogenic origin are known to show interhemispheric gradients (e.g. Carpenter et al., 2014). Our results from interhemispheric flights of the CARIBIC aircraft are shown in Figure 5.12. Even though slightly higher mixing ratios are found in the Northern Hemisphere, the gradient with latitude is insignificant for either CFC-114 or CFC-114a (within the 1σ measurement uncertainty, i.e. 1.2% on average for both gases – compared to gradients of 0.8 and 1.0% for CFC-114 and CFC-114a respectively when looking at the variability of the atmospheric mixing ratios averaged over both flights). This is consistent with the Cape Grim data that indicate that global emissions of both of these gases have largely ceased. As the GC-MS analyses of the CARIBIC air samples revealed no exceptionally high mixing ratios of many other trace gases (e.g. CFC-11, H-1301, HCFC-142b, HFC-134a), it can be concluded that the sampled air masses are representative of well-mixed mid and upper tropospheric background air during February 2015.

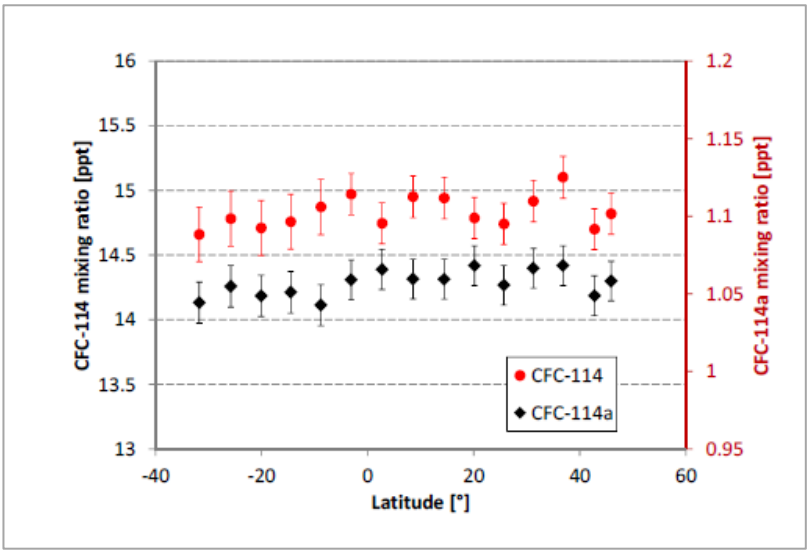

Figure 5.12: *CFC-114 and CFC-114a observations from air samples collected during two interhemispheric aircraft flights from Germany to South Africa and back on 10–11 February 2015.*

However, although the global estimated emissions of both of these gases have largely ceased, we can see clearly in Section 5.3.2 that they do not reach zero by the end of the record for either isomer. As previously discussed in Section 5.3.2, a substantial bank of the CFCs within long-lived applications can potentially produce continued emissions to the atmosphere (AFEAS, 2009.). Alternatively, the persisting emissions could also be generated by the industry that produce or consume CFC-114 and CFC-114a in their manufacturing process.

To understand and assess the relationship between the emissions in developing countries and persisting emissions of CFC-114 and CFC-114a, we utilised our measurements during the field campaign in southern Taiwan in 2015 (Hengchun site, 22.1N, 120.7E; 7m a.s.l.; similar to the 2013 campaign reported by Vollmer et al., 2015). However, our observational data is limited to further asses the origin of those emissions, which suggest the importance to conduct more atmospheric observation in the East Asian region.

CFC-114a exhibited mixing ratios that, on average, were 17% higher than the average mixing ratios observed at Cape Grim (Figure 5.13). Even samples that show no significantly elevated mixing ratios for several other trace gases that are known to have continuing strong East Asian sources (e.g. HCFC-141b, HFC-227ea) exhibited CFC-114a mixing ratios more than 2% higher than at Cape Grim. In contrast, mixing ratios of CFC-114 are not enhanced significantly throughout the campaign confirming that the regional source of CFC-114a is not due to the emission of an isomeric mixture.

I also performed the NAME trajectory analysis in order to identify the possible source regions of both isomers measured in Taiwan. The air masses predominantly originated from China and the Peninsular of Korea with no significant influence from the local industrial regions in Taiwan. Figure 5.14 shows examples of NAME footprints during 2 days that relate to the highest mixing ratios (range: 1.15 - 1.25ppt) of CFC-114a during our sampling. Footprints for the rest of the days that we have measurement are provided in Appendix.

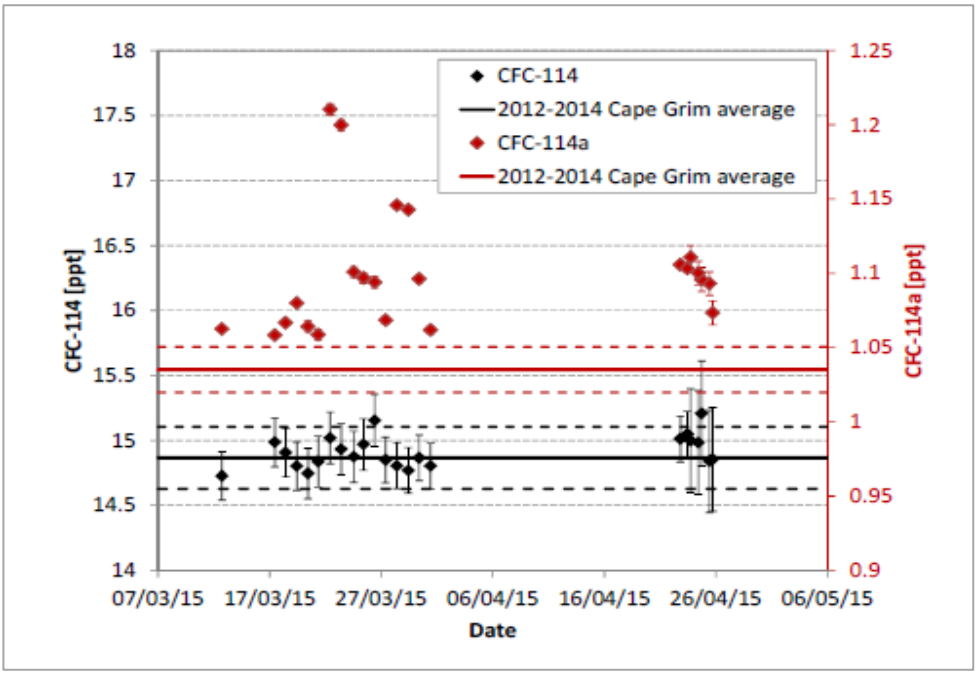

Figure 5.13: *Mixing ratios of CFC-114 and CFC-114a from samples collected during a ground-based campaign near Hengchun, Taiwan, in early 2015 (diamonds) compared to mixing ratios observed at Cape Grim averaged from 2012 to 2014 (lines). Uncertainties (error bars and dashed lines) are 1 σ standard deviations.*

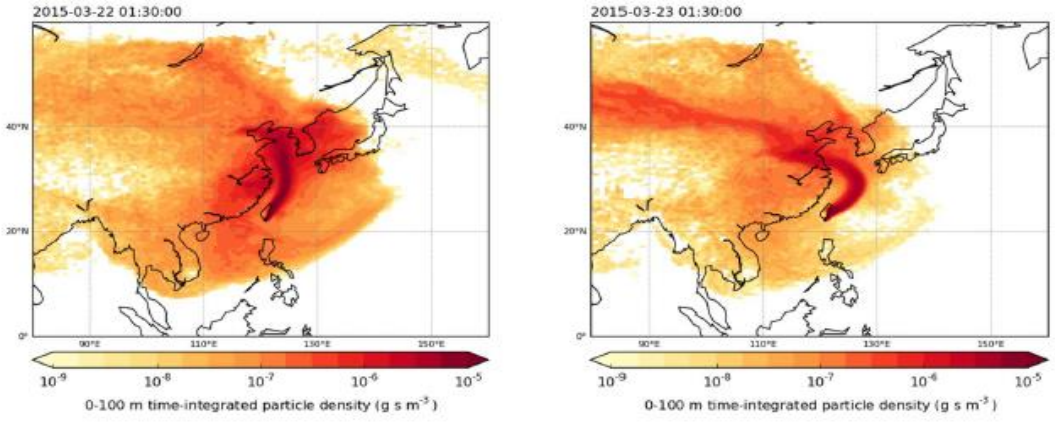

(a) (b)

Figure 5.14: *NAME footprints derived from 12-day backward simulation showing the time integrated density of particles below 100 m altitude on (a) 22/03/2015 and (b) 23/03/2015. Both days experienced large enhancements of CFC-114a mixing ratios during the 2015 campaign in Taiwan.*

During this campaign, HFC-134a showed mixing ratios close to background (six samples between 84 and 88 ppt) as well as enhancements of up to 132 ppt. However, we find no significant correlation ($R^2 < 0.1$) with CFC-114a, implying that either (i) most of the regional HFC-134a emissions originate from production pathways not involving CFC-114a and/or (ii) HFC-134a does not contain CFC-114a as an impurity and the latter is only emitted during HFC-134a production. The connection of these regional CFC-114a emissions to HFC-134a production processes is however supported by the fact that we see the biggest enhancements of CFC-115 (between 5 and 10% above background) and CFC-113a (between 90 and 200 %) in the four samples with the highest CFC-114a mixing ratios– with both these compounds being involved in the same HFC-134a production process (where CFC-113 is isomerised to form CFC-113a, which is then fluorinated to produce CFC-114a, followed by hydrogenolysis to HFC-134a, with CFC-115 being a small by-product as a result of overfluorination; Banks et al., 1994). In addition we cannot rule out the possibility of a new onset of CFC-114a emissions as the Taiwan samples were collected after the end of our current Cape Grim record.

5.4 Conclusions

This study has filled the gap in knowledge of 2 of the so-called neglected CFCs i.e. CFC-114 and 114a. For the first time, we achieved a complete quantification of CFC-114 and CFC-114a and successfully report the long term trend and emissions of the two isomeric forms separately.

The full separation of the two isomers reveals some additional new information. In the past, the isomers have routinely been reported as the sum of the isomers with the assumption that the abundance of CFC-114a is 10% that of CFC-114. However, we found that that the fraction of CFC-114a mixing ratio relative to that of CFC-114 increased from 4.2 to 6.9% over the 37-year period. This contradicts the current tacit assumption used in international climate change and ozone depletion assessments that both isomers have been largely co-emitted and that their atmospheric concentration ratio has remained approximately constant in time Carpenter et al. (2014).

Furthermore, we also present how we used the observational dataset (firn air and Cape Grim archive) in combination with a 2D global model to reconstruct atmospheric histories of these compounds for assessing their global emissions. We estimate global cumulative emissions of 514 Gg (range: 415 to 617 Gg) of CFC-114 and 39 Gg (32 to 47 Gg) of CFC-114a up until 2014, which is broadly consistent with bottom-up estimates derived by industry. The emissions for both compounds grew steadily during the 1980s, followed by a substantial reduction from the late 1980s onwards, which is consistent with the reduction of emission in response to the Montreal Protocol demonstrating the success of the Montreal Protocol regulations, which banned production and consumption in developed countries from 1996 (UNEP, 2014). Nevertheless, there is evidence of small continuing, but significant, emissions of both isomers still in 2014. From our derived emission estimates and comparison with the AFEAS bottom-up emission estimates, we can conclude that there is a persisting emission of 1.8Gg yr^{-1} (range: 1.0 to 2.7 Gg yr^{-1}) and 0.25 Gg yr^{-1}(range: 0.18 to 0.32 Gg yr^{-1}), for CFC-114 and CFC114a, respectively. Moreover the inferred changes to the ratio of emissions of the two isomers since the 1990s also indicate that the sources of the two gases are partly unrelated. Ultimately, the source and trends of each isomer have varied over time, which suggest that CFC-114 and CFC-114a were not always being co-produced or co-emitted. This is further supported by the datasets from Taiwan and CARIBIC, which shows a source of CFC-114a from East Asia but not of CFC-114.

In conclusion, based on the differences in trends and emissions of both isomers presented in this study, we recommend that the two isomers should be reported separately in the future, or that time-dependent speciation factors, should be used to approximate global concentrations of CFC-114 and CFC-114a. Also, the fact that the emissions do not reach zero by 2014 highlights the importance of continued research and monitoring of all ozone-depleting substances (ODSs) in order to ensure compliance with the Montreal Protocol for environmental protection against ozone loss. Further observations are also required to understand the origin of these emissions, especially in the East Asian region. It should however be noted that such emissions are not necessarily in breach of the Montreal Protocol given that CFCs used as intermediates in the production of other compounds (such as HFC-134a) do not have to be reported under that treaty.

5.5 References

AFEAS: Production Sales of Fluorocarbons. Alternative Fluorocarbons Environmental Acceptability Study (AFEAS): Production and Sales of Fluorocarbons (last access: 4 March 2015), 2009.

Andersen, S. O., Sarma, K. M. and Taddonio, K. N. Technology transfer for the ozone layer: Lessons for climate change. London, UK, Earthscan Press. 2007

Banks, R. E., Smart, B. E. and Tatlow, J. C.: Organofluorine Chemistry: Principles and Commercial Applications, 1994.

Burkholder, J. B., Mellouki, W., Fleming, E. L., George, C., Heard, D. E., Jackman, C. H., Kurylo, M. J., Orkin, V. L., Swartz, W. H. and Wallington, T. J.: Evaluation of atmospheric loss processes, SPARC. Lifetimes of Stratospheric Ozone-DepletingSubstances, Their Replacements, Related Species, 2013.

Carpenter, L. J., Reimann, S., Burkholder, J. B., Clerbaux, C., Hall, B. D., Hossaini, R., Laube, J. C. and Yvon-Lewis, S. A. Ozone-Depleting Substances (ODSs) and Other Gases of Interest to the Montreal Protocol, Chapter 1 in Scientific Assessment of Ozone Depletion: 2014, Global Ozone Research and Monitoring Project – Report No. 55. Geneva, Switzerland, World Meteorological Organization.2014

Chan, C. Y., Tang, J. H., Li, Y. S. and Chan, L. Y.: Mixing ratios and sources of halocarbons in urban, semi-urban and rural sites of the Pearl River Delta, South China, Atmospheric Environment, 40, 38, 7331-7345, 10.1016/j.atmosenv.2006.06.041, 2006.

Chen, L., Makide, Y. and Tominaga, T.: Determination of 1, 2-dichlorotetrafluoroethane (CFC-114) concentration in the atmosphere, Chem. Lett., 3, 571-574, 1994.

Davis, M. E., Bernard, F., McGillen, M. R., Fleming, E. L. and Burkholder, J. B.: UV and infrared absorption spectra, atmospheric lifetimes, and ozone depletion and global warming potentials for CCl2FCCl2F (CFC-112), CCl3CClF2 (CFC-112a), CCl3CF3 (CFC-113a), and CCl2FCF3 (CFC-114a), Atmospheric Chemistry and Physics, 16, 12, 8043-8052, 10.5194/acp-16-8043-2016, 2016.

Derwent, R. G., Simmonds, P. G., O'Doherty, S. and Ryall, D. B.: The impact of the Montreal Protocol on halocarbon concentrations in northern hemisphere baseline and European air masses at Mace Head, Ireland over a ten year period from 1987–1996, Atmospheric Environment, 32, 21, 3689-3702.

EIA. Emission of greenhouse gases in United States 1995. United States, Energy Information Administration/ US Dept. of Energy 1996

Farman, J. C., Gardiner, B. G. and Shanklin, J. D.: Large losses of total ozone in Antarctica reveal seasonal ClO x/NOx interaction, Nature, 315, 6016, 207-210, 10.1038/315207a0, 1985.

Fisher, D. A. and Midgley, P. M.: The production and release to the atmosphere of CFCs 113, 114 and 115, Atmospheric Environment Part A, General Topics, 27, 2, 271-276, 10.1016/0960-1686(93)90357-5, 1993.

Hodnebrog, Ø., Etminan, M., Fuglestvedt, J. S., Marston, G., Myhre, G., Nielsen, C. J., Shine, K. P. and Wallington, T. J.: Global warming potentials and radiative efficiencies of halocarbons and related compounds: A comprehensive review, Reviews of Geophysics, 51, 2, 300-378, 10.1002/rog.20013, 2013.

IPCC. IPCC Special Reports on Climate Change. The Hague, Intergovernmental Panel on Climate Change.2000

Laube, J. C., Mohd Hanif, N., Martinerie, P., Gallacher, E., Fraser, P. J., Langenfelds, R., Brenninkmeijer, C. A. M., Schwander, J., Witrant, E., Wang, J. L., Ou-Yang, C. F., Gooch, L. J., Reeves, C. E., Sturges, W. T. and Oram, D. E.: Tropospheric observations of CFC-114 and CFC-114a with a focus on long-term trends and emissions, Atmospheric Chemistry and Physics, 16, 23, 15347-15358, 10.5194/acp-16-15347-2016, 2016.

Laube, J. C., Newland, M. J., Hogan, C., Brenninkmeijer, C. A. M., Fraser, P. J., Martinerie, P., Oram, D. E., Reeves, C. E., Röckmann, T., Schwander, J., Witrant, E. and Sturges, W. T.: Newly detected ozone-depleting substances in the atmosphere, Nature Geoscience, 7, 4, 266-269, 10.1038/ngeo2109, 2014.

Lee, J. M. Determination of stratospheric lifetimes of HCFCs and other halogenated hydrocarbons from balloon-borne profile measurements. UK, University of East Anglia. PhD Thesis.1994

Liang, Q., Stolarski, R. S., Douglass, A. R., Newman, P. A. and Nielsen, J. E.: Evaluation of emissions and transport of CFCs using surface observations and their seasonal cycles and the GEOS CCM simulation with emissions-based forcing, Journal of Geophysical Research: Atmospheres, 113, D14, n/a-n/a, 10.1029/2007JD009617, 2008.

Martinerie, P., Nourtier-Mazauric, E., Barnola, J. M., Sturges, W. T., Worton, D. R., Atlas, E., Gohar, L. K., Shine, K. P. and Brasseur, G. P.: Long-lived halocarbon trends and budgets from atmospheric chemistry modelling constrained with

measurements in polar firn, Atmospheric Chemistry and Physics, 9, 12, 3911-3934, 10.5194/acp-9-3911-2009, 2009.

Montzka, S. A., Butler, J. H., Myers, R. C., Thompson, T. M., Swanson, T. H., Clarke, A. D., Lock, L. T. and Elkins, J. W.: Decline in the tropospheric abundance of halogen from halocarbons: Implications for stratospheric ozone depletion, Science, 272, 5266, 1318-1322, 1996.

Newland, M. J. Long term trends of halogenated trace gases, hydrocarbons, alkyl nitrates and of the oxidative capacity of the atmosphere, University of East Anglia. Ph.D.2013

Oram, D. E.: Trends of Long-lived Anthropogenic Halocarbons in the Southern Hemisphere and Model Calculations of Global Emissions, 1999.

Prinn, R. G., Weiss, R. F., Fraser, P. J., Simmonds, P. G., Cunnold, D. M., Alyea, F. N., O'Doherty, S., Salameh, P., Miller, B. R., Huang, J., Wang, R. H. J., Hartley, D. E., Harth, C., Steele, L. P., Sturrock, G., Midgley, P. M. and McCulloch, A.: A history of chemically and radiatively important gases in air deduced from ALE/GAGE/AGAGE, Journal of Geophysical Research: Atmospheres, 105, D14, 17751-17792, 10.1029/2000JD900141, 2000.

Reimann, S., Schaub, D., Stemmler, K., Folini, D., Hill, M., Hofer, P., Buchmann, B., Simmonds, P. G., Greally, B. R. and O'Doherty, S.: Halogenated greenhouse gases at the Swiss High Alpine Site of Jungfraujoch (3580 m asl): Continuous measurements and their use for regional European source allocation, Journal of Geophysical Research D: Atmospheres, 109, 5, D05307 05301-05312, 2004.

Rigby, M., Prinn, R. G., O'Doherty, S., Montzka, S. A., McCulloch, A., Harth, C. M., Mühle, J., Salameh, P. K., Weiss, R. F., Young, D., Simmonds, P. G., Hall, B. D., Dutton, G. S., Nance, D., Mondeel, D. J., Elkins, J. W., Krummel, P. B., Steele, L. P. and Fraser, P. J.: Re-evaluation of the lifetimes of the major CFCs and CH<inf>3</inf>CCl<inf>3</inf> using atmospheric trends, Atmospheric Chemistry and Physics, 13, 5, 2691-2702, 10.5194/acp-13-2691-2013, 2013.

Rowland, F. S. and Molina, M. J.: Chlorofluoromethanes in the environment, Reviews of Geophysics, 13, 1, 1-35, 10.1029/RG013i001p00001, 1975.

Sturrock, G. A., Etheridge, D. M., Trudinger, C. M., Fraser, P. J. and Smith, A. M.: Atmospheric histories of halocarbons from analysis of Antarctic firn air: Major Montreal Protocol species, Journal of Geophysical Research Atmospheres, 107, 24, 10.1029/2002JD002548, 2002.

Tobiszewski, M. and Namiesnik, J.: PAH diagnostic ratios for the identification of pollution emission sources, Environ Pollut, 162, 110-119, 10.1016/j.envpol.2011.10.025, 2012.

UNEP. Handbook for the Montreal protocol on Substances that Deplete the Ozone Layer. (9th ed.), Ozone Secretariat: United Nations Environment Programme (UNEP).2012

UNEP (2014, last access: 27 May 2016). "Status of Ratification, List of Parties Categorised as Operating under Article 5 Paragraph 1 of the Montreal Protocol."

Chapter 6

Conclusions

The main results of this thesis are summarised in this chapter. Section 6.1 provides an overview of each of three result-related chapters and highlights the principal scientific findings. The aforementioned chapters focused on the three different halocarbon subgroups, namely (1) very short-lived (VSLS) gases (i.e. chlorinated VSLSs), (2) short-lived gases (i.e. methyl halides), as well as (3) long-lived gases (i.e. CFC-114 and -114a). Meanwhile, Section 6.2 suggests the potential methods and techniques to address the limitation of this thesis. These lay the foundation for further expansions of this study, with reference to its findings.

6.1 Significant findings

6.1.1 Regional studies on halogenated substances

The outcomes of the regional studies on chlorinated VSLSs and methyl halides have been presented in Chapters 3 and 4 respectively.

As per Chapter 3, during the regional campaigns in East Asia and South East Asia, the mixing ratios of four species of interest – dichloromethane (CH_2Cl_2), dichoroethane (CH_2ClCH_2Cl), chloroform ($CHCl_3$), and tetrachloroethene or PCE (C_2Cl_4) – were generally higher than their respective background levels, thereby demonstrating widespread regional enhancements. The fact that the mixing ratios at Taiwan were often higher than those of Bachok, indicated that the former was located relatively closer to the major source regions. Moreover, examinations of the NAME footprints and relative particle concentrations suggested that the enhancements of mixing ratios of chlorinated VSLSs in East and Southeast Asia were mostly attributable to anthropogenic sources at the mid-latitude, primarily East

China. Evidently, the elevated mixing ratios of all chlorinated VSLS were consistently associated with industrial emissions. Meanwhile, biomass-burning was also a potential contributor to the variability of the abovementioned mixing ratios. Nevertheless, there are still limited robust ground-based measurements which can support the rationale that biomass-burning has an extensive influence towards the mixing ratios of chlorinated VSLS. It is important to note that this thesis has attempted to use a more quantitative approach to thoroughly analyse the contributions of each sector (natural/ anthropogenic) and each potential region to the variability of the halogenated substance levels at Taiwan and Bachok. In previous works, qualitative analyses (i.e. comparisons of the time series of halogenated substances with their daily NAME air history maps) enabled the formulation of somewhat general conclusions on the possible source regions of the same. This thesis has employed an ArcGIS-generated shapefile whereby the NAME runs were split subjectively into the main geographical areas with differing source characteristics. As a result, the contribution of each source location can be quantified and subsequently helped explain the chemical species' mixing ratio enhancements at the sampling sites. Notably, this study has utilised an improved version of the particle concentration analysis. Previously, the regional divisions were rather crude and not accurately representative. For example, there were mixtures of land and sea areas. However, using the shapefile, the regions were accurately represented; thereby allowing the contributions of specific regions to be assessed correctly.

Similar to Chapter 3, Chapter 4 has also focused on interpretations of the observational datasets that were generated from the ground-based campaigns in East Asia and South East Asia. However, in the latter chapter, the species of interest were methyl halides – methyl chloride (CH_3Cl) and methyl bromide (CH_3Br). At both Taiwan and Bachok, the mixing ratios of the methyl halides also exceeded their respective global background values, hence demonstrating widespread regional enhancements once again. Unlike most of halogenated substances in Chapter 3, the atmospheric abundances of CH_3Cl and CH_3Br were influenced by emissions originated from multiple type of sources. There were two main possible shared sources of methyl halides at Taiwan and Bachok, namely (1) Industry (combustion and processing) and (2) agriculture (waste burning on fields). Additionally, (1) forest burning and grassland burning emissions were suspected to also contribute

to the methyl halide variations, especially at Bachok and (2) oceanic emissions potentially influence the variability of methyl halides in Taiwan. In addition, terrestrial emissions were suspected to contribute to the extraordinarily high mixing ratios of CH_3Cl, especially at Bachok. However, their contributions to the said ratios have not been quantified in this study. As such, further investigations on the same are warranted in the future.

Interestingly, in the regional studies on halogenated substances, some of the strongest enhancements of the gases have also been observed concurrently with the cold surges – an important meteorological process during the Northeast Monsoon. In this thesis, a new cold surge index has been devised to enable more thorough analyses of cold surges and their influences on the variations in the halogenated substances' mixing ratios. As mentioned, the results have shown that high concentrations of halogenated substances corresponded to the occurrence of the Northeast Monsoon's cold surges. Thus, these findings have provided further evidence of the ability of cold surges to rapidly transport gases of relatively short atmospheric lifetimes (~1 year) from highly industrialised regions (i.e. East Asia) to the tropics. Even though evidences of cold surges during the Bachok campaigns have been demonstrated (e.g. Oram et al., 2017), this work has, for the first time, utilised a cold surge index (which is generally used in climatology) to define the same, thereby strengthening the understanding of the associations of cold surges with the variability of very short-lived and short-lived gases. Additionally, an alternative index is assigned further south and called as V_8 to better represent the transport of trace gases closer to Bachok

Importantly, both studies in Chapters 3 and 4 have provided further evidences of the elevated emissions of VSLSs and short-lived gases. Historically, these have not been considered as ozone-damaging in light of the belief that their relatively short atmospheric lifetimes would not enable them to reach the stratosphere in large quantities. As such, they have not been controlled under the Montreal Protocol at that time. However, their impact on the climate, particularly in terms of stratospheric ozone-depletion, depended on the location at which they were liberated. Emissions that were close to the major stratospheric input regions

were of far greater significance with regards to ozone-depletion. On another note, the aforementioned studies have also demonstrated the important roles of the Northeast Monsoon's cold surges as well as East Asian and South East Asian emissions in the enhancement of halogenated substance mixing ratios in those regions. Evidently, East Asia and South East Asia were of particular importance because (1) they can be potential emitters since the sources of chlorinated VSLSs and methyl halides found to be co-located with various emissions generated either from industrial, non-industrial or natural activities found in the regions, and that (2) they had the potential to increase the contribution of halogenated substances to the stratospheric halogens loading. As we have no control over the natural weather patterns (including cold surges, our main concern should be over the copious emissions of halogenated substances from East Asia. In the absence of control over regional emissions, the contributions of chlorinated VSLSs and methyl halides to the stratospheric halogens loading would be likely to substantially increase in the coming years, which in turn would give rise to delays in the long-term recovery of the ozone layer. This highlights the importance of conducting further regional studies not only as few measurements have been made so far but also the proximity of this region to prevalent deep convection, which increases the chance of pollutants emitted from here being transported to the upper tropical troposphere – the point of entry into the stratosphere and subsequently impacting the ozone layer.

6.1.2 Global study on halogenated substances

The study in Chapter 5 has filled the knowledge gap in terms of the so-called neglected long-lived gases (i.e. CFC-144 and -144a). For the first time, complete quantifications of CFC-114 and -114a have been achieved. Likewise, the long-term trends and emissions of the two isomeric forms have been successfully reported separately. Evidently, these achievements were attributable to analyses of a combination of archived remote Southern Hemispheric tropospheric air and firn air data that enabled the reconstruction of tropospheric records from 1960 to 2014. Overall, the mixing ratios of both isomers no longer increased significantly at the

end of that record. Also, the stabilisation of the global atmospheric mixing ratios of both CFCs was proof of the success of the Montreal Protocol.

Chapter 5 has also presented the top-down estimated global annual emissions of CFC-114 and -114a via a two-dimensional atmospheric chemistry-transport model. In general, the emissions of both compounds have increased from around 1960 to the 1980s. A substantial reduction of the same since the late 1980s was in line with the reduction of emissions in response to the Montreal Protocol. However, substantial emissions of both isomers were still the case in 2014. Moreover, changes in the emission ratio of the two isomers since the 1990s have confirmed that the sources of the same were partly unrelated. Complementary ground-based observations of the Taiwanese air samples supported this hypothesis and suggested the presence of a persistent source of CFC-114a in East Asia.

In conclusion, significant global atmospheric emissions of CFC-114 and -114a have persisted until at least 2014, thus highlighting the need for continual efforts to ensure that these substances eventually disappear from the atmosphere. Since the exact factors that contributed to the abundances of both isomers post-implementation of the Montreal Protocol are yet to be identified, further investigations are necessary to determine the origins of the said compounds, especially in East Asia. Given the differences in the trends and emissions, the differentiation of CFC-114 & -114a should be taken into consideration when reporting to the Montreal Protocol in the future.

6.2 Suggestions and future research directions

In general, further observations are required to assess the abundances of halogenated substances and locate the exact origins of the emissions, especially in East Asia and South East Asia. Although this thesis has characterised the East Asian and South East Asian emissions according to the source regions and types, further evaluations should be done in order to generate more solid conclusions which can inform and guide future campaigns. At this stage, the exact mechanisms or pathways of the regional emissions of short-lived, very short-lived, and long-lived gases are still uncertain. Therefore, I recommend the following improvements to expand this work further:

1. The frequencies and durations of the campaigns should be increased. While Taiwan is an ideal location to study the Asian outflow of trace gases including ozone-depleting substances (ODS), constant monitoring at Bachok will provide an opportunity to assess the long-range transportation of ODS from neighbouring regions, apart from further exploring the influences of weather systems (e.g. cold surges) on the variability of the chemical compositions.

2. A more robust modelling approach i.e. combining NAME dispersion studies with source apportionment models that extract the source of the emissions to more than just a region but to a particular type of natural or anthropogenic emission.

3. Correlations with other tracers can also be helpful since this thesis has been restricted to the available compounds. For example, observational datasets of acetonitrile (CH_3CN) concentrations may indicate the contributions of biomass-burning to the anthropogenic release of halogenated substances. Also, correlations can be established between the mixing ratios of naturally-emitted gases and certain parameters like chlorophyll abundance (as marker for phytoplankton abundance) in order to attribute the variations in the mixing ratios of the naturally produced halogenated substances (e.g. methyl halides) to the air masses that originate from the oceanic regions. Also, a more detailed survey of the possible contributors (plants, soil, leaf litter, etc.)

will complement the knowledge of the separate sources and sinks within the terrestrial ecosystem.

4. Datasets of the concentrations of short-lived and very short-lived halogenated substances need to be generated during aircraft campaigns that collect East Asian and South East Asian air samples at altitudes of 10 - 12 km. These samples will provide an opportunity to determine whether the short-lived and very short-lived halogenated substances can be rapidly channelled to the upper tropical troposphere (lower TTL) and have the impact on the stratospheric ozone.

5. Inter-annual comparisons of cold surges should be executed to enable the identification of the presence of consistent or usual year-on-year patterns of the cold surge. Also multi-winter comparison will help determine the existence of a relationship between cold surges and climate change (e.g. El-Nino events).

To summarise, it is hoped that the outcomes of this thesis can assist future investigation of the tropospheric abundances, emissions, and transportation of halogenated substances at the regional as well as global scales. Also, it is hoped that research and monitoring of halogenated substances would be continuously conducted in order to ensure compliance with the Montreal Protocol for the protection of the environment against ozone loss.

Appendix

Chapter 3 & Chapter 4

Appendix A: Mixing ratios of chlorinated VSLS and methyl halides in Taiwan during campaigns in 2013, 2014, 2015 and 2016

Date and Time (UTC)	Mixing ratios (ppt)					
	CH_2Cl_2	CH_2ClCH_2Cl	$CHCl_3$	C_2Cl_4	CH_3Cl	CH_3Br
07/03/2013 03:20	171.81	95.33	22.38	3.81	885.77	18.65
08/03/2013 03:00	328.51	40.23	19.72	2.73	789.67	15.85
11/03/2013 03:33	207.99	103.44	25.95	4.25	806.75	16.87
12/03/2013 02:56	354.61	196.45	40.26	4.38	925.45	35.06
13/03/2013 02:40	226.50	258.97	58.10	3.05	875.82	22.86
14/03/2013 03:00	331.42	140.15	36.08	7.72	912.12	20.60
15/03/2013 01:50	137.56	56.24	19.79	4.64	756.39	18.31
18/03/2013 01:55	108.13	33.12	14.71	2.55	928.96	17.66
19/03/2013 02:30	193.20	80.77	20.42	4.02	861.09	17.40
20/03/2013 01:30	90.26	473.30	91.57	2.20	856.54	16.06
21/03/2013 01:20	671.78	327.72	69.84	16.56	1236.97	23.53
22/03/2013 02:45	408.45	182.89	38.41	6.64	1082.50	34.64
25/03/2013 01:50	296.93	118.51	32.80	7.31	939.89	23.88
27/03/2013 03:20	351.19	820.06	32.99	6.05	1056.66	18.95
28/03/2013 02:40	157.49	65.01	22.37	3.65	923.97	16.85
01/04/2013 02:40	248.54	494.84	199.26	4.69	977.27	17.25
03/04/2013 02:27	476.81	186.62	57.23	10.76	1037.42	23.12
04/04/2013 02:15	239.27	93.26	32.95	6.36	1111.36	48.76
05/04/2013 03:02	76.77	23.67	11.55	1.66	818.90	21.42
11/03/2014 10:22	208.49	63.26	40.79	5.97	726.79	22.86
13/03/2014 15:50	675.41	290.20	85.13	18.55	1086.76	19.76
14/03/2014 14:15	354.85	143.20	55.99	11.34	777.16	17.80
15/03/2014 14:30	209.46	75.86	35.70	6.39	699.12	11.57
16/03/2014 14:22	359.39	166.11	44.92	7.60	772.37	12.77
17/03/2014 14:23	459.94	188.83	44.57	8.33	819.63	16.47
18/03/2014 14:27	331.99	81.93	34.39	4.53	841.31	16.75
19/03/2014 14:40	303.74	90.95	33.53	4.36	802.95	18.53
21/03/2014 14:21	92.46	23.53	21.53	3.58	576.64	9.34
22/03/2014 14:20	77.87	18.96	14.78	3.04	613.32	8.90
24/03/2014 14:15	79.13	17.64	14.71	2.70	613.05	9.28
25/03/2014 14:15	495.50	142.12	42.33	4.57	753.43	12.29
26/03/2014 14:25	204.90	35.89	19.00	3.43	679.23	18.53
27/03/2014 14:20	307.13	95.97	25.72	5.09	735.65	13.84

28/03/2014 14:15	741.02	244.28	61.33	14.88	981.68	18.57
29/03/2014 14:05	78.20	18.17	13.82	1.65	602.63	13.48
30/03/2014 15:20	665.30	245.85	103.23	16.64	1048.54	19.42
31/03/2014 14:20	407.37	122.49	55.33	8.57	947.47	25.17
01/04/2014 14:25	208.29	63.91	31.42	5.30	761.69	13.56
02/04/2014 14:10	226.80	82.82	34.47	5.67	695.13	15.71
03/04/2014 14:25	197.02	63.71	30.82	4.94	676.32	10.66
04/04/2014 14:15	190.52	58.30	36.42	5.61	673.14	11.17
12/03/2015 17:35	97.39	24.22	20.87	4.33	771.22	15.09
17/03/2015 11:26	66.60	15.44	13.65	2.02	640.91	8.98
18/03/2015 10:40	59.38	12.80	12.73	1.78	711.86	14.21
19/03/2015 10:40	211.49	87.82	27.31	2.38	815.78	10.93
20/03/2015 10:42	225.50	355.80	125.09	3.03	965.95	16.62
21/03/2015 08:45	82.47	18.93	13.47	1.85	734.56	10.77
22/03/2015 10:20	510.22	215.12	103.84	17.73	1091.42	20.61
23/03/2015 10:11	391.82	126.66	69.00	8.86	1009.04	18.09
24/03/2015 13:03	135.18	45.32	34.65	4.92	677.92	8.74
25/03/2015 10:20	109.84	30.52	26.10	4.79	693.20	12.53
26/03/2015 10:10	100.65	27.20	20.55	3.46	676.16	9.61
27/03/2015 09:45	325.83	221.50	65.52	4.75	1005.11	19.49
28/03/2015 13:07	536.68	144.05	38.85	7.19	783.44	15.06
29/03/2015 08:50	237.14	77.86	24.72	3.91	751.95	10.51
30/03/2015 09:38	128.74	35.21	18.72	2.53	814.32	11.37
31/03/2015 10:12	88.89	19.05	15.22	2.24	672.28	12.00
22/04/2015 19:45	238.15	100.43	39.40	7.35	660.93	11.15
23/04/2015 10:04	233.11	63.01	33.23	5.80	792.27	15.07
23/04/2015 17:50	235.45	70.15	35.43	5.05	788.08	16.38
24/04/2015 10:40	198.63	58.98	29.16	5.01	770.28	11.70
24/04/2015 17:40	306.15	99.32	44.56	4.62	875.08	15.57
25/04/2015 10:40	175.61	49.11	27.96	3.90	735.62	13.94
25/04/2015 17:20	138.67	39.75	24.29	3.33	645.44	9.20
16/03/2016 17:14	158.15		14.36		874.90	15.75
20/03/2016 12:16	401.20		50.60		958.93	19.42
21/03/2016 13:52	167.87		30.18		790.19	11.65
24/03/2016 12:34	84.46		17.93		670.75	10.62
24/03/2016 14:22	85.15		17.82		702.07	10.50
25/03/2016 12:17	91.55		19.17		705.92	12.26
25/03/2016 14:18	92.27		21.01		703.12	13.39
26/03/2016 12:19	546.47		93.70		1040.74	19.42
26/03/2016 14:07	530.94		95.03		1119.71	17.16
27/03/2016 12:41	270.66		66.19		910.37	16.43
08/04/2016 12:16	423.56		56.31		1162.36	26.84
08/04/2016 14:09	334.22		46.38		859.10	18.03
09/04/2016 10:01	225.93		28.30		821.15	15.31
09/04/2016 11:51	226.20		27.95		794.66	16.68
10/04/2016 11:54	202.64		27.26		785.65	13.15
11/04/2016 12:56	116.76		19.42		774.31	12.46
11/04/2016 14:06	112.26		18.20		790.12	11.72

12/04/2016 12:19	164.59		27.83		747.92	13.73
12/04/2016 14:12	157.11		26.89		826.37	14.15
14/04/2016 11:09	623.30		49.63		879.09	22.64
14/04/2016 12:09	636.92		48.90		899.74	20.38
14/04/2016 14:44	470.59		36.81		892.89	17.17
15/04/2016 10:06	175.00		24.97		738.56	11.17
15/04/2016 12:13	191.40		26.26		773.54	13.85
18/04/2016 12:20	242.05		51.13		804.14	11.85
19/04/2016 11:37	284.40		41.87		816.55	14.69
25/04/2016 12:08	354.64		40.59		807.79	14.92
25/04/2016 14:03	348.18		39.22		837.04	14.22
28/04/2016 11:57	1203.40		136.95		1326.38	34.03
28/04/2016 14:07	1040.18		113.52		1160.79	21.63
29/04/2016 10:17	1106.59		149.43		1268.84	27.33
29/04/2016 12:05	1173.34		147.23		1291.08	28.21
29/04/2016 13:57	1110.87		136.15		1260.54	24.50

Appendix B: Mixing ratios of chlorinated VSLS and methyl halides in Bachok during campaigns in 2013/2014 and 2015/2016

Date and Time (UTC)	Mixing ratios (ppt)					
	CH_2Cl_2	CH_2ClCH_2Cl	$CHCl_3$	C_2Cl_4	CH_3Cl	CH_3Br
20/01/2014 04:05	132.17	50.76	19.74	3.41	804.55	14.24
20/01/2014 08:10	170.36	61.30	20.35	4.26	831.44	18.17
21/01/2014 04:10	200.77	69.90	22.80	4.89	873.92	15.60
22/01/2014 03:45	162.51	62.16	26.09	4.83	835.00	15.67
23/01/2014 04:50	352.22	119.51	30.48	9.48	882.83	12.91
24/01/2014 09:40	183.14	66.47	27.16	4.79	781.24	20.75
25/01/2014 04:08	175.39	66.07	26.76	4.50	864.23	11.76
26/01/2014 04:15	158.50	53.09	22.37	4.24	793.43	9.83
27/01/2014 09:55	92.93	30.52	17.16	2.12	664.36	9.87
28/01/2014 04:25	75.36	21.51	14.68	2.06	606.10	11.41
28/01/2014 09:05	72.67		14.44	2.03	592.83	8.10
29/01/2014 09:00	80.13		14.68	1.99	613.38	9.31
30/01/2014 03:55	92.48		16.25	2.43	642.46	10.40
30/01/2014 09:45	86.99		15.00	2.00	647.43	9.84
30/01/2014 11:40	82.05		14.62	1.88	679.02	9.39
30/01/2014 15:59	82.83	25.20	14.52	1.86	614.84	8.43
31/01/2014 00:00	88.98	27.05	23.23	2.61	1554.32	12.49
31/01/2014 04:00	83.52		14.81	1.95	698.11	8.86
31/01/2014 08:00	81.89		14.04	1.87	633.76	10.26
31/01/2014 12:00	85.16		15.37	1.85	625.33	8.66
31/01/2014 15:59	101.10		17.37	2.32	768.40	11.74
01/02/2014 00:00	89.58	28.90	24.18	3.15	1574.10	17.77
01/02/2014 04:00	81.92		14.95	2.01	716.74	9.32
01/02/2014 08:00	76.44	21.66	14.65	1.85	616.02	8.78
01/02/2014 12:00	73.65		13.50	1.79	687.12	12.18

02/02/2014 04:10	73.83	20.01	14.70	1.90	701.05	9.09
03/02/2014 06:15	66.38	16.43	12.81	1.57	784.29	11.70
05/02/2014 09:55	69.34		13.75	1.57	712.83	8.95
19/11/2015 08:10	49.93	10.97	12.92	1.67	1010.06	15.04
22/11/2015 09:10	67.85	10.41	13.27	4.42	739.36	7.56
23/11/2015 08:38	51.25	8.46	12.88	1.36	709.25	14.27
25/11/2015 09:49	70.79	12.77	13.73	2.39	695.04	9.78
26/11/2015 09:21	69.15	16.14	13.27	2.12	642.24	8.75
29/11/2015 08:45	53.96	12.32	11.43	1.55	661.94	8.28
30/11/2015 09:33	79.88	12.15	18.29	4.00	1014.67	10.05
01/12/2015 09:18	56.34	13.33	13.05	1.53	625.39	8.50
02/12/2015 08:40	90.83	22.13	19.30	2.50	634.71	8.27
03/12/2015 08:30	84.18	23.33	18.06	2.89	728.98	11.06
06/12/2015 09:11	64.09	13.30	12.91	1.56	773.01	9.53
08/12/2015 08:47	62.18	13.17	11.79	1.53	659.93	9.01
09/12/2015 08:58	51.20	10.08	11.24	1.65	653.09	9.42
12/12/2015 09:33	236.58	65.90	35.41	7.18	833.22	10.50
13/12/2015 09:12	86.81	21.52	15.48	2.58	706.07	8.75
16/12/2015 09:53	128.74	38.67	16.78	3.66	743.98	9.78
17/12/2015 08:24	267.96	78.17	30.43	7.85	831.82	12.54
20/12/2015 08:50	204.73	71.61	29.09	7.25	751.63	9.66
27/12/2015 08:30	67.54	15.88	14.10	2.03	645.54	12.90
28/12/2015 08:36	82.40	23.20	16.94	2.67	695.11	10.64
29/12/2015 09:15	110.48	36.21	21.60	3.72	640.72	11.85
30/12/2015 08:29	96.98	31.98	18.47	3.62	641.23	7.98
31/12/2015 05:24	95.81	30.05	17.90	3.74	681.60	8.41
04/01/2016 02:41	98.84	25.55	19.41	2.91	793.39	9.15
04/01/2016 08:26	97.06	24.87	14.95	3.03	634.59	9.25
05/01/2016 08:39	49.36	9.56	11.00	1.44	612.06	7.96
06/01/2016 08:44	61.67	11.29	12.33	1.48	632.82	8.33
10/01/2016 09:25	69.18	20.33	12.34	1.89	710.61	9.56
11/01/2016 08:34	77.53	18.72	13.95	1.99	681.71	9.44
12/01/2016 08:50	88.35	22.59	14.39	2.16	684.52	9.67
13/01/2016 08:24	66.85	12.98	12.50	1.44	731.87	9.51
14/01/2016 08:21	54.05	9.64	11.72	1.33	702.23	8.50
17/01/2016 07:40	60.32	13.96	11.99	1.54	699.58	8.53
18/01/2016 08:35	54.82	13.17	10.84	1.57	680.61	10.56
19/01/2016 07:44	47.35	10.35	9.94	1.33	663.37	9.21
20/01/2016 08:16	48.96	10.78	9.58	1.27	647.87	8.57
21/01/2016 07:24	53.09	12.92	10.47	1.43	662.15	9.69
24/01/2016 08:53	103.09	28.96	16.50	2.78	698.21	10.83
26/01/2016 12:23	171.24	64.24	24.87	6.72	715.08	8.56
27/01/2016 07:44	137.65	44.99	22.68	5.30	690.22	8.04

Appendix C: Meridional wind extracted at 8°N and 15°N during the Bachok campaigns in 2013/2014 and 2015/2016.

Day	V= 8^{0}N				V= 15^{0}N			
	00:00	06:00	12:00	18:00	00:00	06:00	12:00	18:00
1 Jan 2014	-8.45	-7.78	-8.00	-8.39	-7.50	-6.07	-5.60	-3.66
2 Jan 2014	-6.69	-4.55	-3.65	-4.69	-2.40	-0.18	-0.36	1.29
3 Jan 2014	-5.07	-4.20	-4.87	-5.35	1.76	-2.03	-4.84	-4.44
4 Jan 2014	-5.83	-5.75	-7.05	-6.41	-6.54	-9.32	-9.79	-8.21
5 Jan 2014	-6.54	-6.96	-7.45	-6.38	-8.51	-5.48	-5.65	-2.17
6 Jan 2014	-5.31	-5.96	-6.35	-5.30	-3.51	-2.14	-2.46	-1.59
7 Jan 2014	-5.34	-4.64	-6.94	-6.62	-2.29	0.61	-1.26	-0.31
8 Jan 2014	-6.24	-3.95	-6.10	-6.57	-1.67	-4.36	-7.38	-7.74
9 Jan 2014	-6.23	-6.88	-7.84	-5.87	-9.58	-8.14	-9.29	-7.34
10 Jan 2014	-6.88	-5.52	-7.13	-5.15	-8.33	-6.41	-6.92	-4.71
11 Jan 2014	-6.06	-6.53	-7.77	-8.15	-5.54	-5.75	-7.15	-5.81
12 Jan 2014	-8.43	-8.15	-9.71	-8.98	-8.27	-9.62	-11.05	-10.29
13 Jan 2014	-9.95	-8.98	-9.69	-9.17	-11.88	-12.69	-14.54	-12.92
14 Jan 2014	-8.79	-9.58	-10.64	-9.51	-15.50	-13.34	-13.66	-12.11
15 Jan 2014	-10.25	-9.67	-9.21	-8.03	-13.86	-11.67	-11.92	-8.64
16 Jan 2014	-7.61	-7.46	-8.66	-7.51	-9.23	-7.15	-8.64	-8.58
17 Jan 2014	-8.29	-8.76	-9.07	-8.74	-10.56	-10.67	-13.14	-11.87
18 Jan 2014	-10.04	-10.63	-11.33	-9.10	-12.71	-13.08	-13.60	-10.01
19 Jan 2014	-9.97	-8.45	-9.36	-9.24	-8.65	-7.17	-9.33	-6.90
20 Jan 2014	-8.86	-7.23	-7.88	-8.78	-9.19	-9.27	-10.91	-10.55
21 Jan 2014	-9.10	-10.04	-10.58	-9.76	-13.57	-12.73	-14.23	-11.58
22 Jan 2014	-10.90	-10.06	-9.49	-8.14	-13.43	-12.17	-13.85	-10.57
23 Jan 2014	-8.09	-6.83	-7.37	-4.90	-9.70	-7.73	-7.99	-4.57
24 Jan 2014	-5.16	-5.52	-5.57	-2.90	-4.80	-4.23	-3.54	1.20
25 Jan 2014	-3.18	-1.92	-3.35	-3.99	-0.72	-2.69	-3.84	-2.41
26 Jan 2014	-3.89	-3.68	-4.97	-4.74	-3.82	-4.96	-7.02	-6.32
27 Jan 2014	-4.80	-4.55	-4.85	-4.46	-7.43	-5.55	-6.70	-4.26
28 Jan 2014	-5.39	-4.70	-5.77	-4.34	-5.12	-5.62	-6.24	-4.34
29 Jan 2014	-4.60	-5.17	-6.44	-4.45	-5.22	-4.28	-6.22	-4.36
30 Jan 2014	-5.54	-5.39	-7.10	-6.04	-4.49	-4.45	-5.52	-2.48
31 Jan 2014	-5.15	-3.71	-6.09	-4.92	-3.34	-3.91	-3.97	-4.01
1 Feb 2014	-4.47	-3.24	-5.03	-3.60	-4.33	-5.10	-7.11	-4.38
2 Feb 2014	-2.04	-1.67	-2.54	-1.42	-3.71	-1.27	-1.69	0.48
3 Feb 2014	-1.66	-0.79	-1.13	-1.34	-0.85	0.28	-0.90	0.08
4 Feb 2014	-0.99	-0.16	-1.66	-0.79	-0.83	-0.13	0.08	0.73
5 Feb 2014	-0.58	-0.58	-1.69	-0.43	-0.67	0.78	0.71	2.24
6 Feb 2014	-0.46	-0.36	-1.68	-0.98	1.54	2.17	1.44	4.35
7 Feb 2014	-0.50	-0.50	-0.18	-0.65	1.49	2.08	0.69	1.90
8 Feb 2014	-0.48	-1.99	-2.18	-1.22	1.08	1.36	2.10	3.33
9 Feb 2014	-1.79	-1.83	-2.64	-1.97	1.68	1.78	1.18	-0.30
10 Feb 2014	-3.19	-3.15	-4.26	-3.64	-4.52	-5.09	-7.62	-7.25
11 Feb 2014	-4.10	-4.53	-5.36	-3.90	-9.53	-6.93	-6.69	-5.91
12 Feb 2014	-4.17	-3.97	-3.97	-2.82	-6.54	-4.78	-3.26	-2.07

13 Feb 2014	-4.46	-6.32	-6.58	-6.10	-4.62	-3.03	-6.12	-6.34
14 Feb 2014	-5.69	-6.27	-7.04	-5.74	-9.91	-8.53	-9.94	-6.18
15 Feb 2014	-5.50	-6.14	-5.37	-2.79	-6.44	-5.46	-3.67	-2.07
16 Feb 2014	-2.77	-3.40	-3.79	-1.55	-1.71	-0.38	-0.39	1.58
17 Feb 2014	-1.28	-2.18	-3.06	-1.87	0.49	1.66	1.93	1.36
18 Feb 2014	-1.41	-2.02	-2.51	-1.35	1.01	1.87	1.01	-0.29
19 Feb 2014	-1.91	-1.79	-3.95	-4.86	-4.29	-5.33	-10.14	-9.50
20 Feb 2014	-5.32	-4.24	-4.95	-3.96	-10.35	-8.57	-8.78	-7.10
21 Feb 2014	-5.59	-4.28	-6.20	-5.35	-8.13	-5.03	-5.74	-4.94
22 Feb 2014	-7.06	-6.78	-7.24	-5.29	-6.12	-5.33	-6.48	-6.59
23 Feb 2014	-5.25	-6.61	-7.58	-5.98	-6.50	-4.70	-6.00	-3.62
24 Feb 2014	-5.13	-4.42	-5.26	-3.25	-3.26	-1.72	-0.91	1.95
25 Feb 2014	-3.74	-3.74	-4.91	-2.77	0.91	0.57	-0.30	1.26
26 Feb 2014	-2.40	-1.85	-3.77	-3.45	-1.21	-0.66	-1.50	-1.73
27 Feb 2014	-3.56	-3.53	-4.72	-3.40	-3.34	-3.29	-2.17	0.46
28 Feb 2014	-2.84	-1.82	-2.69	-1.09	-0.32	1.72	2.20	2.48
1 Nov 2015	-3.36	-4.60	-4.21	-2.97	-5.95	-4.80	-6.94	-5.84
2 Nov 2015	-4.04	-4.81	-5.35	-2.73	-7.63	-6.92	-8.53	-6.16
3 Nov 2015	-3.62	-2.88	-4.86	-4.67	-6.82	-5.69	-5.66	-4.22
4 Nov 2015	-3.70	-0.22	-0.65	-1.74	-2.94	1.27	0.11	2.34
5 Nov 2015	-0.09	0.23	0.58	0.98	0.75	0.45	-1.40	-0.20
6 Nov 2015	1.46	1.37	-0.19	0.26	-1.10	0.53	-0.27	0.85
7 Nov 2015	-0.49	-1.06	-2.35	-1.58	-0.57	-1.33	-2.46	-2.04
8 Nov 2015	-0.91	-0.40	-2.55	-1.32	-1.84	-1.00	-3.10	-1.97
9 Nov 2015	-1.34	-0.62	-1.49	-0.86	-3.96	-3.39	-3.91	-2.37
10 Nov 2015	-1.82	-1.93	-3.11	-0.99	-3.67	-2.88	-3.29	-1.29
11 Nov 2015	-1.30	-0.71	-1.65	0.18	-1.38	-0.66	-1.63	-0.74
12 Nov 2015	-0.34	0.65	-1.01	-0.28	-0.83	-1.32	-2.18	-0.28
13 Nov 2015	0.07	0.32	-1.74	-1.26	-0.24	1.34	-0.75	-1.35
14 Nov 2015	-1.70	-0.54	-1.82	-0.61	-0.71	-0.19	-1.39	-1.12
15 Nov 2015	-1.81	-3.73	-3.97	-2.01	-1.46	-0.60	-1.62	-0.66
16 Nov 2015	-2.60	-1.28	-0.59	0.74	-0.58	-0.36	0.58	1.27
17 Nov 2015	-0.78	-0.64	-0.88	0.89	-0.37	-1.07	-0.16	0.08
18 Nov 2015	-0.36	0.12	-2.38	-1.79	-0.95	-2.09	-4.22	-4.02
19 Nov 2015	-3.12	-3.41	-4.84	-3.31	-3.46	-2.89	-3.14	-3.63
20 Nov 2015	-4.65	-5.63	-4.23	-2.94	-3.07	-1.10	-1.20	-1.36
21 Nov 2015	-3.04	-3.40	-4.10	-1.88	-3.53	-2.16	-4.80	-3.93
22 Nov 2015	-1.45	-0.78	-2.74	-2.39	-4.71	-4.01	-5.39	-5.11
23 Nov 2015	-3.54	-2.29	-4.79	-4.08	-7.12	-7.14	-8.31	-7.12
24 Nov 2015	-3.89	-2.60	-3.80	-2.93	-7.06	-5.93	-6.40	-4.91
25 Nov 2015	-3.57	-3.29	-4.62	-5.13	-7.02	-6.99	-9.60	-10.15
26 Nov 2015	-5.96	-5.34	-7.53	-6.94	-11.79	-9.94	-10.05	-7.22
27 Nov 2015	-6.14	-2.89	-3.17	-2.78	-7.89	-5.63	-4.92	-3.55

28 Nov 2015	-4.28	-3.24	-4.16	-3.62	-4.95	-5.32	-6.41	-5.25
29 Nov 2015	-4.64	-4.26	-5.21	-3.37	-4.84	-4.98	-5.87	-6.78
30 Nov 2015	-3.39	-1.97	-2.46	-1.02	-8.21	-6.48	-6.04	-5.03
1 Dec 2015	-2.65	-3.76	-3.67	-2.12	-4.65	-4.21	-4.31	-2.82
2 Dec 2015	-2.52	-3.04	-3.15	-2.94	-3.81	-3.84	-4.13	-3.37
3 Dec 2015	-2.86	-3.75	-4.41	-1.78	-5.38	-4.27	-4.65	-5.82
4 Dec 2015	-2.36	-2.89	-4.14	-2.15	-4.96	-3.27	-2.94	-1.24
5 Dec 2015	-1.40	-1.14	-3.97	-4.86	0.58	0.87	-4.21	-5.83
6 Dec 2015	-5.27	-5.18	-6.35	-5.67	-8.34	-7.06	-8.65	-8.45
7 Dec 2015	-5.82	-5.05	-5.84	-5.35	-10.52	-9.64	-10.75	-7.60
8 Dec 2015	-5.27	-4.00	-3.94	-1.72	-5.93	-3.63	-1.36	1.72
9 Dec 2015	-2.59	-1.97	-1.69	-1.35	2.87	3.50	1.58	0.01
10 Dec 2015	-3.19	-3.12	-3.36	-3.02	-2.42	-3.83	-4.87	-3.55
11 Dec 2015	-2.85	-2.56	-3.48	-2.09	-4.36	-4.57	-6.91	-4.43
12 Dec 2015	-3.16	-3.13	-4.03	-3.50	-4.41	-3.03	-3.98	-3.48
13 Dec 2015	-4.08	-2.46	-4.75	-4.17	-4.08	-4.91	-5.11	-4.93
14 Dec 2015	-5.37	-6.60	-6.73	-5.46	-6.91	-6.35	-7.68	-8.90
15 Dec 2015	-5.99	-6.78	-6.78	-8.79	-11.75	-12.94	-14.34	-14.52
16 Dec 2015	-7.95	-9.66	-10.39	-9.50	-17.72	-16.83	-18.19	-15.90
17 Dec 2015	-10.24	-9.64	-11.05	-10.46	-18.76	-16.61	-14.89	-11.12
18 Dec 2015	-10.63	-10.11	-10.38	-10.74	-13.09	-11.16	-11.63	-10.43
19 Dec 2015	-9.63	-9.73	-10.21	-9.56	-10.92	-7.27	-7.68	-6.99
20 Dec 2015	-8.72	-5.88	-7.18	-6.81	-6.25	-3.86	-3.29	-0.19
21 Dec 2015	-4.12	-2.80	-2.85	-0.15	0.74	1.51	0.40	1.72
22 Dec 2015	1.02	2.12	0.80	1.45	1.67	2.71	0.35	0.91
23 Dec 2015	0.97	0.55	-1.49	-1.49	-0.37	-0.70	-0.41	-0.97
24 Dec 2015	-1.35	-1.90	-2.79	-1.81	-1.49	0.55	-2.68	-4.21
25 Dec 2015	-3.61	-4.23	-5.80	-4.68	-5.78	-6.73	-8.72	-7.09
26 Dec 2015	-5.43	-6.06	-5.86	-5.19	-4.86	-2.33	-3.34	-3.43
27 Dec 2015	-7.45	-7.49	-6.38	-4.82	-4.31	-4.90	-7.22	-4.61
28 Dec 2015	-6.18	-7.20	-7.42	-6.85	-8.49	-7.90	-7.68	-5.28
29 Dec 2015	-8.07	-8.29	-8.17	-6.25	-7.02	-4.18	-6.82	-6.40
30 Dec 2015	-7.62	-6.67	-7.49	-6.28	-8.21	-6.23	-8.01	-9.72
31 Dec 2015	-7.72	-8.31	-9.28	-9.40	-10.55	-9.81	-12.16	-10.04
1 Jan 2016	-9.58	-9.32	-9.78	-7.30	-9.70	-8.06	-8.29	-4.57
2 Jan 2016	-6.09	-4.49	-4.53	-3.36	-3.09	-0.18	-1.06	0.26
3 Jan 2016	-4.07	-2.60	-2.87	-1.29	0.50	1.37	0.61	1.09
4 Jan 2016	-1.45	-1.69	-2.19	-1.03	1.09	1.91	1.46	1.90
5 Jan 2016	-2.16	-2.50	-3.42	-2.23	1.77	1.43	-1.36	-1.07
6 Jan 2016	-2.78	-2.94	-3.87	-3.46	-1.02	-3.14	-5.27	-5.31
7 Jan 2016	-3.66	-3.52	-4.03	-2.69	-5.27	-3.03	-6.03	-3.54
8 Jan 2016	-3.41	-4.17	-4.07	-3.81	-5.30	-5.61	-5.96	-4.29
9 Jan 2016	-3.19	-2.98	-3.47	-2.53	-4.81	-3.62	-2.92	-1.31
10 Jan 2016	-2.54	-1.59	-1.87	-0.59	0.04	2.67	2.26	2.92
11 Jan 2016	-0.76	-1.71	-3.12	-2.38	0.55	0.46	-1.88	-2.37
12 Jan 2016	-3.12	-2.49	-2.72	-2.43	-3.84	-2.74	-3.46	-3.50
13 Jan 2016	-2.35	-2.83	-2.84	-2.83	-4.59	-4.18	-4.92	-5.47
14 Jan 2016	-4.16	-2.01	-3.35	-1.26	-4.57	-2.27	-2.03	-1.45

15 Jan 2016	-0.73	-0.38	-1.33	0.34	-1.05	1.98	1.60	0.89
16 Jan 2016	-0.34	-0.55	-0.64	0.12	0.39	3.52	2.60	3.64
17 Jan 2016	-0.59	0.85	-0.73	-0.52	3.94	3.01	0.92	-1.00
18 Jan 2016	-0.68	-2.20	-2.78	-2.56	-2.13	1.01	-0.36	0.57
19 Jan 2016	-2.42	-2.44	-2.39	-1.88	-0.16	0.33	-0.73	0.49
20 Jan 2016	-2.59	-2.38	-2.07	-1.52	1.03	2.52	1.61	3.52
21 Jan 2016	-3.21	-3.45	-3.18	-1.70	2.36	3.27	2.09	2.04
22 Jan 2016	-2.23	-3.18	-4.26	-3.22	-0.15	-0.05	-1.03	-2.12
23 Jan 2016	-3.62	-3.73	-5.40	-5.06	-5.08	-7.09	-12.70	-12.44
24 Jan 2016	-6.69	-8.06	-10.56	-11.25	-15.01	-16.32	-18.56	-16.79
25 Jan 2016	-11.75	-11.80	-11.73	-8.93	-15.31	-12.11	-10.74	-8.45
26 Jan 2016	-7.23	-6.12	-4.59	-3.94	-5.74	-2.92	-2.35	-0.59
27 Jan 2016	-4.05	-2.93	-2.49	-2.07	-0.13	1.76	1.31	2.25
28 Jan 2016	-2.36	-2.10	-2.84	-2.23	4.30	6.73	4.49	2.65
29 Jan 2016	-3.15	-3.60	-3.52	-2.54	0.78	1.06	0.16	0.34
30 Jan 2016	-2.88	-3.21	-3.24	-3.78	-2.21	-1.92	-2.90	-2.82
31 Jan 2016	-4.08	-4.35	-5.30	-3.71	-2.83	-2.08	-1.09	-0.25

Chapter 5

Appendix D: NAME footprints for the Hengchun, Taiwan during 2015 campaign

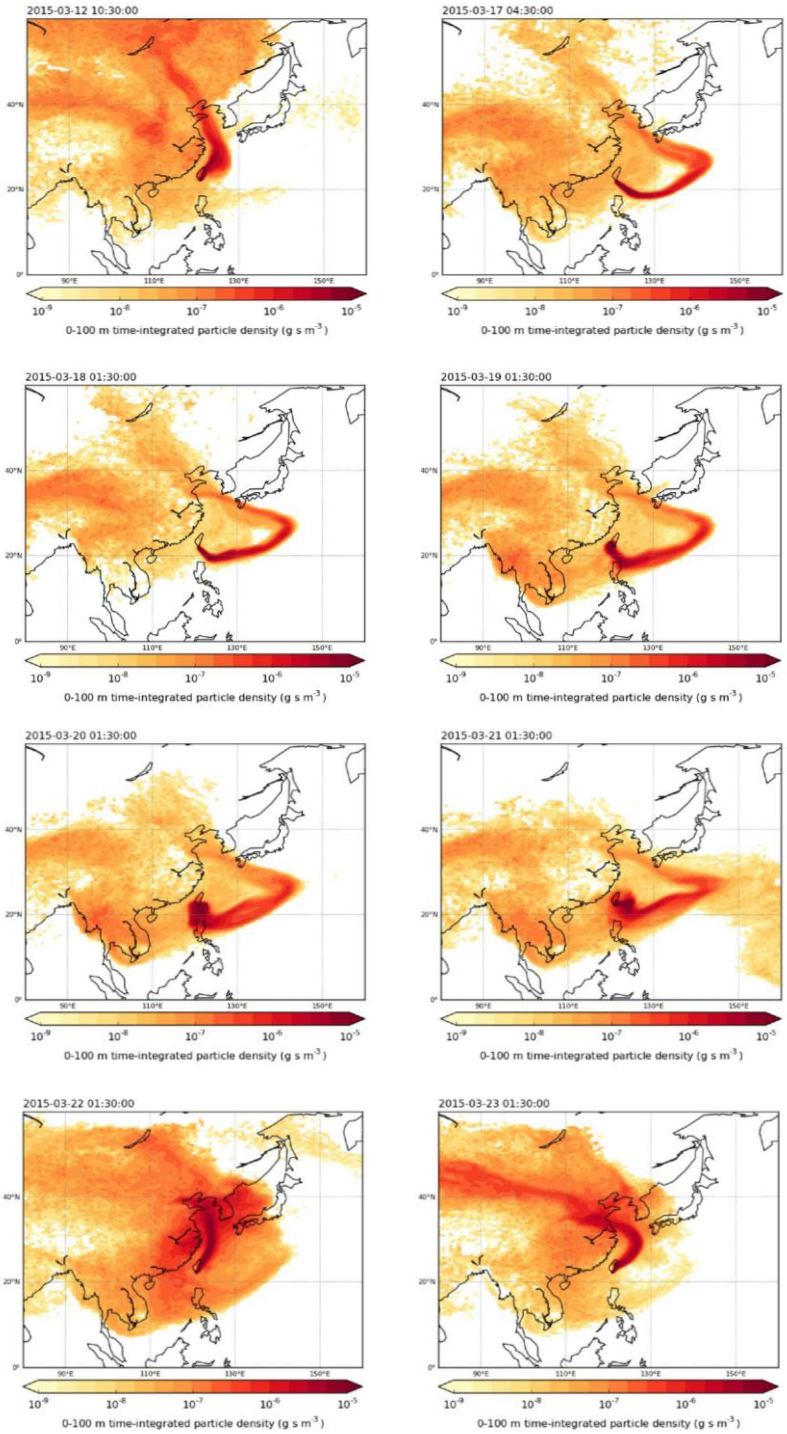

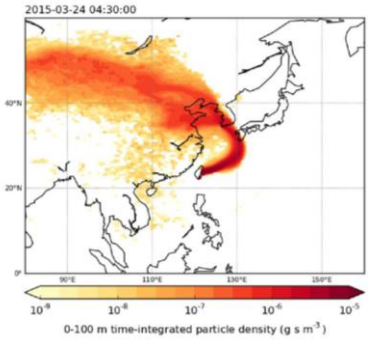
2015-03-24 04:30:00
0-100 m time-integrated particle density (g s m-3)

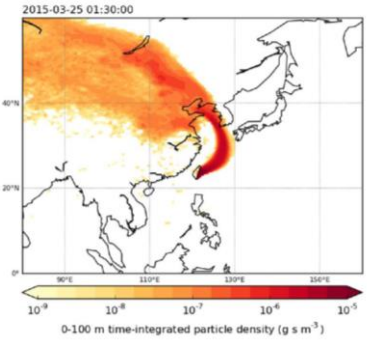
2015-03-25 01:30:00
0-100 m time-integrated particle density (g s m-3)

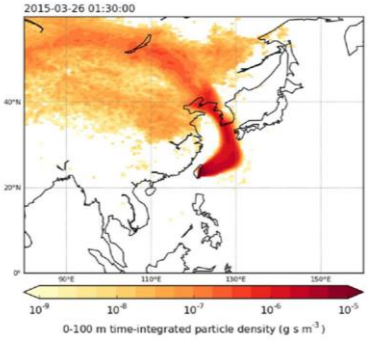
2015-03-26 01:30:00
0-100 m time-integrated particle density (g s m-3)

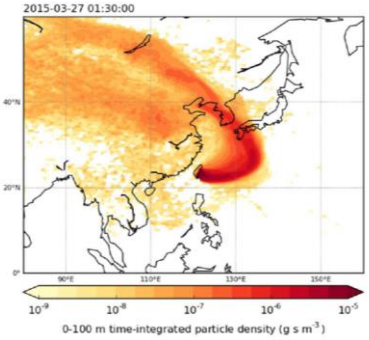
2015-03-27 01:30:00
0-100 m time-integrated particle density (g s m-3)

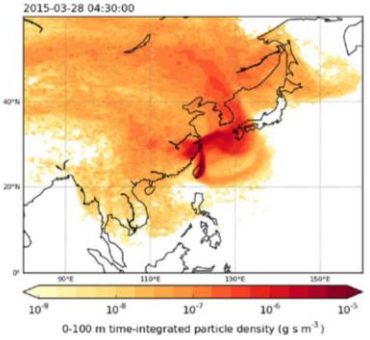
2015-03-28 04:30:00
0-100 m time-integrated particle density (g s m-3)

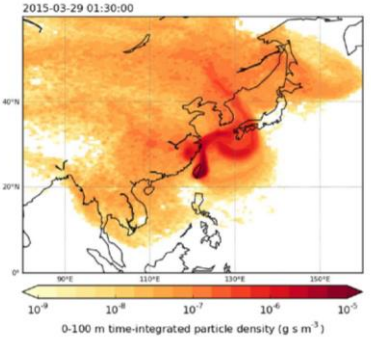
2015-03-29 01:30:00
0-100 m time-integrated particle density (g s m-3)

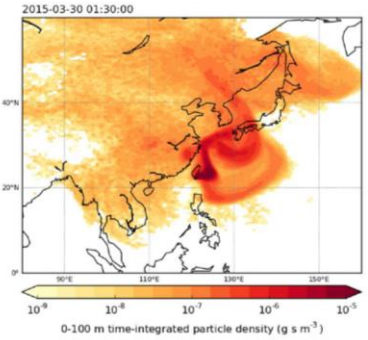
2015-03-30 01:30:00
0-100 m time-integrated particle density (g s m-3)

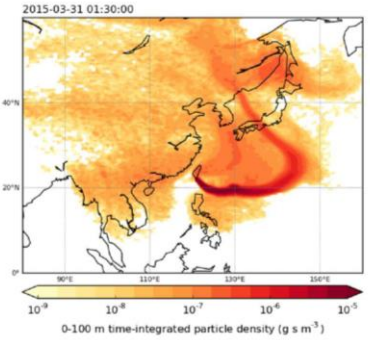
2015-03-31 01:30:00
0-100 m time-integrated particle density (g s m-3)

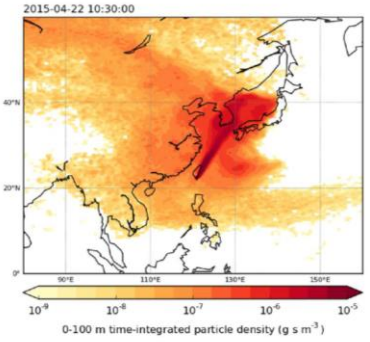
2015-04-22 10:30:00
0-100 m time-integrated particle density (g s m-3)

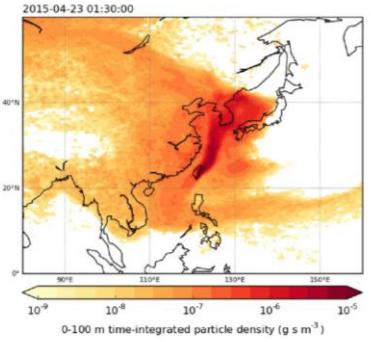
2015-04-23 01:30:00
0-100 m time-integrated particle density (g s m-3)

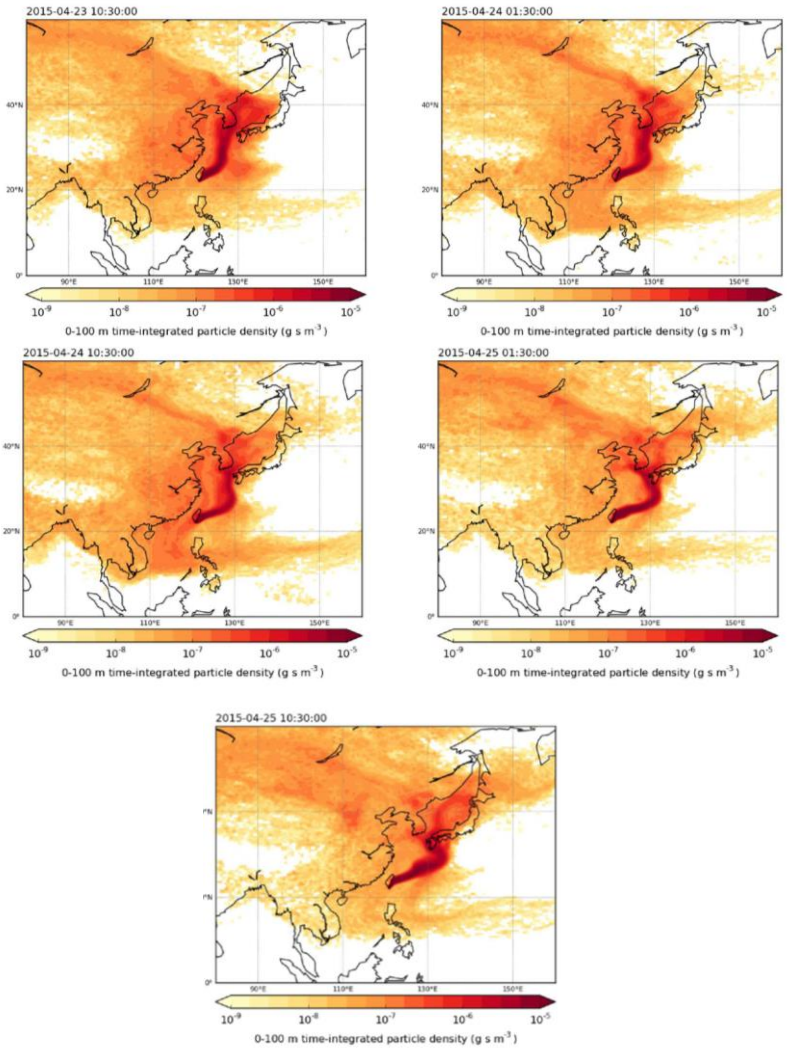
2015-04-23 10:30:00
2015-04-24 01:30:00
2015-04-24 10:30:00
2015-04-25 01:30:00
2015-04-25 10:30:00
0-100 m time-integrated particle density (g s m^{-3})